Thesis

Aspects of non standard cosmology

VONLANTHEN, Marc

Abstract

Divers aspects de la cosmologie au-delà du modèle standard ont été explorés durant cette thèse. Le modèle standard fait face à de nombreux problèmes (énergie noire...), à tel point qu'un consensus s'est établi dans la communauté scientifique portant sur la nécessité de dépasser ce modèle. Nous avons successivement étudier des modèles à dimensions spatiales additionnelles, analyser des données cosmologiques de façon indépendante du modèle standard, étudier les conséquences d'une expansion anisotrope causée par un champ magnétique en présence de neutrinos et finalement, nous avons remis en question le principe d'homogénéité du modèle standard au travers d'un modèle comportant une densité d'énergie dépendant des coordonnées spatiales.

Reference

VONLANTHEN, Marc. *Aspects of non standard cosmology*. Thèse de doctorat : Univ. Genève, 2012, no. Sc. 4428

UNIVERSITÉ DE GENÈVE
Département de physique théorique

FACULTÉ DES SCIENCES
Prof. Ruth DURRER

Aspects

of

non standard cosmology

THÈSE

présentée à la Faculté des Sciences de l'Université de Genève

pour obtenir le grade de

Docteur ès sciences, mention physique

par

Marc Vonlanthen

de

Romont (FR)

Thèse N° XXXXXX

GENÈVE

Atelier de reproduction de la Section de physique

2012

Remerciements

En premier lieu, je tiens à sincèrement remercier ma directrice de thèse Ruth Durrer. Tout au long de ces quatre années de thèse, Ruth Durrer a su réunir et mettre à ma disposition une intelligence et des qualités qui vont largement au-delà de ses compétences purement scientifiques unaniment reconnues. Elle est encore parvenue à mettre en place et à maintenir un climat de travail serein basé sur la confiance, qui m'a largement permis de mener à terme ce travail, tout en le conjuguant avec les exigences de mon heureuse paternité et de mes autres engagements. Davantage qu'une simple et banale formation scientifique, c'est une manière de former et de guider l'étudiant, de lui montrer un chemin en y investissant de sa personne, tout en le laissant libre de faire ses propres détours, dont j'ai eu la chance de bénéficier. Et c'est avant tout ceci que je retiendrai de Ruth.

Je remercie ensuite celles et ceux qui m'ont apporté une aide quelconque ou avec qui j'ai eu la chance de discuter ou de collaborer scientifiquement: Marcus Ruser, Peter Wittwer, Syksy Räsänen, Domenico Sapone, Julian Adamek, Elisa Fenu, Enea Didio, Martin Kunz et Andreas Malaspinas. Pour leur travail et leur gentillesse, je remercie encore les deux secrétaires du département, Francine Gennai-Nicole et Cécile Jaggi.

Tout aussi important que la dimension scientifique, et sans doute même davantage, je remercie celles et ceux avec qui, au fil des doutes, des interrogations, des discussions et des joies, j'ai eu le privilège de cheminer durant ces années passées. Parmi ces dernières et derniers, je ne peux manquer de citer mes amies et amis, compagnons et compagnes de groupe ou de bureau, Géraldine Haack, Elisa Fenu, Mona Frommert, Lukas Hollenstein, Umberto Canella et Enea Didio.

Finalement, mais à ce niveau-là d'engagement, ce ne sont plus des remerciements qu'elle mérite, mais ma plus profonde reconnaissance à Julia, ma compagne de coeur et de route, dont la patience, la tendresse, la confiance et les encouragements continuels ont été la clef de voûte de ce travail. Julia m'a de plus donné celle dont les yeux rayonnent à en faire pâlir de jalousie les feux célestes les plus intenses, Jeanne ma fille, que je remercie simplement de me rappeler tous les jours, sans mots, ce qui est essentiel pour moi.

Examinateurs

Le jury de cette thèse se compose de

- Prof. Dr. Ruth Durrer, Département de Physique Théorique de l'Université de Genève (Suisse)
- Dr. Chiara Caprini, CEA-Saclay (France)
- Dr. Martin Kunz, Département de Physique Théorique de l'Université de Genève (Suisse)
- Dr. Julien Lesgourgues, CERN (Genève, Suisse) et École Polytechnique Fédérale de Lausanne (EPFL)

Je les remercie chaleureusement d'avoir accepté de faire partie du jury, ainsi que d'avoir consacré du temps à la lecture de cette thèse.

Préliminaires

Une science se définit par son objet. Celui de la cosmologie est l'univers, le *cosmos* pour en référer à l'éthymologie grecque du mot. L'extension du concept de *cosmos* n'est pas demeurée figée depuis l'avénement de la longue chaîne de penseurs dont les réflexions ont été nourries de l'insatiable curiosité à comprendre l'infini qui nous entoure.

De manière simple, l'évolution de la cosmologie depuis les philosophes présocratiques, Thalès (VII^e siècle av. J.-C.), Anaximandre (VI^e siècle av. J.-C.), Anaximène (VI^e siècle av. J.-C.) et consorts, peut se comprendre comme un mouvement double ayant des composantes

- verticale de démythologisation du *cosmos* et plus largement de la nature s'accompagnant d'une dramatique réduction de la densité ontologique de l'univers à sa seule réalité physique et
- horizontale d'hyper-scientifisation et de mécanisation irrésistiblement conduites par la mathématisation de cette réalité physique et des succès consécutifs en termes de prédictions.

Pour illustrer correctement ce mouvement double, il conviendrait de dresser un historique de l'idée de nature lors des deux derniers millénaires. Un tel travail dépasse le cadre de cette introduction, et a de plus déjà été mené par le philosophe Pierre Hadot[1]. Il est néanmoins intéressant d'en relever quelques caractéristiques permettant d'en appréhender le contenu essentiel.

Dans les grands systèmes cosmologiques antiques, tels celui décrit par Platon (428-347 av. J.-C.) dans le *Timée*, par Aristote (384-322 av. J.-C.) dans *Du Ciel* ou par Plotin (205-270 ap. J.-C.) dans les *Ennéades*, le réél définit une hiérarchie de mondes dont le monde sensible, objet exclusif de la cosmologie moderne, représente le niveau le plus grossier, celui dans lequels les objets naissent et meurent, croissent et décroissent, sont générés et corrompus. Le monde sensible est le monde du devenir. A ce titre, la connaissance du monde sensible possède une valeur toute relative, car elle ne porte pas sur des lois ou principes immuables, mais bien sur des corps appelés à disparaître. C'est en ce sens que pour Platon, la science du monde physique n'est pas une connaissance à proprement parler, mais une opinion incertaine. Néanmoins, l'intérêt de la connaissance de la réalité physique tient au fait qu'elle manifeste des réalités supérieures dans la hiérarchie des mondes, dont elle est en quelque sorte le signe qui invite à la connaissance de principes plus fondamentaux, lesquels sont à leur tour eux-mêmes signes de principes supérieurs. Il s'agit donc, dans ces systèmes antiques, d'une conception du *cosmos* en pyramide, dont la base est constituée par le monde sensible, les étages intermédiaires par des principes immuables dépendants du système en question (les Idées platoniciennes, les différentes Âmes plotiniennes...) et le sommet par un principe premier qui produit et met en mouvement l'ensemble du réel. Ce premier principe est nommé Démiurge dans le système de Platon, Moteur Immobile chez Aristote, l'Un chez Plotin, ou encore, plus tard, Dieu dans la vision cosmologique du christianisme et des autres monothéismes. Il convient toutefois de se garder d'identifier ces différentes dénominations, chacune ayant des spécificités propres au *corpus* philosophique dont elle est

[1] P. Hadot, *Le Voile d'Isis*, 2004, Gallimard

issue. Nous avons déjà mentionné que du point de vue épistémologique, la connaissance du monde physique n'a pas de valeur en soi. Ceci demande à être complété en ajoutant que le type de connaissance présente un degré de certitude d'autant plus élevé et ferme que son objet affiche un caractère principiel ou fondamental. Ainsi, le degré suprême de la connaissance est la connaissance du principe premier ou divin, et n'est accessible que par la raison (Aristote, Thomas d'Acquin) ou par l'extase mystique (Platon, Plotin, Augustin).

L'impulsion cruciale au mouvement double brièvement décrit ci-dessus se situe au tournant de la Renaissance (XVI^e-$XVII^e$ siècles). Outre un contexte socio-culturel favorable (apparition des universités, démocratisation du savoir), cette impulsion est due à une poignée de philosophes et scientifiques dont les idées novatrices ne tarderont pas à s'imposer. Galilée (1564-1642) compte bien évidemment parmi ces penseurs:

> "La philosophie est écrite dans ce livre immense qui se tient ouvert sous nos yeux - l'univers - et qui ne peut se comprendre si l'on n'a préalablement appris à en comprendre la langue et à connaître les caractères employés pour l'écrire. Ce livre est écrit dans la langue mathématique; ses caractères sont des triangles, des cercles et d'autres figures géométriques, sans l'intermédiaire desquels il est impossible d'en comprendre humainement un seul mot." [2]

Clairement, cette citation illustre la réduction verticale du *cosmos* antique et de sa hiérarchie des mondes à sa dimension la plus superficielle, celle que l'homme appréhende par ses sens, la dimension physique. De plus, les phénomènes y prenant place sont décrits par le langage mathématique, lequel, par sa capacité de cerner et de reproduire l'ordre du monde, a dès lors champs libre pour s'imposer comme outil exclusif de toute description définitve de la réalité. La méthode empirique tend aussi à se propager comme moyen d'investigation de la nature ou du *cosmos*, notamment sous la propagation de l'idéologie d'un autre artisan majeur de la révolution qui s'opère, le philosophe anglais Francis Bacon (1561-1626)

> "Les secrets de la nature se révèlent plutôt sous la torture des expériences que lorsqu'ils suivent leur cours naturel." [3]

Dans de tels textes apparaît ce qui sera, pour le meilleur et pour le pire, le paradigme de la science moderne, soit l'être humain qui se pose hors ou au-dessus d'une nature qu'il s'agit de soumettre à une procédure aux allures judiciaires afin d'en extirper les secrets. Pierre Hadot qualifie cette attitude de *prométhéenne*, par opposition à l'attitude *orphique* dominante à l'Antiquité selon laquelle l'humain est partie indisociable de la nature ou *cosmos*. L'autorité chrétienne conforte encore cette position dominatrice nouvellement acquise:

> "Croissez et multipliez-vous et remplissez la terre et dominez-la. Commandez aux poissons de la mer, aux oiseaux du ciel et à toutes les bêtes qui se meuvent sur la terre." [4]

S'appuyant sur ce passage de la Genèse, Bacon proclame

> "Laissons le genre humain recouvrer ses droits sur la nature, droits dont l'a doué la munificence divine." [5]

[2] Galilée, *Il saggiatore*, 1623
[3] F. Bacon, *Novum Organum*, I, trad. M. Malherbe et J.M.Pousseur, Paris 1986
[4] Genèse 1, 28
[5] F. Bacon, op. cit.

Ceci achève d'esquisser le mouvement double dont la science de la nature a fait l'objet. Le *cosmos* réduit à sa réalité physique, celle-ci fait l'objet d'une étude intensive décrite par le langage mathématique et menée de manière exclusive selon la méthode empirique. Durant les derniers siècles du second millénaire, le mouvement de désacralisation du *cosmos* va encore se radicaliser. Témoin en est la célèbre réponse faite par Laplace (1749-1827) à Napoléon qui l'interroge sur la place de Dieu dans son système:

"Sire, je n'ai pas eu besoin de cette hypothèse." [6]

À partir du $XVIII^e$ siècle, et davantange au XIX^e siècle, le champ de recherche de la cosmologie exclut totalement la considération des causes, des fins et des principes, pour s'en tenir à la seule description des phénomènes. La cosmologie contemporaine n'a en ce sens aucunement infirmé l'existence de Dieu ou d'un principe premier, elle est simplement devenue totalement indifférente à la question. Cette désacralisation du *cosmos* s'accompagne d'une hyper-sophistication de la description quantitative de la réalité physique. Un désaveu de la magie et de la poésie au profit de la pensée mécaniste et cartésienne qui fera dire à l'illustre Schiller (1759-1805):

"Inconsciente des joies qu'elle donne,
Sans jamais s'extasier de sa propre splendeur,
Sans jamais prendre conscience de l'esprit qui la mène,
Sans jamais être heureuse par ma félicité,
Insensible même à la gloire de son créateur,
Comme le battement mort d'un pendule,
Comme une esclave, elle obéit à la loi de pesanteur,
La Nature, dépouillée de sa divinité." [7]

Schiller regrette amèrement la mécanisation de la Nature, le soleil n'est plus qu'un globe de feu, la Nature une horloge. Le poète pleure la perte de la description poétique et esthétique au profit de l'unique description mathématique.

Par ces quelques remarques préliminaires sur l'homme, le *cosmos*, la science et son évolution, je n'ai pas voulu prétendre apporter quelque réponse. Ma seule intention fut d'utiliser cette modeste contribution scientifique qu'est ma thèse pour rappeler la question essentielle, et qui, me semble-t-il après mon court passage dans le monde de la recherche, a été largement évacuée des préoccupations de nombreux scientifiques, la question du rapport de l'homme à la nature. À l'heure où l'attitude *prométhéenne*, pour reprendre le vocabulaire de P. Hadot, en est parvenue, en l'espace de quelques décennies, à modifier irrémédiablement le climat de notre planète vieille de 4.5 milliards d'années, il me semble urgent que la communauté scientifique se réapproprie cette question du rapport de l'homme à la nature, des statuts de la science et de son objet, la nature.

[6] cité par A. Koyré, *Du monde clos à l'univers infini*, Paris, 1973, p. 336
[7] F. von Schiller, *Les Dieux de la Grèce*, strophe XIV.

Introduction

La cosmologie est l'étude de l'univers envisagé dans sa globalité. De par les seules portée et complexité de l'objet que la cosmologie se propose d'étudier, il est nécessaire d'y appliquer des descriptions théoriques portant sur l'immensément petit tout comme sur l'immensément grand. Pour illustrer ce propos, l'énigme de la matière noire peut être prise en exemple. Il existe en effet diverses évidences plaidant pour une densité totale de matière sans pression dans l'univers constituée à près de quatre-vingts pour cent de matière non baryonique, la matière noire. Cette dernière influence le comportement de systèmes physiques à de très importantes échelles. Le spectre de puissance des anisotropies du fonds diffus cosmologique (CMB pour l'anglais cosmic microwave background) est tout-à-fait sensible à la quantité de matière noire sur des échelles physiques caractéristiques de l'univers observable, soient des ordres de grandeur de 10^{28} cm. De même, la concentration de matière noire modifie la dynamique des galaxies en affectant leurs vitesses orbitales dans les clusters de galaxies correspondant à des échelles de 10^{25} cm, ou encore la dynamique des étoiles contenues dans une galaxie particulière à des distances de 10^{22} cm. Néanmoins, la matière noire est un terme générique sous lequel se cache très probablement une particule encore inconnue, si ce n'est qu'elle doit être stable et sans charge. Ainsi, cette énigme cosmologique non encore résolue qu'est la matière noire requiert des outils conceptuels empruntés aussi bien à des théories physiques de l'immensément grand, comme la Relativité Générale, que de l'immensément petit, comme la physique des particules. Un autre exemple illustrant la richesse scientifique de la cosmologie est la formation des grandes structures dans l'univers, distributions et halos de galaxies. Nous avons décrit ci-dessus les ordres de grandeur de ces structures, qui ont pour origine des fluctuations générées pendant une phase inflationaire de l'histoire de notre univers. Cette phase d'expansion extrêmement rapide a eu lieu une petite fraction de seconde après le Big-Bang, en comparaison des treize milliards d'années d'âge de l'univers. Originellement, la taille caractéristique de ces fluctuations est proche de l'échelle de Planck, soit 10^{-33} cm, et en accord avec les équations d'Einstein, ces fluctuations ont par la suite été amplifiées par la gravité pour finalement donner lieu aux structures observées aujourd'hui. À nouveau, la cosmologie est le lieu de rencontre de l'immensément grand et de l'immensément petit.

Ces dernières décennies ont vu l'avénement d'une nouvelle ère en cosmologie, celle des observations de précision qui permettent de tester et de contraindre avec une efficacité grandissante les différents modèles censés décrire notre univers. Parmi eux figure le modèle standard de la cosmologie, ainsi nommé en raison de sa plus grande fidélité à reproduire les observations. Malgré ses succès, le modèle standard ne remporte pas l'adhésion unanime de la communauté scientifique, loin s'en faut, et ceci surtout à cause d'une de ses composantes, la constante cosmologique, dont la densité d'énergie équivaut à plus de soixante-dix pour cent du budget total de l'univers, alors que sa nature et son origine physiques demeurent inconnues ou font l'objet de controverses difficilement résolvables. Des modèles alternatifs sont intensément étudiés et impliquent par exemple des modifications de la Relativité Générale à grandes échelles ou encore l'abandon de certains principes essentiels du modèle standard, telles l'homogénéité ou l'isotropie de l'univers.

Ma thèse de doctorat s'inscrit dans un contexte de recherches théoriques dans le domaine de la cosmologie. Dans une telle approche, l'outil théorique de base sont les équations

d'Einstein qu'il est possible de comprendre sous la forme de l'identité suivante :

$$\text{Géométrie de l}'\text{espace} - \text{temps} = \text{énergie} - \text{impulsion de l}'\text{espace} - \text{temps}.$$

Ces équations expriment la relation intime qui existe entre le contenu en énergie et les aspects géométriques d'un espace quelconque, notre univers en particulier. Elles permettent, sous certaines hypothèses supplémentaires, d'expliquer par exemple en quoi diffère la dynamique d'un univers rempli de radiation de celle d'un univers rempli de matière sans pression, ou encore et dans une certaine mesure, d'établir des scénarios possibles pour l'évolution future de l'univers. Elles constituent de plus le fondement théorique du modèle standard de la cosmologie, et conjointes à la théorie des perturbations, elles expliquent, entre autres, les observations du CMB. Pour la bonne intelligibilité du titre et du contenu de ma thèse, il est utile de s'attarder un peu plus longtemps sur le modèle standard de la cosmologie. Ce dernier suit directement de l'imposition de deux symétries aux équations d'Einstein. Nous supposons en effet que notre universe est homogène et isotrope. Il en suit alors un modèle cosmologique dont la géométrie est entièrement décrite par une fonction dépendant du temps uniquement, le facteur d'échelle, et dont la forme explicite est en rapport direct avec le contenu de l'univers. Ce facteur d'échelle permet de comprendre les observations de Hubble en 1929 montrant indubitablement que les galaxies s'éloignent de l'observateur à une vitesse proportionnelle à la distance. L'espace-temps est en expansion, laquelle est mathématiquement décrite par le facteur d'échelle. Toutefois, en 1998, de nouvelles observations ont prouvé que non seulement l'univers était en expansion, mais que cette dernière est accélérée. Ceci est pour le moins troublant, car si notre univers est rempli de matière et de radiation, sous l'effet de l'attraction gravitationnelle, l'expansion devrait ralentir. Ainsi, une des premières tentatives visant à construire un modèle cosmologique expliquant cette expansion accélérée a consisté dans l'ajout d'un terme nouveau dans la partie décrivant le contenu de l'espace des équations d'Einstein. Ce terme comporte une pression négative capable de jouer le rôle de source pour l'accélération, et dans sa version la plus simple il s'agit d'une constante cosmologique. Nous avons à ce stade tous les ingrédients du modèle standard de la cosmologie, à savoir de la matière sans pression (noire et baryonique) et une constante cosmologique pour le contenu et une géométrie caractérisée par les propriétés d'isotropie et d'homogénéité. Ce modèle, bien qu'il soit loin de faire l'unanimité des scientifiques, a néanmoins l'avantage de reproduire de nombreuses observations indiscutables. Parmi celles-là, il convient de s'attarder quelque peu sur le CMB. Cette radiation quasi isotrope est une relique d'un état extrêmement chaud et dense de l'univers primordial, alors que les photons interagissaient encore fortement avec la matière. Elle est de plus une confirmation de la théorie du Big-Bang, qui veut que notre univers se soit développé à partir d'une singularité initiale d'un état très chaud (10^{32} K) et dense vers ce que nous observons aujourd'hui à environ 2.7 K. Le CMB présente néanmoins de petites anisotropies de température, qu'il est possible d'étudier et de calculer au moyen de la théorie des perturbations linéaires. Le spectre des puissances des anisotropies alors obtenu dépend principalement des conditions initiales et des paramètres cosmologiques. Les conditions initiales décrivent l'état des inhomogénéités à la fin de l'inflation, une période d'expansion très rapide et de dilution de ces inhomogénéités. Les paramètres cosmologiques indiquent le contenu en matière ainsi que la courbure de l'univers, qui en déterminent l'expansion. Parmi les nombreux modèles cosmologiques prétendant expliquer l'accélération actuelle de l'expansion de l'univers, le modèle standard est celui dont les prévisions reproduisent au mieux le spectre des anisotropies du CMB.

Toutefois, comme l'indique le titre de la présente thèse, je me suis davantage intéréssé à des aspects théoriques de la cosmologie qui peuvent être qualifiés de non standards. Dans le bref résumé ci-dessous de mes divers projets, je m'efforce pour chacun de justifier en quoi il revêt des traits qui vont au-delà du modèle standard de la cosmologie.

Le cadre de mon premier projet est celui des théories à dimensions spatiales additionnelles. Ce cadre justifie déjà la place de ce projet dans ma thèse et son titre, le modèle standard de la cosmologie ne comportant que trois dimensions spatiales. De telles théories postulent, en plus des trois dimensions spatiales et de la dimension temporelle usuelles, l'existence de dimensions spatiales supplémentaires. Un tel postulat est motivé par des raisons de consistance de la théorie des cordes qui est une théorie de la gravité quantique. Nous nous sommes intéressés à un modèle qui, en plus du temps, admet quatre dimensions spatiales. Notre espace-temps quadrimensionnel est alors un sous-espace de ce volume à cinq dimensions. En langage technique, ce sous-espace est appelé une brane, et le nombre de branes présentes dans le volume englobant n'est en principe pas restreint à une seule. De plus, toutes les particules du modèle standard des particules sont confinées sur notre brane, alors que seuls les gravitons sont capables de se propager dans l'ensemble du volume englobant. Ce dispositif constitue le modèle cosmologique de mon premier projet. Le problème particulier que nous nous sommes proposés d'étudier est la production des gravitons lorsque notre brane, i.e. notre espace-temps quadridimensionnel, s'approche et s'éloigne d'une autre brane statique. Ceci est en parfaite analogie avec un effet déjà théorisé et observé de la théorie des champs quantiques, l'effet Casimir dynamique, qui explique la création de photons à partir des fluctuations quantiques du vide entre deux miroirs conducteurs et parfaitement réfléchissants en mouvement. Dans notre cas, le rôle des photons est joué par les gravitons, et nous en avons investigué la production en fonction de la vitesse à laquelle notre brane se meut en direction de la seconde brane statique ainsi qu'en fonction de la masse des gravitons. Conceptuellement, mon premier projet est d'un grand intérêt, quoique ne laissant que peu d'espace à l'aspect empirique de la cosmologie. Néanmoins, cela ne signifie pas que de manière générale, l'hypothèse des dimensions spatiales additionnelles échappe à toute testabilité. En 1998 par exemple, Arkani-Ahmed, Dvali et Dimopoulos [5] ont placé des contraintes sur le nombre possible de dimensions additionnelles. Ainsi, une seule dimension supplémentaire est exclue, car cela produirait de trop fortes déviations de la gravité sur des échelles du système solaire.

Mon second projet présente quant à lui nettement plus d'affinités avec l'aspect observationnel de la cosmologie, l'idée directrice étant de fournir une analyse des données du CMB. En effet, comme il en a été fait mention ci-dessus, de nombreuses interrogations subsistent au sujet de la phase la plus récente de l'histoire de l'univers, dont la dynamique est principalement caractérisée par une expansion accélérée. Comme l'interprétation des données et la dérivation de contraintes sur les paramètres cosmologiques principaux (densité de matière noire ou baryonique, index spectral ...) passent par l'approbation d'un modèle cosmologique, et qu'aucun consensus n'existe sur un modèle définitivement valable, il était pertinent d'établir des contraintes ne dépendant pas de la physique méconnue de la dynamique tardive de l'univers. Le modèle standard de la cosmologie intervenant essentiellement comme une possible explication de cette dynamique tardive, notre volonté de l'exclure de l'analyse explique pourquoi ce projet n'appartient pas au cadre du modèle standard de la cosmologie. L'intérêt de la démarche réside dans le fait qu'en principe, toute théorie

cosmologique prétendant expliquer l'accéleration actuellement observée de l'expansion de l'univers doit également être à même de placer des contraintes sur les paramètres cosmologiques fondamentaux. De telles contraintes devront alors impérativement satisfaire celles que nous avons établies dans notre analyse. Sans entrer dans des détails techniques dépassant le cadre de cette introduction, notre méthode a consisté en un premier lieu dans une mise à l'écart des données correspondant à des processus physiques s'étant déroulés dans l'univers tardif, ce qui a permis de prendre comme modèle de référence un modèle ne contenant que de la matière sans pression (noire et baryonique), lequel constitue une bonne approximation pour des époques ou la physique inconnue de l'énergie sombre n'influence pas la dynamique de manière significative. Afin de prendre en compte la différente évolution entre notre modèle de référence et les données à partir du moment où les photons du CMB ont cessé d'interagir avec la matière, nous avons encore introduit et contraint un paramètre supplémentaire. Ce dernier exprime la distance observée à la surface de dernière diffusion définie comme la surface de l'espace-temps sur laquelle les photons ont interragi pour la dernière fois avec la matière, avant que l'univers ne leur devienne transparent et qu'ils ne se propagent librement jusqu'à aujourd'hui.

Dans mon projet suivant, nous nous sommes intéressés à de possibles signatures dans le CMB, signatures produites par l'existence d'un champ magnétique homogène. Par homogène est compris un champ dont la longueur de cohérence est de l'ordre de la taille de l'univers observable, et qui peut donc être considéré comme constant sur de telles échelles de distance. Un tel champ a la particularité d'agir comme source d'une expansion anisotrope de l'univers affectant le spectre de puissance des anisotropies du CMB, dont l'étude permettrait alors de placer des contraintes sur l'intensité du champ magnétique. Le cadre général adopté étant celui d'une expansion anisotrope, le modèle présente des différences géométriques fondamentales avec le modèle standard. Cependant, et c'est là le résultat important de notre étude, si des particules relativistes se propageant librement sont également présentes, elles génèrent une pression anisotrope contrecarrant celle du champs magnétique, et par conséquent, d'anisotrope, l'expansion de l'univers devient rapidement isotrope. Les neutrinos sont de particulièrement bons candidats pour jouer le rôle d'isotropisants, car ils existent en densité suffisante, et nous savons que durant une grande partie de l'histoire thermique de l'univers pertinente pour notre analyse, les neutrinos ont eu une dynamique relativiste. Mais, des expériences ont aussi mis en évidence le fait que les neutrinos ont des masses, sur lesquelles des contraintes provenant de divers domaines de la physique ont été placées. Tout ceci permet de différencier trois phases. La première durant laquelle le taux d'interaction des neutrinos avec le fluide cosmique domine largement le taux d'expansion de l'univers. Les neutrinos ne peuvent alors se propager librement, et le champ magnétique peut agir sur l'expansion alors anisotrope de l'univers. Puis, à mesure que l'univers se refroidit, le taux d'interaction des neutrinos baisse, jusqu'à ce que ces derniers cessent progressivement d'interagir avec le fluide cosmique. L'univers devient alors transparent pour les neutrinos, et leurs pressions anisotropes annulent l'expansion anisotrope de l'univers. Finalement, au moment où la température de l'univers devient inférieure à la masse des neutrinos, ces derniers deviennent non-relativistes, leurs pressions respectives deviennent nulles et ne sont dès lors plus en mesure de contrebalancer l'expansion anisotrope causée par le champ magnétique, laquelle reprend alors. Nous avons, au moyen d'approximations analytiques et de simulations numériques, étudié de manière quantitative l'expansion de l'univers et la possible signature dans le CMB de ce scénario pour des champs de différentes

intensités satisfaisant des contraintes physiques indépendantes et pour des neutrinos de masses différentes, avec comme résultat principal la suppression par plusieurs ordres de grandeur d'un possible signal dans le CMB pour un univers contenant des neutrinos dont les masses se situent dans les valeurs permises par les expériences par rapport au signal attendu dans un univers sans neutrinos.

Dans le cadre de mon quatrième et dernier projet, nous avons choisi d'explorer une alternative au modèle standard de la cosmologie. L'idée directrice du projet consiste à évaluer la possibilité de reproduire certaines observables en se passant de la constante cosmologique ou d'autres composantes physiques dynamiques censées agir comme source de l'expansion accélérée que nous observons. Toutefois, il est indubitable qu'un modèle reprenant toutes les hypothèses du modèle standard, mais sans constante cosmologique, échoue à expliquer les observables qui nous intéressent, lesquelles ne sont autres que différentes sortes de distances. Il est donc nécessaire de relâcher certaines hypothèses. Notre choix s'est porté sur un modèle simple d'univers rempli exclusivement de matière sans pression, mais distribuée de manière inhomogène. Ces inhomogénéités prennent la forme de successions parallèles de surdensités et de sous-densités de matière. Les photons que nous observons voyagent donc à travers ces structures semblables à des murs. Nous avons alors procédé de deux manières. D'abord, nous avons imposé à notre modèle des inhomogénéités dont la taille correspond à celle d'inhomogénéités observées dans notre univers, et en avons calculé des observables d'intérêt. Le résultat ne diffère pas significativement du résultat obtenu pour un univers dans lequel la matière sans pression est répartie de manière homogène, et donc, n'est pas en mesure de reproduire les données. Puis, nous avons imposé au modèle de reproduire les distances voulues, et nous sommes intéressés à la taille des inhomogénéités engendrées par cette contrainte. Nos simulations ont alors montré que pour générer les distances observées, des sous-densités de la taille de l'univers observable étaient nécessaires. Or, les observations indiquent que de telles sous-densités n'existent pas. Nos résultats pour ce modèle simple ne montrent aucun départ significatif du cas homogène, et par là, offrent un désaveu aux modèles prétendant expliquer la présente accélération par des inhomogénéités dans la répartition de la matière. Toutefois, il convient de préciser que notre étude n'a pas un degré de généralité suffisant pour exclure totalement et définitivement cette hypothèse.

Je terminerai cette introduction à mon travail de doctorat par ma liste de publications (page suivante). Il s'ensuit une introduction plus détaillée et théorique ainsi que les publications auxquelles j'ai eu le bonheur de contribuer, le tout rédigé en anglais.

Liste de publications

- Ruser M., Durrer R., Vonlanthen M. and Wittwer P., *Graviton production in anti-de Sitter braneworld cosmology: A fully consistent treatment of the brane motion*, Phys. Rev. **D79**, 083529 (2009), [e-print: arXiv:astro-ph/0901.3683v3]

- Durrer R., Ruser M., Vonlanthen M. and Wittwer P., *Braneworlds, graviton production, dynamical Casimir effect Physics and Mathematics of Gravitation*, Proceedings of the Spanish Relativity Meeting 2008, eds. K.E. Kunze, M. Mars and M.A. Vàsquez-Mozo, AIP Conference Proceedings **1122**, 39 (2009). [e-print: arXiv:astro-ph/0902.0872]

- Vonlanthen M., Rasanen S., Durrer R., *Model-independent cosmological constraints from the CMB*, JCAP08(2010)023, [e-print arXiv:astro-ph/1003.0810v2]

- Adamek J., Durrer R., Fenu E. , Vonlanthen M., *A large scale coherent magnetic field: interactions with free streaming particles and limits from the CMB* , JCAP06(2011)017, [e-print arXiv:astro-ph/1102.5235v1]

- Di Dio E., Vonlanthen M. and Durrer R., *Back Reaction from Walls*, JCAP06(2011)017 [e-print arXiv:astro-ph/1111.5764]

À Julia
et Jeanne,

Le connu est fini,
l'inconnu infini;
ce que nous comprenons n'est qu'un îlot perdu
dans l'océan illimité de l'inexplicable

T.H. HUXLEY

Contents

Chapter 1

Introduction

First of all, in this introduction, I give a short overview of the history of cosmology. This overview is based on [130]. Then, in a second section, I explain some fundamental and basic knowledge of modern and contemporary cosmology, which is helpful to understand the following chapters. Moreover, in this section, I stress on the standard model of cosmology. The title of my thesis being "Aspects of non standard cosmology", it is therefore necessary to give an overview of standard cosmology in order to understand in which sense the works presented hereafter belong to non standard cosmology. In a third and last section, I briefly review and comment on all the projects, which are elaborated in details in the following chapters.

1.1 Some history

1.1.1 The pioneers of modern cosmology

It is commonly admitted to start with the history of cosmology from the ancient Greece. Though peoples like the Babylonians or the early Chinese already made many astronomical observations, their explanations were still full of mythological elements, and it is therefore justified to attribute the first attempts to give a rational picture of the universe to the old Greeks.
It is interesting to note that at the same time as Aristotle's geocentric cosmology, whose influence lasted more than a millenium, the Pythagorean Philolaus of Croton (ca. 480-385 B.C.) and Aristarchos (ca. 310-230 B.C.) proposed some heliocentric models. However, their influences remained small. Indeed, one widespread criticism to Aristarchos' system was the fact that if the earth were to move around the sun, the observer would then have to see the stars on different angles in winter or in summer. Since this is not the case, the stars have to be extremly far away, and Aristarchos' universe needs to be very large.
More precisely, Aristotle (384-322 BC) was certainly the first philosopher-scientist to provide an overall idea of the *cosmos* as a set of physical objects. In his worldview, the Earth was at the center of the universe and surrounded by three-dimensional rotating spheres. All the stars and planets, as well as the Moon and the Sun, were carried by these spheres. Moreover, the whole system was divided in two regions, one below the Moon, to which the Earth belongs, and a second one above the Moon. The first region was characterized by birth and death, generation and corruption, and composed of the four usual elements, earth, fire, air and water. The most important feature of the second region is its perfection

and the incorruptibility of its components composed of a fifth element, the aether.
Ptolemy (90-168) was a greek astronomer and mathematician who spent most of his life in Egypt. Ptolemy's cosmological system (Fig.1.1) relies on Aristotle's, even though he improved it with more accurate geometrical descriptions and added some new elements. For instance, Ptolemy in his book on astronomy, the *Almageste*, decribed in great detail the mechanisms of the rotating spheres.

With the fall of the roman empire, most of the old greeks' astronomical treatises have

Figure 1.1: Ptolemy's system

been transmitted to the Islamic civilzation, while Europe was going through dark ages. At the end of the Middle Ages, translated from Arabic into medieval Latin, Europe, mainly by means of the Church and its monks, rediscovered this scientific inheritance with the contributions added by the Islamic civilization (use of the zero and trignometric techniques).

1.1.2 The way towards scientific cosmology

The way towards scientific modern cosmology went through some of the most decisive revolutions of the history of ideas. After more than fifteen centuries of a geocentric system, Nicholas Copernicus (1473-1543), a Polish monk, proposed to switch the places of the Earth and the Sun. The Sun was meant to be in the center of the universe, and the Earth in revolution around it. Moreover, for observational reasons, he claimed that the Earth was also rotating around its own axis. Copernicus system had the advantage to provide automatic and natural explanations to astronomical phenomena whose explanations looked quite *ad hoc* in geocentric theories. But a heliocentric worldview was unimaginable to many at that time, above all for the Church. Indeed, for the Church, the idea of the Earth not being the center of the universe, and therefore a planet by no means special, was properly intolerable.
Galileo Galilei (1564-1642) made decisive contributions to astronomy. He built a telescope, which allowed him to observe the sky as no one had before. Among his several surprising observations, he discovered for instance Jupiter's four satellites and the fact that the Moon was not a perfect and smooth sphere. At this time still under strong influence of Aristotle's cosmology, such a statement was in conflict with well-established beliefs and dogma.
Another discovery shaded Aristotelian systems: Tycho Brahe (1546-1601) observed comets moving through the sky, but following trajectories forbidden by the theory of rotating spheres. However, Brahe was reluctant to Copernician heliocentric ideas. He built another complicated geocentric system where some planets rotate around the Sun, while the Sun

rotates around the Earth.
Kepler (1571-1630) overtook most of the moral and religious difficulties of the heliocentric worldview. He adopetd a symbolic identification of the Sun with God, God being, in his view, at the center of the spiritual reality as the Sun is at the center of the physical one. In his book *Astronomia nova*, Kepler expounded his three famous laws on the motion of planets.
Newton (1643-1727) (Fig.1.2) applied the same physical laws used to described the motion on Earth to the astronomical objects, the laws of mechanics. He also discovered a mathematical description of gravity, which is still used nowadays for a wide range of physical phenomena and which, for some given scales, is an excellent approximation of the more fundamental description of gravity, Einstein's General Relativity. For completeness, one

Figure 1.2: Portrait of Newton at the age of 46.

should also quote scientists like Euler (1707-1783) or Laplace (1749-1827). The former developed mathematical tools useful to describe a wide range of physical processes and the latter put forward some remarkable hypotheses on the formation of our solar system and made some decisive contributions to theoretical physics. For instance, he predicted the existence of very massive objets or black holes, whose gravity is so strong that not even light can escape. He also brought decisive contributions to celestial mechanics.
In the late 18th century, an english astronomer, William Herschel (1738-1822) discovered Uranus and made some very interesting observations on the structure of the Milky Way and the distribution of stars in the sky. Thanks to his huge telescope (Fig.1.3), Herschel was able to probe deeper regions of our universe than no one had seen before. He first described our galaxy as a branching compound of many millions of stars.
The nineteenth century saw the appearance of new observational techniques, such as spectroscopy or photography. These techniques provided interesting possibilities to learn more on the dynamics and the composition of astrophysical systems.

The first decades of the twentieth century have been marked by the growing influence of the two most important theories in physics: Relativity and Quantum Physics. In the twenties, Einstein's General Relativity was widely admitted as providing a theoretical foundation for modern cosmology. At this time, the belief in a static universe was still incontested. But a consequence of Einstein's gravitational field equation for a cosmological model containing only matter is that it has to collapse upon itself, and was therefore unstable. Einstein then stabilized the model by adding a constant term to the equations, which is not forbidden by the theory. But the evidence for our universe not being static

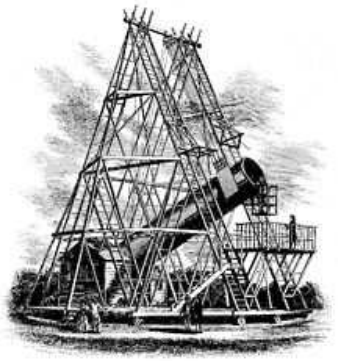

Figure 1.3: Herschel's telescope, focal distance of 12 meters

came from observations. In 1929, based on observations of nebulae, Hubble presented a roughly linear relation (Fig.1.4) between distances and velocities of nebulae. These undeniable observations eventually ruled out the idea that a static universe might match the reality, as admitted by Einstein himself in 1930 at a meeting of the Royal Society in London. In 1922, a Russian mathematician Alexander Friedmann and later in 1927, a Belgian astrophysicist Georges Lemaître, independently, found solutions to Einstein's equations that describe a dynamical universe. Moreover, Lemaître was the first to derive the linear velocity-distance relationship $v \propto d$ that states the proportionality of the relative velocity v of an object to Earth and its distance d to Earth. Combining available data sets, Lemaître found some values for the constant of proportionality. But at the time of their publications, the belief in a static universe was so powerful that nobody really thought of these dynamical solutions as a true description of our universe. The usual story about the discovery of the expansion of the universe tells us that Hubble was the first to combine theory and data to conclude that the universe was in expansion described by Hubble's law $v = H_0 d$, where now the constant of proportionality is Hubble's constant. But indeed, it was Lemaître. The discovery of the expansion of the universe, along with a theoretical

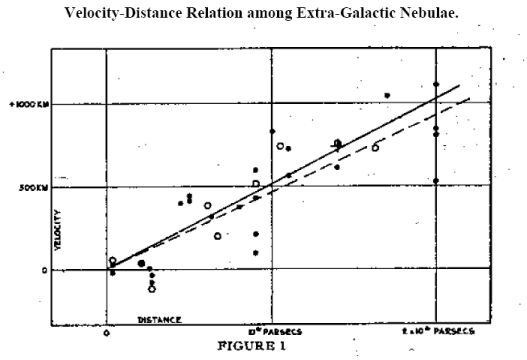

Figure 1.4: The original graph found in Hubble's paper (1929)

model which describes it, is certainly one of the greatest scientific discoveries. Each of the galaxies observed by Hubble was moving away from other galaxies, as a consequence of the expansion of space itself. Of course, in principle, some galaxies may also be moving towards each other. But the trend is clear and indicated the expansion of space.

In the early thirties, most of the ingredients are present to give rise to the Big-Bang model in cosmology, which I will comment on in the next section.

1.2 The Big-Bang model and the standard model of cosmology

Einstein equations relate the geometry of the universe to its matter and energy content

$$G_{\mu\nu} = 8\pi G T_{\mu\nu} - \Lambda g_{\mu\nu} \tag{1.1}$$

Here, G is Newton's constant, $G_{\mu\nu}$ represents Einstein's tensor, $T_{\mu\nu}$ denotes the energy momentum tensor, $g_{\mu\nu}$ is the metric tensor that defines lengths and angles in the universe and Λ is the cosmological constant. Einstein's tensor defines the geometry of the universe and the energy momentum tensor describes its matter and energy content. For a homogeneous and isotropic universe, the metric reads

$$ds^2 = g_{\mu\nu}dx^\mu dx^\nu = -dt^2 + a^2(t)\gamma_{ij}dx^i dx^j, \tag{1.2}$$

where $a(t)$ is the scale factor and γ_{ij} is the metric of a 3-space of constant curvature K. Together with Einstein equations Eq.(1.1), this metric leads to the Friedmann equations

$$\left(\frac{\dot{a}}{a}\right)^2 + \frac{K}{a^2} = \frac{8\pi G}{3}\rho + \frac{\Lambda}{3} \tag{1.3}$$

$$\frac{\ddot{a}}{a} = -\frac{4\pi G}{3}(\rho + 3P) + \frac{\Lambda}{3} \tag{1.4}$$

where ρ is the energy density of the universe and P its pressure. The dot stands for a derivative with respect to the cosmic time. The scale factor describes the dynamics of the expansion, and for a homogeneous universe, it only depends on time, as well as the energy density and the pressure. The Friedmann equations Eq.(1.3-1.4) directly follow from imposing symmetries on the metric Eq.(1.2). Eq.(1.3-1.4) describe the geometry of a homogeneous and isotropic universe. All the information about the geometrical evolution is encoded in the scale factor a. The right hand side of Eq.(1.3-1.4) describes the evolution of the content of the universe, which is caracterized by its pressure P and its energy density ρ. Since there are three unknowns, $a(t)$, $\rho(t)$ and $P(t)$ for two equations, a third relation is necessary. For instances, in case the energy density is dominated by one component, it is provided by an equation of state $w = P/\rho$ which relates the energy density to the pressure of the universe. As long as this component is in a given state, w is constant. But in general it is not, for instance for particles that are initially relativistic and then become non-relativistic (neutrinos), $w \neq$ constant, or for a scalar field ϕ whose equation of state is not constant, but involves time-derivatives of the field $\dot{\phi}$ and its potential $V(\phi)$. In addition, if one assumes the strong energy condition $w \geq -1/3$ that implies gravitation is attractive, one obtains the Big-Bang model, since when going back into the past, it describes a universe whose temperature and energy density always increase while it contracts until a singularity called the Big-Bang. After the decisive discovery of the Cosmic Microwave Background in 1965 by Wilson and Penzias, the Big-Bang model became the prevailing cosmological paradigm. Indeed, the CMB is a relic of a much hotter and denser state of the universe.

Nevertheless, if the geometry of our universe were to be definitely described by Eq. (1.2), we would never have observed the CMB anisotropies or the large scale structure we do now. These observations can be explained in the framework of the theory of linear perturbations of the Friedmann-Lemaître universe. The idea is that both the CMB anisotropies and the large scale structures originate from tiny quantum fluctuations generated during inflation. Inflation is a period of accelerated expansion of the universe which started 10^{-36} seconds after the Big-Bang. During inflation, these quantum fluctuations are streched to cosmic size and give rise to the largest structures observed today (Fig.1.5 (a)). Inflation also generates the right initial fluctuations that correspond to those observed today in the CMB anisotropies (Fig.1.5 (b)).

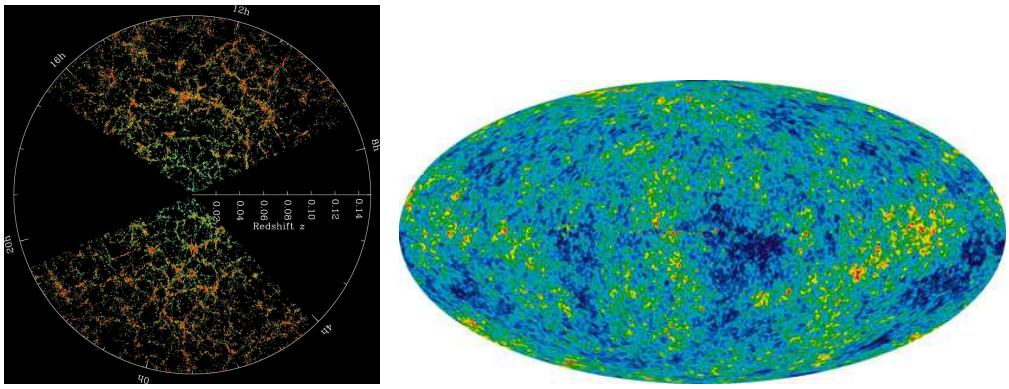

(a) Large scale structures (b) CMB anisotropies

Figure 1.5: On the left panel, a plot of sky coordinates vs. distance for galaxies in the Sloan Digital Sky Survey, and on the right panel, the WMAP7 map of the CMB temperature anisotropies.

However in 1998, the Big-Bang model with radiation and matter only ran into tension with cosmological observations. At this time, two groups of astronomers [105] concluded from supernovae observations that the universe is currently undergoing a phase of accelerated expansion. This surprising discovery brought them the Nobel Prize in Physics 2011. In the context of an isotropic and homogeneous universe filled with ordinary pressureless matter and radiation, the accelerated expansion of the universe has no explanations. Indeed, an accelerating universe requires $\ddot{a} > 0$. But from Eq.(1.4), it follows that this requirement is equivalent to $P < -\frac{\rho}{3}$. Clearly, for ordinary non-relativistic matter or radiation, this is not the case. For the former, we have $P_m = 0$ and for the later, $P_r = \frac{\rho_r}{3}$, meaning that the pressure is either null or positive. Therefore, one can modify the right hand side of Friedmann equations by adding a new component with a negative pressure, called Dark Energy. This is usually achieved by means of a constant term, the cosmological constant Λ, with equation of state $P_\Lambda = -\rho_\Lambda$. It is interesting to note that though it succeeds in describing the accelerated expansion of our universe, we have no fundamental understanding of the cosmological constant.

Another big puzzle in our universe is dark matter. Already in 1933, Zwicky noticed that the amount of visible matter inside the Coma Cluster was too small to explain the velocities of galaxies [129]. Since then, Zwicky's results of missing matter have been confirmed by several observations, including the observations of the motion of stars within

galaxies. Assuming the amount of visible matter and Newtonian gravity still to be valid at these scales shows that the velocity of stars in the outer part of the galaxy is much larger than expected. In order to make theory and observations compatible, one has to postulate more matter than the visible, called for this reason dark matter.

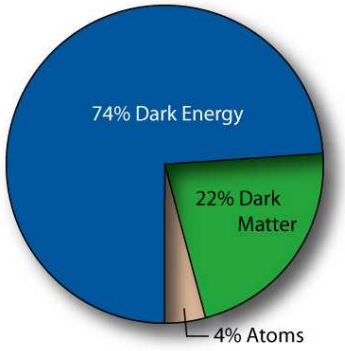

Figure 1.6: Energy budget of the standard model of cosmology

At this stage, all the necessary ingredients of the standard model of cosmology have been introduced. It can be summarized as an isotropic and homogeneous universe whose most important contributions to the current overall energy budget are those of the cosmological constant (74%), cold dark matter (22%) and baryonic matter (4%). The cosmological constant drives the present accelerated expansion. Since this model best fits the observations, it is called the standard model of cosmology or the ΛCDM model in reference to its two main components.

1.3 Overview

In this section, I introduce the subsequent chapters containing the research work of my thesis: given the wide range of topics studied, it is convenient to provide a short overwiev of each of them as well as of the main theoretical concepts. I explain the cosmological background of the problem, the methodology used to tackle the problem and summarize the main results. Finally, I stress on the aspects of the problem that belong to non standard cosmology.

1.3.1 Graviton production in braneworlds

1.3.1.1 Background

String theory is only consistent in spacetime with extra spatial dimensions. In such a spacetime called the bulk, lower dimensional objects called branes may be moving and interacting. In these models, our universe is a 3 (space) +1 (time) dimensional brane moving into the bulk. Braneworlds scenarios are particularly well motivated, since they can provide a solution to a problem of particle physics, the hierarchy problem of the huge difference between the Planck scale and the electroweak scale. In the simplest scenarios, only the gravitons can propagate in the entire bulk and the standard model particles

are confined to our brane. Among all the available models, we consider a 5-dimensional bulk with two branes in it. The bulk has the geometry of an anti-de Sitter space, AdS_5, a maximally symmetric, vacuum solution of Einstein's equations with a negative cosmological constant. This geometry is decribed by the following metric

$$ds^2 = g_{AB}dx^A dx^B = \frac{L^2}{y^2}\left[-dt^2 + \delta_{ij}dx^i dx^j + dy^2\right] \ , \tag{1.5}$$

where $i, j = 1, 2, 3$, L is the AdS_5 curvature radius and y denotes the extra spatial dimension. The first brane is at rest and the second, our universe moves along the y-direction towards and backwards the first static brane. The motion of our brane in the bulk induces its contraction and expansion, depending on the direction of motion. Indeed, the metric (1.5) induces a Friedmann-Robertson-Walker geometry on our brane

$$ds^2 = a^2(\eta)\left[-\mathrm{d}\eta^2 + \delta_{ij}dx^i dx^j\right] \ , \tag{1.6}$$

where η is the conformal time on the brane. The scale factor $a(\eta)$ is given by the brane position $y_b(t)$ in the bulk

$$a(\eta) = \frac{L}{y_b(t)} \tag{1.7}$$

When our brane moves towards the static brane located at y_s ($0 \leq y_b(t) \leq y_s$), the scale factor decreases and our universe is in a contraction phase. When our brane moves in the opposite direction, the scale factor increases and our universe undergoes an expansion phase. For this reason, this model of braneworlds may also be called bouncing braneworlds. The fact that our universe moves in the bulk represents a spacetime with moving boundaries that can lead to particle creation, in this case graviton, via the dynamical Casimir effect, mechanism explained in the next paragraph.

1.3.1.2 Methodology

The Casimir effect is a well-know effect of quantum field theory. The most typical example involves two uncharged metallic plates in a vacuum. In such a set-up, the vacuum quantum fluctuations produce an attractive force called the Casimir force. Depending on the geometry of the set-up, the Casimir force can also be repulsive. If now the geometry of the system varies in time, for instance if one plate is allowed to move, particle creation (photon) occurs. In the formalism of the second quantization, a state denotes one particular configuration of the field. The second important actors are the operators acting on the states. We adopt the Heisenberg picture in which the operators are time-dependent, but the state vectors are time-independent. The lowest energy state is called the vacuum state and is usually written $|0\rangle$. Moreover, in this formalism, a creation operator $\hat{a}^\dagger$ acts on given state $|n\rangle$ by creating a particle

$$\hat{a}^\dagger|n\rangle = \sqrt{n+1}|n+1\rangle \qquad \hat{a}^\dagger|0\rangle = |1\rangle \tag{1.8}$$

where n is the number of particle, and the annihilation operator $\hat{a}$ acts by annihilating a particle

$$\hat{a}|n\rangle = \sqrt{n}|n-1\rangle \qquad \hat{a}|0\rangle = 0. \tag{1.9}$$

The operator $\hat{N} = \hat{a}^\dagger \hat{a}$ counts the number of particle of a given state

$$\hat{N}|n\rangle = n|n\rangle. \tag{1.10}$$

If we denote by a subscript *in* and *out* the configuration of the field in the vacua before and after the motion of the plate, we have

$$\hat{N}_{in}|0\rangle_{in} = 0 \tag{1.11}$$

but

$$\hat{N}_{out}|0\rangle_{in} \neq 0, \tag{1.12}$$

which means that with respect to the initial vacuum state, particles have been created. The existence of an attractive force between the plates has been theorized by Casimir in the forties. The dynamical Casimir effect leading to particle creation has been theoretically predicted in the seventies [49, 87] and has only been recently observed experimentally [123]. In our work, we apply the dynamical Casimir effect formalism to the braneworld scenario. Instead of having an electromagnetic field, two plates and photon creation, we consider gravitons propagating in the bulk, two branes and graviton production.

1.3.1.3 Results

In previous papers [38, 109], it has been shown that the energy density ρ_0 of the massless zero mode gravitons scales like radiation $\rho_0 \propto a^{-4}$ and the energy density of the massive Kaluza-Klein modes ρ_{KK} scales like stiff matter $\rho_{KK} \propto a^{-6}$ on the brane. The scaling of the Kaluza-Klein modes is a bit surprising, since one would naively expect $\rho_{KK} \propto a^{-3}$, i.e. the same behaviour as pressure-less matter. This first analysis of the problem was limited to a brane moving in the bulk at small velocity $v_{max} \lesssim 0.1$ (speed of light $c = 1$). We developed a new approach valid for arbitrary brane velocities. We proved the consistency between our method and the approximated one at low velocities and we derived numerical solutions for the final number of gravitons depending on their mass and on the brane velocity.

In the first chapter, we report results of a first approach where the velocity v_b of the moving brane is small compared to the speed of light. This assumption leads to Neumann boundary conditions, where a term linear in the velocity v_b has been neglected with respect to the original junction conditions. In the second chapter, we present a fully consistent treatment of the junction conditions, valid for arbitrary velocity of the brane. Brane cosmology differs from standard cosmology by the number of spatial dimensions. Interactions of our $3 + 1$ dimensional brane with the bulk or other branes can influence the physical processes in our universe. It can then create new effects that do not exist in standard cosmology, and describes thus some aspects of non standard cosmology.

1.3.2 Model-independent constraints from the CMB

1.3.2.1 Background

In the very hot early universe, no hydrogen could be formed without being immediately dissociated by high energy photons. But as the universe expands, it cools down until a

given temperature T_{dec} when this reaction stops. This moment is called the photon decoupling, and after decoupling, thermal photons freely stream through the universe without any further scattering. The generic name for this radiation is the Cosmic Microwave Background (CMB). The CMB has an almost perfect black-body spectrum at $T = 2.725\,K$ with tiny fluctuations of the order $10^{-5}\,K$. The study of its angular temperature fluctuations gives us a direct picture of the distribution of radiation and energy when the universe was a hundred thousand times younger than today. Since the CMB anisotropies are a function on the sphere, they can be expanded in spherical harmonics

$$\frac{\Delta T}{T_0}(\mathbf{n}) = \frac{T(\mathbf{n}) - T_0}{T_0} = \sum_{l=0}^{\infty} \sum_{m=-l}^{m=l} a_{lm} Y_{lm}(\mathbf{n}). \tag{1.13}$$

where $T(\mathbf{n})$ is the temperature measured in the direction $\mathbf{n}$ and T_0 is the mean temperature in the sky. The CMB power spectrum C_l is the average of the coefficients a_{lm}

$$C_l = \langle a_{lm}^* a_{lm} \rangle. \tag{1.14}$$

The two main physical effects on the CMB are the physics at decoupling and the evolution of the universe after decoupling. The former is well understood by means of atomic physics, general relativity and perturbation theory, but the latter, specially the late time evolution of the universe, is very controversial, since it deviates from the predictions of a linearly perturbed Friedmann-Lemaître universe with radiation and matter only. This difference is still poorly understood, and a wide range of models are studied to solve this so-called "Dark Energy" problem. In this work, we are not interested in any particular model describing the evolution of the universe at late times. But since we do not know which of the models is correct, we decided to perform an analysis of the CMB which is as independent of the details of late-time cosmology as possible. This has the advantage of making clear the constraints that all models of late-time cosmology have to satisfy in order to agree with CMB observations.

1.3.2.2 Methodology

The standard model of cosmology, the ΛCDM model, has six parameters that can be contrained using different cosmological observations:

- ω_b is the physical density of baryonic matter
- ω_c is the physical density of dark matter
- n_s is the spectral index of the primordial spectrum of fluctuations
- A_s is the amplitude of the primordial spectrum of fluctuations
- Ω_Λ is the cosmological constant density parameter
- τ is the optical depth

Ω_Λ and τ are related to the late-time evolution of the universe, and have therefore to be excluded from our analysis. The observed amplitude of CMB perturbations is determined by A_s and late-time physics like reionization and accelerated expansion. Without a model for the late-time universe, it is not posible to disentangle theses effects. Therefore, we treat

A_s as a nuisance parameter. Finally, for our purposes, it is useful to introduce the scale parameter S, defined as the ratio of the angular diameter distance to the last scattering surface to the value of this distance in the simplest cosmological model.

$$S \equiv \frac{D_A(z_*)}{D_{A,EdS}(z_*)} \tag{1.15}$$

where $D_{A,EdS}$ is the angular diameter distance in the Einstein-de Sitter (EdS) universe (the matter-dominated spatially flat Friedmann-Lemaître model) and z_* is the redshift to the last scattering surface. The shift parameter S contains the information about the distance to the last scattering surface. Finally, since we want to perform a model independent data analysis of the CMB, we have to exclude the multipoles that have been affected by the late time evolution of the universe. This concerns the last wavelengths that entered the sound horizon or equivalently the lowest multipoles. Excluding the multipoles $l \leq 40$, we have numerically shown that the effect of reionization on the remaining multipoles is less than 2%, and the effect of the cosmological constant or any other model for Dark Energy is mainly contained in the fourty lowest multipoles, since it modifies the CMB anisotropies power spectrum via the late integrated Sachs-Wolfe (LISW) effect. The LISW effect happened recently in the history of the universe, as Dark Energy started to drive its expansion. During the matter-dominated era, strong large-scale potential wells remain constant, such that there is no integrated effect over the time it takes a photon to travel through them. The energy gained by the photon when falling into the well is exactly lost when escaping it. Once Dark Energy starts to dominate, the potential wells decay with time, and thus, lead some observable signatures on the CMB anisotropies.

1.3.2.3 Results

We have derived model-independent limits on the physical density of baryonic matter ω_b, the physical density of cold dark matter ω_c and the spectral index n_s, and the scale parameter S or equivalently the angular diameter distance to the last scattering surface $D_A(z_*)$. The interest of our results is their validity for most models of late-time cosmology, whether they include dark energy, modified gravity, a local void or backreaction.

The standard model of cosmology with the cosmological constant playing the role of Dark Energy is one among many propositions to explain the late time accelerated expansion of our universe. Since our analysis of the CMB does not depend on the late-time cosmology, it puts constraints on some aspects of non standard cosmology.

1.3.3 A large scale coherent magnetic field and free streaming particles

1.3.3.1 Background

In addition to a perfect fluid, we suppose that our universe is permeated by a large scale coherent magnetic field. By large scale coherence, we mean that the field is coherent over a Hubble scale, and it can therefore be treated as a homogeneous magnetic field. This magnetic field has a direction and acts thus as a source of anisotropic expansion of our universe, which would then in turn leave imprints on the Cosmic Microwave Background. The anisotropic geometry induced by the magnetic field leads to a plane-symmetric Bianchi

I model with metric

$$ds^2 \;=\; -dt^2 + a_\perp^2(t)(dx^2+dy^2) + a_\parallel^2(t)\,dz^2\,, \tag{1.16}$$

where the scale factor $a_\perp(t)$ governs the expansion in the $x-$ and $y-$ directions and the scale factor $a_\parallel(t)$ in the z-direction, for a magnetic field $\mathbf{B} = B\boldsymbol{e}_z$ in the z-direction. Indeed, the contribution to the stress-energy tensor from the magnetic field is intrinsically anisotropic

$$P_{B,\perp} = -P_{B,\parallel} = \rho_B\,, \tag{1.17}$$

with $P_{B,\perp,\parallel}$ the pressure of the magnetic field in the directions perpendicular respectively parallel to its direction, and ρ_B is its energy density. In principle, the study of CMB anisotropies puts constraints on the intensity of the magnetic field. However, when free streaming relativistic particles are present, their anisotropic pressure counteracts the anisotropic expansion sourced by the magnetic field and therefore, they tend to cancel possible signatures in the CMB. We found that they effectively reduce them by several orders of magnitude. In our universe, we know that neutrinos behave like relativistic free streaming particles and may therefore play the role of isotropizers in our scenario.

1.3.3.2 Methodology

The observations show that the expansion of the universe is nearly isotropic. Motivated by these observations, we assume that the scale factors difference always remains small

$$\frac{a_\perp - a_\parallel}{a} \equiv \delta \ll 1\,. \qquad a \equiv a_\perp^{2/3} a_\parallel^{1/3}\,, \tag{1.18}$$

We can then expand all the relevant physical quantities up to the first order in δ. Three different periods of the thermal history of our universe can then be distinguished. First, at very high temperature during the radiation dominated era, the neutrinos are still very tightly coupled to the baryons. Their caracteristic free streaming length is very small, and their pressure remains isotropic. In this case, nothing prevents the anisotropic stress of the homogeneous magnetic field to source the anisotropic expansion of the universe. But then, as the universe expands, it also cools down and reaches the temperature of neutrinos decoupling, $T^\nu_{dec} \sim 1.4\,\mathrm{MeV}$, when they stop interacting with baryons and begin to free-stream. During this second phase, the neutrinos are sill relativistic, and they develop an anisotropic stress that counteracts the anisotropic stress of the magnetic field. In our case, for the neutrinos and the magnetic field, the anisotropic stress is actually the pressure difference and we have

$$P_{\nu,\perp} - P_{\nu,\parallel} = -\left(P_{B,\perp} - P_{B,\parallel}\right) \tag{1.19}$$

where the subscripts ν and B respectively stand for neutrinos and magnetic field. Eq.(1.19) shows that as long as the temperature T of the universe is smaller than the neutrino decoupling temperature and larger than the neutrino mass $m_\nu < T < T^\nu_{dec}$, both anisotropic stresses cancel and δ is then constant, since the expansion is isotropic. The start of the third phase depends on the neutrino mass m_ν. Once the temperature of the universe drops below the neutrino mass scale, they become non-relativistic, their pressure vanishes very fast and the anisotropic expansion driven by the magnetic field restarts. To understand our results, one has also to take into acount that photon decoupling occurs much later than neutrino decoupling.

1.3.3.3 Results

The temperature of photon decoupling is $T^{\gamma}_{dec} \sim 0.3\,\mathrm{eV}$. Current bounds [95, 2] on the sum of the mass eigenstate indicate that $\sum_{\nu} m_{\nu} < 0.36\,\mathrm{eV}$. Qualitatively, two cases correponding to two different results can be distinguished. In the first case, the neutrinos become non-relativistic before photon decoupling. Then the isotropization effect of relativistic free streaming particles will not be present, and the CMB will be affected by the anisotropic expansion sourced by the magnetic field. In the second case, the neutrinos become non-relativistic after photon decoupling. Here, the imprints on the CMB of the anisotropic expansion will be significantly reduced because the neutrinos maintain expansion isotropic until they become non-relativistic.

Since the standard model of cosmology assumes isotropic expansion, the study of a model whose geometry is described by the metric (1.16) covers aspects of non standard cosmology.

1.3.4 Back reaction from walls

1.3.4.1 Background

The present universe seems to be in an accelerating phase and dark energy is the name we give to our poor understanding of this phenomenon. Most of the cosmological evidences for this accelerated expansion rely on measurements of distance-redshift relation in a Friedmann universe. The distance-redshift relation is defined in the following way. We call L the luminosity corresponding to the energy emitted per second of a source at redshift z, and let F be its flux, corresponding to the energy received by the observer per second per square centimeter. Then, the luminosity distance to the source is

$$D_L(z) = \left(\frac{L}{4\pi F}\right)^{1/2}. \tag{1.20}$$

The flux F describes how the energy is distributed over a sphere, whose radius encodes the particular geometry of the spacetime. The luminosity distance is thus measured and compared with the predictions of different models. As previously explained, the ΛCDM model assumes that our universe is homogeneous and isotropic, and faces the problem of the cosmological constant. One alternative to this model is Backreaction, which states that inhomogeneities can indeed affect the average expansion rate of the universe and lead to the present acceleration. Backreaction models do not need to introduce some exotic component to the stress energy tensor, but they give up homogeneity. Several models of universes containing only pressure-less matter can be studied. For this project, we choose to investigate universes which are symmetric under translations and rotations in a plane called the y-plane. This geometry is described by the metric

$$ds^2 = -dt^2 + a^2(t,x)dx^2 + b^2(t,x)(dy_1^2 + dy_2^2)\,. \tag{1.21}$$

where we denote the proper time coordinate by t and the spatial coordinates by $\mathbf{x} = (x, y_1, y_2)$. The universe is then filled with walls of pressure-less matter separated by under dense regions. Of interest to us is how light propagates through these walls, and whether the corresponding luminosity distance can reproduce the observations.

1.3.4.2 Methodology

The existence in our universe of huge inhomogeneities is a well-known fact. Their typical size is around 80 Mpc. On the one hand, it is possible to impose on our model such inhomogeneities of matter, and to predict what would be the observed luminosity distance. We have tried this approach for several matter density profiles. On the other hand, it is also possible to require that our model mimics Dark Energy, i.e. reproduces the observed luminositiy distance, and to see the size of the inhomogeneities necessary to satisfy this condition.
For both approaches, we use the existing analytical solutions to the Einstein equations for this geometry with pressure-less matter. In order to know how light rays propagate through spacetime, we then solve numerically the geodesic equations and finally calculate the luminosity distance as a function of the redshift of the source.

1.3.4.3 Results

Based on the two different approaches described in the precedent paragraph, we have obtained the following results. First, requiring the size of the underdensities to be of the order of the observed voids and taking into account two different density profiles, we have clearly found that we cannot mimic acceleration by a series of dense walls of reasonable overdensities and spacings in agreement with observations. If an effect were to be observed, it would rely on a significant change in the photon energy on its path. But because the photon goes through many walls on its path, the energy gained when falling into a gravitational well is lost when escaping from it. The effect on the luminosity distance is therefore minute, and since this effect is quite general, we think that our conclusions can be extended to other density profiles. After having shown that realistic wall models cannot reproduce the observed luminosity distance, we have determined the density profile which can mimic it. We have found that an underdensity of the size of the order of the Hubble distance is necessary to mimic ΛCDM with our walls. Such underdensities do not seem to exist in our universe. Thus, our study tends to disfavour Backreaction as a sound alternative to standard cosmology.

Chapter 2

Graviton production in brane worlds by the dynamical Casimir effect

AIP Conf.Proc.**1122:39-54,2009**

Graviton production in brane worlds by the dynamical Casimir effect

Ruth Durrer, Marcus Ruser, Marc Vonlanthen and Peter Wittwer

If our Universe is a $3+1$ brane in a warped $4+1$ dimensional bulk so that its expansion can be understood as the motion of the brane in the bulk, the time dependence of the boundary conditions for arbitrary bulk fields can lead to particle creation via the dynamical Casimir effect. In this talk I report results for the simplest such scenario, when the only particle in the bulk is the graviton and the bulk is the 5 dimensional anti-de Sitter spacetime.

PACS numbers 98.80.Cq, 04.50.-h, 04.30.-w

2.1 Introduction

The idea that our Universe be a $3+1$ dimensional membrane in a higher dimensional 'bulk' spacetime has opened new exciting prospects for cosmology, for reviews see [83, 35]. In the simplest braneworlds motivated by string theory, the standard model particles are confined to the brane and only the graviton can propagate in the bulk. Of particular interest is the Randall-Sundrum (RS) model [97, 98], where the bulk is 5-dimensional anti-de Sitter space, AdS_5. If the so called RS fine tuning condition is satisfied, it can be shown that gravity on the brane 'looks 4-dimensional' at low energies.

Within this model, cosmological evolution can be interpreted as the motion of the physical brane, i.e. our Universe, through the 5d bulk. Such a time-dependent boundary does in general lead to particle production via the dynamical Casimir effect [13].

Of course one can always choose coordinates with respect to which the brane is at rest, e.g. Gaussian normal coordinates. But then usually (except in the case of de Sitter expansion on the brane [53]), the perturbation equation describing the evolution of gravitons is not separable and can be treated only with numerical simulations [64, 71, 113]. Furthermore, in a time-dependent bulk a mode decomposition is in general ambiguous and one cannot split the field in a zero mode and Kaluza-Klein (KK) modes in a unique way.

Based on the picture of a moving brane in AdS_5, we have studied graviton production in an ekpyrotic type scenario [63] where our Universe first approaches a second static brane. After a 'collision' the physical brane reverses direction and moves away from the static brane, see Fig. 2.1. For an observer on the brane, the first phase corresponds to a contracting Universe and the collision represents the 'Big Bang' after which the Universe starts expanding.

Here I report on the results which we have obtained in our previous papers [38, 109, 110]. We have found that the energy density of KK gravitons in AdS_5 scales like stiff matter,

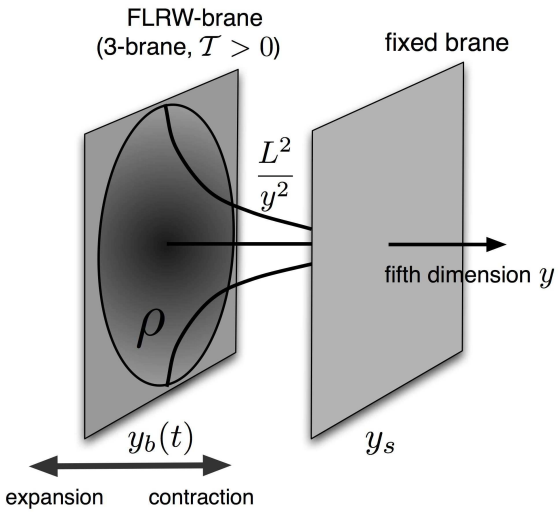

Figure 2.1: Two branes in an AdS_5 spacetime. The physical brane is to the left. While it is approaching the static brane its scale factor is decreasing, the Universe is contracting, and when it moves away from the static brane the Universe is expanding. The AdS curvature radius L (dashed line) and value of the scale factor of the brane metric as function of the extra dimension y (light (blue) line) are also indicated.

$\rho_{\rm KK} \propto a^{-6}$, here a denotes the scale factor defined in Eq. (2.2). Therefore, KK gravitons in AdS_5 cannot represent the dark matter in the Universe. This finding is in contrast with the results of Ref. [86] and we comment on this below. We have also found that in the early Universe the back reaction from KK gravitons on the bulk geometry is likely to be important.

Finally, we have derived a limit for the maximal brane velocity, the bounce velocity, $v_b \lesssim 0.2$ in order not to over-produce zero-mode (i.e. 4d) gravitons, the energy density of which is constrained by the nucleosynthesis bound. We have calculated the spectra of both, the zero-mode and the KK gravitons. In Refs. [38, 109] we have, however, neglected a term linear in the brane velocity v in the boundary conditions. In our latest work, Ref. [110] we derived a method which includes this term and allows to treat the problem without any low velocity approximation. We have shown that the low velocity results previously obtained are not modified.

The remainder of this paper is organized as follows. In the next section we present the basic equations for the evolution of tensor perturbations (gravitons) and we explain why it is not straight forward to include the velocity term of the boundary condition. In Section 3 we quantize the system. In Section 4 we discuss our results and in Section 5 we conclude.

2.2 A moving brane in AdS$_5$

2.2.1 The background

In Poincaré coordinates $(x^A) = (t, \mathbf{x}, y)$ with $\mathbf{x} = (x^1, x^2, x^3)$ and $A = 0, ..., 4$, the AdS$_5$ (bulk) metric is given by

$$ds^2 = g_{AB}dx^A dx^B = \frac{L^2}{y^2}\left[-dt^2 + \delta_{ij}dx^i dx^j + dy^2\right] , \tag{2.1}$$

where $i, j = 1, 2, 3$ and L is the AdS$_5$ curvature radius which is related to the bulk cosmological constant by the 5d Einstein equation, $-\Lambda = 6/L^2$. The physical brane representing our (spatially flat) Universe is located at some time dependent position $y = y_b(t)$ in the bulk, and the metric induced on the brane is the Friedman-Robertson-Walker metric,

$$ds^2 = a^2(\eta)\left[-\mathrm{d}\eta^2 + \delta_{ij}dx^i dx^j\right] , \tag{2.2}$$

with scale factor $a(\eta)$ which is given by the brane position,

$$a(\eta) = \frac{L}{y_b(t)} . \tag{2.3}$$

The conformal time η of an observer on the brane, is related to the bulk time t via

$$d\eta = \sqrt{1 - v^2}dt \equiv \gamma^{-1}dt . \tag{2.4}$$

Here we have introduced the brane velocity

$$v \equiv \frac{dy_b}{dt} = -\frac{LH}{\sqrt{1 + L^2H^2}} \quad \text{and} \quad \gamma = \frac{1}{\sqrt{1 - v^2}} . \tag{2.5}$$

H is the usual Hubble parameter,

$$H \equiv \frac{1}{a^2}\frac{\partial a}{\partial \eta} \equiv a^{-1}\mathcal{H} = -L^{-1}\gamma v . \tag{2.6}$$

The brane dynamics, as a result of the second junction condition, is determined by the modified Friedmann equation [83]

$$H^2 = \frac{\kappa_4\rho}{3}\left(1 + \frac{\rho}{2\mathcal{T}}\right) \tag{2.7}$$

where $\mathcal{T}$ is the brane tension, ρ the energy density on the brane, and we assume the RS fine tuning condition [97]

$$\frac{\kappa_5^2\mathcal{T}^2}{12} = \frac{3}{L^2} , \qquad \text{and} \qquad \kappa_4 \equiv 8\pi G_4 \equiv \frac{\kappa_5^2\mathcal{T}}{6} . \tag{2.8}$$

We define the string and Planck scales by

$$\kappa_5 = \frac{1}{M_5^3} = L_s^3 , \qquad \kappa_4 = \frac{1}{M_{\mathrm{Pl}}^2} = L_{\mathrm{Pl}}^2 . \tag{2.9}$$

Note that the RS fine-tuning condition is equivalent to

$$\kappa_5 = \kappa_4 L \quad \text{or} \quad \frac{L_s}{L} = \frac{L_{\rm Pl}^2}{L_s^2}. \tag{2.10}$$

2.2.2 Tensor perturbations

We now consider 3d tensor perturbations $h_{ij}(t, \mathbf{x}, y)$ of the spatial three-dimensional geometry on this background. The perturbed bulk metric reads

$$ds^2 = \frac{L^2}{y^2}\left[-dt^2 + (\delta_{ij} + 2h_{ij})dx^i dx^j + dy^2\right] \ . \tag{2.11}$$

Tensor modes satisfy the traceless and transverse conditions, $h^i_i = \partial_i h^i_j = 0$. These conditions imply that h_{ij} has only two independent degrees of freedom, the two polarization states $\bullet = \times, +$. We decompose h_{ij} into spatial Fourier modes,

$$h_{ij}(t, \mathbf{x}, y) = \int \frac{d^3k}{(2\pi)^{3/2}} \sum_{\bullet=+,\times} e^{i\mathbf{k}\cdot\mathbf{x}} e^{\bullet}_{ij}(\mathbf{k}) h_\bullet(t, y; \mathbf{k}) \ , \tag{2.12}$$

where $e^{\bullet}_{ij}(\mathbf{k})$ are unitary constant transverse-traceless polarization tensors which form a basis of the two polarization states $\bullet = \times, +$. Since we assume parity symmetry, we shall neglect in the following the distinction between the two graviton polarizations and consider only one of them. We then have to multiply the final results for e.g. particle number or energy density by a factor of two to account for both polarizations.

The perturbed Einstein equations and the second junction condition lead to the following boundary value problem

$$\left[\partial_t^2 + k^2 - \partial_y^2 + \frac{3}{y}\partial_y\right] h(t, y; \mathbf{k}) = 0 \ \text{ in the bulk}, \quad k^2 = |\mathbf{k}|^2 \, , \tag{2.13}$$

and

$$\gamma\left(v\partial_t + \partial_y\right) h\big|_{y_b(t)} = 0 \ \text{ on the brane} \, . \tag{2.14}$$

We introduce also a second, static brane at position y_s, which requires the additional boundary condition

$$\partial_y h\big|_{y_s} = 0 \ \text{ on the static brane} \, . \tag{2.15}$$

Eq. (2.13) is the Klein-Gordon equation for a minimally coupled massless mode in AdS$_5$, i.e. the operator acting on h is just the Klein-Gordon operator

$$\Box = \frac{1}{\sqrt{-g}}\partial_A\left[\sqrt{-g}g^{AB}\partial_B\right] \ . \tag{2.16}$$

Equation (2.14) is the time-dependent boundary condition (BC) coming from the fact that the moving brane acts like a "moving mirror" for the gravitational perturbations. Only in the rest-frame of the brane do we have pure Neumann BC. In a generic frame we have the Lorentz transformed BC which contains a velocity term $v\partial_t$.

We assume that the brane is filled with a perfect fluid such that there are no anisotropic stress perturbations in the brane energy momentum tensor, i.e. there is no coupling of gravitational waves to matter. If this were the case, the r.h.s. of Eq. (2.14) would not be

zero but a term coupling h_{ij} to the matter on the brane, see Eq. (2.25) of [109].

For the tensor perturbations the gravitational action up to second order in the perturbations reads

$$\mathcal{S}_h = 4\,\frac{L^3}{2\kappa_5}\int dt \int d^3k \int_{y_b(t)}^{y_s} \frac{dy}{y^3}\left[|\partial_t h|^2 - |\partial_y h|^2 - k^2|h|^2\right] . \tag{2.17}$$

One factor of two in the action is due to $\mathbb{Z}_2$ symmetry while a second factor comes from the two polarizations.

2.2.3 Dynamical Casimir effect approach

The wave equation (2.13) itself has no time dependence and simply describes the propagation of free modes. It is the time dependence of the BC (2.14) that sources the non-trivial time-evolution of the perturbations. As it is well known, such a system of a wave equation and time-dependent BC lead, within a quantum mechanical formulation, to particle production from vacuum fluctuations. In the context of the photon field perturbed by a moving mirror this goes under the name "dynamical Casimir effect" [13].

In [109] we have extended a formalism which has been successfully employed for the numerical investigation of photon production in dynamical cavities [106, 107, 108] to the RS braneworld scenario. We have studied graviton production by a moving brane, which we call dynamical Casimir effect for gravitons, for a bouncing braneworld scenario.

However, in order to solve the problem, we have neglected the velocity term in Eq. (2.14). The ansatz

$$h = \sum_\alpha a_\alpha(t) e^{-i\omega_\alpha t}\phi_\alpha(t,y) + \text{h.c.}\ , \quad \omega_\alpha^2 = k^2 + m_\alpha(t)^2$$

then leads to a Sturm–Liouville problem for the instantaneous eigenfunctions $\phi_\alpha(t,y)$ which satisfy

$$\left(-\partial_y^2 + \frac{3}{y}\partial_y\right)\phi_\alpha = m_\alpha^2\phi_\alpha\ . \tag{2.18}$$

The solutions of (2.18) are

$$\phi_0(t) = \frac{y_s y_b(t)}{\sqrt{y_s^2 - y_b^2(t)}}\,, \tag{2.19}$$

$$\begin{aligned} \phi_n(t,y) &= N_n(t) y^2 C_2(m_n(t), y_b(t), y) \qquad \text{with} \\ C_\nu(m,x,y) &= Y_1(mx)J_\nu(my) - J_1(mx)Y_\nu(my)\,. \end{aligned} \tag{2.20}$$

The function ϕ_0 is the zero mode which corresponds to the ordinary $(3+1)$d graviton on the brane while the ϕ_n are the KK modes. The masses m_n are determined by the boundary condition at the static brane, see, e.g. [21] for more details. Since ϕ_α satisfies Neumann boundary conditions, we know that the solutions $(\phi_\alpha)_\alpha$ form a complete orthonormal set of functions on the interval $[y_b(t), y_s]$ normalized by the scalar product

$$(\phi_\alpha, \phi_\beta) \equiv 2\int_{y_b(t)}^{y_s} \frac{dy}{y^3}\phi_\alpha\phi_\beta = \delta_{\alpha\beta}\ .$$

Therefore, any general solution which satisfies Neumann BC can be expanded in these instantaneous eigenfunctions. If we add the term $v\partial_t$ to the boundary condition this feature

is lost, and we can no longer expect to find a complete set of instantaneous eigenfunctions.

However, since the entire effect disappears when the velocity tends to zero, neglecting a term which is first order in the velocity seems not to be consistent. This problem led us to search for another approach which is discussed in Ref. [110] where we transform to a coordinate system where the velocity term disappears identically. There also show that for low velocities $v < 0.3$, say the corrections obtained with this consistent treatment are below a few percent. We therefore ignore it in the following.

2.3 Quantization

2.3.1 Equation of motion

The gravitational wave amplitude $h(t, y; \mathbf{k})$ subject to Neumann boundary conditions can be expanded as

$$h(t, y; \mathbf{k}) = \sqrt{\frac{\kappa_5}{L^3}} \sum_{\alpha=0}^{\infty} q_{\alpha,\mathbf{k}}(t)\phi_\alpha(t, y) \ . \tag{2.21}$$

The coefficients $q_{\alpha,\mathbf{k}}(t)$ are canonical variables describing the time evolution of the perturbations and the factor $\sqrt{\kappa_5/L^3}$ has been introduced in order to render the $q_{\alpha,\mathbf{k}}$'s canonically normalized. For $h(t, y, \mathbf{x})$ to be real, we have to impose the following reality condition on the canonical variables,

$$q^*_{\alpha,\mathbf{k}} = q_{\alpha,-\mathbf{k}} \, . \tag{2.22}$$

One could now insert the expansion (2.21) into the wave equation (2.13), multiply it by $\phi_\beta(t, y)$ and integrate out the $y-$dependence by using the orthonormality to derive the equations of motion for the variables $q_{\alpha,\mathbf{k}}$. However, as we explain in Refs. [109, 110], a Neumann boundary condition at a moving brane is not compatible with a free wave equation. The only consistent way to implement Neumann boundary conditions is therefore to consider the action (2.17) of the perturbations as the starting point to derive the equations of motion for $q_{\alpha,\mathbf{k}}$. Inserting (2.21) into (2.17) leads to the action

$$\begin{aligned} \mathcal{S} \ = \ & \frac{1}{2} \int dt \int d^3k \Big\{ \sum_\alpha \left[|\dot{q}_{\alpha,\mathbf{k}}|^2 - \omega^2_{\alpha,k} |q_{\alpha,\mathbf{k}}|^2 \right] + \\ & \sum_{\alpha\beta} \left[M_{\alpha\beta} \left(q_{\alpha,\mathbf{k}} \dot{q}_{\beta,-\mathbf{k}} + q_{\alpha,-\mathbf{k}} \dot{q}_{\beta,\mathbf{k}} \right) + N_{\alpha\beta} q_{\alpha,\mathbf{k}} q_{\beta,-\mathbf{k}} \right] \Big\} \ . \end{aligned} \tag{2.23}$$

We have introduced the time-dependent frequency of a graviton mode

$$\omega^2_{\alpha,k} = \sqrt{k^2 + m^2_\alpha} \, , \tag{2.24}$$

and the time-dependent coupling matrices

$$M_{\alpha\beta} \ = \ (\partial_t \phi_\alpha, \phi_\beta) \ , \tag{2.25}$$

$$N_{\alpha\beta} \ = \ (\partial_t \phi_\alpha, \partial_t \phi_\beta) = \sum_\gamma M_{\alpha\gamma} M_{\beta\gamma} = (M M^T)_{\alpha\beta} \, , \tag{2.26}$$

which are given explicitely in Ref. [109] (see also [21]). The equations of motion for the

canonical variables are the Euler–Lagrange equations from the action (2.23),

$$\ddot{q}_{\alpha,\mathbf{k}} + \omega_{\alpha,k}^2 q_{\alpha,\mathbf{k}} + \sum_\beta \left[M_{\beta\alpha} - M_{\alpha\beta}\right] \dot{q}_{\beta,\mathbf{k}} + \sum_\beta \left[\dot{M}_{\alpha\beta} - N_{\alpha\beta}\right] q_{\beta,\mathbf{k}} = 0 \ . \tag{2.27}$$

The motion of the brane through the bulk, i.e. the expansion of the universe, is encoded in the time-dependent coupling matrices $M_{\alpha\beta}$ and $N_{\alpha\beta}$. These mode couplings are caused by the time-dependent boundary condition $\partial_y h_\bullet(t,y)|_{y_b} = 0$ which forces the eigenfunctions $\phi_\alpha(t,y)$ to be explicitly time-dependent. In addition, the frequency of the KK modes $\omega_{\alpha,k}$ is also time-dependent since the distance between the two branes changes when the brane is in motion. Both time dependencies can lead to the amplification of tensor perturbations and, within a quantum treatment which is developed below, to graviton production from vacuum.

Because of translational invariance with respect to the directions parallel to the brane, modes with different $\mathbf{k}$ do not couple in (2.27). The three-momentum $\mathbf{k}$ enters the equation of motion for the perturbation only via the frequency $\omega_{\alpha,k}$. Equation (2.27) is similar to the equation describing the time evolution of electromagnetic field modes within a three-dimensional dynamical cavity [107] and may effectively be described by a massive scalar field on a time-dependent interval [108]. For the electromagnetic field, the dynamics of the cavity, or more precisely the motion of one of its walls, leads to photon creation from vacuum fluctuations. This phenomenon is usually referred to as dynamical Casimir effect. Inspired by this, we call the production of gravitons by the moving brane the *dynamical Casimir effect for gravitons*.

2.3.2 Quantization

Asymptotically, i.e. for $t \to \pm\infty$, the physical brane approaches the Cauchy horizon ($y_b \to 0$), moving very slowly. Then, the coupling matrices vanish and the KK masses become constant,

$$\lim_{t\to\pm\infty} M_{\alpha\beta}(t) = 0 \ \ , \ \ \lim_{t\to\pm\infty} m_\alpha(t) = \text{const.} \ \ \forall\alpha,\beta \ \ . \tag{2.28}$$

In this limit, the system (2.27) reduces to an infinite set of uncoupled harmonic oscillators. This allows to introduce an unambiguous and meaningful particle concept, i.e. the notion of (massive) gravitons.

Canonical quantization of the gravity wave amplitude is performed by replacing the canonical variables $q_{\alpha,\mathbf{k}}$ by the corresponding operators $\hat{q}_{\alpha,\mathbf{k}}$

$$\hat{h}(t,y;\mathbf{k}) = \sqrt{\frac{\kappa_5}{L^3}} \sum_\alpha \hat{q}_{\alpha,\mathbf{k}}(t)\phi_\alpha(t,y) \ . \tag{2.29}$$

Adopting the Heisenberg picture to describe the quantum time evolution, it follows that $\hat{q}_{\alpha,\mathbf{k}}$ satisfies the same equation (2.27) as the canonical variable $q_{\alpha,\mathbf{k}}$.

Under the assumptions outlined above, the operator $\hat{q}_{\alpha,\mathbf{k}}$ can be written for very early times, $t < t_{\rm in}$, as

$$\hat{q}_{\alpha,\mathbf{k}}(t < t_{\rm in}) = \frac{1}{\sqrt{2\omega_{\alpha,k}^{\rm in}}} \left[\hat{a}_{\alpha,\mathbf{k}}^{\rm in} e^{-i\,\omega_{\alpha,k}^{\rm in}\,t} + \hat{a}_{\alpha,-\mathbf{k}}^{\rm in\dagger} e^{i\,\omega_{\alpha,k}^{\rm in}\,t}\right] , \tag{2.30}$$

where we have introduced the reference frequency

$$\omega^{\rm in}_{\alpha,k} \equiv \omega_{\alpha,k}(t < t_{\rm in}) \ . \tag{2.31}$$

This expansion ensures that Eq. (2.22) is satisfied. The set of annihilation and creation operators $\{\hat{a}^{\rm in}_{\alpha,\mathbf{k}},\, \hat{a}^{\rm in\dagger}_{\alpha,\mathbf{k}}\}$ corresponding to the notion of gravitons for $t < t_{\rm in}$ is subject to the usual commutation relations

$$\left[\hat{a}^{\rm in}_{\alpha,\mathbf{k}}, \hat{a}^{\rm in\dagger}_{\alpha',\mathbf{k}'}\right] = \delta_{\alpha\alpha'}\delta^{(3)}(\mathbf{k}-\mathbf{k}') \ , \tag{2.32}$$

$$\left[\hat{a}^{\rm in}_{\alpha,\mathbf{k}}, \hat{a}^{\rm in}_{\alpha',\mathbf{k}'}\right] = \left[\hat{a}^{\rm in\dagger}_{\alpha,\mathbf{k}}, \hat{a}^{\rm in\dagger}_{\alpha',\mathbf{k}'}\right] = 0. \tag{2.33}$$

For very late times, $t > t_{\rm out}$, i.e. after the motion of the brane has ceased, the operator $\hat{q}_{\alpha,\mathbf{k}}$ can be expanded in a similar manner,

$$\hat{q}_{\alpha,\mathbf{k}}(t > t_{\rm out}) = \frac{1}{\sqrt{2\omega^{\rm out}_{\alpha,k}}}\left[\hat{a}^{\rm out}_{\alpha,\mathbf{k}} e^{-i\,\omega^{\rm out}_{\alpha,k}\,t} + \hat{a}^{\rm out\,\dagger}_{\alpha,-\mathbf{k}} e^{i\,\omega^{\rm out}_{\alpha,k}\,t}\right] \tag{2.34}$$

with final state frequency

$$\omega^{\rm out}_{\alpha,k} \equiv \omega_{\alpha,k}(t > t_{\rm out}) \ . \tag{2.35}$$

The annihilation and creation operators $\{\hat{a}^{\rm out}_{\alpha,\mathbf{k}}, \hat{a}^{\rm out\,\dagger}_{\alpha,\mathbf{k}}\}$ correspond to a meaningful definition of final state gravitons (they are associated with positive and negative frequency solutions for $t \geq t_{\rm out}$) and satisfy the same commutation relations as the initial state operators[1].

Initial $|0,{\rm in}\rangle \equiv |0, t < t_{\rm in}\rangle$ and final $|0,{\rm out}\rangle \equiv |0, t > t_{\rm out}\rangle$ vacuum states are uniquely defined via [2]

$$\hat{a}^{\rm in}_{\alpha,\mathbf{k}}|0,{\rm in}\rangle = 0 \ , \ \hat{a}^{\rm out}_{\alpha,\mathbf{k}}|0,{\rm out}\rangle = 0 \ , \ \ \forall\ \alpha,\ \mathbf{k} \ . \tag{2.36}$$

The operators counting the number of particles defined with respect to the initial and final vacuum state, respectively, are

$$\hat{N}^{\rm in}_{\alpha,\mathbf{k}} = \hat{a}^{\rm in\,\dagger}_{\alpha,\mathbf{k}}\hat{a}^{\rm in}_{\alpha,\mathbf{k}} \ , \ \ \hat{N}^{\rm out}_{\alpha,\mathbf{k}} = \hat{a}^{\rm out\,\dagger}_{\alpha,\mathbf{k}}\hat{a}^{\rm out}_{\alpha,\mathbf{k}} \ . \tag{2.37}$$

The number of gravitons created during the motion of the brane for each momentum $\mathbf{k}$ and quantum number α is given by the expectation value of the number operator $\hat{N}^{\rm out}_{\alpha,\mathbf{k}}$ of final-state gravitons with respect to the initial vacuum state $|0,{\rm in}\rangle$:

$$\mathcal{N}^{\rm out}_{\alpha,\mathbf{k}} = \langle 0,{\rm in}|\hat{N}^{\rm out}_{\alpha,\mathbf{k}}|0,{\rm in}\rangle. \tag{2.38}$$

If the brane undergoes a non-trivial dynamics between $t_{\rm in} < t < t_{\rm out}$ we have $\hat{a}^{\rm out}_{\alpha,\mathbf{k}}|0,{\rm in}\rangle \neq 0$ in general, i.e. graviton production from vacuum fluctuations takes place.

[1] Of course the brane never really stops moving, but before a certain time $t_{\rm in}$ and after a certain time $t_{\rm out}$ the motion is so slow that no particle production takes place. We have chosen these times sufficiently early (rsp. late) so that the numerical results are independent of their choice.

[2] Note that the notations $|0, t < t_{\rm in}\rangle$ and $|0, t > t_{\rm out}\rangle$ do not mean that the states are time-dependent; states do not evolve in the Heisenberg picture.

2.4 Results

2.4.1 Energy density

For a usual four-dimensional tensor perturbation $h_{\mu\nu}$ on a background metric $g_{\mu\nu}$ an associated effective energy momentum tensor can be defined unambiguously by

$$T_{\mu\nu} = \frac{1}{\kappa_4}\langle h_{\alpha\beta\|\mu} h^{\alpha\beta}{}_{\|\nu}\rangle \ , \tag{2.39}$$

where the bracket stands for averaging over several periods of the wave and "$\|$" denotes the covariant derivative with respect to the unperturbed background metric. The energy density of gravity waves is the 00-component of the effective energy momentum tensor. We shall use the same effective energy momentum tensor to calculate the energy density corresponding to the four-dimensional spin-2 graviton component of the five-dimensional tensor perturbation on the brane, i.e. for the perturbation $h_{ij}(t, \mathbf{x}, y_b)$. For this it is important to remember that in our low energy approach, and in particular at very late times for which we want to calculate the energy density, the conformal time η on the brane is identical to the conformal bulk time t. The energy density of four-dimensional spin-2 gravitons on the brane produced during the brane motion is then given by

$$\rho = \frac{1}{\kappa_4\, a^2}\left\langle\left\langle 0, \mathrm{in}|\dot{\hat{h}}_{ij}(t, \mathbf{x}, y_b)\dot{\hat{h}}^{ij}(t, \mathbf{x}, y_b)|0, \mathrm{in}\right\rangle\right\rangle . \tag{2.40}$$

Here the outer bracket denotes averaging over several oscillations, which we embrace from the very beginning. The factor $1/a^2$ comes from the fact that an over-dot indicates the derivative with respect to conformal time $t \simeq \eta$. The detailed calculation given in Ref. [109] leads to

$$\rho = \frac{2}{a^4}\sum_\alpha \int \frac{d^3k}{(2\pi)^3}\omega_{\alpha,k}\mathcal{N}_{\alpha,k}(t)\mathcal{Y}^2_\alpha(a) \tag{2.41}$$

where again $\mathcal{N}_{\alpha,k}(t)$ is the instantaneous particle number and $\mathcal{Y}_\alpha$ is related to value of the wave function on the brane by

$$\mathcal{Y}_\alpha(a) = \frac{a}{L}\phi_\alpha(t, y_b(t)) .$$

The factor two reflects the two polarizations. At late times, $t > t_{\mathrm{out}}$, after particle creation has ceased, the energy density is

$$\rho = \frac{2}{a^4}\sum_\alpha \int \frac{d^3k}{(2\pi)^3}\omega^{\mathrm{out}}_{\alpha,\mathrm{k}}\, \mathcal{N}^{\mathrm{out}}_{\alpha,\mathbf{k}}\, \mathcal{Y}^2_\alpha(a). \tag{2.42}$$

This expression looks at first sight very similar to a "naive" definition of energy density as integration over momentum space and summation over all quantum numbers α of the energy $\omega^{\mathrm{out}}_{\alpha,\mathrm{k}}\, \mathcal{N}^{\mathrm{out}}_{\alpha,\mathbf{k}}$ of created gravitons. However, the important difference is the appearance of the function $\mathcal{Y}^2_\alpha(a)$ which exhibits a different dependence on the scale factor for the zero mode compared to the KK-modes.

Let us decompose the energy density into zero mode and KK contributions

$$\rho = \rho_0 + \rho_{KK}. \tag{2.43}$$

Evaluating $\mathcal{Y}_0(a)$ one then obtains for the energy density of the massless zero mode

$$\rho_0 = \frac{2}{a^4}\int \frac{d^3k}{(2\pi)^3}\, k\, \mathcal{N}^{\rm out}_{0,\mathbf{k}} \ . \tag{2.44}$$

This is the expected behavior; the energy density of standard four-dimensional gravitons scales like radiation.
In contrast, the energy density of the KK-modes at late times is found to be

$$\rho_{\rm KK} = \frac{L^2}{a^6}\frac{\pi^2}{2}\sum_{n=1}^{\infty}\int \frac{d^3k}{(2\pi)^3}\omega^{\rm out}_{n,k}\, \mathcal{N}^{\rm out}_{n,\mathbf{k}}\, m_n^2 Y_1^2(m_n y_s), \tag{2.45}$$

which decays like $1/a^6$. As the universe expands, the energy density of massive gravitons on the brane is therefore rapidly diluted. The total energy density of gravitational waves in our universe at late times is dominated by the standard four-dimensional graviton (massless zero mode). In the large mass limit, $m_n y_s \gg 1$, $n \gg 1$, the KK-energy density can be approximated by

$$\rho_{\rm KK} \simeq \frac{\pi L^2}{2a^6 y_s}\sum_n \int \frac{d^3k}{(2\pi)^3}\, \mathcal{N}^{\rm out}_{n,\mathbf{k}}\, \omega^{\rm out}_{n,k}\, m_n \ . \tag{2.46}$$

Due to the factor m_n coming from the function $\mathcal{Y}_n^2$, i.e. from the normalization of the functions $\phi_n(t,y)$, in order for the summation over the KK-tower to converge, the number of produced gravitons $\mathcal{N}^{\rm out}_{n,\mathbf{k}}$ has to decrease faster than $1/m_n^3$ for large masses and not just faster than $1/m_n^2$ as one might naively expect.

2.4.2 Escaping of massive gravitons and localization of gravity

As we have shown, the energy density of the KK modes scales, at late times when particle production has ceased, with the expansion of the universe like

$$\rho_{\rm KK} \propto 1/a^6\,, \tag{2.47}$$

i.e. it decays by a factor $1/a^2$ faster than the corresponding expression for the zero mode graviton and behaves effectively like stiff matter. Mathematically, this difference arises from the distinct behavior of the functions $\mathcal{Y}_0(a)$ and $\mathcal{Y}_n(a)$, $n \geq 1$, and is a direct consequence of the warping of the fifth dimension which affects the normalization of the mode functions ϕ_α. But what is the underlying physics? As we shall discuss now, this scaling behavior for the KK particles has indeed a straight forward very appealing physical interpretation.

First, the mass m_n is a comoving mass. The (instantaneous) 'comoving' frequency or energy of a KK graviton is $\omega_{n,k} = \sqrt{k^2 + m_n^2}$, with comoving wave number k. The physical mass of a KK mode measured by an observer on the brane with cosmic time $d\tau = a dt$ is therefore m_n/a, i.e. the KK masses are redshifted with the expansion of the universe. This comes from the fact that m_n is the wave number corresponding to the y-direction with respect to the bulk time t which corresponds to *conformal time* η on the brane and not to physical time. It implies that the energy of KK particles on a moving AdS brane redshifts like that of massless particles. From this alone one would expect the energy density of KK-modes on the brane to decay like $1/a^4$ (see also Appendix D of [54]).

Now, let us define the normalized "wave function" for a graviton

$$\Psi_\alpha(t,y) = \frac{\phi_\alpha(t,y)}{y^{3/2}}\,, \qquad 2\int_{y_b}^{y_s} dy \Psi_\alpha^2(t,y) = 1\,. \tag{2.48}$$

From the expansion of the gravity wave amplitude Eq. (2.21) and the normalization condition it is clear that $\Psi_n^2(t,y)$ gives the probability to find a graviton of mass m_α for a given (fixed) time t at position y in the $\mathbb{Z}_2$-symmetric AdS-bulk.

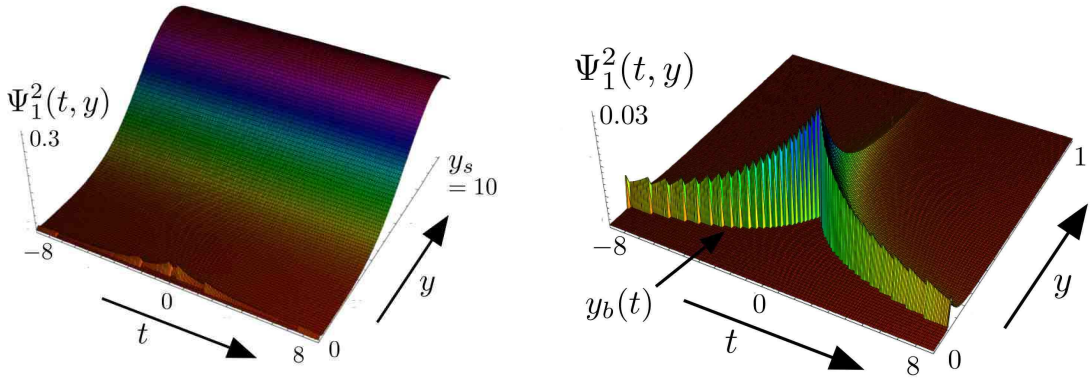

Figure 2.2: Evolution of $\Psi_1^2(t,y) = \phi_1^2(t,y)/y^3$ corresponding to the probability to find the first KK graviton at time t at the position y in the AdS-bulk. The static brane is at $y_s = 10L$ and the maximal brane velocity is given by $v_b = 0.1$. On the right hand panel a zoom into the bulk-region close to the moving brane is shown.

In Fig. 2.2 we plot the evolution of $\Psi_1^2(t,y)$ under the influence of the brane motion with $v_b = 0.1$. For this motion, the physical brane starting at $y_b \to 0$ for $t \to -\infty$ moves towards the static brane, corresponding to a contracting universe. After a bounce, it moves back to the Cauchy horizon, i.e. the universe expands. The second brane is placed at $y_s = 10L$ and y ranges from $y_b(t)$ to y_s. As it is evident from this Figure, Ψ_1^2 is effectively localized close to the static brane, i.e. the weight of the KK-mode wave function lies in the region of less warping, far from the physical brane. Thus the probability to find a KK-mode is larger in the region with less warping. Since the effect of the brane motion on Ψ_1^2 is hardly visible in Fig. 2.2, we also show the behavior of Ψ_1^2 close to the physical brane (right hand panel).

This shows that Ψ_1^2 peaks also at the physical brane but with an amplitude roughly ten times smaller than the amplitude at the static brane. While the brane, coming from $t \to -\infty$, approaches the point of closest encounter, Ψ_1^2 slightly increases and peaks at the bounce $t = 0$ where, as we shall see, the production of KK particles takes place. Afterwards, for $t \to \infty$, when the brane is moving back towards the Cauchy horizon, the amplitude Ψ_1^2 decreases again and so does the probability to find a KK particle at the position of the physical brane, i.e. in our universe. The parameter settings used in Fig. 2.2 are typical parameters which we use in the numerical simulations. However, the effect is illustrated much better if the second brane is closer to the moving brane. In Figure 2.3 (left panel) we show Ψ_1^2 for the same parameters as in Figure 2.2 but now with $y_s = L$. In this case, the probability to find a KK particle on the physical brane is of the same order as in the region close to the second brane during times close to the bounce. However, as the universe

expands, Ψ_1^2 rapidly decreases at the position of the physical brane.

The behavior of the KK-mode wave function suggests the following interpretation: If KK gravitons are created on the brane, or equivalently in our universe, they escape from the brane into the bulk as the brane moves back to the Cauchy horizon, i.e. when the universe undergoes expansion. This is the reason why the power spectrum and the energy density imprinted by the KK-modes on the brane decrease faster with the expansion of the universe than for the massless zero mode.

The zero mode, on the other hand, is localized at the position of the moving brane. The profile of ϕ_0 does not depend on the extra dimension, but the zero-mode wave function Ψ_0 does. Its square is

$$\Psi_0^2(t,y) = \frac{y_s^2 y_b^2}{y_s^2 - y_b^2}\frac{1}{y^3} \to \frac{y_b^2}{y^3} = \left(\frac{L}{a}\right)^2 \frac{1}{y^3} \quad \text{if} \quad y_s \gg y_b \ , \tag{2.49}$$

such that on the brane ($y = y_b$) it behaves as

$$\Psi_0^2(t,y_b) \simeq \frac{a}{L}. \tag{2.50}$$

Equation (2.49) shows that, at any time, the zero mode is localized at the position of the moving brane. For a better illustration we show Eq. (2.49) in Fig. 2.3, right panel for the same parameters as in the left panel. This is the "dynamical analog" of the localization mechanism for four-dimensional gravity discussed in [97, 98].

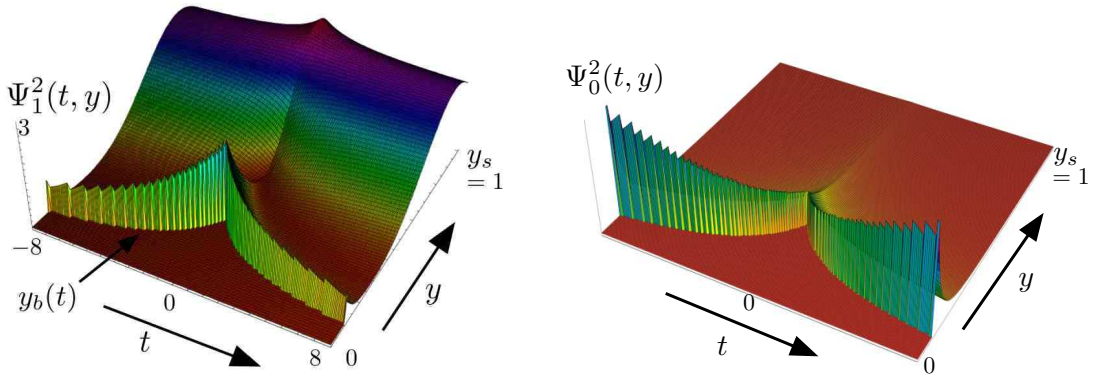

Figure 2.3: Left panel: evolution of $\Psi_1^2(t,y)$ for $y_s = L$ and $v_b = 0.1$. Right panel: localization of four-dimensional gravity on a moving brane. Evolution of $\Psi_0^2(t,y)$. Note the opposite behavior of zero mode and massive mode.

This result is in contradiction with the findings of Ref. [86] where the authors conclude that for an observer on the brane KK gravitons behave like dust with a negative energy density. To arrive at this result, they use Gaussian normal coordinates,

$$ds^2 = -N^2(t,z)dt^2 + Q^2(t,z)a^2(t)\delta_{ij}dx^i dx^j + dz^2 \qquad \text{with} \tag{2.51}$$

$$Q = \cosh(z/L) - \gamma^{-1}\sinh(|z|/L) \quad N = \cosh(z/L) - \left(\gamma^{-1} - \frac{\dot{\gamma}}{\gamma^2 H}\right)\sinh(|z|/L)$$

$$\gamma(t)^{-1} = \sqrt{(HL)^2 + 1} \quad \text{see Eq. (2.5).} \tag{2.52}$$

They then argue that at low velocity, $\gamma \simeq 1$, one may neglect the difference between N and Q so that one obtains the metric

$$ds^2 \simeq dz^2 + e^{-2|z|/L}\left(-dt^2 + a^2(t)\delta_{ij}dx^i dx^j\right) \ .$$

In this metric, the mode equation for the KK modes separates and their time evolution can be determined by simply solving the time part of the equation, see [86]. There is, however, a flaw in this argument: the above approximation is only valid sufficiently close to the brane (which is positioned at $z \equiv 0$ in these coordinates), but far from the brane, when, e.g., $(\gamma^{-1} - 1)\sinh(|z|/L) > \exp(-2|z|/L)$ the above metric is no longer a good approximation and the difference between N and Q does become important. As we have seen, the wave function of the KK gravitons actually is large far away from the brane and the time dependence enters in an important way in the normalization of the mode function which changes its scaling with time.

2.4.3 Spectra

In Fig. 2.4 we show the results of a numerical simulation for three-momentum $k = 0.01/L$, static brane position $y_s = 10L$ and maximal brane velocity $v_b = 0.1$. Depicted is the graviton number for one polarization $\mathcal{N}_{\alpha,k}(t)$ for the zero mode and the first ten KK-modes as well as the evolution of the scale factor $a(t)$ and the position of the physical brane $y_b(t)$.

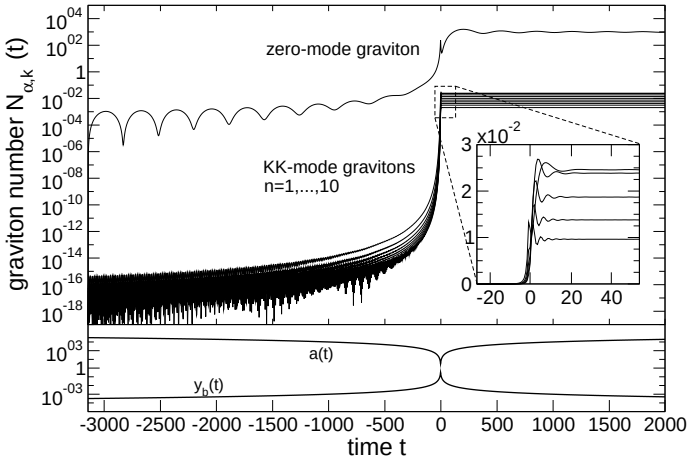

Figure 2.4: Evolution of the graviton number $\mathcal{N}_{\alpha,k}(t)$ for the zero mode (one polarization) and the first ten KK-modes for three-momentum $k = 0.01/L$ and $v_b = 0.1$, $y_s = 10L$.

In Fig. 2.5 we show some KK spectra which we have obtained by integrating the equation of motion numerically. More details about the numerics and results for different values of the parameters can be found in Ref. [109]. In this paper we also derive an analytical approximation for the spectrum which is good for KK masses $m_n < 1$. The numerical calculations are in very good agreement with the analytical estimates, where applicable.

Integrating the zero-mode energy density over frequency with a cutoff given by the strong scale, $k_{\max} = 1/L_s$ leads to the following simple result for the gravitational wave

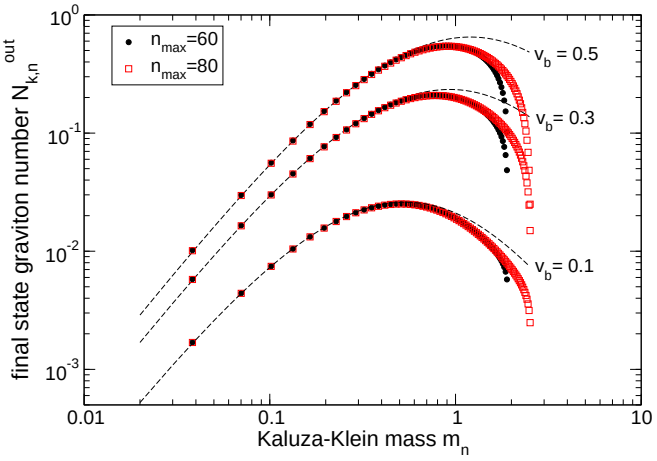

Figure 2.5: Final state KK graviton spectra for $k = 0.001$, $y_s = 100$, different maximal brane velocities v_b at $t_{\rm out} = 400$ for one polarization. The numerical results are compared with the analytical prediction (dashed line).

density parameter [109]

$$\Omega_{h0} \simeq \frac{v_b}{2}\Omega_{\rm rad} \quad \text{so that} \quad v_b \lesssim 0.2\,. \tag{2.53}$$

$\Omega_{\rm rad}$ is the density parameter of the relativistic degrees of freedom at nucleosynthesis, the photon and three species of neutrini. The limit $v_b < 0.2$ follows from the nucleosynthesis constraint which tells us that during nucleosynthesis $\Omega_{\rm rad}$ should not deviate by more than 10% from its standard value [36]. The graviton spectrum is blue with tensor spectral index $n_T = 2$. Its amplitude on Hubble scales is therefore severely suppressed and it leaves no detectable imprint on the cosmic microwave background [36].

Also the energy density of the KK modes grows like k^2 for suffiently large k,

$$\frac{d\rho_{\rm KK}(k)}{d\log k} \propto k^2\,, \qquad k \gtrsim 1$$

and its maximum comes from the cutoff scale $k_{\rm max} = 1/L_s$. We find

$$\rho_{\rm KK} \simeq \frac{\pi^5 v_b^2}{a^6 y_s}\frac{L^2}{L_s^5}\,, \qquad \left(\frac{\rho_{\rm KK}}{\rho_{\rm rad}}\right)_{\rm max} \simeq 100\, v_b^3 \left(\frac{L}{y_s}\right)\left(\frac{L}{L_s}\right)^2\,. \tag{2.54}$$

It is easy to see that low energy requires $y_b < L$ at all times. Therefore, to initiate a bounce, where y_b should be close to y_s, we expect $y_s \lesssim L$. For typical values of the string scale, $L_s \ll L$ and $y_s \sim L$, the above ratio is not small and back reaction of the KK gravitons on the geometry has to be taken into account. The ratio indicated is the one directly after the big bang. As time goes on the KK mode energy density dilutes faster than radiation and rapidly becomes subdominant.

2.5 Conclusions

In braneworld cosmology where expansion is mimicked by a brane moving through a warped higher dimensional spacetime, the brane motion leads to particle creation via the dynamical Casimir effect for all bulk modes. Here we have studied the generation of gravitons.

The KK gravitons scale like stiff matter, $\rho_{\rm KK} \propto 1/a^6$, and can therefore not represent dark matter. In an 'ekpyrotic type' scenario with an AdS_5 bulk, the nucleosynthesis bound on gravitational waves requires $v_b < 0.2$. Furthermore, back reaction of KK gravitons on the evolution of spacetime is most probably not negligible at early times.

In the RSII model where only one brane is present, graviton generation is negligible [21].

2.6 Acknowledgments

RD thanks the Organizers of the Spanish Relativity meeting for inviting her to Salamanca, to assist and talk at this stimulating meeting. This work is supported by the Swiss National Science Foundation. Thanks go also the the Galileo Galilei Institut in Florence where part of the writing was done.

Chapter 3

Graviton production in anti-de Sitter braneworld cosmology: A fully consistent treatment of the boundary condition

PHYSICAL REVIEW D **79**, 083529 (2009)

Graviton production in anti-de Sitter braneworld cosmology: A fully consistent treatment of the boundary condition

Marcus Ruser, Ruth Durrer, Marc Vonlanthen and Peter Wittwer

In recent work by two of us, [Durrer & Ruser, PRL **99**, 071601 (2007); Ruser & Durrer PRD **76**, 104014 (2007)], graviton production due to a moving spacetime boundary (braneworld) in a five dimensional bulk has been considered. In the same way as the presence of a conducting plate modifies the electromagnetic vacuum, the presence of a brane modifies the graviton vacuum. As the brane moves, the time dependence of the resulting boundary condition leads to particle creation via the so called 'dynamical Casimir effect'. In our previous work a term in the boundary condition which is linear in the brane velocity has been neglected. In this work we develop a new approach which overcomes this approximation. We show that the previous results are not modified if the brane velocity is low.

DOI: 10.1103/PhysRevD.79.083529 **PACS** numbers 98.80.Cq, 04.50.+h

3.1 Introduction

The idea that our Universe is a $3+1$ dimensional membrane in a higher dimensional 'bulk' spacetime has opened new exciting prospects for cosmology, for reviews see [83, 35]. In the simplest braneworlds motivated by string theory, the standard model particles are confined to the brane and only the graviton can propagate in the bulk. Of particular interest is the Randall-Sundrum (RS) model [97, 98], where the bulk is 5-dimensional anti-de Sitter space. If the so called RS fine tuning condition is satisfied, it can be shown that gravity on the brane 'looks 4-dimensional' at low energies.

Within this model, cosmological evolution can be interpreted as the motion of the physical brane, i.e. our Universe, through the 5d bulk, acting as a moving boundary for bulk fields, in particular for 5d gravitational perturbations. Such a time-dependent boundary does in general lead to particle production via the dynamical Casimir effect [13, 29].

Of course one can always choose coordinates with respect to which the brane is at rest, e.g. Gaussian normal coordinates. This leads to a time dependent bulk resulting in the same effect, particle production from vacuum due to a time varying background metric. But then, usually (except in the case of de Sitter expansion on the brane [53]), the perturbation equation describing the evolution of gravitons is not separable and can only be treated with numerical simulations [64, 71, 113]. Furthermore, in a time dependent bulk, a mode decomposition is in general ambiguous and one cannot split the field in a zero mode and Kaluza-Klein (KK) modes in a unique way. One of the advantages of the dynamical Casimir effect approach presented in [38, 109] is that it allows for a clear physical interpretation and in addition exhibits an analogy with quantum electrodynamics.

Based on the picture of a moving brane in AdS_5, we have studied graviton production in an ekpyrotic type scenario [63] where our Universe first approaches a second static brane. After a 'collision' the physical brane reverses direction and moves away from the static brane, see Fig. 3.1. For an observer on the brane, the first phase corresponds to a contracting Universe, the collision represents the 'Big Bang' after which the Universe starts expanding (see Fig. 1). We do not model the details of this collision, but assume that the brane distance is still finite at the collision. This corresponds to a cutoff of all the physics which happens at scales smaller than the minimal brane distance when contraction reverses into expansion. In our results we assume this to be of the order of the string scale. We cut off the spectra at the string scale. This is a conservative assumption which signifies that we neglect all the particle creation at energies higher than this scale.

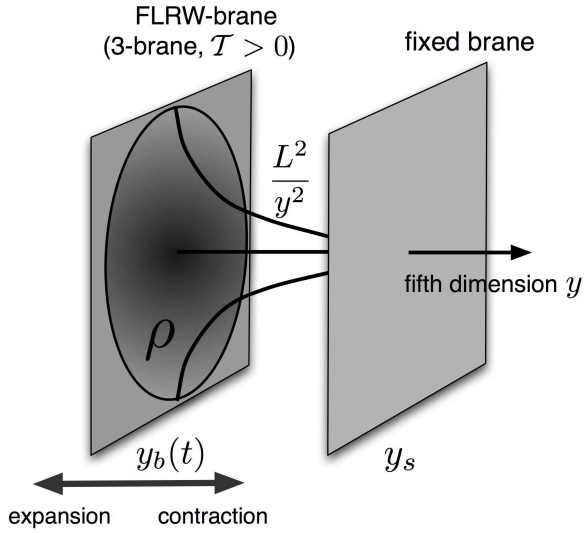

Figure 3.1: Two branes in an AdS_5 spacetime. The physical brane, a Friedmann universe with energy density ρ is on the left. While it is approaching the static brane its scale factor is decreasing, the Universe is contracting, and when it moves away from the static brane the Universe is expanding. L is the AdS curvature radius which is related to the brane tension $\mathcal{T}$ via Eq. (3.8). The value of the scale factor of the brane metric as a function of the extra dimension y is also indicated.

We have obtained the following important results in our previous papers [38, 109]: first of all, the energy density of KK gravitons in AdS_5 scales like stiff matter, $\propto a^{-6}$, where a denotes the scale factor introduced in Eq. (3.2). Therefore, KK gravitons in AdS_5 cannot represent the dark matter in the Universe [1]. We have also seen that in the early Universe the back reaction from KK gravitons on the bulk geometry is likely to be important. Finally, we have derived a limit for the maximal brane velocity, the bounce velocity, $v_{\max} \lesssim 0.2$ in order not to over-produce zero-mode (i.e. 4d) gravitons, the energy density of which is constrained by the nucleosynthesis bound. We have also calculated the spectra of both, the zero-mode and the KK gravitons.

In this previous work we have, however, neglected a term linear in the brane velocity v in the boundary conditions (junction conditions) for the tensor perturbations. Here we derive a method which includes this term and allows to treat the problem without any low

[1] See [39] for a discussion on a contradicting result in the literature.

velocity approximation. We show that the low velocity results previously obtained are not modified. Especially, the nucleosynthesis bound on the maximal brane velocity, $v_{\max} \lesssim 0.2$, remains valid. In a subsequent study we shall investigate graviton production from branes which achieve high velocities in detail [41].

The paper is organized as follows. In the next section we repeat the basic equations for the evolution of tensor perturbations (gravitons) and we explain why it is not straight forward to include the velocity term of the boundary condition. In Section 3.3 we present the new approach and obtain the modified perturbation equations via a coordinate transformation which is such that the velocity term in the boundary condition disappears. We then quantize the system in the new coordinates. In Section 5.3.3 we show numerical results for graviton production at relatively low velocities. In Section 6.4 we conclude. Technical details are deferred to appendices.

3.2 A moving brane in AdS_5

3.2.1 The background

In Poincaré coordinates $(x^A) = (t, \mathbf{x}, y)$ with $\mathbf{x} = (x^1, x^2, x^3)$ and $A = 0, ..., 4$, the AdS_5 (bulk) metric is given by

$$ds^2 = g_{\sigma AB} dx^{\sigma A} dx^{\sigma B} = \frac{L^2}{y^2}\left[-dt^2 + \delta_{ij} dx^i dx^j + dy^2\right] \ , \tag{3.1}$$

where $i, j = 1, 2, 3$ and L is the AdS_5 curvature radius which is related to the bulk cosmological constant by the 5d Einstein equation, $-\Lambda = 6/L^2$. The physical brane representing our (spatially flat) Universe is located at some time dependent position $y = y_b(t)$ in the bulk, and the metric induced on the brane is the Friedman-Robertson-Walker metric

$$ds^2 = a^2(\eta)\left[-\mathrm{d}\eta^2 + \delta_{ij} dx^i dx^j\right] \ , \tag{3.2}$$

with scale factor $a(\eta)$ which is given by the brane position,

$$a(\eta) = \frac{L}{y_b(t)} \ . \tag{3.3}$$

The conformal time η of an observer on the brane, is related to the bulk time t via

$$d\eta = \sqrt{1 - v^2}\, dt \equiv \gamma^{-1} dt \ . \tag{3.4}$$

Here we have introduced the brane velocity

$$v \equiv \frac{dy_b}{dt} = -\frac{LH}{\sqrt{1 + L^2 H^2}} \quad \text{and} \quad \gamma = \frac{1}{\sqrt{1 - v^2}} \ . \tag{3.5}$$

H is the usual Hubble parameter,

$$H \equiv \frac{1}{a^2}\frac{da}{d\eta} \equiv a^{-1}\mathcal{H} = -L^{-1}\gamma v \ . \tag{3.6}$$

Its dynamics, as a result of the second junction condition, is determined by the modified Friedmann equation [83]

$$H^2 = \frac{\kappa_4 \rho}{3}\left(1 + \frac{\rho}{2\mathcal{T}}\right) , \tag{3.7}$$

where $\mathcal{T}$ is the brane tension, ρ the energy density on the brane, and we assume the RS fine tuning condition [97]

$$\frac{\kappa_5^2 \mathcal{T}^2}{12} = \frac{3}{L^2} . \tag{3.8}$$

Furthermore (see [97]),

$$\kappa_4 = 8\pi G_4 = \frac{\kappa_5^2 \mathcal{T}}{6} . \tag{3.9}$$

We define the string and Planck scales by

$$\kappa_5 = \frac{1}{M_5^3} = L_s^3 , \qquad \kappa_4 = \frac{1}{M_{\rm Pl}^2} = L_{\rm Pl}^2 . \tag{3.10}$$

Note that the RS fine-tuning condition is equivalent to

$$\kappa_5 = \kappa_4 L \quad \text{or} \quad \frac{L_s}{L} = \frac{L_{\rm Pl}^2}{L_s^2}. \tag{3.11}$$

Identifying κ_5 with the string scale is based on the assumption that this phenomenological model comes from string theory with one large extra-dimension L, the y direction, while all the other extra-dimensions remain of the order of the string scale, L_s. In this case the 4d observed Planck scale is related to the string scale by Eq. (3.11).

3.2.2 The setup

We consider a radiation dominated brane which moves frome the Cauchy horizon, $y = 0$, at $t = -\infty$ to a position $y_b(0) < y_s$ at $t = 0$, where it bounces and changes its direction. In a radiation dominated universe $\rho \propto a^{-4} \propto y_b(t)^4$. Defining

$$r(t) \equiv \frac{L_{\rm Pl}^2 L^2 \rho}{3} , \tag{3.12}$$

we have $HL = \sqrt{r(1 + r/4)}$. Inserting this in Eq. (3.5) yields

$$\dot{y}_b(t) = v(t) = \pm \frac{\sqrt{r(t)(1 + r(t)/4)}}{1 + r(t)/2} . \tag{3.13}$$

Here the upper sign is chosen for negative times, when y is growing and the universe is contracting while the lower sign corresponds to positive times (expanding universe). At the bounce the maximal velocity, $v(0)$ is reached corresponding to the maximal radiation density given by

$$r(0) = \frac{1}{2}\left(\sqrt{1 + \frac{v^2(0)}{1 - v^2(0)}} - 1\right) \tag{3.14}$$

At $t \neq 0$ the radiation density is

$$r(t) = r(0) \left(\frac{y_b(t)}{y_b(0)} \right)^4 .$$

Note that since the differential equation (3.13) is first order, only one initial condition, e.g $v(0)$ can be chosen. $y_b(0)$ is then determined by the implicit equation

$$y(0) = \int_{-\infty}^{0} v(t) dt \ .$$

(Implicit because it contains $y(0)$ also in the integrand.) Because of this complication it is simpler to choose the initial conditions at some early time, $t_{\rm in} \ll 0$ so that $r(t_{\rm in}) \ll 1$. For $t \lesssim t_{\rm in}$ we can then approximate Eq. (3.13) to

$$\dot{y}_b(t) = \sqrt{r(t)} = \sqrt{r(t_{\rm in})} \frac{y_b^2(t)}{y_b^2(t_{\rm in})}$$

with solution

$$y_b(t) = -\frac{\sqrt{r(t_{\rm in})} t_{\rm in}^2}{t} , \qquad t \leq t_{\rm in} \ . \tag{3.15}$$

The initial condition $(t_{\rm in}, r(t_{\rm in}))$ determines the bounce velocity $v(0)$. In this first paper, where we mainly want to present the method how to transform mixed boundary conditions into Neumann boundary conditions, we simplify the background evolution by assuming $HL \ll 1$ or, equivalently, $r(t) \ll 1$ at all times. This is of course not a good approximation if the bounce velocity is high and we shall treat the brane motion correctly in Ref. [40]. With this (3.13) reduces to

$$\dot{y}_b(t) = \sqrt{r(t)} \propto y_b^2(t) \tag{3.16}$$

at all times. The expression

$$y_b(t) = \frac{L^2}{|t| + t_b} , \tag{3.17}$$

with parameter t_b solves Eq. (3.16) for all $t \neq 0$. Furthermore, it has the correct asymptotics and the bounce velocity is given by

$$v(0) = \frac{L^2}{t_b^2} = \frac{y_b(0)^2}{L^2} \equiv v_b \ .$$

The kink at $t = 0$ can be regularized by replacing $|t|$ by $\sqrt{t^2 + t_c^2}$, where t_c is a small regularization parameter. For $|t| \ll t_c$ this does not affect the dynamics but for $|t| < t_c$ the velocity is reduced and it actually passes through zero at $t = 0$. For graviton frequencies with $\omega t_c \ll 1$ the particle production obtained is independent of this regularization.

3.2.3 Tensor perturbations

Allowing for tensor perturbations $h_{ij}(t, \mathbf{x}, y)$ of the spatial three-dimensional geometry at fixed y, the perturbed bulk metric reads

$$\mathrm{d}s^2 = \frac{L^2}{y^2}\left[-\mathrm{d}t^2 + (\delta_{ij} + 2h_{ij})\mathrm{d}x^i\mathrm{d}x^j + dy^2\right] \ . \tag{3.18}$$

Tensor modes satisfy the traceless and transverse conditions, $h^i_i = \partial_i h^i_j = 0$. These conditions imply that h_{ij} has only two independent degrees of freedom, the two polarization states $\bullet = \times, +$. We decompose h_{ij} into spatial Fourier modes,

$$h_{ij}(t, \boldsymbol{x}, y) = \int \frac{d^3k}{(2\pi)^{3/2}} \sum_{\bullet=+,\times} e^{i\boldsymbol{k}\cdot\boldsymbol{x}} e^{\bullet}_{ij}(\mathbf{k}) h_{\bullet}(t, y; \mathbf{k}) \ , \tag{3.19}$$

where $e^{\bullet}_{ij}(\mathbf{k})$ are unitary constant transverse-traceless polarization tensors which form a basis of the two polarization states $\bullet = \times, +$. Since the problem at hand obeys parity symmetry, we shall neglect in the following the distinction between the two graviton polarizations and consider only one of them. We then have to multiply the final results for e.g. particle number or energy density by a factor of two to account for both polarizations.

Here we only consider 4d gravitational waves. The 5d metric has in principle five different spin-2 polarizations. Two of them are the ones discussed here. In addition there are the two helicities of the so-called gravi-vector and a gravi-scalar (see, e.g. [20]). The gravi-vector and the gravi-scalar obey exactly the same propagation equation as the 4d gravitational waves in the bulk, only their boundary conditions are different. In principle they would add to the results obtained here. In this sense our results are conservative, but since the different polarization states do not interact at the linear level they can be calculated independently. These polarizations are expected to contribute on the same level as the two considered here.

The perturbed Einstein equations and the second junction condition lead to the boundary value problem

$$\left[\partial_t^2 + k^2 - \partial_y^2 + \frac{3}{y}\partial_y\right] h(t, y; \mathbf{k}) = 0 \ \text{ in the bulk} \tag{3.20}$$

and

$$\gamma\left(v\partial_t + \partial_y\right) h\big|_{y_b(t)} = 0 \tag{3.21}$$

describing the time-evolution of the tensor perturbations as the brane moves through the bulk. We introduce also a second, static brane at position y_s, which requires the additional boundary condition

$$\partial_y h\big|_{y_s} = 0 \ . \tag{3.22}$$

Eq. (3.20) is the Klein-Gordon equation for a minimally coupled massless mode in AdS$_5$, i.e. the operator acting on h is just the Klein-Gordon operator

$$\Box = \frac{1}{\sqrt{-g}}\partial_A\left[\sqrt{-g}g^{AB}\partial_B\right] \ . \tag{3.23}$$

Equation (3.21) is a time-dependent boundary condition (BC) coming from the fact that the moving brane acts like a "moving mirror" for the gravitational perturbations.

Only in the rest-frame of the brane do we have pure Neumann BCs. In a generic frame we have the Lorentz transformed BC which contains a velocity term $v\partial_t$.

We assume that the brane is filled with a perfect fluid such that there are no anisotropic stress perturbations in the brane energy momentum tensor, i.e. there is no coupling of gravitational waves to matter. If this were the case, the r.h.s. of Eq. (3.21) would not be zero but a term coupling h_{ij} to the matter on the brane, see Eq. (2.25) of [109], would be present.

The analogy to a moving mirror is actually not just a pictorial one. Transverse-magnetic modes of the electromagnetic field in an ideal, i.e. perfectly conducting, dynamical cavity are subject to the very same boundary condition, see, e.g., [28]. In this context, the boundary condition (3.21) is sometimes referred to as "generalized Neumann" boundary condition, a terminology which we also adopt here. If the cavity is non-perfect, then also in the case of the electromagnetic field, the right hand side of the boundary condition contains a term describing the interaction of the photon field with cavity material, similar to the anisotropic stress perturbations for the gravitational case considered here. This suggests that a brane with no anisotropic stresses could be termed "ideal brane".

For the tensor perturbations the gravitational action up to second order in the perturbations reads

$$\mathcal{S}_h \;=\; 4\,\frac{L^3}{2\kappa_5}\int dt\int d^3k\int_{y_b(t)}^{y_s}\frac{dy}{y^3}\Big[|\partial_t h|^2-|\partial_y h|^2-k^2|h|^2\Big]\;. \tag{3.24}$$

One factor of two in the action is due to $\mathbb{Z}_2$ symmetry while a second factor comes from the two polarizations. As we have shown in [109], the BC's (3.21,3.22) are indeed the only ones for which $\delta\mathcal{S}_h=0$ leads to the free wave equation (3.20). (In principle also Dirichlet BC's, i.e. h vanishing identically on the brane, lead to a wave equation in the bulk. But besides leaving no room for a non-trivial dynamics of the gravitational waves on the brane, these are not obtained from the Einstein equations in the bulk.)

3.2.4 Dynamical Casimir effect approach

The wave equation (3.20) itself is not time dependent and simply describes the propagation of free modes. It is the time dependence of the BC (3.21) that sources the non-trivial time-evolution of the perturbations. As it is well known, such a system of a wave equation and a time-dependent BC leads, within a quantum mechanical formulation, to particle production from vacuum fluctuations. In the context of the photon field perturbed by a moving mirror this goes under the name "dynamical Casimir effect" [13, 29].

In [38, 109] we have extended a formalism which has been successfully employed for the numerical investigation of photon production in dynamical cavities [106, 107, 108] to the RS braneworld scenario. We have studied graviton production by a moving brane, which we call dynamical Casimir effect for gravitons, for a bouncing braneworld scenario.

However, in order to solve the problem, we have neglected the velocity term in the BC (3.21). The ansatz

$$h=\sum_{\alpha=0}^{\infty}a_\alpha(t)e^{-i\omega_{\alpha,k}t}\phi_\alpha(t,y)+\text{h.c.}\;,\quad \omega_{\alpha,k}^2=k^2+m_\alpha^2(t)$$

then leads to a Sturm–Liouville problem for the instantaneous eigenfunctions $\phi_\alpha(t,y)$ con-

sisting of the differential equation

$$\left[-\partial_y^2 + \frac{3}{y}\partial_y\right]\phi_\alpha(t,y) = m_\alpha^2(t)\phi_\alpha(t,y) \tag{3.25}$$

and Neumann BC's at both branes. The solutions of (3.25) respecting Neumann BC's at both branes are

$$\begin{aligned} \phi_0(t) &= \frac{y_s y_b(t)}{\sqrt{y_s^2 - y_b^2(t)}} \qquad (3.26)\\ \phi_n(t,y) &= N_n(t) y^2 C_2(m_n(t), y_b(t), y) \\ &\text{with} \\ C_\nu(m,x,y) &= Y_1(mx)J_\nu(my) - J_1(mx)Y_\nu(my)\,. \qquad (3.27) \end{aligned}$$

They form a complete orthonormal system with respect to the inner product

$$(\phi_\alpha, \phi_\beta) = 2\int_{y_b(t)}^{y_s} \frac{dy}{y^3}\phi_\alpha(t,y)\phi_\beta(t,y) = \delta_{\alpha\beta} \tag{3.28}$$

and the completeness relation implies

$$2\sum_\alpha \phi_\alpha(t,y)\phi_\alpha(t,\tilde{y}) = \delta(y-\tilde{y})y^3\ . \tag{3.29}$$

The factor two accounts for the $\mathbb{Z}_2$ symmetry of the bulk.

In [109] we call ϕ_0 and ϕ_n the zero-mode and Kaluza-Klein (KK)- mode solution, respectively. Here ϕ_0 is the massless mode, $m_0 = 0$, which reduces to the usual $3+1$ - dimensional graviton on the brane. The KK masses $m_n \neq 0$ are determined by the BC at the static brane, see, e.g. [109, 21] for more details.

Due to the completeness and ortho-normality of the functions $\{\phi_\alpha\}$ at any instant in time, any general solution of (3.25) subject to Neumann BC's can be expanded in these instantaneous eigenfunctions. If we add the term $v\partial_t$ to the boundary condition this feature is lost and we can no longer expect to find a complete set of instantaneous eigenfunctions.

However, since the entire effect disappears when the velocity tends to zero, neglecting a term which is first order in the velocity seems not to be a consistent approach. This problem prompted us to search for another description allowing us to treat the boundary condition (3.21) in full.

3.3 Graviton production in a time-dependent bulk with a moving brane

In this section we introduce a new time coordinate which is chosen such that the velocity term in the boundary condition disappears but the mode equation for the instantaneous eigenfunctions still remains the Bessel equation (3.25) with its solution given by Eqs. (3.26) and (3.27). We then extend the formalism of [109] to this case and shall see that for small velocities our previous results are not modified.

3.3.1 A new time coordinate

We introduce new variables $(\tilde{x}^A) = (\tau, \mathbf{x}, z)$ given by

$$\tau(t, y) = t + s(t, y) \ , \quad z = y \ . \tag{3.30}$$

The idea is to find a function $s(t, y)$ such that $\tau \to t$ for all y, when $v \to 0$ and that the junction condition (3.21) reduces to a normal Neumann BC in the new variables. We can then use the mode functions (3.26) and (3.27) to formulate the problem quantum mechanically. One might first be tempted to make a y-dependent Lorentz transformation to the rest frame of the moving brane, but actually this does not lead to Neumann BC's in our case as the transformation induces new terms in the metric. We therefore first leave the function $s(t, y)$ completely general and formulate the conditions which have to be satisfied in order for the new BC's to be purely Neumann.

In $(\tau, \mathbf{x}, z)$-coordinates, the brane trajectory is given by the implicit equation

$$z_b(\tau) = y_b\big[t(\tau, z_b(\tau))\big] \ . \tag{3.31}$$

Once we have specified the function $s(t, y)$, the new brane trajectory $z_b(\tau)$ can be found. This is done numerically since neither $s(t, y)$ nor the inverse $t(\tau, z)$ of (3.30) exist in closed form. As in [109] we restrict ourselves to brane motions where asymptotically, i.e. for $t \to \pm\infty$, the physical brane approaches the Cauchy horizon ($y_b \to 0$), moving very slowly ($v \to 0$).

The new metric given by

$$ds^2 = \tilde{g}_{AB}(\tau, z) d\tilde{x}^A \tilde{x}^B \tag{3.32}$$

is time dependent and contains non-vanishing cross terms $\tilde{g}_{0z}$. The explicit expression is given in (3.57). We now show that the function $s(t, y)$ can be chosen such that the time-derivative term in the boundary condition disappears.

In the coordinates defined in Eq. (3.30), the junction condition (3.21) becomes

$$\begin{aligned} \left[v(t)\frac{\partial \tau}{\partial t} + \frac{\partial \tau}{\partial y}\right] \partial_\tau h(\tau, z) + \partial_z h(\tau, z) &= \\ \left[v(t)\left\{1 + \partial_t s(t, y)\right\} + \partial_y s(t, y)\right] \partial_\tau h(\tau, z) + \partial_z h(\tau, z) &= 0 \quad \text{at } z = z_b(\tau) \ . \end{aligned} \tag{3.33}$$

In order to obtain Neumann boundary conditions, we require that the term in square brackets vanish at $z_b(\tau)$. This leads to the condition

$$-\left.\frac{\partial_y s(t, y)}{1 + \partial_t s(t, y)}\right|_{y = y_b(t)} = v(t) \tag{3.34}$$

for the function $s(t, y)$. Furthermore, we want to maintain the Neumann BC at the static brane $y_s = z_s$. This yields the additional condition for the function $s(t, y)$

$$\partial_y s(t, y)|_{y = y_s} = 0 \ . \tag{3.35}$$

Hence, if we can find a function $s(t, y)$ which satisfies Eqs. (3.34) and (3.35), the junction conditions in the new coordinates reduce to Neumann BC's

$$\partial_z h(\tau, z) = 0 \text{ at } \ z = z_s \ \text{ and } \ z = z_b(\tau) \ . \tag{3.36}$$

To find a suitable function $s(t,y)$ we choose the separation ansatz

$$s(t,y) = f(t)\sigma(y) \tag{3.37}$$

leading to

$$v(t) = -\frac{f(t)\partial_y\sigma\big(y_b(t)\big)}{1+\big(\partial_t f(t)\big)\sigma\big(y_b(t)\big)} \ . \tag{3.38}$$

For the transformation (3.30) to be regular, we have to require $1+\partial_t s(t,y) = 1+\frac{df}{dt}(t)\sigma(y) \neq 0 \ \forall(t,y)$. If we choose σ such that $\partial_y\sigma(y_b(t))$ is bounded from below, $0 < A < \partial_y\sigma\big(y_b(t)\big)$, this ansatz ensures the required asymptotics, $f(t) \to 0$ for $v(t) \to 0$. In addition we need

$$\partial_y\sigma(y)|_{y=y_s} = 0 \ . \tag{3.39}$$

The function $f(t)$ is determined by the differential equation

$$\frac{df(t)}{dt} + \frac{1}{v(t)}\frac{\sigma'(y_b(t))}{\sigma(y_b(t))}f(t) + \frac{1}{\sigma(y_b(t))} = 0 \ . \tag{3.40}$$

A simple choice for $\sigma(y)$ is

$$\sigma(y) = 1 + \frac{1}{\sigma_0}\left(1-\frac{y}{y_s}\right)^2 \ , \quad \sigma_0 = \text{const.}, \ \sigma_0 > 1 \ , \tag{3.41}$$

so that $1 \leq \sigma(y) < 2$. With this, condition (3.35) is automatically satisfied. In addition, we want the brane collision, i.e. the bounce to happen at the fixed time $\tau = 0$. For this we chose the initial condition

$$f(t=0) = 0. \tag{3.42}$$

Since $f(t) \to 0$ for $v(t) \to 0$, the transformation (3.30) satisfies

$$\tau \to t \ \text{ for } \ t \to \pm\infty \ \text{ and } \ \tau(t=0,y) = 0. \tag{3.43}$$

For the first of these equations we use that $v(t) \to 0$ for $t \to \pm\infty$ and the form of the differential equation (3.40).

With (3.38), $f(0) = 0$ implies that the velocity vanishes at the brane, $v(0_-) = v_b = v(0_+) = 0$. Hence the velocity does not jump from a large value v_b to $-v_b$ at the bounce but it evolves very rapidly but smoothly from a high positive value $v_{\max} = v(-\epsilon)$ to a large negative value $-v_{\max} = v(\epsilon)$, $\epsilon > 0$ and small (see Fig. 3.2), like the regularized brane motion proposed in Section 3.2.2. Confirming that the results are independent of the choice of σ_0 is of course a crucial test.

The coordinate transformation maps the problem of a moving brane in a static bulk (3.1) onto the problem of a brane moving according to (3.31) in a time-dependent bulk. At first glance a further complication of the problem. Its benefits, however, will become clear in the next sections. The transformation of the metric is given explicitely in Appendix 3.6.1.

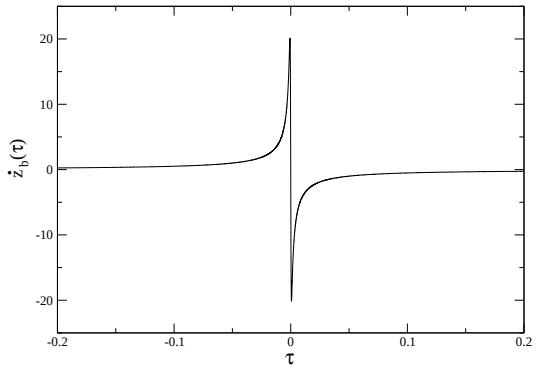

Figure 3.2: The velocity in the new coordinates, $\frac{dz_b}{d\tau}$. Note that this is a coordinate velocity, not a physical quantity. It is easy to check that $\tilde{g}_{AB}\frac{d\tilde{x}_b^A(\tau)}{d\tau}\frac{d\tilde{x}_b^B(\tau)}{d\tau} < 0$ at all times, hence the physical velocity remains timelike also if $\frac{dz_b}{d\tau}$ becomes larger than 1. The maximal velocity for this case is $v_{\max} = 0.3$.

3.3.2 Wave equation

Transforming the Klein-Gordon operator (3.23) to the new coordinates $\tilde{x}^A$, we obtain the wave equation

$$\Big[g_1(\tau,z)\partial_\tau^2 + g_2(\tau,z)\partial_\tau - 2s_2(\tau,z)\partial_z\partial_\tau + \frac{3}{z}\partial_z - \partial_z^2 + k^2\Big]h(\tau,z) = 0\ . \tag{3.44}$$

The definitions of the functions $g_1(\tau,z)$, $g_2(\tau,z)$ and $s_2(\tau,z)$ in terms of the coordinate transformation $s(t,y)$ are given in Appendix 3.6.1. These functions manifest that the bulk itself is now time-dependent and that the metric is no longer diagonal. In Poincaré coordinates the non-triviality of the time-evolution of the perturbations is purely a consequence of the time-dependent junction condition, no time-dependent functions enter the wave equation (3.20). Our coordinate transformation which transforms the generalized Neumann BC into a pure Neumann BC, induces explicite time-dependence in the wave equation itself. What is important, however, is that in (3.44), in the instantaneous rest frame where we neglect time derivatives, we get the operator (3.25) of the original Bessel equation with normalized solutions (3.26) and (3.27). We just have to replace the variables (t,y) by (τ,z).

Writing the action (3.24) in terms of the new coordinates yields

$$\begin{aligned} S &= 4\int d\tau\frac{L^3}{2\kappa_5}\int d^3k\int_{z_b(\tau)}^{z_s}\frac{dz}{z^3}\frac{1}{1+s_1}\times \\ &\Big[g_1|\partial_\tau h|^2 - 2\,s_2\mathrm{Re}\,[(\partial_\tau h)(\partial_z h^*)] - |\partial_z h|^2 + k^2|h|^2\Big]\ . \end{aligned} \tag{3.45}$$

Using the expressions for s_1, s_2, g_1 and g_2 given in Appendix 3.6.1, it is readily shown that

the variation of (3.45), demanding Neumann boundary conditions at the brane positions, leads to the wave equation (3.44).

In the next subsections we take the action (3.45) as the starting point to set up the dynamical Casimir effect formulation of graviton production along the same lines as in [38, 109]. For the physical interpretation of gravitons we are using the fact that asymptotically, when the velocity of the brane goes to zero, the action (3.45) and the wave equation (3.44) reduce to (3.24) and (3.20), respectively. However, in the new coordinates, the junction conditions are always simple Neumann boundary conditions.

3.3.3 Mode decomposition and Hamiltonian

As a basis for a mode decomposition we chose the eigenfunctions $\{\phi_\alpha(\tau, z)\}$ obtained by replacing $(t, y) \to (\tau, z)$ in (3.26) and (3.27). As in [109] we call ϕ_0 and ϕ_i the zero-mode and KK mode solution, respectively. For a brane at rest, and hence $\tau = t$, the solutions ϕ_0 and ϕ_i do indeed represent the physical zero mode and the KK modes, see, e.g. [97]. When the brane is moving, however, these solutions are 'instantaneous modes', provided that the boundary condition is Neumann. This approach is widely employed in the context of the dynamical Casimir effect, see [106, 107, 108] and references therein. Here, working in the (τ, z)-coordinates, the modes (3.26) and (3.27), are proper eigenfunctions respecting the full junction condition which we have reduced to a Neumann BC. At early and late times, i.e. asymptotically $|t| \to \infty$, where the brane velocity tends to zero, these eigenfunctions agree with the physical eigenfunctions corresponding to the zero mode and the KK modes. Since the eigenfunctions $\{\phi_\alpha(\tau, z)\}$ form a complete and orthonormal set. and satisfy the correct junction conditions at both branes, we may decompose the graviton field in ϕ_α's and the pre-factors $q_{\alpha,\mathbf{k}}(\tau)$ become canonical variables which can then be quantized [109],

$$h(\tau, z, \mathbf{k}) = \sqrt{\frac{\kappa_5}{L^3}} \sum_{\alpha=0}^{\infty} q_{\alpha,\mathbf{k}}(\tau)\phi_\alpha(\tau, z) \ . \tag{3.46}$$

Our coordinate transformation and the expansion (3.46) satisfy two major requirements. First, the expansion (3.46) is consistent with the full junction condition (generalized Neumann BC). This overcomes the problem of our approach in [38, 109]. Secondly, even if at arbitrary times the $q_{\alpha,\mathbf{k}}$'s cannot a priori be identified with physical modes, asymptotically, i.e. when the brane moves very slowly, they do represent the independent physical graviton modes. This allows us to introduce a proper notion of particles and vacuum states for asymptotic times. Initial and final vacuum states are then linked by the time-evolution of the $q_{\alpha,\mathbf{k}}$'s exactly as in [109].

We divide the wave equation (3.44) by g_1 in order to isolate the second time derivative and insert the expansion (3.46). Note that $g_1 \to 1$ for $|t| \to \infty$ and for a sufficiently large choice of σ_0, $g_1 > 0$ at all times. As we shall see below, this is also needed for the Hamiltonian to be positive at all times. Inserting the expansion (3.46) into (3.44), multiplying it by ϕ_β and integrating over $2\int_{z_b(\tau)}^{z_s} dz/z^3$ leads to a system of differential equations for the $q_{\alpha,\mathbf{k}}$ which has the same form as the one of Refs. [38, 109],

$$\ddot{q}_{\alpha,\mathbf{k}}(\tau) + \sum_\beta \left[A_{\beta\alpha}(\tau)\dot{q}_{\beta,\mathbf{k}}(\tau) + B_{\beta\alpha}(\tau)q_{\beta,\mathbf{k}}(\tau)\right] = 0 \ . \tag{3.47}$$

The explicite expressions for the time-dependent coupling matrices $A_{\beta\alpha}$ and $B_{\beta\alpha}$ are given

by integrals over the bulk which are rather cumbersome. The details can be found in Appendix 3.6.2. Inserting the expansion (3.46) into the action (3.45) we obtain the Lagrangian $L(\tau)$ in terms of the variables $q_{\alpha,\mathbf{k}}(\tau)$. We can then define the canonical momenta $p_{\alpha,\mathbf{k}} = \partial L/\partial \dot{q}_{\alpha,\mathbf{k}}$ from which, by means of a Legendre transformation, we derive the Hamiltonian

$$\begin{aligned} H(\tau) &= \frac{1}{2}\int d^3k \sum_{\alpha\beta} \Big[p_{\alpha,\mathbf{k}}\, E^{-1}_{\alpha\beta}\, p_{\beta,-\mathbf{k}} + q_{\alpha,\mathbf{k}} \left[\frac{1}{2}\left(\omega^2_{\alpha,k}(\tau) + \omega^2_{\beta,k}(\tau)\right)\delta_{\alpha\beta} + V_{\alpha\beta} \right] q_{\beta,-\mathbf{k}} \\ &- (M_{\beta\alpha} - S_{\beta\alpha})\left[q_{\beta,\mathbf{k}} p_{\alpha,\mathbf{k}} + p_{\alpha,\mathbf{k}} q_{\beta,\mathbf{k}} \right] \Big] \end{aligned} \tag{3.48}$$

The matrices $E^{-1}_{\alpha\beta}$, $V_{\alpha\beta}$, $M_{\beta\alpha}$ and $S_{\beta\alpha}$ are given explicitely in Appendix 3.6.2. It is important to note that $E^{-1}_{\alpha\beta}$ is positive definite as long as $g_1 > 0$ and $1 + s_1 > 0$, which we have to require for our approach to be consistent. In the old treatment, $E_{\alpha\beta}$ was the identity matrix and the couplings $S_{\beta\alpha}$ and $V_{\alpha\beta}$ were missing. They are due to the time-dependence of the bulk spacetime in the new coordinates and therefore originate from the term $v\partial_t$ of the boundary condition in Poincaré coordinates. The coupling matrix $M_{\beta\alpha}$ which is also present in our previous treatment comes from the time dependent Neumann BC. Finally, the time dependence of the bulk volume $z_s - z_b(\tau)$, induces the time dependence in the frequency $\omega_{\alpha,k}$ (squeezing effect, see [109]).

All the coupling matrices tend to zero when $v \to 0$. But we have not been able to show that the new couplings, $E^{-1}_{\alpha\beta} - \delta_{\alpha\beta}$, $V_{\alpha\beta}$ and $S_{\beta\alpha}$ are parametrically smaller than $M_{\beta\alpha}$, e.g. that they are of order v^2. Therefore, the result that the particle production obtained in our previous treatment [38, 109] is not modified if the velocity is sufficiently low is not evident and has to be checked numerically.

3.3.4 Quantum Generation of Gravitons

The quantization procedure goes along the same lines as in [109]. The canonical variables $q_{\alpha,\mathbf{k}}(\tau)$, $p_{\alpha,\mathbf{k}}(\tau)$ and the Hamiltonian $H(\tau)$ are promoted to operators $\hat{q}_{\alpha,\mathbf{k}(\tau)}$, $\hat{p}_{\alpha,\mathbf{k}}(\tau)$ and $\hat{H}(\tau)$, subject to the usual commutation relations. In the Heisenberg picture where the time evolution of an operator $\hat{O}$ is determined by

$$\dot{\hat{O}}(\tau) = i[\hat{H}(\tau), \hat{O}(\tau)] + \left(\frac{\partial \hat{O}(\tau)}{\partial \tau}\right)_{\text{expl.}} ,$$

the operators $\hat{q}_{\alpha,\mathbf{k}}(\tau)$ and $\hat{p}_{\alpha,\mathbf{k}}(\tau)$ satisfy the same Hamiltonian equations of motion as their classical counterparts, i.e.

$$\dot{q}_{\alpha,\mathbf{k}} = \frac{\partial H}{\partial p_{\alpha,\mathbf{k}}} , \qquad \dot{p}_{\alpha,\mathbf{k}} = -\frac{\partial H}{\partial q_{\alpha,\mathbf{k}}} \tag{3.49}$$

Remember that we assume that asymptotically, $|t| \to \infty$, the brane is at rest, i.e. the brane velocity vanishes and both coordinate systems agree, $\tau = t$. We extend this notion of asymptotic behavior by introducing two times, t_{in} and t_{out}, and we shall assume that the brane is at rest for $t \le t_{\text{in}}$ and $t \ge t_{\text{out}}$, respectively. This corresponds to a scenario where the motion of the brane is switched on and off at finite times. Such a brane dynamics may

seem rather artificial from a physical point of view, but what is important for us is that before $t_{\rm in}$ and after $t_{\rm out}$ no significant particle creation takes place. Numerically, we test this by varying $t_{\rm in}$ and $t_{\rm out}$ and choosing them large enough so that the particle number is independent of the value chosen.

In the (τ, z)-coordinates, the brane is then at rest for times $\tau \equiv t \leq \tau_{\rm in} \equiv t_{\rm in}$ and $\tau \equiv t \geq \tau_{\rm out} \equiv t_{\rm out}$, respectively. When the brane velocity is zero, the matrix $E_{\alpha\beta}(\tau)$ defined in Appendix 3.6.2 becomes the identity, $E_{\alpha\beta}(\tau) \to_{|\tau|\to\infty} \delta_{\alpha\beta}$, and all other matrices which represent the coupling terms vanish identically in this limit. Consequently, for asymptotic times the Hamiltonian reduces to the familiar form of a collection of independent harmonic oscillators,

$$\hat{H}^{\rm in/out} = \frac{1}{2}\int d^3k \sum_\alpha \left[|\hat{p}_{\alpha,\mathbf{k}}|^2 + \left(\omega^{\rm in/out}_{\alpha,k}\right)^2 |\hat{q}_{\alpha,\mathbf{k}}|^2 \right] \tag{3.50}$$

with

$$\hat{p}_{\alpha,\mathbf{k}} = \dot{\hat{q}}_{\alpha,-\mathbf{k}}\,. \tag{3.51}$$

We have introduced the notation

$$\omega^{\rm in}_{\alpha,k} \equiv \omega_{\alpha,k}(\tau \leq \tau_{\rm in})\,, \quad \omega^{\rm out}_{\alpha,k} \equiv \omega_{\alpha,k}(\tau \geq \tau_{\rm out})\,. \tag{3.52}$$

Following [109], we decompose $\hat{q}_{\alpha,\mathbf{k}}$ in creation and annihilation operators,

$$\hat{q}_{\alpha,\mathbf{k}}(\tau) = \sum_\beta \frac{1}{\sqrt{2\,\omega^{\rm in}_{\beta,k}}} \left[\hat{a}^{\rm in}_{\beta,\mathbf{k}} \epsilon^{(\beta)}_{\alpha,k}(\tau) + \hat{a}^{\rm in\dagger}_{\beta,-\mathbf{k}} \epsilon^{(\beta)*}_{\alpha,k}(\tau) \right]\,, \tag{3.53}$$

which are defined via $\hat{a}^{\rm in}_{\alpha,\mathbf{k}}|0,{\rm in}\rangle = 0 \;\forall\; \alpha,\mathbf{k}$. The initial vacuum state $|0,{\rm in}\rangle$ is the ground state of the Hamiltonian (3.50) for times $\tau \leq \tau_{\rm in}$. This initial state is linked to the final vacuum state defined by $\hat{a}^{\rm out}_{\alpha,\mathbf{k}}|0,{\rm out}\rangle = 0\,;\; \forall\; \alpha,\mathbf{k}$, by means of a Bogoliubov transformation (see [109])

$$\hat{a}^{\rm out}_{\beta,\mathbf{k}} = \sum_\alpha \left[\mathcal{A}_{\alpha\beta,k}(\tau_{\rm out}) \hat{a}^{\rm in}_{\alpha,\mathbf{k}} + \mathcal{B}^*_{\alpha\beta,k}(\tau_{\rm out}) \hat{a}^{\rm in\dagger}_{\alpha,-\mathbf{k}} \right] \tag{3.54}$$

which determines the number of produced gravitons (for each polarization)

$$N^{\rm out}_{\alpha,k} = \sum_\beta |\mathcal{B}_{\beta\alpha,k}(\tau_{\rm out})|^2\,. \tag{3.55}$$

As we have discussed in detail in [109], the graviton number after the time $\tau_{\rm out}$, (3.55), represents a physically meaningful quantity .

3.4 Numerical Results

In order to solve the equations of motion (3.47) numerically, we transform the system to a first order system and introduce a mass cutoff, $n_{\rm max}$, i.e. we neglect all modes with masses higher than $m_{n_{\rm max}}$, in other words $q_\alpha = 0$ for $\alpha > n_{\rm max}$, along the lines explained in detail in Ref. [109]. Modes close to this cutoff are of course seriously affected by it as is seen in Figs. 3.3, 3.4 and 3.5. We have tested the stability of the results for modes $n \ll n_{\rm max}$ by varying the cutoff. The stability of the zero mode is illustrated in the lower panel of Figs. 3.3 and 3.4. Typically modes with $n \lesssim 0.7 n_{\rm max}$ can be trusted. An indication for this

is also the Bogoliubov test shown in Fig. 3.6 and discussed in Ref. [109].

The first order system is given explicitly in Appendix 3.6.2.3 and differs from the original one in [109] only by additional mode couplings. We have compared our new results with those of Ref. [38, 109] and find excellent agreement at low velocity, $v_{\max} \lesssim 0.1$. This is illustrated in Figs. 3.3 and 3.4. At bounce velocities $v_{\max} \gtrsim 0.5$ we do find differences as expected, but these results cannot be taken literally since for these velocities the low energy evolution of the scale factor adopted in this work is no longer sufficient. We will present the full high velocity results in a forthcoming paper [40].

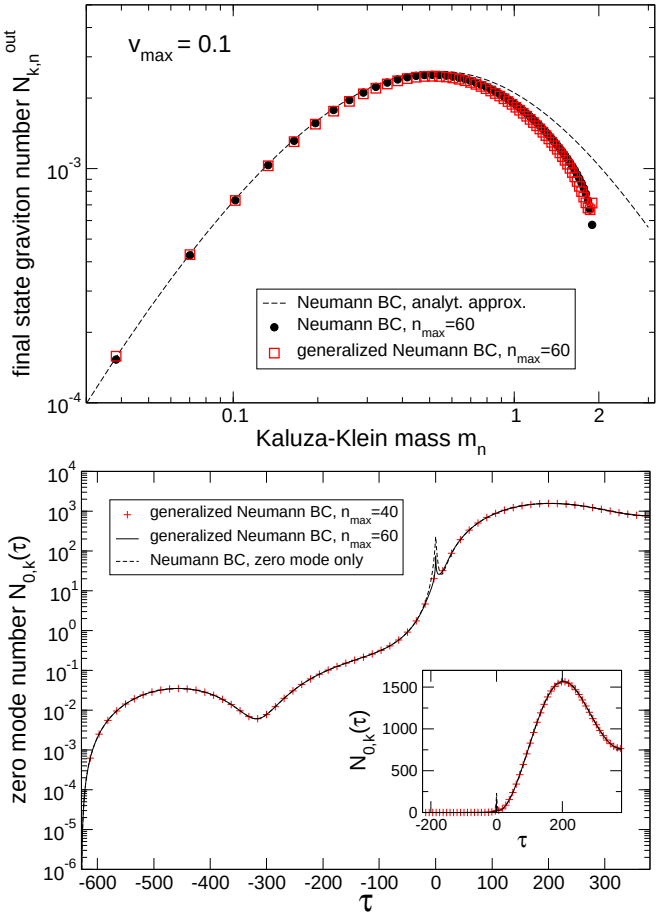

Figure 3.3: The final graviton spectrum for three-momentum $k = 0.01$, brane separation $y_s = 100$ and bounce velocity $v_{\max} = 0.1$. The top panel shows the final KK mode spectrum and the lower panel depicts the time evolution of the zero mode. What we plot here is a kind of instantaneous particle number (see Appendix C of [109]). The numerical result for the KK spectrum is compared with the old one (shown in Fig. 13 of [109]). Like there, lengths are in units of L and momenta/masses in the units of L^{-1}. For low velocities $v_{\max} \leq 0.1$ the new spectra (generalized Neumann BC) are identical with the old ones (Neumann BC) within the numerical error which are estimated by the Bogoliubov test (see Appendix). $N_{0,k}(\tau)$ is shown for two cut-off parameters $n_{\max}$ to underline stability of the solution.

The agreement between the old results for pure Neumann boundary conditions and the new ones with the generalized Neumann boundary conditions is similar for other values of

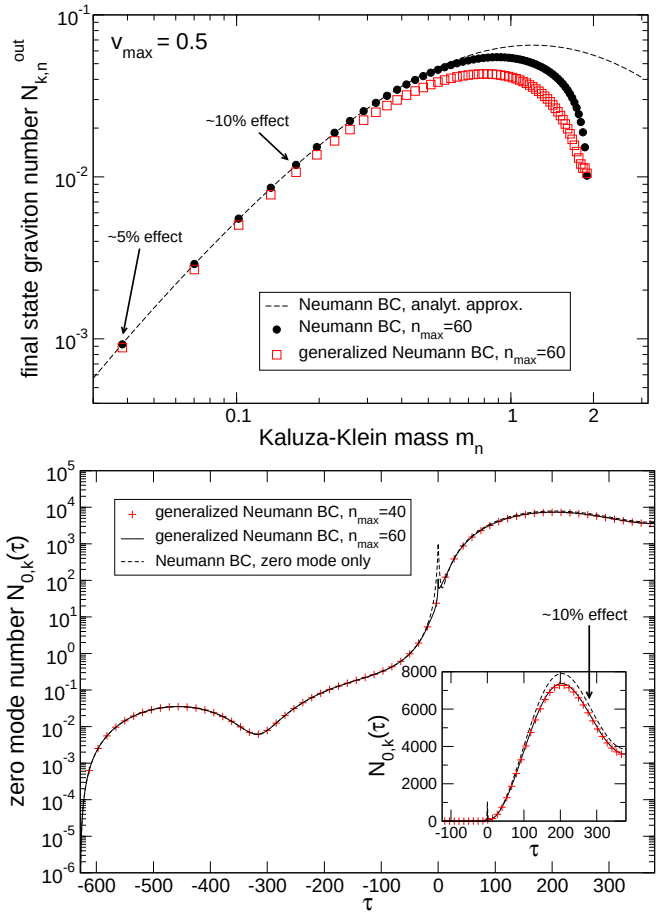

Figure 3.4: As Figure 3.3 but for $v_{\max} = 0.5$. For this velocity we do see a difference of about 10% between the previous, inconsistent approach and the new generalized Neumann BC for both, the KK modes as well as the zero mode. Again, the 4d graviton number is shown for two cut-off parameters $n_{\max}$ to indicate numerical stability. .

y_s and k.

In Fig. 3.5 we show the KK spectra for $v_{\max} = 0.1$ and $v_{\max} = 0.3$ for the wave number $k = 0.1$ and position of the static brane, $y_s = 10$. In this case, the analytic approximation derived in Ref. [109] which is valid for $m_n < 1$ can only be trusted for the first two modes. The slight difference between the old and the new spectra towards the end, i.e. for $m_n > 10$, is due to changes how we numerically evolve the solutions through the bounce (see Appendix 3.6.3). This affects the sensitivity of the solutions to the cut-off. What we observe here as a slight bending of the spectrum for generalized Neumann BC's is also found in our previous approach if we increase the number of modes; compare to the $n_{\max} = 100$ results shown in Fig. 15 of [109] and the discussion related to Fig. 25 of [109]. The drop in the final part of the spectrum is just an artefact of the finite cut-off (see [109] for a detailed discussion).

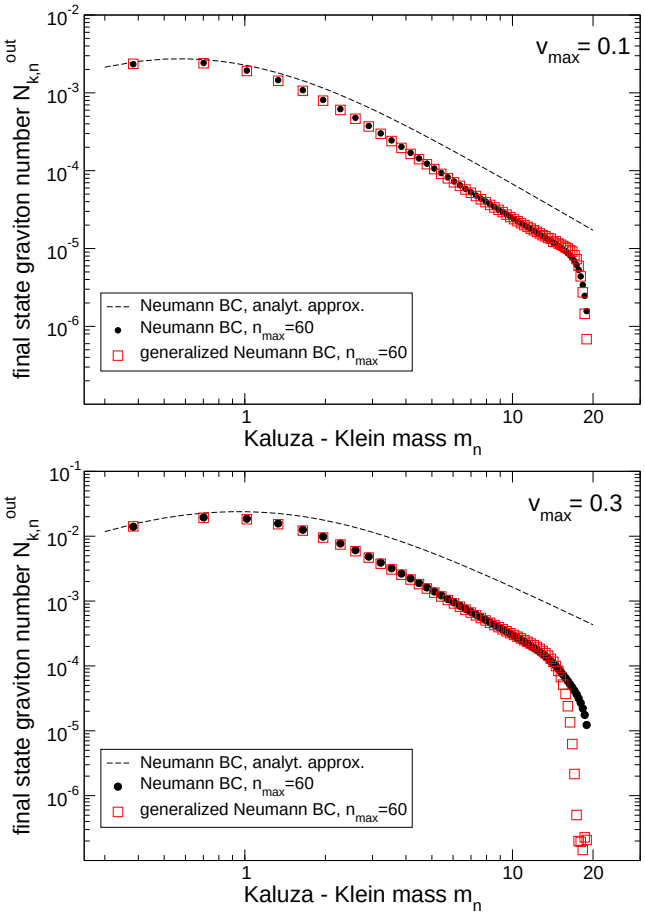

Figure 3.5: Final graviton spectra for three-momentum $k = 0.1$ and brane separation $y_s = 10$ for the bounce velocities $v_{\max} = 0.1$ and 0.3. Again, the new (generalized Neumann BC) numerical results are compared with the ones of the previous inconsistent approach (Neumann BC), see Fig. 15 of [109], and the agreement is excellent in the regime $m_n < 13$, where the numerics can be trusted.

3.5 Conclusions

In this paper we have derived a method to calculate graviton production in bouncing AdS_5 braneworlds by the dynamical Casimir effect taking into account the full generalized Neumann boundary condition. We have achieved this by transforming to a new time coordinate, in which the generalized Neumann BC become ordinary Neumann BC. We have shown numerically that for low bounce velocities, $v_{\max} \lesssim 0.1$, the number of generated particles agrees with the one from the simpler treatment which neglects the velocity term in the boundary condition. Since this term is of first order in the velocity, we believe that our result is not obvious. Furthermore, the method developed in this work can be used to calculate particle creation for branes moving at arbitrarily high velocities. In this case, one will have to take into account the modification of the Friedmann equation at high energy, $HL \gtrsim 1$. This is the goal of a forthcoming paper [40].

In this work we have not derived new physical results, but we have developed a new, fully consistent method to calculate graviton production due to the motion of a braneworld.

Our method overcomes a shortcoming of our previous treatment [38, 109], and we have verified that at low brane velocity, $v_{\max} \lesssim 0.3$ the previous results are not affected.

Acknowledgment

This work is supported by the Swiss National Science Foundation. The numerical simulations have been carried out on the Myrinet cluster of Geneva University. RD thanks the Galileo Galilei Institute of theoretical physics, where this work was finalized, for hospitality.

3.6 Appendix

3.6.1 The coordinate transformation

The Jacobian $\mathbf{T}$ of the transformation

$$(t, y) \mapsto (\tau = t + s(t, y), z = y)$$

reads

$$\mathbf{T} = \frac{\partial(\tau, \mathbf{x}, z)}{\partial(t, \mathbf{x}, y)} = \begin{pmatrix} 1+\partial_t s & 0 & 0 & 0 & \partial_y s \\ 0 & 1 & 0 & 0 & 0 \\ 0 & 0 & 1 & 0 & 0 \\ 0 & 0 & 0 & 1 & 0 \\ 0 & 0 & 0 & 0 & 1 \end{pmatrix}, \tag{3.56}$$

and its inverse is

$$\mathbf{T}^{-1} = \frac{\partial(t, \mathbf{x}, y)}{\partial(\tau, \mathbf{x}, z)} = \begin{pmatrix} \frac{1}{1+\partial_t s} & 0 & 0 & 0 & \frac{-\partial_y s}{1+\partial_t s} \\ 0 & 1 & 0 & 0 & 0 \\ 0 & 0 & 1 & 0 & 0 \\ 0 & 0 & 0 & 1 & 0 \\ 0 & 0 & 0 & 0 & 1 \end{pmatrix}.$$

Under this coordinate transformation the AdS_5 metric in Poincaré coordinates given in (3.1) transforms to

$$\begin{aligned} \tilde{g}_{AB} d\tilde{x}^A d\tilde{x}^B &= \left((\mathbf{T}^{-1})^T g \mathbf{T}^{-1}\right)_{AB} d\tilde{x}^A d\tilde{x}^B \\ &= \frac{L^2}{z^2}\Big[\frac{1}{(1+s_1(\tau,z))^2}\Big(-d\tau^2 + 2s_2(\tau,z)d\tau dz + g_1(\tau,z)dz^2\Big) + \delta_{ij}dx^i dx^j\Big]. \end{aligned}$$

We introduce the functions

$$s_1(\tau, z) = (\partial_t s)\big(t(\tau, z), z\big) \tag{3.57}$$

$$s_2(\tau, z) = (\partial_z s)\big|_{t=\text{const}}\big(t(\tau, z), z\big) \tag{3.58}$$

$$s_{11}(\tau, z) = (\partial_t^2 s)\big(t(\tau, z), z\big) \tag{3.59}$$

$$s_{22}(\tau, z) = (\partial_z^2 s)\big|_{t=\text{const}}\big(t(\tau, z), z\big) \tag{3.60}$$

and

$$g_1(\tau,z) = \big(1+s_1(\tau,z)\big)^2 - s_2(\tau,z)^2 \tag{3.61}$$

$$g_2(\tau,z) = s_{11}(\tau,z) - s_{22}(\tau,z) + \frac{3}{z}s_2(\tau,z)\ , \tag{3.62}$$

of which g_1 and g_2 will be used in Appendix 3.6.2.
The determinant is

$$\tilde{g} = \det(\tilde{g}_{AB}) = -\left(\frac{L}{z}\right)^{10} \frac{1}{(1+s_1(\tau,z))^2}\ . \tag{3.63}$$

3.6.2 Details on evolution equations

3.6.2.1 Wave equation

The coupling matrices which determine the mode evolution equation (3.47) are given in terms of the following bulk integrals:

$$\begin{aligned} A_{\alpha\beta}(\tau) &= 2\int_{z_b(\tau)}^{z_s}\frac{dz}{z^3}\left[2\dot{\phi}_\alpha + \frac{g_2(\tau,z)}{g_1(\tau,z)}\phi_\alpha(\tau,z)\right. \\ &\qquad \left. -\frac{2s_2(\tau,z)}{g_1(\tau,z)}\phi'_\alpha(\tau,z)\right]\phi_\beta(\tau,z) \end{aligned} \tag{3.64}$$

$$\begin{aligned} B_{\alpha\beta}(\tau) &= 2\int_{z_b(\tau)}^{z_s}\frac{dz}{z^3}\left[\ddot{\phi}_\alpha(\tau,z) + \frac{g_2(\tau,z)}{g_1(\tau,z)}\dot{\phi}_\alpha(\tau,z)\right. \\ &\quad \left. -\frac{2s_2(\tau,z)}{g_1(\tau,z)}\dot{\phi}'_\alpha(\tau,z) + \frac{\omega^2_{\alpha,k}(\tau)}{g_1(\tau,z)}\phi_\alpha(\tau,z)\right]\phi_\beta(\tau,z) \end{aligned} \tag{3.65}$$

with

$$\omega_{\alpha,k}(\tau) = \sqrt{m^2_\alpha(\tau)+k^2}\ . \tag{3.66}$$

The over-dot denotes the derivative w.r.t. the time τ and a prime stands for the derivative w.r.t. the coordinate z. Compared to our former work [109], the present problem is more complicated due to the additional couplings which are caused by the time-dependence of the bulk spacetime. Also the Lagrangian and Hamiltonian equations for $q_{\alpha,k}$ are more complicated. Furthermore, the functions s_1, s_2, g_1 and g_2 are only known numerically. This induces additional numerical difficulties. Note also that it is important that g_1 does not pass through zero for these integrals to be well defined, hence $g_1(\tau,z) > 0\ \forall\tau,z$. This is, however, easily achieved with our ansatz (3.37, 3.41) for $s(t,y)$ if we choose σ_0 sufficiently large.

3.6.2.2 Lagrangian and Hamiltonian formulation

Inserting the expansion (3.46) into the action (3.45) leads (for each of the polarizations) to the Lagrangian

$$\begin{aligned} L(\tau) &= \frac{1}{2}\int d^3k \sum_{\alpha\beta}\Big[E_{\alpha\beta}\dot{q}_{\alpha,\mathbf{k}}\dot{q}_{\beta,-\mathbf{k}} \\ &\quad +(\mathcal{M}_{\alpha\beta}-\mathcal{K}_{\alpha\beta})(q_{\alpha,\mathbf{k}}\dot{q}_{\beta,-\mathbf{k}}+q_{\alpha,-\mathbf{k}}\dot{q}_{\beta,\mathbf{k}}) \\ &\quad +(\mathcal{N}_{\alpha\beta}-\mathcal{P}_{\alpha\beta}-Q_{\alpha\beta}-\omega^2_{\alpha\beta,k})q_{\alpha,\mathbf{k}}q_{\beta,-\mathbf{k}}\Big] \end{aligned}$$

containing several time-dependent coupling terms. In detail, these read

$$\begin{aligned} E_{\alpha\beta}(\tau) &= 2\int_{z_b(\tau)}^{z_s}\frac{dz}{z^3}\frac{g_1(\tau,z)}{1+s_1(\tau,z)}\phi_\alpha(\tau,z)\phi_\beta(\tau,z) \\ \mathcal{M}_{\alpha\beta}(\tau) &= 2\int_{z_b(\tau)}^{z_s}\frac{dz}{z^3}\frac{g_1(\tau,z)}{1+s_1(\tau,z)}\dot{\phi}_\alpha(\tau,z)\phi_\beta(\tau,z) \\ \mathcal{N}_{\alpha\beta}(\tau) &= 2\int_{z_b(\tau)}^{z_s}\frac{dz}{z^3}\frac{g_1(\tau,z)}{1+s_1(\tau,z)}\dot{\phi}_\alpha(\tau,z)\dot{\phi}_\beta(\tau,z) \\ \mathcal{K}_{\alpha\beta}(\tau) &= 2\int_{z_b(\tau)}^{z_s}\frac{dz}{z^3}\frac{s_2(\tau,z)}{1+s_1(\tau,z)}\phi'_\alpha(\tau,z)\phi_\beta(\tau,z) \\ \mathcal{P}_{\alpha\beta}(\tau) &= 2\int_{z_b(\tau)}^{z_s}\frac{dz}{z^3}\frac{s_2(\tau,z)}{1+s_1(\tau,z)}\big[\dot{\phi}_\alpha(\tau,z)\phi'_\beta(\tau,z) \\ &\quad +\phi'_\alpha(\tau,z)\dot{\phi}_\beta(\tau,z)\big] \\ \mathcal{Q}_{\alpha\beta}(\tau) &= \int_{z_b(\tau)}^{z_s}\frac{dz}{z^3}\frac{s'_1(\tau,z)}{(1+s_1(\tau,z))^2}\big[\phi_\alpha(\tau,z)\phi'_\beta(\tau,z) \\ &\quad +\phi'_\alpha(\tau,z)\phi_\beta(\tau,z)\big] \\ \omega^2_{\alpha\beta,k}(\tau) &= 2\left[\frac{1}{2}\left(m^2_\alpha(\tau)+m^2_\beta(\tau)\right)+k^2\right]\times \\ &\quad \int_{z_b(\tau)}^{z_s}\frac{dz}{z^3}\frac{\phi_\alpha(\tau,z)\phi_\beta(\tau,z)}{1+s_1(\tau,z)}\,. \end{aligned}$$

Since we require $g_1(\tau,z)>0$ and $1+s_1(\tau,z)>0$, the matrix $E_{\alpha\beta}$ is positive definite. This is important for the above Lagrangian to lead to consistent second order equations of motion for the variables $q_{\alpha,\mathbf{k}}$ (no ghosts).

The equation of motion for the canonical variables obtained from the Euler–Lagrange equations become

$$\begin{aligned} \sum_\alpha\Big[&E_{\alpha\gamma}\ddot{q}_{\alpha,\mathbf{k}}+\dot{E}_{\alpha\gamma}\dot{q}_{\alpha,\mathbf{k}}+\left(\dot{\mathcal{M}}-\dot{\mathcal{K}}\right)_{\alpha\gamma}q_{\alpha,\mathbf{k}} \\ &+\left[(\mathcal{M}-\mathcal{K})_{\alpha\gamma}-(\mathcal{M}-\mathcal{K})_{\gamma\alpha}\right]\dot{q}_{\alpha,\mathbf{k}} \\ &-(\mathcal{N}_{\alpha\gamma}-\mathcal{P}_{\alpha\gamma}-Q_{\alpha\gamma}-\omega_{\alpha\gamma,k})\,q_{\alpha,\mathbf{k}}\Big]=0\,. \end{aligned} \tag{3.67}$$

Note that all the matrices introduced above apart from $E_{\alpha\beta}$ tend to zero when $v\to 0$, i.e. for $|\tau|\to\infty$. In this limit $E_{\alpha\beta}$ tends to $\delta_{\alpha\beta}$ so that Eq. (3.67) becomes the free, uncoupled

mode evolution equation in this limit as is expected. Introducing the canonically conjugate variables

$$p_{\alpha,\mathbf{k}} = \frac{\partial L}{\partial \dot{q}_{\alpha,\mathbf{k}}} = \sum_{\beta} \left[E_{\alpha\beta} \dot{q}_{\beta,-\mathbf{k}} + (\mathcal{M}_{\beta\alpha} - \mathcal{K}_{\beta\alpha}) q_{\beta,-\mathbf{k}} \right] \tag{3.68}$$

leads by means of a Legendre transformation to the Hamiltonian (3.48) with coupling matrices

$$\begin{aligned} V_{\alpha\beta}(\tau) &= 2 \int_{z_b(\tau)}^{z_s} \frac{dz}{z^3} \frac{1}{1+s_1} \Big[\left(\frac{s_2^2}{g_1} - s_1 \right) \phi_\alpha^{'}(\tau,z) \phi_\beta^{'}(\tau,z) \\ &\qquad - k^2 s_1(\tau,z) \phi_\alpha(\tau,z) \phi_\beta(\tau,z) \Big] \qquad (3.69) \\ M_{\alpha\beta}(\tau) &= 2 \int_{z_b(\tau)}^{z_s} \frac{dz}{z^3} \dot{\phi}_\alpha(\tau,z) \phi_\beta(\tau,z) \qquad (3.70) \\ S_{\alpha\beta}(\tau) &= 2 \int_{z_b(\tau)}^{z_s} \frac{dz}{z^3} \frac{s_2}{g_1} \phi_\alpha'(\tau,z) \phi_\beta(\tau,z) \ . \qquad (3.71) \end{aligned}$$

Thereby $E^{-1}_{\alpha\beta}$ is the inverse of $E_{\alpha\beta}$, i.e.

$$E^{-1}_{\alpha\beta} = 2 \int_{z_b(\tau)}^{z_s} \frac{dz}{z^3} \frac{1+s_1(\tau,z)}{g_1(\tau,z)} \phi_\alpha(\tau,z) \phi_\beta(\tau,z) \ . \tag{3.72}$$

The Hamilton equations

$$\dot{q}_{\alpha,\mathbf{k}} = \frac{\partial H}{\partial p_{\alpha,\mathbf{k}}} \ , \ \ \dot{p}_{\alpha,\mathbf{k}} = -\frac{\partial H}{\partial q_{\alpha,\mathbf{k}}} \tag{3.73}$$

then provide the equations of motion for the variables $q_{\alpha,\mathbf{k}}$ and $p_{\alpha,\mathbf{k}}$.

Using certain relations of the coupling matrices following from the completeness (3.29) and ortho-normality (3.28) of the functions ϕ_α and the properties of the functions s_1, s_2, s_{11} and s_{22} one can show that the three systems of equations (3.47), (3.67) and the Hamilton equations (3.73) are consistent with each other, i.e. one system follows from the other one. This seems to be at first sight a rather trivial statement but we have to remind the reader that this is not the case in our previous work [38, 109] as we have discussed in detail in Section II. D of Ref. [109]. The new coupling matrices $V_{\alpha\beta}$, $S_{\alpha\beta}$ and $E_{\alpha\beta} - \delta_{\alpha\beta}$ are missing in our previous work. Even though they do become very small when the brane velocity becomes small, it is not evident that these new terms must be smaller than e.g. $M_{\alpha\beta}$, which also tends to zero with v. In other words, it is not straight forward to show that these contributions are, e.g., of order v^2.

3.6.2.3 Bogoliubov coefficients

Performing the quantization as in Ref. [109] we again transform to a first order system of equation. In the new coordinates the system of equations (3.34), (3.35) of [109] is replaced

by

$$\begin{aligned}\dot{\xi}^{(\gamma)}_{\alpha}(\tau) &= \sum_{\beta}\Big\{ -\Big[ia^{+}_{\alpha\beta}(\tau)+c^{-}_{\alpha\beta}(\tau)\Big]\,\xi^{(\gamma)}_{\beta}(\tau) \\ &\quad +\Big[ia^{-}_{\alpha\beta}(\tau)-c^{+}_{\alpha\beta}(\tau)\Big]\,\eta^{(\gamma)}_{\beta}(\tau)\Big\} \qquad (3.74)\\ \dot{\eta}^{(\gamma)}_{\alpha}(\tau) &= \sum_{\beta}\Big\{ \Big[ia^{+}_{\alpha\beta}(\tau)-c^{-}_{\alpha\beta}(\tau)\Big]\,\eta^{(\gamma)}_{\beta}(\tau) \\ &\quad -\Big[ia^{-}_{\alpha\beta}(\tau)+c^{+}_{\alpha\beta}(\tau)\Big]\,\xi^{(\gamma)}_{\beta}(\tau)\Big\} \qquad (3.75)\end{aligned}$$

where

$$\begin{aligned}a^{\pm}_{\alpha\beta}(\tau) &= \frac{1}{2}\Big[\omega^{\rm in}_{\beta,k}E^{-1}_{\alpha\beta}(\tau)\pm\frac{1}{\omega^{\rm in}_{\alpha,k}}\Big(\frac{1}{2}(\omega^{2}_{\alpha,k}(\tau) \\ &\quad +\omega^{2}_{\beta,k}(\tau))\delta_{\alpha\beta}+V_{\alpha\beta}(\tau)\Big)\Big] \qquad (3.76)\end{aligned}$$

$$\begin{aligned}c^{\pm}_{\alpha\beta}(\tau) &= \frac{1}{2}\Big[M_{\beta\alpha}(\tau)-S_{\beta\alpha}(\tau) \\ &\quad \pm\frac{\omega^{\rm in}_{\beta,k}}{\omega^{\rm in}_{\alpha,k}}\left(M_{\alpha\beta}(\tau)-S_{\alpha\beta}(\tau)\right)\Big]\,. \qquad (3.77)\end{aligned}$$

(Note that in Ref. [109] a factor of two is missing in the expression for $M^{\rm N}_{ij}$ in Eq. (B8), a simple misprint.)

3.6.3 Numerics

To compute the graviton spectra we have adapted the code described in Ref. [109] to the new problem. Apart from calculating the new coupling matrices we also have to solve the differential equation (3.40) numerically to calculate the coordinate transformation and its inverse in order to determine $z_b(\tau)$ via the implicit equation (3.31) as well as the functions $s_1(\tau,z)$, $s_2(\tau,z)$, $g_1(\tau,z)$ and $g_2(\tau,z)$ which enter the integrals for the coupling matrices. For numerical purposes we have smoothed the function $y_b(t)$. Due to this implicit nature of the coordinate transformation, the calculation of these coupling matrices is numerically significantly more involved than in our previous approach.

As in [109], splines are used to interpolate the various matrix elements between time steps. The time steps used to produce the splines are not uniformly distributed but carefully selected to take into account the steepness of the time dependence of the couplings. Close to the bounce we use very short time steps to produce the splines ($\sim 10^{-6}$) while far away we can increase the step up to 0.2 (in units of L). Furthermore, due to the complex time dependence of some of the couplings very close to the bounce, exact integration of the matrix elements when propagating the solutions through the bounce is necessary in order to obtain satisfactory accuracy for large KK masses as in Fig. 3.5. In this way the bounce is taken into account as accurate as possible. This affects the speed of convergence of the solutions w.r.t. $n_{\rm max}$, leading to the behavior described below Fig. 3.5.

As an indicator for the accuracy of our calculations we use the Bogoliubov test as described in Appendix D of [109] (Eq. (D6)). This is presented in Fig. 3.6 for the $v_{\rm max}=0.3$

result given in Fig. 3.5. The quantity denoted by 'Bogoliubov test' and shown as solid line in Fig. 3.6 should ideally vanish. Given the complex nature of the numerical problem, the accuracy of the results is satisfactory for $m_n \lesssim 10/L$.

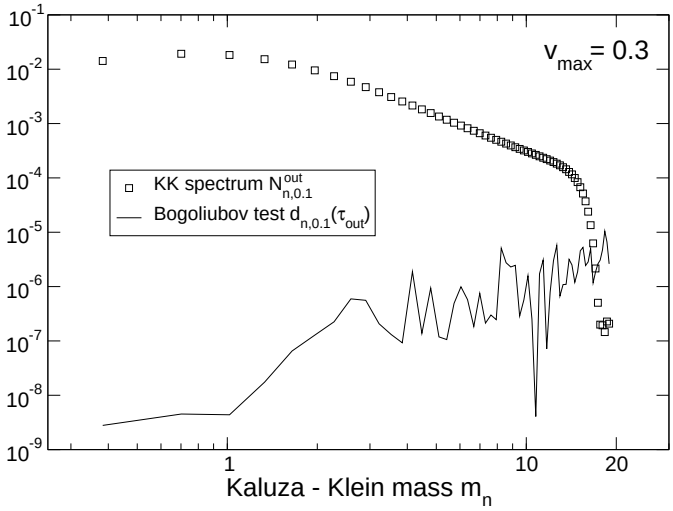

Figure 3.6: Comparison of the final KK spectrum $N^{\rm out}_{n,0.1}$ and the corresponding quantity $d_{n,0.1}(\tau_{\rm out})$ given in Eq. (D6) of [109]. The quantity $d_{n,0.1}(\tau_{\rm out})$ is supposed to vanish identically, see [109]. The comparison is a measure for the accuracy of the $v_{\rm max} = 0.3$ result depicted in Fig. 3.5. In the region of the spectrum which is free from numerical artefacts, i.e. no dependence on cut-off $n_{\rm max}$, $d_{n,0.1}(\tau_{\rm out})$ is at least about two orders of magnitude smaller than the physically relevant quantity $N^{\rm out}_{n,0.1}$ indicating a satisfactory accuracy.

Chapter 4

Model-independent cosmological constraints from the CMB

JOURNAL OF ASTROPHYSICS AND ASTROPARTICLE PHYSICS **08**, 023 (2009)

Model-independent cosmological constraints from the CMB

Marc Vonlanthen, Syksy Räsänen, Ruth Durrer

We analyse CMB data in a manner which is as independent as possible of the model of late-time cosmology. We encode the effects of late-time cosmology into a single parameter which determines the distance to the last scattering surface. We exclude low multipoles $\ell < 40$ from the analysis. We consider the WMAP5 and ACBAR data. We obtain the cosmological parameters $100\omega_{\rm b} = 2.13 \pm 0.05$, $\omega_{\rm c} = 0.124 \pm 0.007$, $n_s = 0.93 \pm 0.02$ and $\theta_A = 0.593^\circ \pm 0.001^\circ$ (68% C.L.). The last number is the angular scale subtended by the sound horizon at decoupling. There is a systematic shift in the parameters as more low ℓ data are omitted, towards smaller values of $\omega_{\rm b}$ and n_s and larger values of $\omega_{\rm c}$. The scale θ_A remains stable and very well determined.

4.1 Introduction

The cosmic microwave background (CMB) is one of the most important cosmological probes. The pattern of acoustic oscillations of the baryon-photon plasma is imprinted on the CMB at the time of decoupling, and then rescaled (and on large scales modified) as the CMB photons propagate from the last scattering surface to the observer. The CMB is thus sensitive to cosmological parameters in two ways, via the physics at decoupling and via the evolution of the universe after that.

While the physics at decoupling –essentially atomic physics and general relativity of a linearly perturbed Friedmann-Lemaître (FL) universe– is well understood, the evolution at late times deviates from the predictions of linearly perturbed FL models with radiation and matter. The difference may be due to an exotic matter component with negative pressure such as vacuum energy, deviation of gravity from general relativity [37, 82, 72, 18], or a breakdown of the homogeneous and isotropic approximation [99, 14, 47, 100, 127, 22]. It is not known which of these possibilities is correct, and there are large differences between the various models. It is therefore worthwhile to analyse the CMB in a manner which is as independent of the details of late-time cosmology as possible. On the one hand, this clarifies the minimal constraints that all models of late-time cosmology, whatever their details, have to satisfy in order to agree with CMB observations. On the other hand, our analysis provides limits on the physical parameters at decoupling that are independent of the details of what happens at later times. This is particularly important for cosmological parameters such as the density of baryons, density of dark matter and the spectral index, which are used to constrain particle physics models of baryogenesis, supersymmetry and inflation, which are independent of late-time cosmology.

Such a separation of constraints is possible because the physics after decoupling affects the CMB in a rather limited manner (except at low multipoles), by simply changing the angular scale and modifying the overall amplitude of the CMB pattern. We encode the change in the angular scale in a single parameter related to the angular diameter distance

to the last scattering surface and treat the amplitude as a nuisance parameter. We aim to be transparent about how the different cosmological parameters enter the calculation and the assumptions that go into the analysis.

In section 2 we discuss how the physics at early and late times affects the CMB and explain our assumptions. In section 3 we present the results of the analysis of the WMAP 5-year data [66, 32, 58] and the ACBAR data [104] and give the constraints on cosmological parameters. In section 4 we summarise our results. Some details are collected in two appendices.

4.2 Parameter dependence of the CMB

4.2.1 Our assumptions

The pattern of CMB anisotropies can be summarised in terms of a few parameters. It was noted in [44] that models with the same primordial perturbation spectra and same values of $\omega_{\rm b}, \omega_{\rm c}$ and the shift parameter R have an identical CMB spectrum today, apart from low multipoles ($\ell \lesssim 30$). The discussion in [44] was in the context of a family of Friedmann-Lemaître (FL) models, but the statement is true more generally. The shift parameter is defined as

$$\begin{aligned} R &\equiv \omega_{\rm m}^{1/2}(1+z_*)H_0 h^{-1} D_A(z_*) \\ &= \left(\frac{\Omega_m}{\Omega_K}\right)^{1/2} \sinh\left(\Omega_K^{1/2}\int_0^{z_*} {\rm d}z' \frac{H_0}{H(z')}\right) \ , \end{aligned} \tag{4.1}$$

where z_* is the redshift of decoupling, $D_A(z)$ is the angular diameter distance between today and redshift z, $H_0 = 100h$km/s/Mpc is the Hubble parameter today, and the second equation holds for all FL models. The density parameter $\omega_{\rm b}$ is the normalized dimensionless physical density of baryonic matter, $\omega_{\rm b} = 8\pi G_{\rm N}\rho_b/3/(100\ {\rm km/s/Mpc})^2$, $\omega_{\rm c}$ is the normalized dimensionless physical density of cold dark matter defined the same way, $\omega_{\rm m} = \omega_{\rm b} + \omega_{\rm c}$ is the total physical matter density, and $\Omega_{\rm m} = \omega_{\rm m} h^{-2}$ and Ω_K are, respectively, the matter and the spatial curvature density parameter today. With present observations which include polarization data, one has to add a parameter to take into account collisions between the CMB photons and baryonic matter after the cosmic medium becomes reionized. This is usually expressed with the redshift of reionization $z_{\rm ri}$ or the optical depth τ.

The CMB data have been analysed in terms of the shift parameter R in various FL models [70, 66, 46, 122, 27, 89, 67], and a similar approach has been followed for local void models [127, 25]. The model-dependence of parameters such as R has been discussed, but limits on them have always been derived within some specific models, and it has not been clear which assumptions are important and what is the model-independent information.

In this work, we analyse the CMB in a manner which is as model-independent as possible, and we are explicit about the assumptions involved. In particular, we do not restrict our study to models which are close to FL at late times, so our constraints are also applicable to models where the effect of non-linear structures on the expansion rate is important, or where we are located in a large spherically symmetric density fluctuation such as a local void. (Note that the near-isotropy of the CMB does not imply that the universe is close to FL, even coupled with the Copernican principle [101].)

We assume that the physics up to and including decoupling is completely standard, i.e. linearly perturbed FL evolution according to normal four-dimensional general relativity

with Standard Model particle physics and dark matter (which we assume to be cold during decoupling). As for physics after decoupling, we make the minimal assumptions that it changes the small angle CMB spectrum only by 1) modifying the angular diameter distance to the last scattering surface and 2) changing the overall amplitude. Here, small angles refers to scales which are well inside the horizon at late times when the unknown physics can be important, say conservatively at $z \lesssim 60$. We discard low multipoles in our analysis, because typically the unknown physics of dark energy, modified gravity or large deviations from FL geometry affects the large angles in a model-dependent way, for example via the late Integrated Sachs-Wolfe (ISW) effect. In typical perturbed FL models, the late ISW effect is only significant at low multipoles (see appendix 4.5.1), and the Rees-Sciama effect, gravitational lensing and the Sunyaev-Zel'dovich effect do not have a significant impact at the present observational accuracy [80, 36, 115], though their presence is already suggested by the ACBAR data [104]. We assume that such effects remain small in other models, and that any multipole-dependent effect of new physics on the CMB spectrum is below the observational precision, except at low multipoles.

In perturbed FL models, reionization has a significant effect on all angular scales, but at high multipoles it amounts to a simple rescaling of the amplitude, and is thus degenerate with the amplitude of primordial perturbations (see appendix 4.5.2), so we can neglect modeling of reionization.

We assume that the primordial perturbations are adiabatic, and have a power-law spectrum. We only consider scalar perturbations, and assume that vector and tensor contributions are small. (This division refers to the early universe; in the late universe it is not necessarily meaningful, because we do not assume that the late universe is close to FL.) Within our approach it would not be easy to include tensor perturbations in the temperature anisotropy spectrum, because they contribute mainly via the ISW effect and are relevant up to $\ell \approx 100$. However, the contribution of tensors starts to decay already around $\ell \approx 50$ and is probably relatively small, so their presence would not be expected to change our results significantly. (It would be easy to take into account the tensor contribution to the polarization spectrum, though, because it is mainly generated at the last scattering surface.) We also neglect the effect of neutrino masses.

The idea behind these assumptions is that we can treat the CMB with a standard Boltzmann code, and simply exclude low multipoles from the analysis. We have modified the publicly available CAMB code and the corresponding Monte Carlo Markov Chain program [81] to search for best-fit values of our parameters. As long as the rise to the first peak is fully included in the analysis, discarding low multipoles should not involve a significant loss of information, because there are more high multipoles and the cosmic variance is larger on large scales. However, our results in this respect are somewhat surprising, as we discuss in section 4.3. Also, it has been argued that there are anomalies in the angular distribution on large scales [56] (and a dipolar modulation at higher multipoles [57]), which could indicate that some physics affecting the low multipoles is not understood, so they may be unreliable for cosmological analysis; see also [48, 8].

Our assumptions do not hold for models with non-standard physics at or before decoupling, such as new radiation degrees of freedom, early dark energy [16] or dark matter which undergoes significant annihilation at early times [50]. In models where we are located in a large spherically symmetric region, it is possible to obtain a large CMB dipole [61], and there could be a large effect at higher multipoles as well. This can only be checked with perturbation theory adapted to such models, which is now being developed [23].

4.2.2 The physics of the CMB parameters

Let us outline the relation between the features in the CMB spectrum and the cosmological parameters, given our assumptions above. (See [36, 88] for detailed discussion.) We consider five parameters, namely the overall amplitude, the baryon density $\omega_{\rm b}$, the cold dark matter density $\omega_{\rm c}$, the spectral index n_s and the distance to the last scattering surface $D_A(z_*)$.

The observed amplitude of CMB perturbations is determined by a combination of the primordial power spectrum and late-time physics, such as damping due to accelerating expansion and scattering of CMB photons from matter due to reionization. Without specifying a model for the late-time universe, it is not possible to disentangle these effects. Because the overall normalization does not have a model-independent interpretation, we treat it as a nuisance parameter, i.e., we marginalize over it and do not quote limits for it.

The spectral index n_s is related to the early universe physics, such as inflation, which produces the primordial perturbations. Extending the analysis to more complicated primordial spectra would be straightforward, though of course we would not be sensitive to large-scale features.

The relative height and depth of the CMB peaks and troughs is set by the physics of the baryon-photon oscillations, which depends on $\omega_{\rm b}$ and $\omega_{\rm c}$. This pattern also depends on the radiation density $\omega_r = 8\pi G_{\rm N}\rho_r/3/(100\ {\rm km/s/Mpc})^2$, which is however accurately determined by the CMB temperature. Note that the CMB is only sensitive to the densities at the time of decoupling, not to their values today. As is customary, we use the symbols $\omega_{\rm b}$, $\omega_{\rm c}$ and ω_r to refer to the densities at decoupling scaled to today with the factor $(1+z_*)^3$ for baryons and dark matter and $(1+z_*)^4$ for radiation, where $*$ indicates the time of decoupling. At decoupling, the distribution of matter is still very smooth, so the densities at that time can be understood as local or average values; the scaled numbers represent today's average values. In a statistically homogeneous and isotropic space, the mean energy density of baryons and cold dark matter evolves like $(1+z)^3$ due to conservation of mass, and the mean energy density of photons evolves like $(1+z)^4$ due to conservation of photon number and the fact that the change of energy of the CMB photons by scattering can be neglected [102]. FL models are of course a particular case of this. If dark matter has significant pressure, or decays significantly [31], or if there is some extra source of baryons, dark matter or photons, our $\omega_{\rm b}, \omega_{\rm c}$ and ω_r would not correspond to the physical densities today. (Dark matter decay to radiation would also contribute to the late ISW effect [65].) This is already true for neutrinos, which we treat as massless, but which in fact do not contribute to the present-day radiation density, since their mass today is larger than the temperature. This will also be the case if the factor $(1+z)^3$ is not simply proportional to the volume, which can happen if statistical homogeneity and isotropy is broken, such as in local void models where shear can contribute significantly to the redshift.

Our final parameter is the angular diameter distance to the last scattering surface. The angular diameter distance out to redshift z is defined as $D_A(z) = L/\theta$, where L is the proper size of an object at redshift z and θ is its observed angular size. The physical scale of the baryon-photon oscillations is set by the sound horizon at decoupling $r_s(z_*)$ which depends on $\omega_{\rm b}$ and $\omega_{\rm c}$ [59, 36]. With standard physics up to decoupling, the sound speed of the photon-baryon plasma is

$$c_s^2 = \frac{1}{3(1+3\rho_b/4\rho_\gamma)} = \frac{1}{3\left(1+\frac{3\omega_{\rm b}}{(1+z)4\omega_\gamma}\right)} \equiv \frac{1}{3[1+r(1+z)^{-1}]}\ , \tag{4.2}$$

where we have introduced $r \equiv 3\omega_{\rm b}/4\omega_\gamma$. For the sound horizon we obtain[1]

$$\begin{aligned}(1+z_*)r_s(z_*) &= \int_0^{t_*} \frac{c_s(t')}{a(t')}dt' \\ &= \frac{h}{H_0\sqrt{3}}\int_{1+z_*}^{\infty} \frac{dx}{x\sqrt{(x+r)(x\omega_r+\omega_{\rm m})}} \\ &= \frac{2h}{H_0\sqrt{3r\omega_{\rm m}}}\log\left(\frac{\sqrt{1+z_*+r}+\sqrt{\frac{(1+z_*)r\omega_r}{\omega_m}+r}}{\sqrt{1+z_*}\left(1+\sqrt{\frac{r\omega_r}{\omega_{\rm m}}}\right)}\right) . \end{aligned} \tag{4.3}$$

Note that $h/H_0 = 1/(100\text{km/s/Mpc}) \approx 2998$ Mpc is a fixed scale which does not depend on the cosmological model. The photon energy density $\omega_\gamma \approx 2.48\times10^{-5}$ is known as well as the CMB temperature and we do not treat it as a free parameter. Assuming massless neutrinos, the same is true for the radiation density [36], $\omega_r = \omega_\gamma\left(1+3\frac{7}{8}\left(\frac{4}{11}\right)^{4/3}\right) \approx 4.17\times10^{-5}$. Furthermore, for standard radiation content, $z_* \approx 1090$ and it depends weakly on $\omega_{\rm b}$ and $\omega_{\rm c}$ (for an analytical approximation, see [59]). For standard values of the parameters, the log in (4.3) is of order unity. The sound horizon at decoupling therefore depends only on $\omega_{\rm b}$ and $\omega_{\rm c}$. The angle under which it is observed today is given by $\theta_A \equiv r_s(z_*)/D_A(z_*)$. With $\omega_{\rm b}$ and $\omega_{\rm c}$ fixed, the pattern of CMB anisotropies is determined at decoupling (apart from low multipoles), and its angular scale changes as the distance to the last scattering surface grows and the multipole positions of the CMB peaks and troughs scale with $D_A(z_*)$. Given our assumptions, the CMB (apart from low multipoles) has no sensitivity to any physical parameters other than $\omega_{\rm b}, \omega_{\rm c}, n_s, D_A$ and the overall amplitude, and these five parameters are a priori independent. A given model can of course couple them to each other, as well as to parameters which do not directly affect the CMB.

In particular, in linearly perturbed FL models the spatial curvature affects the CMB only via the angular diameter distance (apart from the late ISW effect). It is sometimes said that the spatial curvature can be determined from CMB observations by using the sound horizon as a standard ruler (assuming that the universe can be described by a FL model). However, as (4.1) shows, the effect of spatial curvature on $D_A(z_*)$ is completely degenerate with the expansion history $H(z)$. For example, FL models with matter and significant spatial curvature are consistent with the WMAP observations [117]. In that case, a prior on H_0 is enough to exclude large spatial curvature, but only because of the specific form of the expansion history. The only way to really measure the spatial curvature, as opposed to doing parameter estimation in the context of specific models, is to use independent observations of the distance and expansion rate [24], such as from the ages of passively evolving galaxies [62] and baryon acoustic oscillations [51]. Note also that the CMB (apart from low multipoles) is sensitive to the expansion history between decoupling and today only via the angular diameter distance; in particular, the CMB contains no model-independent information about H_0.

In addition to R, another parameter defined as

$$\ell_A \equiv \frac{\pi}{\theta_A} = \pi\frac{D_A(z_*)}{r_s(z_*)} \tag{4.4}$$

[1]Here r_s is the physical sound horizon at the time of decoupling. In the literature, r_s often denotes the comoving sound horizon.

has also been introduced to parametrise the distance to the last scattering surface [60]. The parameter ℓ_A is related to the position of the first peak in multipole space (for details, see [36, 88, 60, 30]). The quantity ℓ_A has been called an independent shift parameter in addition to R [122]. However, this is somewhat misleading, because R and ℓ_A contain the same information as regards the shift in the angular scale of the CMB anisotropy pattern due to the late-time evolution, the only difference is their dependence on $\omega_{\rm b}$ and $\omega_{\rm c}$. Of course, one can consider any combination of the four parameters $\omega_{\rm b}, \omega_{\rm c}, n_s$ and R. For our purposes, it is useful to introduce the scale parameter S, which is defined as the ratio of the angular diameter distance to the prediction of the simplest cosmological model,

$$S \equiv \frac{D_A(z_*)}{D_{A,EdS}(z_*)} = \frac{H_0(1+z_*)D_A(z_*)}{2[1-(1+z_*)^{-1/2}]} \simeq \frac{1}{2}H_0(1+z_*)D_A(z_*) \ , \qquad (4.5)$$

where $D_{A,EdS}$ is the angular diameter distance in the Einstein-de Sitter (EdS) universe (the matter-dominated spatially flat FL model), $(1+z)D_{A,EdS} = 2H_0^{-1}[1-(1+z)^{-1/2}]$; the last approximation in (4.5) is accurate to 3%. Using (4.1), the scale parameter S is related to R by $S = hR/(2\omega_{\rm m}^{1/2})[1-(1+z_*)^{-1/2}]^{-1} \simeq hR/(2\omega_{\rm m}^{1/2})$. Unlike R and ℓ_A, the scale parameter S depends on the Hubble parameter, to which the CMB has no direct sensitivity. (This arises because FL models predict the distance in units of H_0.) Therefore, the value of S depends on how we fix the Hubble parameter.

We can simply keep H_0 free and quote limits for $h^{-1}S$, and one can then substitute the Hubble parameter given by e.g. local observations of H_0. The mean value is $h^{-1}S = 2.4$ (see table 4.4), so for $h = 0.6$–0.7, the distance to the last scattering surface is a factor of 1.4–1.7 longer than in an EdS model with the observed Hubble parameter. This is in accordance with the usual intuition that physics in the late-time universe acts to increase the distance compared to EdS, for example via accelerated expansion. We could instead keep the age of the universe fixed, i.e. ask how large the distance is compared to the value in an EdS model at the same time after the big bang. In an EdS model $H_0 = 2/(3t_0)$, so we have $S = 2/(3t_0 100{\rm km/s/Mpc}) \times R/(2\omega_{\rm m}^{1/2})[1-(1+z_*)^{-1/2}]^{-1}$, which for $t_0 = 13.4$ Gyr [74] gives $S \approx 1.2$ for our mean values $\omega_{\rm m} = 0.145$ and $R = 1.77$.

Finally, we can ask how long the distance is compared to an EdS model which has the correct matter density. The Hubble parameter is then simply $h = \omega_{\rm m}^{1/2}$, so $S = R/2[1-(1+z_*)^{-1/2}]^{-1} \simeq R/2 \approx 0.9$. This means that in an EdS model with the correct matter density, the predicted distance to the last scattering surface is *longer* than observed. (In other words, the real matter density decays faster as function of the distance to the last scattering surface than in the EdS reference model.) Unless otherwise noted, we follow this last convention, and compare with an EdS model which has the correct matter density, at the expense of the age of the universe and the Hubble parameter. We give constraints for θ_A, ℓ_A, R, S, $h^{-1}S$, and $D_A(z_*)$ in section 4.3. For fixed $\omega_{\rm b}$, $\omega_{\rm c}$ and n_s, these quantities contain the same information, only their correlation properties with the parameters $\omega_{\rm b}$, $\omega_{\rm c}$ and n_s are different (see table 4.5).

4.2.3 The distance to the last scattering surface

Let us now study how the CMB spectrum depends on the angular diameter distance to the last scattering surface $D_A(z_*)$. We consider two positions on the sky denoted by $\mathbf{n}_1$ and $\mathbf{n}_2$ which have the temperature fluctuations $\Delta T(\mathbf{n}_1)$ and $\Delta T(\mathbf{n}_2)$ and which are separated by proper distance L on the last scattering surface. For two different angular diameter

distances D_A and D'_A to the last scattering surface, the length L is seen under the angles $\theta = L/D_A$ and $\theta' = L/D'_A$, see figure 4.1.

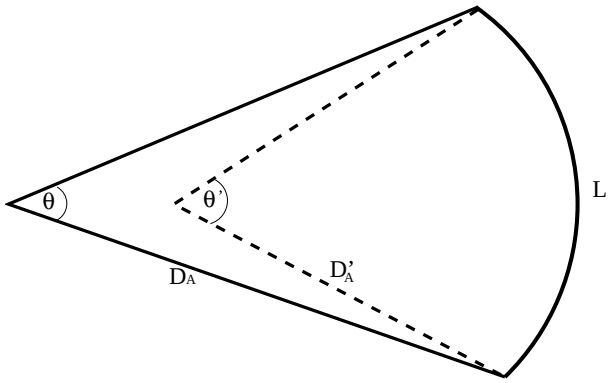

Figure 4.1: The angle under which two fixed points on the sky are seen changes with the angular diameter distance D_A.

The two-point functions $\mathcal{C}$ and $\mathcal{C}'$ which correlate $\mathbf{n}_1$ and $\mathbf{n}_2$ for an observer at distance D_A or D'_A, respectively, can be decomposed in terms of the two angles as

$$\begin{aligned} \mathcal{C}(\theta) \equiv \langle \Delta T(\mathbf{n}_1) \Delta T(\mathbf{n}_2) \rangle &= \frac{1}{4\pi} \sum_\ell (2\ell+1) C_\ell P_\ell(\cos\theta) \\ &= \frac{1}{4\pi} \sum_\ell (2\ell+1) C'_\ell P_\ell(\cos\theta') = \mathcal{C}'(\theta') \,, \end{aligned} \tag{4.6}$$

where P_ℓ is the Legendre polynomial of degree ℓ, and C_ℓ and C'_ℓ are the power spectra corresponding to the angular diameter distances D_A and D'_A respectively. The equality $\mathcal{C}(\theta) = \mathcal{C}'(\theta')$ means that we consider only correlations on the last scattering surface (or very close to it) and neglect line-of-sight effects like, e.g. the late ISW effect which can be different for the two photon paths. Using the orthogonality of the Legendre polynomials, $\int_{-1}^{1} P_{\tilde\ell}(\mu) P_\ell(\mu) d\mu = 2\delta_{\ell,\tilde\ell}/(2\ell+1)$, we obtain the relation

$$C_\ell = \sum_{\tilde\ell} \frac{2\tilde\ell + 1}{2} C'_{\tilde\ell} \int_0^\pi \sin\theta d\theta P_{\tilde\ell}[\cos(\theta D_A / D'_A)] P_\ell(\cos\theta) \,. \tag{4.7}$$

This cumbersome exact expression is only needed for low values of ℓ. At high ℓ we can work in the flat sky approximation (see [36], section 5.4), where

$$Y_{\ell m} \to \frac{1}{2\pi} \exp(i\boldsymbol{\ell} \cdot \mathbf{x}) \quad \text{and } P_\ell(\cos\theta) \to J_0(|\mathbf{x}|\ell) \,.$$

Here $\mathbf{x}$ is a vector on the flat sky, $\boldsymbol{\ell}$ is the variable of its 2-dimensional Fourier transform, with $\ell = |\boldsymbol{\ell}|$, and J_0 is the Bessel function of order 0. Denoting $r \equiv |\mathbf{x}|$, the correlation function is

$$\mathcal{C}(\theta) = \mathcal{C}(r) = \frac{1}{2\pi} \int_0^\infty d\ell \, \ell J_0(r\ell) C_\ell \,. \tag{4.8}$$

The correlation functions corresponding to the two angular diameter distances are related

by $\mathcal{C}(r) = \mathcal{C}'(r')$, where $r' = rD_A/D'_A$,

$$\begin{aligned} \frac{1}{2\pi}\int_0^\infty d\ell\,\ell J_0(r\ell)C_\ell &= \frac{1}{2\pi}\int_0^\infty d\ell\,\ell J_0(r'\ell)C'_\ell \\ &= \frac{1}{2\pi}\left(\frac{D'_A}{D_A}\right)^2\int_0^\infty d\ell\,\ell J_0(r\ell)C'_{\frac{D'_A}{D_A}\ell}\,, \end{aligned} \tag{4.9}$$

where on the second line we have simply performed the change of variables $\ell \to \ell D_A/D'_A$. Using the property $\int_0^\infty r dr J_0(r\ell)J_0(r\ell') = \ell^{-1}\delta(\ell-\ell')$, we obtain

$$C_\ell = \left(\frac{D'_A}{D_A}\right)^2 C'_{\frac{D'_A}{D_A}\ell}\,. \tag{4.10}$$

The relation (4.10) is valid independent of spatial curvature, since we do not invoke three-dimensional Fourier transforms. We are simply using the fact that the CMB anisotropies are functions on a sphere. This result agrees with [128] where it is derived in a different way and contrasts with [25], where there is an extra power of D'_A/D_A. Let us denote the spectrum of a reference EdS Universe by C_ℓ^{EdS} and the measured CMB spectrum by C_ℓ. Recalling the definition (4.5) of the scale parameter S, we can assign C_ℓ to an EdS universe with the same values of $\omega_{\rm b}$, $\omega_{\rm c}$ and n_s and the angular diameter distance $D_A = SD_{A,EdS}$ if we scale the angular power spectrum by

$$C_\ell = S^{-2}C^{EdS}_{S^{-1}\ell}\,. \tag{4.11}$$

The basic assumption here is that the CMB fluctuations at decoupling are the same for both models and the only difference is the distance to the last scattering surface. If this is true, the relation (4.11) is exact in the flat sky limit. Without the flat sky approximation it has to be replaced by (4.7) with $D_A/D'_A = S$. Note that despite of the factor S^{-2} in (4.11), the shift parameter S is not strongly correlated with the amplitude, it just *shifts* the spectrum in angular space. This is visible on the 2D-plots shown in Fig. 4.7. We have tested the flat sky approximation numerically and have found that for $\ell \geq 20$ the difference between (4.11) and the exact expression (4.7) is smaller than 1% for $1.1 \geq S \geq 0.7$, which includes the region which is of interest to us (the mean value we obtain is $S = 0.91 \pm 0.01$, see table 4.4).

To illustrate the dependence of the CMB spectra on the scale parameter S, we show in appendix 4.5.1 the TT, TE and EE spectra for FL models with non-zero spatial curvature or cosmological constant, compared with the EdS result scaled with S. As shown in figures 4.9 to 4.11, the spectra for the scaled model and the model with spatial curvature lie on top of each other for $\ell \gtrsim 20$, except for the case of large negative spatial curvature with $S \approx 1.5$, where there is some difference in the TT spectra until $\ell \approx 100$. For the cosmological constant case, shown in figure 4.12, the approximation is excellent for all of the spectra for $\ell \gtrsim 20$.

$\ell_{\rm min}$	2	20	40	60
$100\omega_{\rm b}$	$2.21^{+0.05}_{-0.05}$	$2.19^{+0.05}_{-0.05}$	$2.18^{+0.07}_{-0.07}$	$2.15^{+0.08}_{-0.08}$
$\omega_{\rm c}$	$0.113^{+0.005}_{-0.005}$	$0.115^{+0.006}_{-0.006}$	$0.118^{+0.007}_{-0.007}$	$0.120^{+0.008}_{-0.008}$
n_s	$0.95^{+0.01}_{-0.01}$	$0.95^{+0.01}_{-0.01}$	$0.94^{+0.02}_{-0.02}$	$0.93^{+0.02}_{-0.02}$
Ω_Λ	$0.72^{+0.03}_{-0.03}$	$0.71^{+0.04}_{-0.03}$	$0.70^{+0.04}_{-0.04}$	$0.68^{+0.06}_{-0.05}$
$\ell_{\rm min}$	80	100	120	140
$100\omega_{\rm b}$	$2.09^{+0.10}_{-0.10}$	$2.05^{+0.09}_{-0.09}$	$2.11^{+0.13}_{-0.12}$	$2.07^{+0.14}_{-0.14}$
$\omega_{\rm c}$	$0.127^{+0.012}_{-0.013}$	$0.132^{+0.012}_{-0.012}$	$0.126^{+0.013}_{-0.016}$	$0.131^{+0.018}_{-0.017}$
n_s	$0.91^{+0.03}_{-0.04}$	$0.89^{+0.04}_{-0.03}$	$0.91^{+0.05}_{-0.04}$	$0.90^{+0.05}_{-0.06}$
Ω_Λ	$0.62^{+0.09}_{-0.09}$	$0.58^{+0.10}_{-0.09}$	$0.63^{+0.11}_{-0.10}$	$0.58^{+0.14}_{-0.14}$

Figure 4.2: The change in the mean parameters when more low ℓ data are omitted, in the ΛCDM model with $\tau = 0$. We have used the WMAP5 and ACBAR data.

4.3 Results

4.3.1 Cosmological parameters and the multipole cut

We use the WMAP5 data and the ACBAR data in our analysis. However, disregarding ACBAR does not change the results much. We have performed a Markov Chain Monte Carlo analysis with chain length $N = 2 \times 10^5$. The results change by significantly less than 1σ when going from $N = 1.5 \times 10^5$ to 2×10^5, which indicates that the chains have converged well [81]. As a convergence test, we have checked that when the samples are split in two or three parts, the change of the relevant cosmological parameters is a few percent of one standard deviation. We have also checked that the Raftery and Lewis convergence diagnostic is satisfied [96].

In table 4.2 we show the effect of excluding a successively larger multipole range up to $\ell_{\rm min}$ in the analysis of the ΛCDM model; Ω_Λ is the vacuum energy density today, as usual. We have set $\tau = 0$ for consistency with the treatment of the scaled model. From $\ell_{\rm min} = 2$ to $\ell_{\rm min} = 40$ the errors on $\omega_{\rm b}$ and $\omega_{\rm c}$ increase by 28%, while the error on n_s increases by 57%. The central values move only by 1%, 4% and 1%, respectively, and the results are consistent within 1σ.

Nevertheless, there is a systematic trend that $\omega_{\rm b}$ and n_s decrease and $\omega_{\rm c}$ increases as $\ell_{\rm min}$ grows. Even at $\ell_{\rm min} = 100$, where the shifts are maximized, they are less than 2σ in terms of the new error bars. In terms of the error bars of the model with $\ell_{\rm min} = 2$, the shift is of course larger: for n_s it more than 5σ, and for Ω_Λ more than 4σ. The feature that the error bars on n_s increase more than those of $\omega_{\rm b}$ and $\omega_{\rm c}$ may be related to the fact that as $\ell_{\rm min}$ grows, the pivot scale $k = 0.05$ Mpc^{-1} moves closer to the edge of the data [77].

Part of this shift is due to the fact that reionization is neglected. We know from the absence of the Gunn-Peterson trough in quasar spectra that the Universe is reionized at redshifts $z \lesssim 6$, see [7]. The light decrease towards smaller scales which is usually attributed to reionization is now achieved with a somewhat redder spectrum. In order not to decrease the height of the acoustic peaks, this leads to a higher value of $\omega_{\rm c}$. A redder spectrum also enhances the amplitude difference between the well measured first and second peaks. This can be compensated by a reduction of $\omega_{\rm b}$, since a larger $\omega_{\rm b}$ means a larger difference between the odd contraction and even expansion peaks [36].

However, we have found that reionization is not the dominant effect, the systematic shift is also present if reionization is included in the analysis. We have checked this by including τ as a model parameter. The results of table 4.2 remain valid for also in this case. The problem is that for $\ell_{\rm min} \geq 40$ the value of τ is degenerate with a renormalization of the amplitude (see discussion in Appendix 4.5.2) and the best fit value for τ fluctuates significantly from chain to chain. We therefore prefer to show the results for $\tau = 0$. Note that the change is larger than the increase in the error bars. The shape of the one-dimensional probability distribution for the parameters is not for the most part significantly distorted, and the two-dimensional distributions do not show strong changes in the correlation properties as $\ell_{\rm min}$ increases. Therefore, the error bars do accurately represent the statistical error even at high $\ell_{\rm min}$. In other words, the shift in the parameters is systematic, and is not reflected in the statistical error estimate.

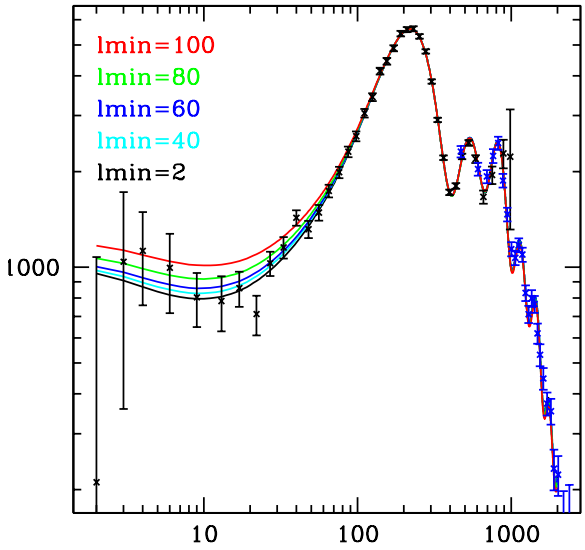

Figure 4.3: The increase in the large-scale power with increasing $\ell_{\rm min}$ in the best-fit ΛCDM models with $\tau = 0$. The lowest line corresponds to a cut at $\ell_{\rm min} = 2$ the subsequent lines have $\ell_{\rm min} = 40,\ 60,\ 80$ and 100, respectively. At $\ell_{\rm min} = 120$ the large scale power no longer increases but it decreases somewhat. The WMAP and ACBAR data are superimposed. The vertical axis is $\ell(\ell+1)C^{TT}/(2\pi)$ in $(\mu K)^2$.

We conclude that the high ℓ data prefer different parameter values than the data which include the low multipoles. In figure 4.3 we show the TT power spectra for the best-fit ΛCDM models with different $\ell_{\rm min}$. There is a trend of increasing large-scale power with higher $\ell_{\rm min}$. In all cases, the overall amplitude is fixed well by the high ℓ data, and the effect is due to the change in $\omega_{\rm b}, \omega_{\rm c}$ and n_s. We have checked that the ISW effect is not the cause: there is a similar shift for both the ΛCDM model and the scaled EdS model. Also, increasing $\ell_{\rm min}$ corresponds to decreasing Ω_Λ and hence a smaller contribution of the ISW effect to the low multipoles.

Parameter	Scaled $\ell_{\rm min} = 40$ mean	ΛCDM $\ell_{\rm min} = 40$ mean	ΛCDM $\ell_{\rm min} = 2$ mean
$100\omega_{\rm b}$	2.13 ± 0.05	2.21 ± 0.07	2.24 ± 0.05
$\omega_{\rm c}$	0.124 ± 0.007	0.113 ± 0.007	0.111 ± 0.005
n_s	0.93 ± 0.02	0.96 ± 0.02	0.97 ± 0.01
S	0.91 ± 0.01	–	–
Ω_Λ	–	0.72 ± 0.04	0.74 ± 0.03
τ	–	$0.09^{+0.04}_{-0.05}$	0.09 ± 0.02
ω_m	0.145 ± 0.007	0.136 ± 0.007	0.133 ± 0.005
$h^{-1}S$	2.40 ± 0.03	–	–
R	1.77 ± 0.02	1.73 ± 0.02	1.72 ± 0.02
θ_A	$0.593^\circ \pm 0.001^\circ$	$0.594^\circ\,^{+0.002^\circ}_{-0.001^\circ}$	$0.593^\circ \pm 0.002^\circ$
ℓ_A	303.7 ± 0.7	303.3 ± 0.8	303.2 ± 0.7
$D_A(z_*)$/Mpc	12.7 ± 0.2	12.9 ± 0.2	13.0 ± 0.1
$r_s(z_*)$/Mpc	0.132 ± 0.002	0.134 ± 0.002	0.134 ± 0.001
$10^{-3} z_{\rm eq}$	3.5 ± 0.2	3.3 ± 0.2	3.2 ± 0.1
z_*	1094 ± 1	1092 ± 1	1091 ± 1

Figure 4.4: The mean values for the scaled model and the ΛCDM model. We have used the WMAP5 and ACBAR data for $\ell \geq \ell_{\rm min} = 40$.

4.3.2 Model-independent parameter estimates

We fix our multipole cut at $\ell_{\rm min} = 40$, which roughly corresponds to neglecting modes which entered the horizon after $z = 60$. The dependence on the redshift is weak, $\ell_{\rm min} \propto (1+z)^{1/2}$ for $z \gg 1$. Choosing $z = 30$ instead would give $\ell_{\rm min} \approx 30$. The cut at $\ell_{\rm min} = 40$ is also motivated by the fact that for $\ell > 40$ reionization is well approximated by a simple rescaling of the amplitude, as well as by the multipole dependence of the late ISW effect, see appendices 4.5.1 and 4.5.2.

In table 4.4 we give the mean values for our primary parameters $\omega_{\rm b}$, $\omega_{\rm c}$, n_s and S, as well as some derived parameters. In addition to the systematic effect discussed above, this table is our main result. As already mentioned, the overall amplitude is treated as a nuisance parameter. For comparison, we give the corresponding results for the ΛCDM model, with non-zero τ. We use $\ell_{\rm min} = 40$ in both cases. The ΛCDM values are in good agreement with the WMAP5 results [32] and have comparable error bars. For the scaled model, the errors in $\omega_{\rm c}$ and n_s are slightly larger than those of the ΛCDM model with $\ell_{\rm min} = 2$. We attribute this to the fact that we start at $\ell_{\rm min} = 40$. Furthermore, our spectral index is somewhat redder, $n_s = 0.93$ compared to $n_s = 0.96$. This shift is also clearly seen in the one-dimensional likelihood functions for the scaled model and the ΛCDM model, shown in figure 4.6. However, these parameter changes are within one standard deviation and are therefore not statistically significant. It is impressive how accurately present CMB data determine ℓ_A. The relative error is less than 0.3% for both the scaled model and ΛCDM. The error in the other parameters related to the angular diameter distance, $S, h^{-1}S, R$ and

	$\omega_{\rm b}$	$\omega_{\rm c}$	n_s	S	$\omega_{\rm m}$	$h^{-1}S$	ℓ_A	$D_A(z_*)$	$r_s(z_*)$	z_*
$\omega_{\rm b}$	1.00	−0.31	0.84	−0.49	−0.23	−0.06	−0.56	0.02	0.14	−0.88
$\omega_{\rm c}$	−0.31	1.00	−0.51	0.96	1.00	−0.91	0.05	−0.94	−0.98	0.72
n_s	0.84	−0.51	1.00	−0.65	−0.45	0.19	−0.51	0.26	0.38	−0.86
S	−0.49	0.96	−0.65	1.00	0.94	−0.78	0.30	−0.82	−0.91	0.83
$\omega_{\rm m}$	−0.23	1.00	−0.45	0.94	1.00	−0.94	−0.004	−0.96	−1.00	0.66
$h^{-1}S$	−0.06	−0.91	0.19	−0.78	−0.94	1.00	0.32	1.00	0.96	−0.40
ℓ_A	−0.56	0.05	−0.51	0.30	−0.004	0.32	1.00	0.27	0.06	0.43
$D_A(z_*)$	0.02	−0.94	0.26	−0.82	−0.96	1.00	0.27	1.00	0.98	−0.47
$r_s(z_*)$	0.14	−0.98	0.38	−0.91	−1.00	0.96	0.06	0.98	1.00	−0.58
z_*	−0.88	0.72	−0.86	0.83	0.66	−0.40	0.43	−0.47	−0.58	1.00

Figure 4.5: The normalized covariance matrix for the scaled model. We have used the WMAP5 and ACBAR data for $\ell \geq \ell_{\rm min} = 40$. At this level of precision, the correlation coefficients of R are the same as those of S, and those of θ_A are minus those of ℓ_A.

D_A, as well as r_s, is about 1%. The errors for $\omega_{\rm b}, \omega_{\rm c}$ and n_s are less than 3%, 6% and 2%, respectively.

In table 4.5 we give the covariance matrix between the different variables, and in figure 4.7 we show selected two-dimensional likelihoods. We see that R and S are strongly positively correlated with $\omega_{\rm c}$ and $\omega_{\rm m}$. In contrast, D_A is strongly anti-correlated with $\omega_{\rm c}$ and $\omega_{\rm m}$. This can be understood by writing $D_A = SD_{A,EdS}$ and noting that $D_{A,EdS} \propto h^{-1} = \omega_{\rm m}^{-1/2}$. The variable ℓ_A is nearly uncorrelated with $\omega_{\rm m}$, but it is quite correlated with $\omega_{\rm b}$ and correspondingly also with n_s. Since most of the statistical weight of the WMAP data come from the first and second peaks, n_s and $\omega_{\rm b}$ are strongly correlated even if the full WMAP data (with $\ell_{\rm min} = 2$) are taken into account [66]. This correlation becomes stronger as some of the low ℓ data are omitted.

The standard deviations for the scaled EdS model are somewhat smaller than those of the ΛCDM model for the same $\ell_{\rm min}$. However, this does not mean that the fit is better, only that the well-fitting region is somewhat smaller. Error bars for a model can be small simply because different parts of the data prefer different regions of parameter space, so that the fit is good only in some small overlap region. In the present case, the scaled model and the ΛCDM model are comparably good fits to the data for $\ell_{\rm min} \geq 20$. In table 4.8 we show $-2\log\mathcal{L}$, where $\mathcal{L}$ is the likelihood of the best-fit, as a function of $\ell_{\rm min}$. There are only differences of ≈ 1 in $-2\log\mathcal{L}$, which is the same order as the differences between different chains of the same model.

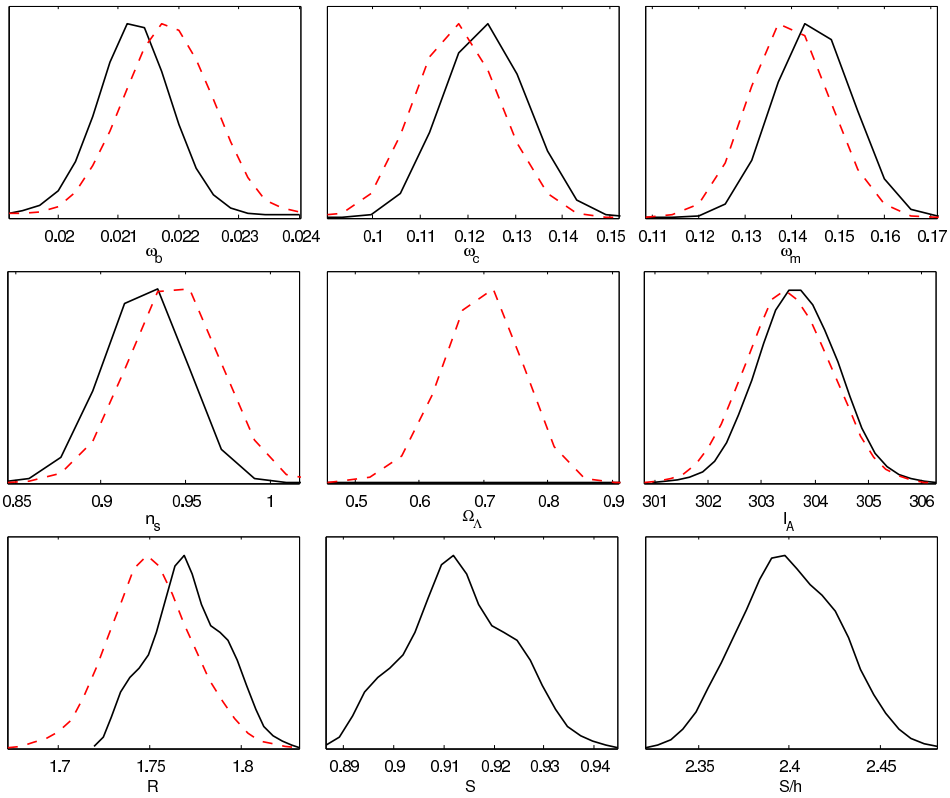

Figure 4.6: One-dimensional likelihoods for the scaled model (black, solid) and the ΛCDM model (red, dashed). We have used the WMAP5 and ACBAR data for $\ell \geq \ell_{\rm min} = 40$.

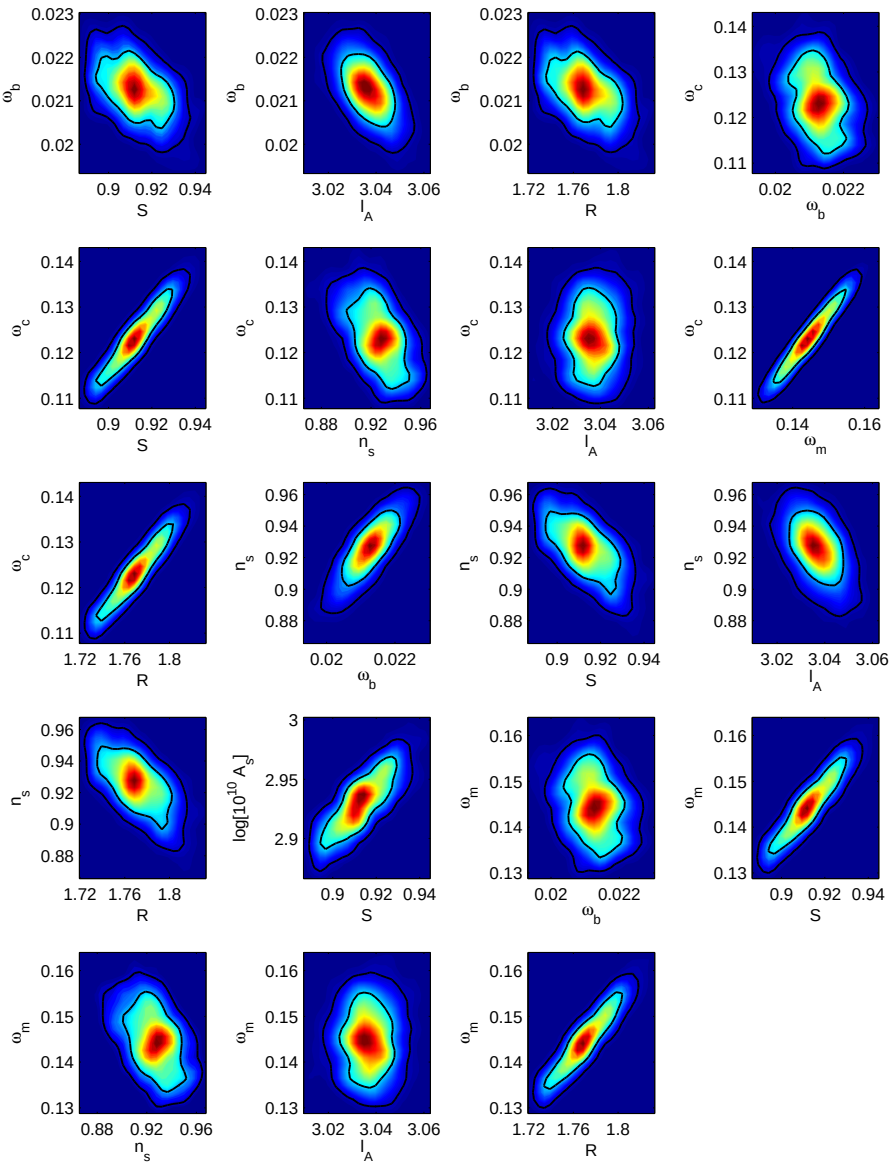

Figure 4.7: Two-dimensional likelihoods for the scaled model. We have used the WMAP5 and ACBAR data for $\ell \geq \ell_{\rm min} = 40$.

4.3.3 Discussion

The CMB contains information about the distance to the last scattering surface, the baryon density, the matter density and the primordial power spectrum (here taken to be a power law), which can be extracted independently of the model used to describe the late universe. In particular, the angular diameter distance to the last scattering surface is a factor of $S = 0.91 \pm 0.01$ smaller than in an EdS Universe with the same mean matter density, $\omega_{\rm m} = 0.145 \pm 0.006$. With baryon density $\omega_{\rm b} = 0.0213 \pm 0.001$ and spectral index $n_s = 0.93 \pm 0.03$, an EdS model scaled by this factor is a good fit to the present CMB data, apart from the low multipoles. Of course such a model is in complete disagreement with local measurements of the Hubble parameter and supernova observations. If we want to

$\ell_{\rm min}$	nr. of points $N(\ell_{\rm min})$	$-2\log\mathcal{L}$ scaled	$-2\log\mathcal{L}$ standard, $\tau = 0$	$-2\log\mathcal{L}$ standard, $\tau \neq 0$
2	2591	2717.12	2715.78	2695.29
20	1385	1508.20	1507.41	1507.72
40	1345	1382.52	1381.24	1381.24
60	1305	1234.44	1233.23	1233.46
80	1265	1073.03	1072.01	1072.16

Figure 4.8: The log of the likelihood $\mathcal{L}$ as function of $\ell_{\rm min}$. In the second column we give the number of C_ℓ estimates (including the polarization data) except for the case $\ell_{\rm min} = 2$ where a pixel-likelihood is added. For $\ell_{\rm min} \geq 20$, $N(\ell_{\rm min}) = 994 + 427 - 2(\ell_{\rm min} - 1)$, which is the number of multipoles for the TT (WMAP5 and ACBAR data) and TE (WMAP5 data) spectra minus twice the number of cut multipoles. The only significant difference between models appears in the first row with $\ell_{\rm min} = 2$, where the ΛCDM model with $\tau \neq 0$ is clearly favoured.

agree with the local value $H_0 = (60–70)$ km/s/Mpc, the observed distance is instead longer than in an EdS model by the factor $h^{-1}S \approx 1.4–1.7$. From the CMB we cannot determine at which point between last scattering and today the distance evolution diverges from the EdS case; from supernova observations, we know that this happens between a redshift of order unity and today. Any viable cosmological model has to explain this change in the distance scale, whether the reason is dark energy, modified gravity or large deviations from the FL geometry.

Constraints on R, ℓ_A and other parameters have been presented earlier in [66, 46, 122, 27, 89, 67], where the data have been analysed in the context of different models for dark energy, also taking into account effects like neutrino masses which we do not consider. Our mean value for R is larger (and $\omega_{\rm b}$ and n_s are smaller) than in those studies, because of the systematic shift due to cutting away the low multipoles. The increase in the error bars is smaller than the change in the mean values, as they do not take into account the systematic shift. The shift indicates that different parts of the data prefer different parameter values, which frustrates the effort to give precise model-independent error bars, because the only way to reduce model-dependence is to exclude the part of the data which is most likely subject to unknown physical effects. We think that cutting the multipoles below $\ell_{\rm min} = 40$ strikes a good balance between reducing model-dependence and not discarding data needlessly.

The cosmological parameter most robustly determined by the CMB in a model-independent manner is the ratio $\ell_A = \pi D_A(z_*)/r_s(z_*)$, which does not undergo a systematic shift with increasing $\ell_{\rm min}$, unlike $\omega_{\rm b}, \omega_{\rm c}, n_s, R$ or $D_A(z_*)$. It is interesting that as low multipoles are cut, the spectral index becomes smaller, making the evidence for violation of scale-invariance in the initial conditions stronger. For $\ell_{\rm min} \geq 80$, values $n_s < 0.9$ are within 1σ of the mean. As for the baryon density, the shift towards smaller values is well within the constraint $1.9 \leq 100\omega_{\rm b} \leq 2.4$ (95% C.L.) from Big Bang Nucleosynthesis [2]. Our value for $\omega_{\rm c}$ is more than 2σ away from the ΛCDM value with no multipole cut, while the error bars increase only by 26%. This model-dependence suggests caution about the value and the error bars of $\omega_{\rm c}$ which enter into codes such as DarkSUSY [52].

In order to be independent of late-time cosmology, we cannot take into account low

ℓ results for the CMB anisotropies. In the final parameters quoted in table 4.4 we have used the data for $\ell \geq \ell_{\rm min} = 40$. At first sight one might hope that our analysis could be significantly improved once the Planck data with precise C_ℓ's up to $\ell \approx 2500$ will be available. However, for $\ell \gtrsim 1000$ CMB lensing can no longer be neglected for data with a precision better than about 4% for the anisotropies and 10% for the polarisation [80, 36]. But lensing and other second order effects depend on the details of the late-time cosmology. Hence our model-independent analysis has to be restricted to the interval of roughly $40 \leq \ell \leq 800$. Higher ℓ data can only be used if the error bars are sufficiently large. For ACBAR this is still marginally possible, but with Planck systematic errors due to late-time effects will have to be added to the high ℓ data. Increased precision in the multipole range $40 \leq \ell \leq 800$ also has to be balanced against contamination by model-dependent secondary effects. We therefore do not expect a substantial improvement of our results from future data.

4.4 Conclusion

We have analysed the CMB data in a way which is independent of the details of late-time cosmology, i.e. the cosmology at redshifts $z \lesssim 60$. The results we have obtained are therefore valid for most models of late-time cosmology, whether they include dark energy, modified gravity, a local void or backreaction.

We have presented model-independent limits on $\omega_{\rm b}$, $\omega_{\rm c}$, n_s and the angular diameter distance to the last scattering surface $D_A(z_*)$, or its ratio with the sound horizon at last scattering, $\theta_A = r_s(z_*)/D_A(z_*)$. The present CMB data give an extraordinarily precise measurement of θ_A, which every realistic model of the late universe must agree with. We can summarize the final result by

$$\begin{aligned} 100\omega_{\rm b} &= 2.13 \pm 0.05 \,, \qquad \omega_{\rm c} = 0.124 \pm 0.007 \\ n_s &= 0.93 \pm 0.02 \,, \qquad \theta_A = 0.593^\circ \pm 0.001^\circ \,. \end{aligned} \tag{4.12}$$

Note that the values of $\omega_{\rm c}$ and $\omega_{\rm b}$ actually determine the matter and baryon density at last scattering via the relation $\rho_x(z_*) = (1+z_*)^3 (H_0/h)^2 \omega_x$. The values of the densities today may be different e.g. if dark matter decays at late times [31].

In summary, every model which satisfies equations (4.12) will automatically be in agreement with the present CMB data for $\ell \geq 40$. Only lower ℓ CMB data, large scale structure, lensing and other observations can distinguish between models which have the above values for $\omega_{\rm b}, \omega_{\rm c}, n_s$ and θ_A.

We have also found that there is a systematic shift in the cosmological parameters as more low ℓ data are cut. As more data from low multipoles is removed, $\omega_{\rm b}$ and n_s decrease, while $\omega_{\rm c}$ becomes larger. These changes keep the power spectrum at small scales fixed, but tend to increase the amplitude on large scales. These changes are not reflected in the statistical error bars: the small angle data prefer different parameter values than the full set of CMB data. This trend is visible to at least $\ell_{\rm min} = 100$. Whether this behaviour has any connection with the various directional features at low multipoles [56, 57, 48, 8], is not clear.

Acknowledgments

We thank Domenico Sapone who participated in the beginning of this project. This work is supported by the Swiss National Science Foundation.

4.5 Appendix

4.5.1 The scale parameter approximation

In this appendix we illustrate the accuracy of the scale parameter approximation for the high multipoles. We consider spectra for FL models with non-zero spatial curvature or cosmological constant, compared with the Einstein-de Sitter result scaled with the parameter S as discussed in section 4.2.3. We keep the matter densities fixed to the WMAP5 best-fit values $\omega_{\rm b} = 0.023$ and $\omega_{\rm c} = 0.11$ [32]. Neglecting the contribution of radiation, the scale parameter in these models is

$$S \simeq \frac{\sqrt{\omega_m}}{2} \int_0^{z_*} \frac{dz}{\sqrt{\omega_m(1+z)^3 + \omega_K(1+z)^2 + h^2 - \omega_m - \omega_K}} \,, \tag{4.13}$$

where $\omega_K \equiv \Omega_K h^2$ and $h^2 - \omega_m - \omega_K = \Omega_\Lambda h^2 \equiv \omega_\Lambda$.

In figure 4.9 we show the TT spectrum for models with positive or negative spatial curvature and the scaled model. The spectra lie on top of each other for $\ell \gtrsim 20$, except for large negative spatial curvature. In figure 4.10 and figure 4.11 we show the TE and EE spectra. The scaled curves are practically indistinguishable from the exact ones at all multipoles, even for large negative spatial curvature. In figure 4.12, we show the spectra for models [illegible] ling approx

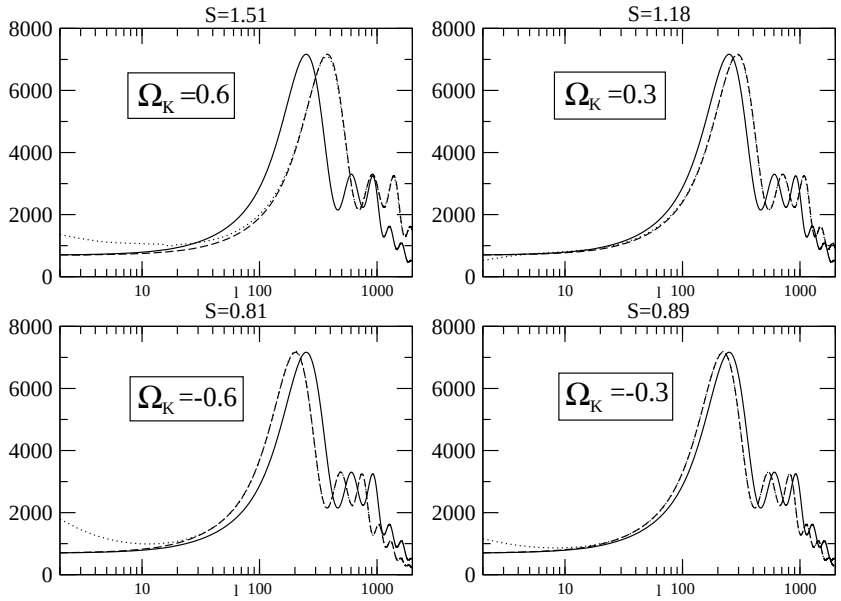

Figure 4.9: The TT spectra for models with $\Omega_\Lambda = 0, \Omega_K \neq 0$. The solid curve corresponds to the Einstein-de Sitter universe, the dotted curve corresponds to a model with Ω_K as specified in the panels, and the dashed curve shows the Einstein-de Sitter universe power spectrum scaled with S. The vertical axis is $\ell(\ell+1)C_\ell^{TT}/(2\pi)$ in $(\mu K)^2$.

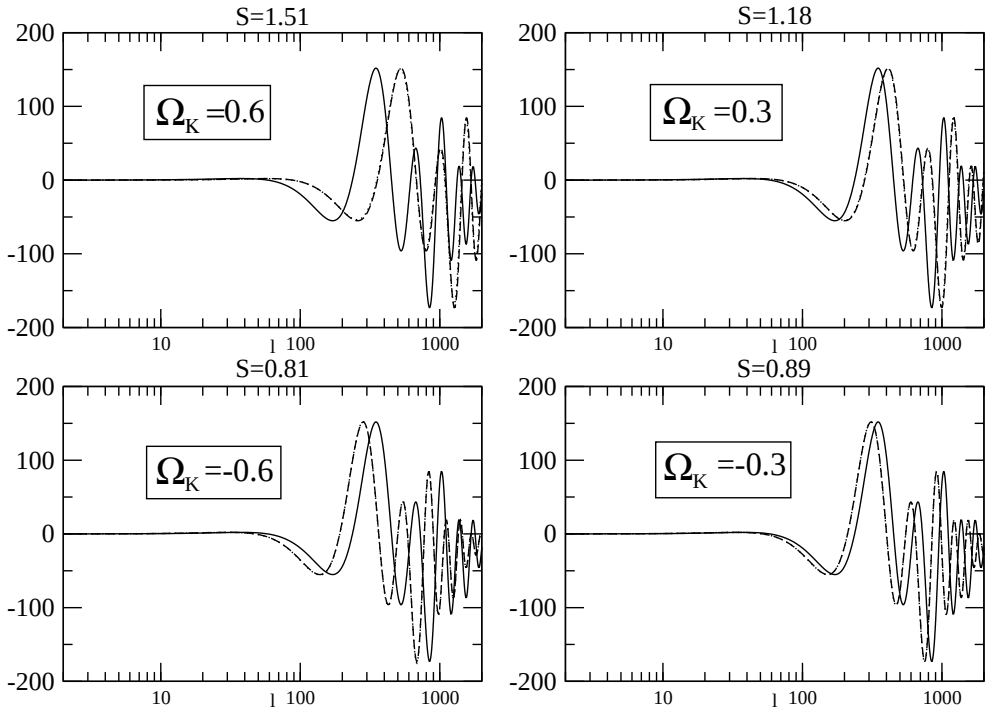

Figure 4.10: As in figure 4.9, but for the TE spectra. The dotted curves are invisible since they are completely overlaid by the dashed ones (scaled model).

4.5.2 Reionization

In this appendix we study the effect of reionization on the angular power spectrum of the CMB. If the baryons are reionized at redshift $z_{\rm ri}$, the effect on scales which are of the order of the horizon size at the time is complicated, and leads to additional polarization and a scale-dependent reduction of the amplitude of anisotropies. However, on scales which are well inside the horizon, the rescattering of photons simply reduces the amplitude of CMB temperature and polarization anisotropies by roughly the same amount on all scales. This effect can therefore be absorbed in a renormalization of the spectrum. In figure 4.13 we show the TT spectrum with and without reionization for the best-fit ΛCDM model, as well as the relative difference of the spectrum with and without reionization. For $\ell \geq 40$, renormalizing the spectrum with a constant reproduces the effect of reionization within about 1.5%. We have done the same with the temperature–polarization cross-correlation and the polarization spectra. Also there renormalization is a very good approximation (better than 0.5% on average) for $\ell \geq 40$, see figures 4.14 and 4.15. To obtain the spectra with $\tau = 0.1$, we have multiplied the spectra with $\tau = 0$ by the factor 0.82.

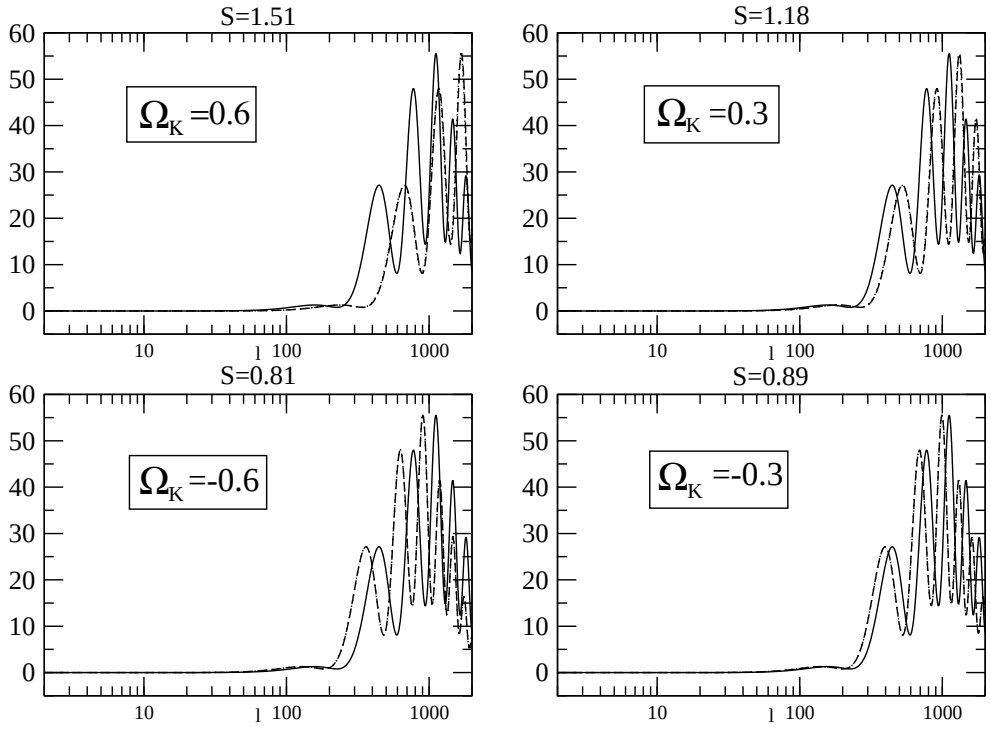

Figure 4.11: As in figure 4.9, but for the EE spectra. The dotted curves are invisible since they are completely overlaid by the dashed ones (scaled model).

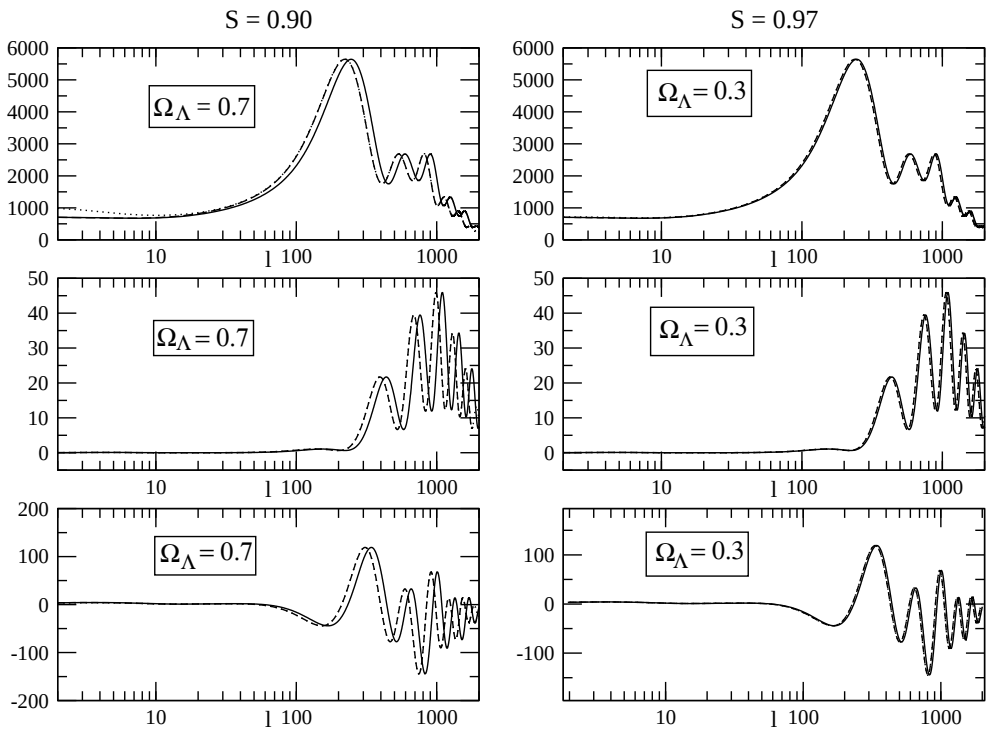

Figure 4.12: As in figure 4.9, but for $\Omega_\Lambda \neq 0, \Omega_K = 0$. We consider two different values for Ω_Λ, corresponding to the two columns. The rows from top to bottom are the TT, EE and TE spectra.

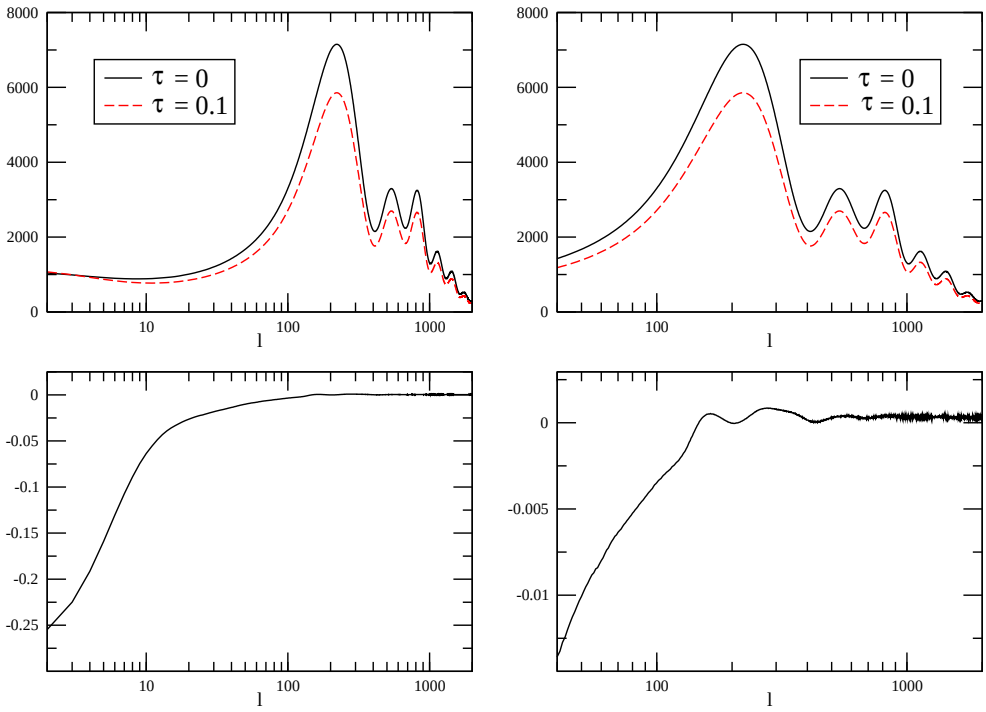

Figure 4.13: The TT power spectrum with (dashed, red) and without (solid, black) reionization for optical depth $\tau = 0.1$ for $\ell \geq 2$ (left upper panel) and $\ell \geq 40$ (right upper panel). For the upper panels, the vertical axis is $\ell(\ell+1)C^{TT}/(2\pi)$ in $(\mu K)^2$. In the lower panel we show the relative difference between the spectrum with and without reionization, when the latter is simply rescaled by a constant. For low ℓ's, the differences are substantial, up to 25%, but for the values $\ell \geq 40$ we consider, the difference is less than 2%.

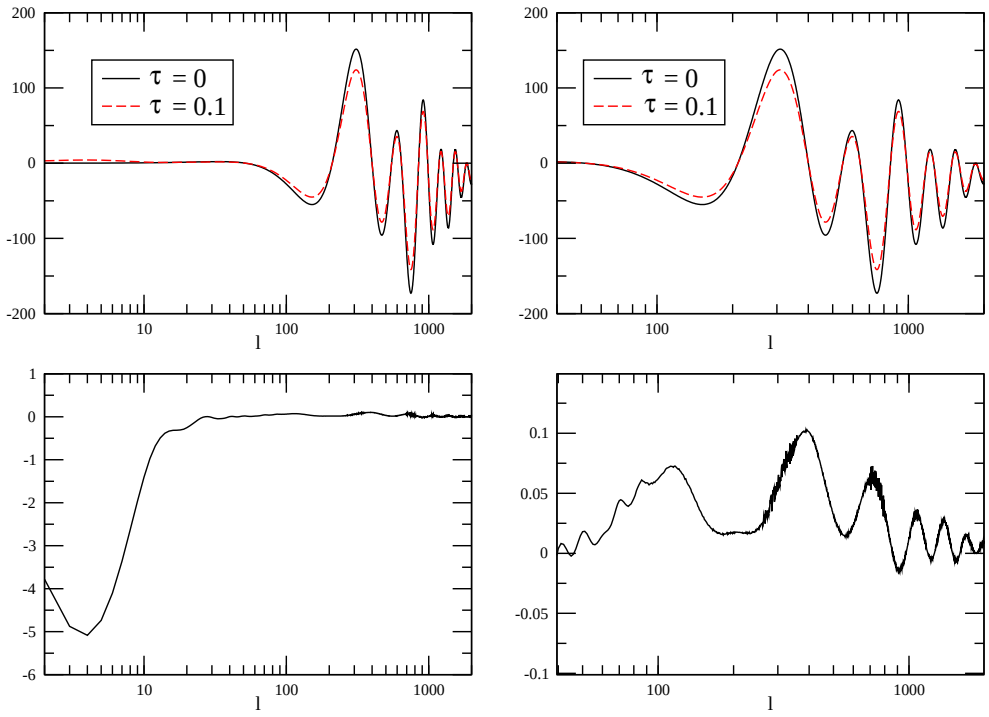

Figure 4.14: The TE correlation spectrum with (dashed, red) and without (solid, black) reionization for optical depth $\tau = 0.1$ for $\ell \geq 2$ (left upper panel) and $\ell \geq 40$ (right upper panel). The vertical axis is $\ell(\ell+1)C^{TT}/(2\pi)$ in $(\mu K)^2$. In the lower panel we show the difference between the spectrum with and without reionization, when the latter is simply rescaled by a constant. For the values $\ell \geq 40$ we consider, the difference is below $0.1(\mu K)^2$.

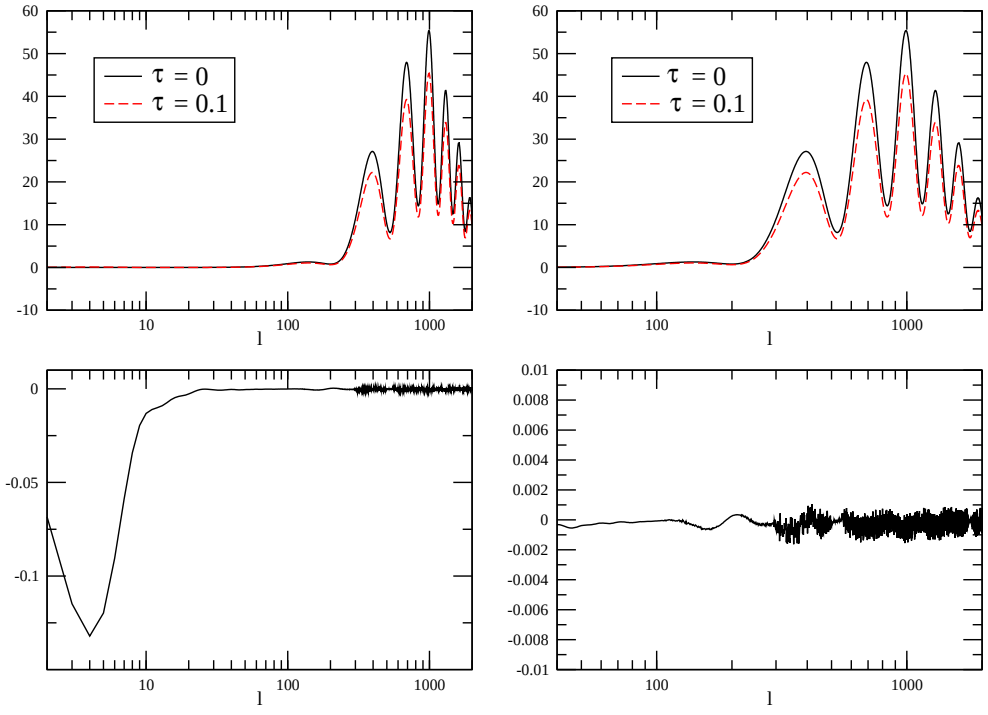

Figure 4.15: As in figure 4.14, but for the EE power spectrum. For $\ell \geq 40$, the difference is below $0.002(\mu K)^2$.

Chapter 5

A large scale coherent magnetic field: interactions with free streaming particles and limits from the CMB

JOURNAL OF ASTROPHYSICS AND ASTROPARTICLE PHYSICS **06**, 017 (2011)

A large scale coherent magnetic field: interactions with free streaming particles and limits from the CMB

Julian Adamek, Ruth Durrer, Elisa Fenu, Marc Vonlanthen

We study a homogeneous and nearly-isotropic Universe permeated by a homogeneous magnetic field. Together with an isotropic fluid, the homogeneous magnetic field, which is the primary source of anisotropy, leads to a plane-symmetric Bianchi I model of the Universe. However, when free-streaming relativistic particles are present, they generate an anisotropic pressure which counteracts the one from the magnetic field such that the Universe becomes isotropized. We show that due to this effect, the CMB temperature anisotropy from a homogeneous magnetic field is significantly suppressed if the the neutrino masses are smaller than 0.3 eV.

5.1 Introduction

On very large scales, the observed Universe is well approximated by a homogeneous and isotropic Friedmann solution of Einstein's equations. This is best verified by the isotropy of the Cosmic Microwave Background (CMB). The small fluctuations observed in the CMB temperature are fully accounted for by the standard model of structure formation from small initial fluctuations which are generated during an inflationary phase. Nevertheless, these small fluctuations are often used to limit other processes or components which may be present in the early Universe, like e.g. a primordial magnetic field.

The generation of the magnetic fields observed in galaxies and clusters [75] is still unclear. It has been shown that phase transitions in the early Universe, even if they do generate magnetic fields, have not enough power on large scale to explain the observed large scale coherent fields [19]. These findings suggest that primordial magnetic fields must be correlated over very large scales.

In this paper, we discuss limits on fields which are coherent over a Hubble scale and which we can therefore treat as a homogeneous magnetic field permeating the entire Universe. We want to derive limits on a homogeneous field from CMB anisotropies. This question has been addressed in the past [4] and limits on the order of $B \lesssim 2 \times 10^{-9}$ Gauss have been derived from the CMB anisotropies [6]. A similar limit can also be obtained from Faraday rotation [111, 69].

We show that the limits from the CMB temperature anisotropy actually are invalid if free streaming neutrinos with masses $m_\nu < T_{\rm dec}$ are present, where $T_{\rm dec}$ denotes the photon temperature at decoupling. This is the case if the neutrino masses are not degenerate, i.e. the largest measured mass splitting is of the order of the largest mass, hence $m_\nu \lesssim 0.04$eV. The same effect can be obtained from any other massless free streaming particle species, like e.g. gravitons, if they contribute sufficiently to the background energy density. This is due to the following mechanism which we derive in detal in this paper: In an anisotropic

Bianchi-I model, free streaming relativistic particles develop an anisotropic stress. If the geometric anisotropy is due to a magnetic field, which scales exactly like the anisotropic stress of the massless particles, this anisotropic stress cancels the one from the magnetic field and the Universe is isotropized. Hence the quadrupole anisotropy of the CMB due to the magnetic field is erased. This 'compensation' of the magnetic field anisotropic stress by free-streaming neutrinos has also been seen in the study of the effects of stochastic magnetic fields on the CMB [90, 116, 12, 76] for the large scale modes. In our simple analysis the mechanism behind it finally becomes clear.

The limits from Faraday rotation are not affected by our arguments.

In the next section we derive the CMB anisotropies in a Bianchi I Universe. In Section 5.3 we show that relativistic free streaming neutrinos in a Bianchi I model develop anisotropic stresses and that these back-react to remove the anisotropy of the Universe if the latter is due to a massless mode. In Section 5.4 we discuss isotropization due to other massless free streaming particles, with special attention to a gravitational wave background. In Section 5.5 we conclude.

5.2 Effects on the CMB from a constant magnetic field in an ideal fluid Universe

We consider a homogeneous magnetic field in $z-$direction, $\mathbf{B} = B\boldsymbol{e}_z$ in a Universe filled otherwise with an isotropic fluid consisting, e.g. of matter and radiation. The metric of such a Universe is of Bianchi type I,

$$ds^2 = -dt^2 + a_\perp^2(t)(dx^2 + dy^2) + a_\parallel^2(t)\, dz^2 \,, \tag{5.1}$$

where t is cosmic time. The Einstein equations in cosmic time read

$$2\frac{\dot{a}_\parallel}{a_\parallel}\frac{\dot{a}_\perp}{a_\perp} + \left(\frac{\dot{a}_\perp}{a_\perp}\right)^2 = 8\pi G\rho \,, \tag{5.2}$$

$$\frac{\ddot{a}_\parallel}{a_\parallel} + \frac{\ddot{a}_\perp}{a_\perp} + \frac{\dot{a}_\parallel}{a_\parallel}\frac{\dot{a}_\perp}{a_\perp} = -8\pi G P_\perp \,, \tag{5.3}$$

$$2\frac{\ddot{a}_\perp}{a_\perp} + \left(\frac{\dot{a}_\perp}{a_\perp}\right)^2 = -8\pi G P_\parallel \,. \tag{5.4}$$

The dot denotes the derivative with respect to t. We have introduced the total energy density $\rho = \rho_B + \rho_m + \rho_\gamma + \rho_\nu + \rho_\Lambda$, where $\rho_B = B^2/8\pi$ is the energy density in the magnetic field, and $\rho_m, \rho_\gamma, \rho_\nu, \rho_\Lambda$ are as usual the energy densities of matter (assumed to be baryons and cold dark matter), photons, neutrinos, and dark energy (assumed to be a cosmological constant), respectively.

All the above constituents of the Universe, except matter (which is assumed to be pressureless) also contribute to the pressure components $P_\parallel, P_\perp$. The contribution from the magnetic field is intrinsically anisotropic and given by

$$P_{B,\perp} = -P_{B,\parallel} = \rho_B \,, \tag{5.5}$$

as can be read off from the corresponding stress-energy tensor. Note that the magnetic field B decays as $a_\perp^{-2}$, so that ρ_B scales as $a_\perp^{-4}$.

For later reference we define an 'average' scale factor

$$a \equiv a_\perp^{2/3} a_\parallel^{1/3} , \tag{5.6}$$

which is chosen such that it correctly describes the volume expansion.

Let us also introduce the expansion rates $H_\perp = \dot{a}_\perp/a_\perp$ and $H_\parallel = \dot{a}_\parallel/a_\parallel$. The anisotropic stress of the homogeneous magnetic field sources anisotropic expansion, which can be expressed as the difference of the expansion rates, $\Delta H = H_\perp - H_\parallel$. We combine eqs. (5.4) and (5.3) to obtain an evolution equation for ΔH,

$$\dot{\Delta H} + \left(2H_\perp + H_\parallel\right) \Delta H = 8\pi G \left(P_\perp - P_\parallel\right) . \tag{5.7}$$

This pressure difference is actually simply the anisotropic stress. More precisely,

$$\begin{aligned} \Pi_i{}^j &\equiv T_i{}^j - P\delta_i{}^j , \qquad P = T_i^i/3 = (2P_\perp + P_\parallel)/3 , \\ \Pi_1{}^1 &= \Pi_2{}^2 = P_\perp - P = \frac{1}{3}\left(P_\perp - P_\parallel\right) , \quad \Pi_3{}^3 = P_\parallel - P = -\frac{2}{3}\left(P_\perp - P_\parallel\right) . \end{aligned} \tag{5.8}$$

At very high temperatures, both photons and neutrinos are tightly coupled to baryons. Their pressure is isotropic and thus their contribution to the right-hand-side of (5.7) vanishes. The collision term in Boltzmann's equation tends to isotropize their momentum-space distribution. Under these conditions the only source of anisotropic stress is the magnetic field. The above equation can then easily be solved to leading order in ΔH, as will be carried out in section 5.3.

However, as soon as the neutrinos decouple and start to free-stream, their momentum-space distribution will be affected by the anisotropic expansion caused by the magnetic field and thus they will develop anisotropic stress. As we will show, the neutrino anisotropic stress counteracts the one from the magnetic field. This behavior will be maintained until the neutrinos become non-relativistic, then their pressure decays. For the temperature anisotropy in the CMB it is relevant whether this happens before or after photon decoupling. This depends, of course, on the neutrino masses.

We introduce the energy density parameters

$$\Omega_x(t) \equiv \frac{8\pi G\rho_x(t)}{3H^2(t)} = \frac{\rho_x(t)}{\rho_c(t)} ,$$

corresponding respectively to the magnetic field, matter and radiation etc., such that e.g. $\Omega_B = B^2/8\pi\rho_c$, $\Omega_m = \rho_m/\rho_c$ and $\Omega_\gamma = \rho_\gamma/\rho_c$. Here we define the 'average' Hubble parameter by

$$H^2 \equiv \frac{1}{3}\left[\left(\frac{\dot{a}_\perp}{a_\perp}\right)^2 + 2\frac{\dot{a}_\perp \dot{a}_\parallel}{a_\perp a_\parallel}\right] . \tag{5.9}$$

With this, eq. (5.2), implies

$$\Omega_{\rm T} \equiv \Omega_B + \Omega_\gamma + \Omega_\nu + \Omega_m + \Omega_\Lambda = 1 \quad \text{ at all times.} \tag{5.10}$$

As an alternative, one could have defined the 'average' Hubble parameter as

$$H_a \equiv \frac{1}{3}\left[2\frac{\dot{a}_\perp}{a_\perp} + \frac{\dot{a}_\parallel}{a_\parallel}\right] .$$

It can easily be verified that the difference between these definitions is of the order of the small quantity $\Delta H = H_\perp - H_\parallel$. More precisely,

$$H^2 = H_a^2 \left[1 - \frac{2}{3}\frac{\Delta H}{H_a} - \frac{1}{3}\left(\frac{\Delta H}{H_a}\right)^2 \right] . \tag{5.11}$$

We shall mainly use the definition which yields the constraint (5.10).

The scaling of the energy densities corresponding to every species follows from the stress energy conservation of every single fluid

$$\rho_\gamma = \rho_\gamma^0 \left(\frac{a_0}{a}\right)^4 , \quad \rho_m = \rho_m^0 \left(\frac{a_0}{a}\right)^3 , \quad \rho_B = \rho_B^0 \left[\frac{a_\perp(t_0)}{a_\perp}\right]^4 . \tag{5.12}$$

To obtain the above behavior for radiation, it is important to impose that the fluid is ideal, i.e. that pressure is isotropic. This is the case if there are sufficiently many collisions, but does not hold for free streaming particles as we shall see in the next section.

At a fixed initial time one may set $a_\perp = a_\parallel$ as initial condition. Motivated by observations, we assume that the scale factor difference always remains small,

$$\frac{a_\perp - a_\parallel}{a} \equiv \delta \ll 1 . \tag{5.13}$$

To first order in $\Delta H \ll H$, as long as the magnetic field is the only anisotropic component, eq. (5.7) becomes (see also [55])

$$\dot{\Delta H} + 3H\Delta H = 8\pi G \left(P_\perp - P_\parallel\right) = 6H^2\Omega_B . \tag{5.14}$$

In the following we consider both Ω_B and ΔH as small quantities and want to calculate effects to first order in them. To first order, $\rho_B \propto a^{-4} \propto \rho_\gamma$. We can therefore introduce the ratio

$$r = \frac{\rho_B}{\rho_\gamma} = \frac{\Omega_B}{\Omega_\gamma} , \tag{5.15}$$

which (to first order) is constant.

In fig. 5.1 we plot the scale factor difference $\delta_0 - \delta$ and $\Delta H/H$ as functions of the temperature in a first stage where neutrinos, photons and baryons are all tightly coupled and the magnetic field is the only source of anisotropy.

5.2.1 Lightlike geodesics in Bianchi I

Let us now determine the CMB anisotropies in a Bianchi I Universe. We are not interested in the usual anisotropies from primordial perturbations, which we disregard in our treatment, but we concentrate on the effect of the global anisotropy, which to leading order will result in a temperature quadrupole.

We choose the tetrad basis $e_0 = \partial_t$, $e_i = a_\perp^{-1}\partial_i$ for $i = 1, 2$ and $e_3 = a_\parallel^{-1}\partial_3$. The dual basis of 1-forms is given by $\theta^0 = dt$, $\theta^i = a_\perp dx^i$, for $i = 1, 2$ and $\theta^3 = a_\parallel dx^3$. The first structure equation,

$$d\theta^a + \omega^a{}_b \wedge \theta^b = 0 ,$$

yields

$$\omega^{i}{}_{0} = \frac{\dot{a_\perp}}{a_\perp}\theta^0\,, \quad i=1,2\,, \qquad \text{and} \quad \omega^{3}{}_{0} = \frac{\dot{a_\parallel}}{a_\parallel}\theta^0\,. \tag{5.16}$$

The other non-vanishing connection 1-forms are determined by anti-symmetry, $\omega_{ab} = -\omega_{ba}$. After photon decoupling, the photon 4-momentum $\boldsymbol{p} = p^a \boldsymbol{e}_a$ satisfies the geodesic equation

$$\frac{dp^a}{d\lambda} + \omega^a{}_c(\boldsymbol{e}_b)\, p^b\, p^c = 0\,. \tag{5.17}$$

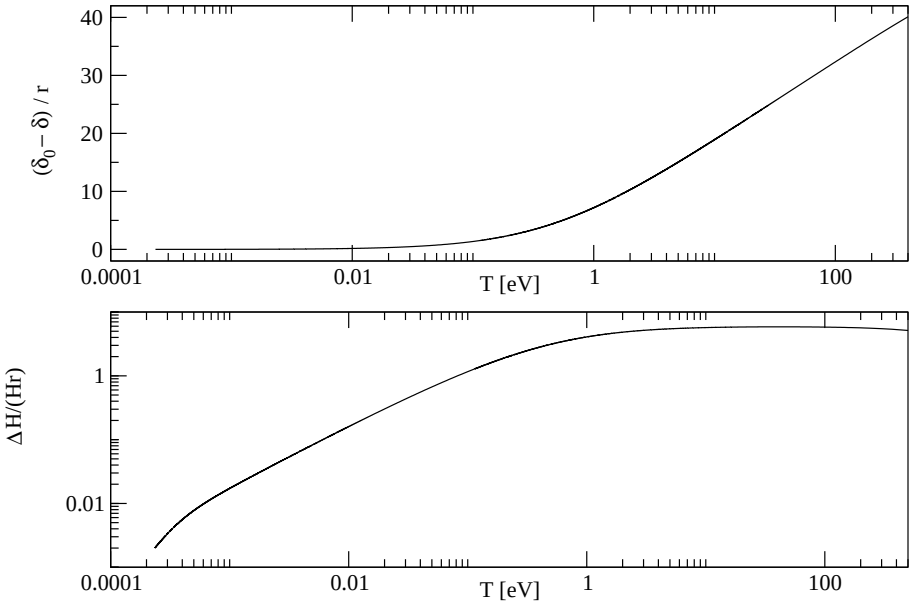

Figure 5.1: Temperature evolution of the scale factor difference $\delta_0 - \delta$ and $\Delta H/H$ in units of $r = \Omega_B/\Omega_\gamma$ when no free-streaming particle compensates the anisotropy produced by the magnetic field anisotropic stress. Here δ_0 denotes the scale factor difference δ today. The evolution of the 'average' scale factor a is the one of a ΛCDM Universe. As it is shown in section 3, $\Delta H/H$ is constant during the radiation dominated era and δ is growing. During the matter dominated era $\Delta H/H$ is decaying, $\Delta H/H \propto 1/a \propto T$, and δ asymptotes to a constant.

Considering the constraint relation for massless particles $p_a p^a = 0$ and setting $\alpha T_0 \equiv p^0 = p = \sqrt{\sum_{i=1}^{3}(p^i)^2}$, where T_0 is a constant with the dimension of energy (or temperature) that multiplies all the components p^a, the above equation is solved by

$$(p^a) = T_0 \left(\alpha, \frac{n^1}{a_\perp}, \frac{n^2}{a_\perp}, \frac{n^3}{a_\parallel}\right)\,, \tag{5.18}$$

where n is a unit vector in the direction of the particle momentum and α is determined by

the condition $p_a p^a = 0$.

$$n^1 = \sin\theta\sin\phi\ , \quad n^2 = \sin\theta\cos\phi \quad \text{and} \quad n^3 = \cos\theta\ .$$

The temperature of photons in such an anisotropic Universe for a comoving observer, $u = \partial_t$, is then given by

$$T(t,\theta) = \eta_{ab}u^a p^b = p^0 = T_0\alpha = T_0\sqrt{\frac{\sin^2\theta}{a_\perp^2} + \frac{\cos^2\theta}{a_\parallel^2}} \simeq \frac{T_0}{a}\left[1 + \delta\cos^2\theta + \mathcal{O}(\delta^2)\right]\ . \quad (5.19)$$

We set

$$\bar{T} = \frac{1}{4\pi}\int T(t,\theta)\sin\theta d\theta d\phi = \frac{T_0}{a}\left[1 + \frac{1}{3}\delta + \mathcal{O}(\delta^2)\right]$$

to be the temperature averaged over directions. Note that for $\delta = 0$ and $a_0 = 1$, T_0 is simply the CMB temperature at time t_0. For the temperature fluctuations to first order in δ we obtain

$$\frac{\Delta T}{T} \equiv \frac{T(t,\theta) - \bar{T}}{\bar{T}} = \frac{1}{3}\delta(3\cos^2\theta - 1) + \mathcal{O}(\delta^2) = \delta\frac{2}{3}\sqrt{\frac{4\pi}{5}}Y_{20}(\mathbf{n}) + \mathcal{O}(\delta^2)\ . \quad (5.20)$$

Hence, to lowest order in δ a homogeneous magnetic field generates a quadrupole which is given by

$$C_2 = \frac{1}{5}\sum_{m=-2}^{2}|a_{2m}|^2 = \frac{1}{5}|a_{20}|^2 = \frac{16\pi}{225}\delta^2 \simeq 0.22\times\delta^2\ . \quad (5.21)$$

Of course, in principle one can set $\delta(t_1) = 0$ at any given moment t_1 which then leads to $\frac{\Delta T}{T}(t_1) = 0$. However, for the CMB we know that photons start free-streaming only at $t_{\rm dec}$ when they decouple from electrons. Before that, scattering isotropizes the photon distribution and no quadrupole can develop[1]. In other words, we have to make sure that the anisotropy-induced quadrupole is fixed to zero at decoupling and only appears as a result of differential expansion between last scattering and today. This can be taken into account by simply choosing the initial condition $\delta(t_{\rm dec}) = 0$. Without this initial condition we have to replace $\delta(t)$ by $\delta(t) - \delta(t_{\rm dec})$ in eq. (5.21) [2]. The general result for the CMB quadrupole today is therefore

$$C_2 = \frac{16\pi}{225}\left[\delta(t_0) - \delta(t_{\rm dec})\right]^2\ . \quad (5.22)$$

5.2.2 The Liouville equation

At this stage it is straightforward to check that the exact expression found above for the temperature, eq. (5.19), satisfies the Liouville equation for photons (see, e.g. [34])

$$p^a \boldsymbol{e}_a(f_\gamma) - \omega^i{}_b(\boldsymbol{p})p^b\frac{\partial f_\gamma}{\partial p^i} = 0\,, \quad (5.23)$$

[1] This is not strictly true and neglects the slight anisotropy of non-relativistic Thomson scattering.

[2] More generally, one can say that δ itself is not a quantity with a physical meaning as long as no reference value is specified. In physical terms, only the difference of δ between two instants of time can be a relevant quantity.

when we make the following Ansatz for the distribution function of massless bosonic particles in our Bianchi I Universe

$$p_\perp \equiv \sqrt{(p^1)^2 + (p^2)^2}\,, \quad p_\parallel = p^3, \quad p = \sqrt{p_\perp^2 + p_\parallel^2} = p^0\,, \tag{5.24}$$

$$f_\gamma(t,T) = \frac{N_\gamma}{(2\pi)^3}\frac{1}{\mathrm{e}^{p/T}-1}, \qquad T = T(t,\theta)\,. \tag{5.25}$$

Indeed, using eqs. (5.16), we find the following differential equation for the temperature T

$$\frac{\partial f_\gamma}{\partial T}\frac{\partial T}{\partial t} - \frac{\dot{a_\perp}}{a_\perp}\frac{\partial f_\gamma}{p_\perp}p_\perp - \frac{\dot{a_\parallel}}{a_\parallel}\frac{\partial f_\gamma}{\partial p_\parallel}p_\parallel = 0\,. \tag{5.26}$$

With (5.25) this can be written as

$$\frac{\dot{T}}{T} + \frac{\dot{a_\perp}}{a_\perp}\left(\frac{p_\perp}{p}\right)^2 + \frac{\dot{a_\parallel}}{a_\parallel}\left(\frac{p_\parallel}{p}\right)^2 = 0\,. \tag{5.27}$$

The time behavior of the different components of the photon momentum are given by eq. (5.18) and one immediately sees that expression (5.19) for the temperature solves the above differential equation.

Moreover, defining the time dependent unit vectors $\hat{p}^i \equiv p^i/p$ and the shear tensor

$$\sigma_{ab} \equiv \vartheta_{ab} - \frac{1}{3}\vartheta_c^c h_{ab}\,, \quad \text{where } \vartheta_{ab} \equiv \frac{1}{2}\left(\nabla_a u_b + \nabla_b u_a\right) \quad \text{and} \quad h_{ab} \equiv \eta_{ab} + u_a u_b\,,$$

one can rewrite the above Liouville equation as

$$\dot{(\tilde{p})} = -\tilde{p}\sigma_{ij}\hat{p}^i\hat{p}^j\,, \tag{5.28}$$

where $\tilde{p}$ denotes the redshift-corrected photon energy defined as $\tilde{p} \equiv ap$. This last expression agrees with the corresponding equation given in [94].

Using the expression for the distribution function of massless fermions, we can also compute the pressure of neutrinos once they start free-streaming. Indeed, given the fact that neutrinos can be considered massless before they become non-relativistic, their geodesic equation has the same solution as the one for photons found above, therefore we immediately obtain the time behavior of their temperature in an anisotropic Bianchi I background. Taking also into account the fact that neutrinos are fermions, their distribution function reads

$$f_\nu(t,T) = \frac{N_\nu}{(2\pi)^3}\frac{1}{\mathrm{e}^{p/T}+1}, \quad \text{with} \quad T(t,\theta) = \frac{T_\nu}{a}\left[1 + \delta\cos^2\theta + \mathcal{O}(\delta^2)\right]\,. \tag{5.29}$$

Note that the parameter T appearing in the neutrino distribution function in not a temperature in the thermodynamical sense as the neutrinos are not in thermal equilibrium. It is simply a parameter in the distribution function and its time evolution has been determined by requiring the neutrinos to move along geodesics i.e. to free-stream.

This distribution function remains valid also in the case where neutrinos are massive, i.e. $T_\nu < m_\nu$. The only difference is that the relation $p^0 = p$ changes to $p^0 = \sqrt{p^2 + (m_\nu a)^2}$ which of course affects the momentum integrals for the neutrino energy density and pressure.

The energy T_ν/a_0 is the present neutrino 'temperature' in the absence of a homogeneous magnetic field ($\delta = 0$). The energy density ρ_ν and the pressure $P_{\nu,i}$ in direction i with respect to our orthonormal basis are

$$\rho_\nu = N_\nu \int d^3p\, f_\nu(t,T) p^0 \tag{5.30}$$

$$P_{\nu,i} = N_\nu \int d^3p\, f_\nu(t,T)\, \frac{p_i^2}{p^0}\,. \tag{5.31}$$

Calculating the integral (5.31) for relativistic neutrinos to first order in δ in the directions perpendicular and parallel to the magnetic field direction, one finds for the neutrino anisotropic stress in the ultra-relativistic limit

$$P_{\nu,\perp} - P_{\nu,\parallel} \simeq -\frac{8}{15}\rho_\nu\,(\delta - \delta_*)\ , \tag{5.32}$$

where δ_* is the value of δ at neutrino decoupling and can be fixed to zero for convenience.

The temperature dependence of the neutrino pressure is shown in fig. 5.2. To leading order, this also gives the temperature dependence of the neutrino anisotropic stress. From the plot it is clear how the pressure scales as a^{-4} as long as the neutrinos are ultra-relativistic. Once they have become effectively non-relativistic, their pressure decays more rapidly, as a^{-5}. The break in the power law is not precisely at $T = m_\nu$, but at a somewhat lower temperature. Because the neutrinos still have the highly relativistic Fermi-Dirac distribution from the time of their thermal freeze-out, it takes some additional redshift until they behave effectively non-relativisic. This will have some effect on the estimates for the residual CMB quadrupole, as we shall see in sec. 5.3, in particular the discussion of fig. 5.5.

5.3 Neutrino free-streaming and isotropization

5.3.1 Massless free-streaming neutrinos

We now calculate the effect of free-streaming neutrinos perturbatively, i.e. to first order in δ, $\Delta H/H$ and Ω_B. We linearize eq. (5.7), taking into account the contribution of a free-streaming relativistic component to the right-hand side. We have shown that this contribution, to leading order in δ, is given by eq. (5.32). Furthermore, up to $\mathcal{O}(\delta^2)$ corrections, δ is just the integral of ΔH,

$$\int_{t_*}^{t} \Delta H(t')dt' = \ln\frac{a_\perp(t)}{a_\parallel(t)} - \ln\frac{a_\perp(t_*)}{a_\parallel(t_*)} \simeq \delta - \delta_*\ , \tag{5.33}$$

so that to first order we can identify $\Delta H \simeq \dot\delta$.

Inserting this back into eq. (5.7) we find, to linear order in δ,

$$\ddot\delta + 3H\dot\delta + \frac{8}{5}H^2\Omega_\nu\,(\delta - \delta_*) = 6H^2\Omega_B\ . \tag{5.34}$$

Note that, because we are working at linear order, it is not important with respect to which scale factor H, Ω_ν and Ω_B are defined in (5.34). We will now give analytic solutions to this equation for different regimes in the evolution of the Universe.

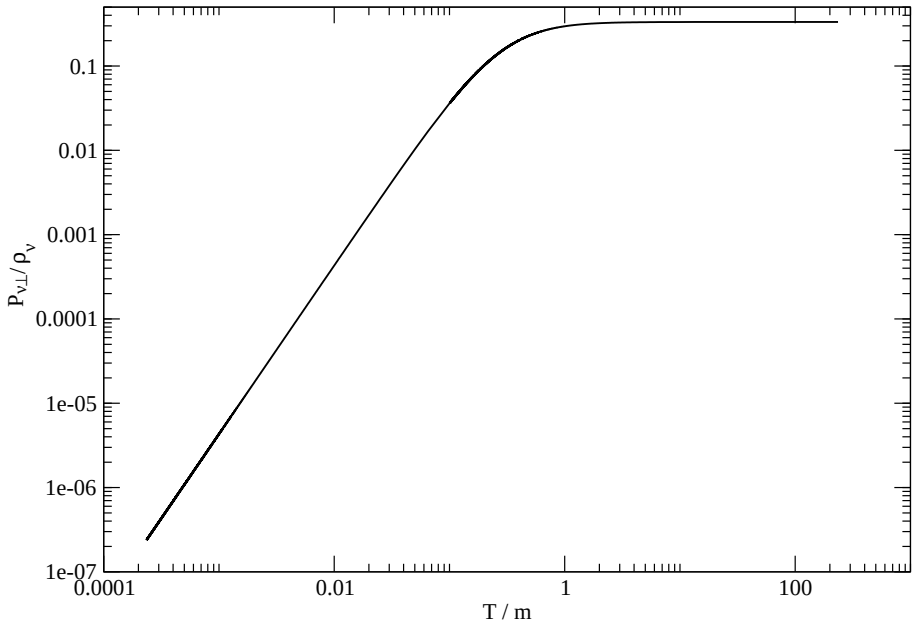

Figure 5.2: Temperature evolution of the neutrino pressure $P_{\nu,\perp}$ normalized to the neutrino energy density ρ_ν. The temperature is given in units of the neutrino mass. Note that the break in the power law is not at $T = m$, but at somewhat lower temperature. This is due to the highly relativistic Fermi-Dirac distribution of the neutrinos, see also the discussion of fig. 5 in sec. 3.3.

Let us begin at very high temperature where the neutrinos are still strongly coupled to baryons. In this case they do not contribute to eq. (5.34) since their pressure is isotropic ($P_{\nu,\perp} - P_{\nu,\parallel} \sim 0$) given the high rate of collisions. Furthermore, since we are in the **radiation dominated era** ($a \propto t^{1/2}$), we have $H = 1/2t$, and Ω_B is constant. The solution to eq. (5.34) in this case is

$$\dot{\delta}(t) = \Delta H(t) = \frac{3\Omega_B}{t} + \frac{C}{t^{3/2}} \; . \tag{5.35}$$

The dimensionless quantity $\Delta H/H$ hence asymptotes to a constant, since the homogeneous piece decays like a^{-1}:

$$\frac{\Delta H}{H} \to 6\Omega_B \; . \tag{5.36}$$

ΔH soon becomes insensitive to the initial conditions and only depends on Ω_B. This also shows that in the absence of an anisotropic source ($\Omega_B = 0$), the expanding Universe isotropizes. Integrating this equation and remembering that $\Omega_B =$ constant to first order in a radiation dominated Universe, we obtain

$$\delta(t) - \delta(t') = 3\Omega_B \ln(t/t') \, . \tag{5.37}$$

As the Universe reaches a temperature of roughly 1.4 MeV, the neutrinos decouple and begin to free-stream, giving rise to the corresponding term in eq. (5.34). In the radiation

dominated era, Ω_ν remains constant as long as neutrinos are ultra-relativistic[3]. This is certainly true for temperatures well above a few eV. In this regime, the general solution of eq. (5.34) is given by

$$\delta(t) - \delta_* = \frac{15}{4}\frac{\Omega_B}{\Omega_\nu} + t^{-1/4}\left(C_+ t^{i\sqrt{2\Omega_\nu/5-1/16}} + C_- t^{-i\sqrt{2\Omega_\nu/5-1/16}}\right) . \tag{5.38}$$

For $\Omega_\nu > 5/32$, the homogeneous part is oscillating with a damping envelope $\propto t^{-1/4} \propto a^{-1/2}$. This means that $\Delta H = \dot{\delta}$ will decay within a few Hubble times, which is a matter of seconds at the temperatures we are talking about. After that, $\delta - \delta_*$ will remain constant at the value of $(15/4)\,\Omega_B/\Omega_\nu$ until the neutrinos become non-relativistic. Then their pressure drops dramatically and so does their anisotropic stress. Until this time, the Universe expands isotropically, because the anisotropic stress of the magnetic field is precisely cancelled by the one of the neutrinos. Remember that a constant δ can always be absorbed in a re-scaling of the coordinates and has no physical effect. Fig. 5.3 shows the temperature evolution of $\delta - \delta_*$ in the radiation dominated era from neutrino decoupling until $T = 100\text{eV}$.

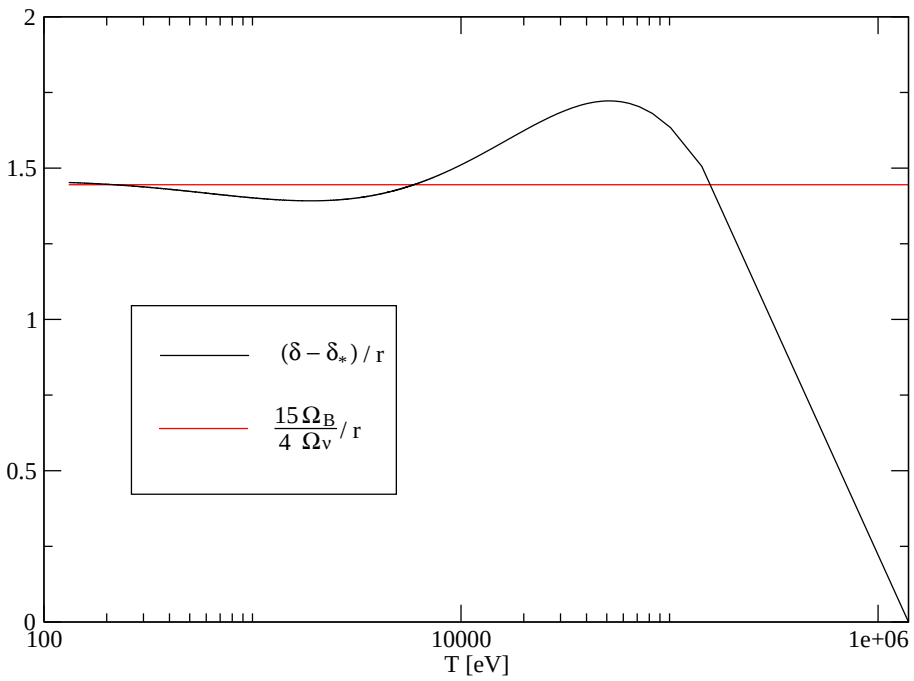

Figure 5.3: Temperature evolution of $\delta - \delta_*$ from neutrino decoupling to $T = 100\text{eV}$. After decoupling, $\delta - \delta_*$ begins to oscillate with a decreasing amplitude around the constant $\frac{15}{4}\frac{\Omega_B}{\Omega_\nu}$, as predicted by the analytic solution (5.38). This qualitative behavior is independent of the initial conditions.

[3] Actually, Ω_ν changes slightly when electron-positron annihilation takes place, a process which heats up the photons but not the neutrinos. This happens at a temperature close to the electron mass. After that, Ω_ν/Ω_γ remains constant until the neutrinos become non-relativistic.

This mechanism rests on two important facts. Firstly, as long as neutrinos are ultra-relativistic, they redshift in the same way as the magnetic field, meaning that Ω_B/Ω_ν is constant. Once the anisotropic stress of the neutrinos has adjusted to the magnetic field, their sum remains zero independent of the expansion of the Universe which is now in a Friedmann phase. Secondly, the efficiency of the effect hinges on the absolute value of Ω_ν. In the radiation dominated era (after positron annihilation), we have $\Omega_\nu \simeq 0.4$ so that $\Omega_\nu > 5/32$, and hence the system behaves as an underdamped oscillator with a damping envelope $\propto t^{-1/4}$. Had the density parameter of the free-streaming particles been less than 5/32, the behavior would be that of an overdamped oscillator. As it is evident from eq. (5.38), for $\Omega_\nu \ll 5/32$ there would be a mode which decays extremely slowly, roughly as $t^{-4\Omega_\nu/5}$. This is why a strongly subdominant free-streaming component cannot damp the anisotropy efficiently. As we shall discuss in section 5.4, a primordial gravitational wave background could play the role of such a free-streaming component if $\Omega_{GW} \gtrsim 5/32$.

5.3.2 Massive neutrinos

The neutrinos become non-relativistic roughly at the time when their temperature drops below their mass scale. Current bounds on the neutrino mass [3] are such that the highest-mass eigenstate is somewhere between ~ 1 eV and ~ 0.04 eV. Since the neutrino mass splitting is much below 1 eV, an eigenstate close to the upper bound would mean that the neutrinos are almost degenerate and hence become non-relativistic all at the same time. If this happens *before* photon decoupling, i.e., if $m_\nu > 0.3$ eV, the isotropization effect will not be present and the CMB will be affected by the anisotropic expansion sourced by the magnetic field. However, if the neutrinos remain ultra-relativistic until long *after* photon decoupling, the CMB quadrupole due to anisotropic expansion will be reduced because the neutrinos maintain expansion isotropic until they become non-relativistic.

In order to quantify this statement, we repeat the above calculations for the **matter dominated era**. For our purposes, this is a reasonable approximation for the time between photon decoupling and today. At decoupling, radiation is already subdominant, and on the other hand vacuum energy only begins to dominate at redshift $z \sim 0.5$. We therefore expect that both give small corrections only.

For completeness, we also give the solution of eq. (5.34) in a matter dominated Universe for the case where we ignore any contributions from free-streaming particles (neutrinos and, after decoupling, also photons). During matter domination we have $H = 2/3t$ and $\Omega_B \propto a^{-1} \propto t^{-2/3}$. The solution to (5.14) hence reads

$$\dot{\delta}(t) = \Delta H(t) = \frac{8\Omega_B(t)}{t} + \frac{C}{t^2} \ . \tag{5.39}$$

The homogeneous mode again decays more rapidly than the particular solution, so that the dimensionless quantity $\Delta H/H$ is again asymptotically proportional to Ω_B. Instead of eqs. (5.36), (5.37), we have

$$\frac{\Delta H}{H} \to 12\Omega_B \ , \qquad \delta(t) - \delta(t_{\rm eq}) = \int_{t_{\rm eq}}^{t} \Delta H dt \simeq 12\left[\Omega_B(t_{\rm eq}) - \Omega_B(t)\right] \ . \tag{5.40}$$

Let us now take into account a free-streaming component. We want to estimate the effect on the photon distribution function caused by anisotropic expansion in two cases. Case A: the neutrinos become non-relativistic *before* photon decoupling. Case B: the neu-

trinos become non-relativistic *after* photon decoupling. As an approximation, we assume that this happens instantaneously to all neutrino species, such that the contribution of neutrinos to eq. (5.34) disappears abruptly. We know that the neutrinos are in fact spread out in momentum space and also have a certain spread in the mass spectrum, so in reality this will be a gentle transition. However, we only want to estimate the order of magnitude of the effect and are not interested in these details at this point. More precice numerical results will be presented in sec. 5.3.3. Let us consider case A first.

5.3.2.1 Case A: neutrinos become non-relativistic before photon decoupling

We know that ΔH is very nearly zero when the neutrinos become non-relativistic. After that, $\Delta H/H$ will start to grow again to approach the value $6\Omega_B$ during radiation domination and $12\Omega_B$ during matter domination. As boundary condition at photon decoupling, we will hence assume $\Delta H/H = x\Omega_B$ with $x \lesssim 12$. This number can in principle be computed given the neutrino masses and the evolution of the scale factor across matter-radiation equality. We shall solve the full equations in subsection 5.3.3; here we just want to understand the results which we obtain there by numerical integration. The free-streaming component we are interested in now are the photons after decoupling. We therefore identify $\delta_* = \delta(t_{\rm dec})$, where $t_{\rm dec}$ denotes the instant of photon decoupling. Furthermore, in eq. (5.34) we replace Ω_ν by Ω_γ, our new free-streaming species. With $\Omega_\gamma \propto t^{-2/3}$ in the matter dominated era, the (not so obvious) analytic solution to eq. (5.34) is

$$\delta(t) - \delta(t_{\rm dec}) = \frac{15}{4}\frac{\Omega_B}{\Omega_\gamma} + C\left[f(t)\cos f(t) - \sin f(t)\right] + D\left[f(t)\sin f(t) + \cos f(t)\right] \ , \quad (5.41)$$

where we have introduced $f(t) \equiv 4\sqrt{2\Omega_\gamma(t)/5}$. The time derivative of eq. (5.41) yields

$$\frac{\Delta H}{H} = \frac{16}{5}\Omega_\gamma\left[C\sin f(t) - D\cos f(t)\right] \ . \quad (5.42)$$

Note that the slowly decaying mode has the same asymptotic behavior as (5.40) – in the matter dominated era, the free-streaming radiation can never catch up to the magnetic field, since both fade away too quickly. In other words, this means that free-streaming photons are never able to counteract the magnetic field anisotropy in order to isotropize again the Universe, even if they represent the main contribution to the background radiation energy density, and the reason for this is that they decouple only after the end of radiation dominantion.

In order to estimate the value of δ today (t_0), we can simply take the limit of small $\Omega_\gamma(t_0) \ll 1$ of (5.41). Correction terms are suppressed at least by $\sqrt{\Omega_\gamma(t_0)} \sim 10^{-2}$. We find

$$\delta(t_0) - \delta(t_{\rm dec}) \simeq \frac{15}{4}\frac{\Omega_B}{\Omega_\gamma} + D \ . \quad (5.43)$$

The constant D is fixed by the boundary conditions at decoupling, given by $\Delta H/H = x\Omega_B$ and $\delta = \delta(t_{\rm dec})$. These boundary conditions translate to

$$\begin{aligned} D &= \frac{\Omega_B(t_{\rm dec})}{\Omega_\gamma(t_{\rm dec})}\left[\frac{\sin f(t_{\rm dec})}{f(t_{\rm dec})}\left(\frac{5}{16}x - \frac{15}{4}\right) - \frac{5}{16}x\cos f(t_{\rm dec})\right] \\ &= \frac{\Omega_B(t_{\rm dec})}{\Omega_\gamma(t_{\rm dec})}\left[-\frac{15}{4} + \left(4 + \frac{2x}{3}\right)\Omega_\gamma(t_{\rm dec}) + \mathcal{O}\left(\Omega_\gamma^2(t_{\rm dec})\right)\right] \ . \end{aligned} \quad (5.44)$$

In order to obtain the essential behavior we have expanded the boundary term as a Taylor series in $\Omega_\gamma(t_{\rm dec}) \ll 1$. Our final result is

$$\delta(t_0) - \delta(t_{\rm dec}) \simeq \left(4 + \frac{2x}{3}\right) \Omega_B(t_{\rm dec}) \lesssim 12\Omega_B(t_{\rm dec}) \ , \tag{5.45}$$

up to corrections suppressed by powers of $\Omega_\gamma(t_{\rm dec})$.

In this case, the CMB quadrupole is not affected by the presence of free-streaming neutrinos and we obtain the same result as when neglecting their presence,

$$C_2 \simeq \frac{16\pi}{225} \left[\delta(t_0) - \delta(t_{\rm dec})\right]^2 \simeq \frac{768\pi}{75} \Omega_B^2(t_{\rm dec}) \simeq 0.1 r^2 \, . \tag{5.46}$$

5.3.2.2 Case B: neutrinos become non-relativistic after photon decoupling

In this case, the presence of the neutrino anisotropic stress will delay the onset of anisotropic expansion until a time t_m when the neutrinos become effectively non-relativistic. As before, we will ignore that this is a gradual process and simply assume that one can define some kind of "effective" t_m at which the neutrino anisotropic stress drops to zero. The full numerical result is given in section 5.3.3. The effect of anisotropic expansion on the photon distribution function is estimated as follows. We assume there is no anisotropic expansion between photon decoupling and t_m. At later times, neutrino anisotropic stress can be ignored. The relevant solution (5.41) is hence obtained with boundary condition $\dot\delta(t_m) = 0$. Working through the steps above once again or simply taking the result (5.45) with $t_{\rm dec} \to t_m$ and $x \to 0$, one finds

$$\delta(t_0) - \delta(t_{\rm dec}) = \delta(t_0) - \delta(t_m) \simeq 4\, \Omega_B(t_m) \ . \tag{5.47}$$

Since Ω_B decays as a^{-1}, the effect of anisotropic expansion in case B is suppressed by roughly a factor of $a(t_{\rm dec})/(3a(t_m))$ with respect to case A. For light neutrinos with a highest-mass eigenstate close to the current lower bound, this factor can be as small as ~ 0.03, loosening the constraint on a constant magnetic field from the CMB temperature anisotropy correspondingly. Constraints coming from Faraday rotation are not affected.

Clearly, the heaviest neutrino becomes massive at redshift $z_m = m_\nu/T_\nu \gtrsim 0.04{\rm eV}/T_\nu \simeq 200$. One might wonder whether isotropization can be supported even if only one neutrino remains massless, since its contribution to the energy density is $\Omega_{\nu 1} \simeq 0.23\Omega_\gamma$. The problem is however that, as soon as one neutrino species becomes massive, the equilibrium between the magnetic field and the neutrino anisotropic stresses is destroyed and, as we have seen under case A, where one still has free streaming photons, it cannot be fully re-established in a matter dominated Universe.

5.3.3 Numerical solutions

In order to go beyond the estimates derived so far, we have solved eqs. (5.2-5.4) numerically with cosmological parameters corresponding to the current best-fit ΛCDM model [78]. We use cosmological parameters $\Omega_\Lambda = 0.73$, $\Omega_m = 0.27$ today, where Ω_m includes a contribution of massive neutrinos[4] which we approximate by $\Omega_\nu h^2 = N_\nu m_\nu/94{\rm eV}$ with $N_\nu \simeq 3$.

[4]CMB observations actually constrain the matter density at decoupling, such that neutrinos with $m_\nu \lesssim 0.3$eV, which are still relativistic at that time, do not contribute to the measurement of Ω_m. However, since

The contribution to the right-hand side of eq. (5.7) from free-streaming neutrinos is obtained by integrating eq. (5.31) with the full distribution function for massive fermions. More precisely, we compute the full distribution function to first order in δ and perform the integration numerically, including the neutrino mass as a parameter. We begin to integrate deep inside the radiation dominated era, when the neutrinos are still relativistic but already free-streaming. The asymptotic behavior of solution (5.37) can be used as initial condition at neutrino decoupling. The constraint equation (5.2) provides the remaining initial condition. We then integrate until the desired time. We define today t_0 by $a(t_0) = 1$.

In fig. 5.4, we present the results of the numerical integration from neutrino decoupling until today. We plot both $\delta - \delta_*$ and $\Delta H/H$ in units of the parameter $r = \Omega_B/\Omega_\gamma$ so that the plots are valid for arbitrary magnetic field strengths, as long as $r \ll 1$. After neutrino decoupling, δ oscillates and reaches its constant value as in eqs. (5.38), (5.41), while $\Delta H = \dot{\delta}$ oscillates and decays. We choose as initial condition $\delta = \delta_* = 0$ at neutrino decoupling. Once the temperature of the Universe reaches the neutrinos mass scale, neutrino pressure decreases and they become non-relativistic. At this point, they can no longer compensate the anisotropic pressure of the magnetic field, and both δ and ΔH begin to grow. However, it is clear from fig. 5.4 (upper plot) how, once neutrinos become non relativistic after photon decoupling (case B), the growth of δ is suppressed with respect to case A, where this happens before photon decoupling. Moreover, the solid black line in the lower plot represents the temperature evolution of $\Delta H/H$ in the case where only the magnetic field sources the anisotropy: this makes clear how the absence of any free-streaming particle able to counteract the magnetic anisotropic stress leaves the anisotropy of the Universe free to grow with respect to its value today.

Our quantitative final result is shown in fig. 5.5, where we plot the value of the quadrupole generated by a constant magnetic field, rescaled by r^2, as function of the neutrino mass. We weight the final C_2 with respect to the quadrupole obtained without considering the isotropization induced by free-streaming particles, in order to underline the relative importance of this effect. These results clearly show that the CMB quadrupole is significantly reduced by neutrino free-streaming only if their mass is smaller than the temperature at photon decoupling, $m_\nu < T_{\rm dec} \simeq 0.26\,\text{eV}$. In fact, for neutrino masses in the range $0.3\,\text{eV} \lesssim m_\nu \lesssim 3\,\text{eV}$, the quadrupole C_2 is reduced by less than a factor 100 from the result without a free-streaming component, whereas for $0 \lesssim m_\nu \lesssim 0.3\,\text{eV}$, it decreases by several orders of magnitude. Note, however, that the effect is not negligible even in the former case with relatively large neutrino masses. Fig. 5.5 also shows our analytical estimation for the final amplitude of the CMB quadrupole produced by this effect as given by eq. (5.47). Of course the value of eq. (5.47) depends on the time at which neutrinos become effectively non-relativistic, t_m. Once we choose t_m to be given by the time at which $T = m_\nu$, we overestimate the final quadrupole amplitude still by one order of magnitude (dashed blue line). This is a consequence of the fact that the neutrino distribution function is highly relativistic and therefore it takes a further redshift for them to start behaving effectively as massive pressureless particles. This has been considered in the more elaborate estimate given by the dashed red line where we fix the time t_m to be given by the time at which $d^3P_\nu/d(\ln T)^3 = 0$, i.e. the time at which the pressure reaches the break in the power law. This is in excellent agreement with the numerical results.

their density parameter today is then also very small, their contribution to the matter density remains practically irrelevant.

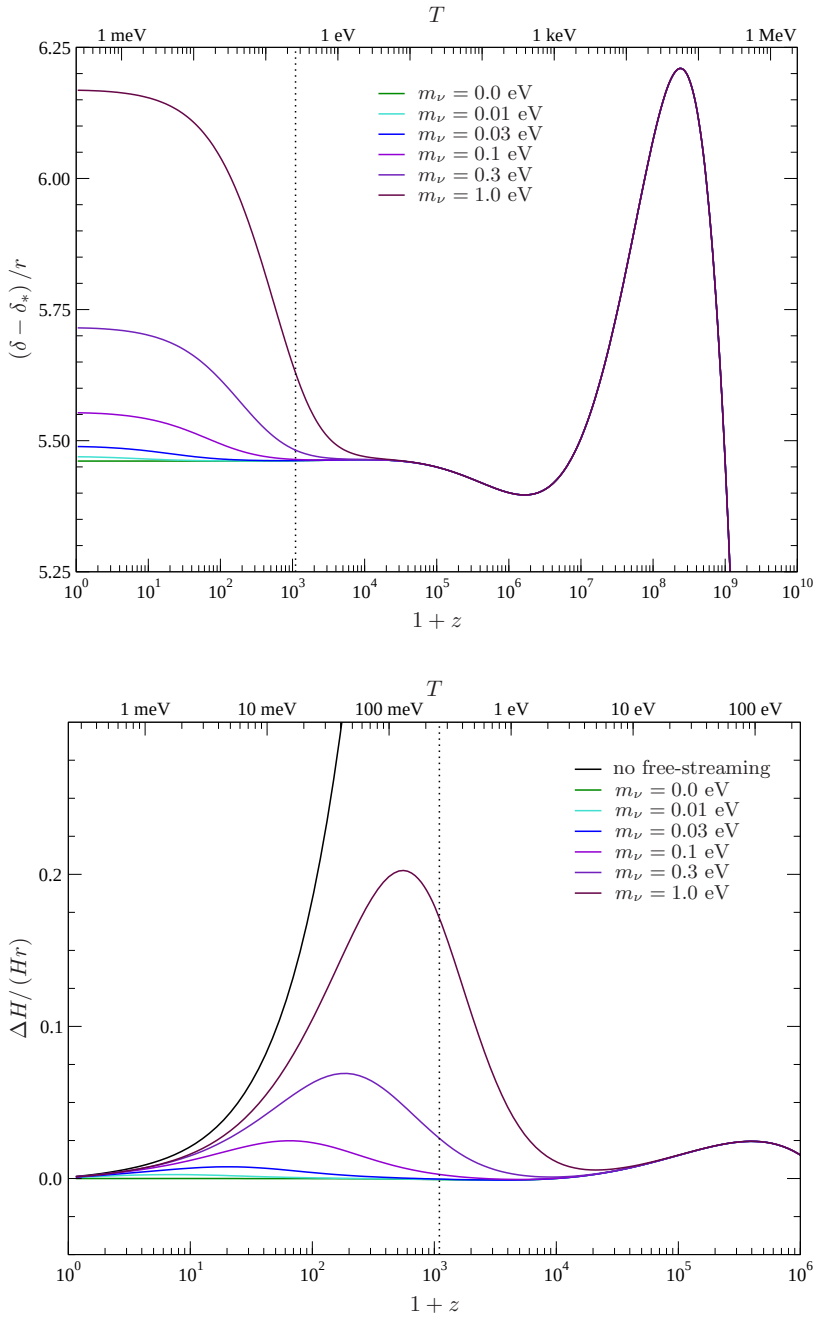

Figure 5.4: Temperature evolution of $\Delta H/H$ and $\delta - \delta_*$ for different neutrino masses. We chose the initial conditions to be given by $\delta_* = 0$ at neutrino decoupling. The black solid line in the lower plot represents the temperature evolution of $\Delta H/H$ in the case where only the magnetic field sources the anisotropy and no free-streaming particle is present to compensate this effect. The dotted vertical line indicates the instant of photon decoupling.

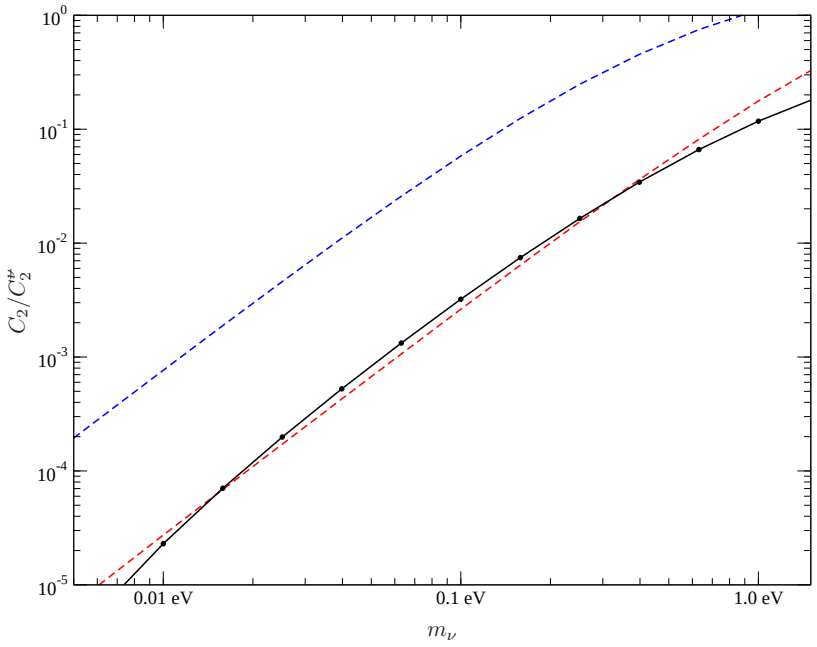

Figure 5.5: Effect of free-streaming neutrinos with different masses on the quadrupole generated by a homogeneous magnetic field, weighted on the quadrupole obtained without considering the effect of any free-streaming particles. The solid black line represents the result of the numerical integration, the dashed blue and red lines correspond to our analytical prediction given by eq. (5.47) for two different choices of t_m, the time at which neutrinos are effectively non-relativistic (see the text for clarification).

5.4 A gravitational wave background and other massless free-streaming components in an anisotropic Universe

From our previous discussion it is evident that any massless free-streaming particle species X can isotropize the Bianchi I model with a constant magnetic field, if present with sufficient contribution Ω_X already in the radiation dominated era. This has to be accounted for if we want to estimate the CMB quadrupole induced by a homogeneous magnetic field.

So far we have discussed the standard model neutrinos as an example of such a particle. However, also other massless particles can play this role, for instance gravitons, but also particle species outside of the spectrum of the standard model. Interestingly, the current bounds on the number of relativistic degrees of freedom during nucleosynthesis, often parameterized by the *effective number of additional neutrino species* ΔN_ν, allow for the possibility that such a species could be sufficiently abundant. The present bound on N_ν from nucleosynthesis is [3]

$$\begin{aligned} N_\nu &= 3.2 \pm 1.2 \ , \\ g_* &= 2 + \frac{7N_\nu}{4}\left(\frac{4}{11}\right)^{4/3} = 3.36 + (N_\nu - 3) \times 0.454 \\ &= 3.36 + (0.2 \pm 1.2) \times 0.454 \quad \text{at } 95\% \text{ confidence.} \end{aligned} \tag{5.48}$$

Here we have taken into account that the photon and neutrino temperatures are related by

$T_\nu = (4/11)^{1/3} T_\gamma$ [36]. The effective g_* from γ and three species of neutrino corresponds to $g_*(\gamma, 3\nu) = 3.36$. This is equivalent to a limit on an additional relativistic contribution at nucleosynthesis of $\Omega_X \lesssim 0.2$. From the solution (5.38) we know that a free-streaming relativistic species with a density parameter $\Omega_X \gtrsim 5/32 \simeq 0.156$ during the radiation dominated era will isotropize expansion within a few Hubble times. Since this species will presumably decouple before the neutrinos (otherwise it should have been discovered in laboratory experiments), expansion can be isotropic already at neutrino decoupling, and thus neither the cosmic neutrino background nor the CMB will be affected by anisotropic expansion. In this case therefore, unless we are able to detect the background of the species X, we will never find a trace of the anisotropic stress produced by a homogeneous magnetic field. An interesting example are gravitons, which we now want to discuss.

Inflationary models generically predict a background of cosmological gravitational waves which are produced from quantum fluctuations during the inflationary phase. The amplitude of this background, usually expressed by the so-called tensor-to-scalar ratio, r_T, has not yet been measured, but for a certain class of inflationary models, forthcoming experiments such as Planck might be able to detect these gravitational waves. This is in contrast to the cosmic neutrino background, for which there is no hope of direct detection with current or foreseeable technology. However, this background typically contributes only a very small energy density,

$$\Omega_{\mathrm{GW,\,inf}}/\Omega_\gamma \simeq 10^{-10} r_T \,, \qquad n_T \lesssim 0 \,.$$

Only non-standard inflationary models which allow for $n_T > 0$ can contribute a significant background, see [17].

Gravitational waves can also be produced during phase transitions in the early Universe [43], after the end of inflation. Such gravitational wave backgrounds can easily contribute the required energy density. Let us therefore concentrate on this possibility.

If the highest energy scales of our Universe remain some orders of magnitude below the Planck scale, gravitational waves are *never* in thermal equilibrium and can be considered as free-streaming radiation throughout the *entire history*. Therefore, if the gravitational wave background was statistically isotropic at some very early time, then any amount of anisotropic expansion taking place between this initial time and today will affect the gravitons in a similar fashion as any other free-streaming component, and therefore our present gravitational wave background would be anisotropic. Loosely speaking, the intensity of gravitational waves would be larger in those directions which have experienced less expansion in total since the initial time when the gravitational wave background was isotropic.

As we have specified above, with the current limits on ΔN_ν, the density parameter of gravitons Ω_{GW} during nucleosynthesis can be as large as ~ 0.2. At higher temperatures (that is, at earlier times), the number of relativistic degrees of freedom increases (more particle species are effectively massless), such that Ω_{GW} at earlier time can even be larger[5]. It is therefore conceivable that gravitons acquire sufficient anisotropic stress to compensate the magnetic field and hence take over the role which neutrinos have played in section 5.3.

[5] During a transition from g_1 relativistic degrees of freedom to $g_2 < g_1$, the temperature changes from T_1 to T_2. Since entropy is conserved during the transition we have $g_1 T_1^3 = g_2 T_2^3$. Hence $\rho_2 = g_2 T_2^4 = g_2 \left[\left(\frac{g_1}{g_2} \right)^{1/3} T_1 \right]^4 = \left(\frac{g_1}{g_2} \right)^{1/3} \rho_1 > \rho_1$. In other words, the energy density of all species which are still in thermal equilibrium increases if one reduces the number of degrees of freedom at constant entropy.

As already pointed out, in this case, neither neutrinos nor photons will ever experience any significant anisotropic expansion, since the Universe remains in a Friedmann phase after the gravitons have adjusted to the magnetic field. Of course, gravitons remain relativistic for all times and the mass effect which we discussed for the neutrinos does not occur.

In order to rule out this scenario, it would be very interesting not only to measure the background of cosmological gravitational waves but also to determine whether or not it shows a quadrupole anisotropy compatible with such a compensating anisotropic stress. Or in other words: just as the smallness of the CMB quadrupole is a direct indication for isotropic expansion between decoupling of photons and today, the smallness of the quadrupole of a gravitational wave background would inform us about the isotropy of expansion between today and a much earlier epoch where this background was generated.

5.5 Conclusions

In this paper we have studied a magnetic field coherent over very large scales so that it can be considered homogeneous. We have shown that in the radiation dominated era the well known Bianchi I solution for this geometry is isotropized if a free streaming relativistic component is present and contributes sufficiently to the energy density, $\Omega_X \gtrsim 5/32$. This is in tune with the numerical finding [90, 116, 76] that the neutrino anisotropic stresses 'compensate' large scale magnetic field stresses. A perturbative explanation of this effect is attempted in [12]. Here we explain the effect for the simple case of a homogeneous magnetic field: free streaming of relativistic particles leads to larger redshift, hence smaller pressure in the directions orthogonal to the field lines where the magnetic field pressure is positive and to smaller redshift, hence larger pressure in the direction parallel to the magnetic field, where the magnetic field pressure is negative. To first order in the difference of the scale factors this effect leads to a build up of anisotropic stress in the free streaming component until it exactly cancels the magnetic field anisotropic stress. This is possible since both these anisotropic stresses scale like a^{-4}.

In standard cosmology this free-streaming component is given by neutrinos. However, as soon as neutrinos become massive, their pressure, $P_\nu \propto a^{-5}$, decays much faster than their energy density, $\rho_\nu \propto a^{-3}$, and the effect of compensation is lost. If this happens significantly after decoupling, there is still a partial cancellation, but if it happens before decoupling, the neutrinos no longer compensate the magnetic field anisotropic stress. Furthermore, a component which starts to free-stream only in the matter era (like e.g. the photons) does not significantly reduce the anisotropic stress. Actually, inserting the dominant part of the constant D from eq. (5.44) in (5.42) one finds

$$\frac{\Delta H}{H} = 12\Omega_B \,, \tag{5.49}$$

like without a free-streaming component.

This cancellation of anisotropic stresses does not affect Faraday rotation. A constant magnetic field with amplitude $B_0 \gtrsim 10^{-9}$Gauss can therefore be discovered either by the Faraday rotation it induces in the CMB [111], or, if a sufficiently intense gravitational wave background exists, by the quadrupole (anisotropic stress) it generates in it.

Finally, Planck and certainly future large scale structure surveys like Euclid will most probably determine the absolute neutrino mass scale. Once this is known, we can infer exactly by how much the CMB quadrupole from a constant magnetic field is reduced by

their presence.

Acknowledgments

We thank Camille Bonvin and Chiara Caprini for discussions. JA wants to thank Geneva University for hospitality and the German Research Foundation (DFG) for financial support. This work is supported by the Swiss National Science Foundation.

Chapter 6

Back Reaction from Walls

JOURNAL OF ASTROPHYSICS AND ASTROPARTICLE PHYSICS **02**, 036 (2012)

Back Reaction from Walls

Enea Didio, Marc Vonlanthen, Ruth Durrer

We study the distance–redshift relation in a universe filled with 'walls' of pressure-less dust separated by under dense regions. We show that as long as the density contrast of the walls is small, or the diameter of the under dense regions is much smaller than the Hubble scale, the distance–redshift relation remains close to what is obtained in a Friedmann universe. However, when arbitrary density contrasts are allowed, every prescribed distance–redshift relation can be reproduced with such models.

6.1 Introduction

Since more than a decade, cosmology research is facing the dark energy problem: the present Universe seems to be in an accelerating phase. This conclusion was first drawn from measurements of the distance–redshift relation from type Ia Supernovae (SNIa) [105, 1] and is confirmed by many other datasets, from the cosmic microwave background [33] to baryon acoustic oscillations and other aspects of large scale structure. Until very recently the measurements inferring the existence of dark energy rely mainly on the distance–redshift relation which is valid in a Friedmann Universe [42]. New *independent* measurements of, e.g. the expansion rate $H(z)$ are now being performed see e.g. [9]. Hence this situation is changing, so that we shall soon know both, $d_A(z)$ and $H(z)$ with good accuracy. The general opinion is that fluctuations on large scales are small so that they can be treated with linear perturbation theory and linear perturbations average out in the mean over many directions and large scales, and therefore fluctuations are not relevant for the determination of quantities like $d_A(z)$ and $H(z)$. This expectation has been confirmed by perturbative calculations. Within linear perturbation theory, the fluctuations of the distance–redshift relation for redshift $z > 0.2$ is on the level of a few percent [11].

However, perturbations on smaller scales can become very large, density fluctuations e.g. in galaxies are $\delta\rho/\rho \sim \rho_{\rm gal}/\rho_m \sim 10^8$. Since the relation between metric perturbations, or more precisely the Christoffel symbols, and density fluctuations is non-linear, it is not evident that large amplitude, non-linear, small scale density fluctuations cannot add up to affect the distance–redshift relation on large scales.

To study the real problem one would need to analyse light rays passing through a realistic Universe with high density fluctuations. So far, this has been done only within Newtonian N-body simulations, see e.g. [121]. However, it is well known that Newtonian gravity misses the terms which are relevant for the back reaction problem [103], hence a full, non-linear relativistic treatment is needed. Since this is very difficult, so far mainly toy models which mimic reality to a certain extent have been studied.

The present work inscribes in this framework. Instead of considering spherically symmetric solutions of general relativity (GR), the so called Lemaître [79]-Tolman [120]-Bondi (LTB) models, for recent reviews see [10], we study a Universe containing high density

walls. We shall consider infinitely extended parallel walls. The considered model is a subcase of the Szekeres solution [119]. Light propagation in general Szekeres model has been studied recently [73, 85]. This is of course a gross over-simplification, but we know that galaxies tend to be aligned in filaments and photons coming to us from a far away supernova, might experience a geometry similar to the one of such a symmetric wall universe. The weakest point of our toy model is that all the walls are parallel while we expect a typical photon to traverse filaments which are aligned in different directions. We shall take this into account to some extent by studying photons coming in from different directions with respect to the walls.

Such walls have been studied in the past [26], but only perturbatively. Since we know that the effects are small within linear perturbation theory, we cannot trust higher order perturbation theory if it predicts large deviations from the Friedmann distance-redshift relation. For this reasons we analyse exact, fully relativistic wall-universes in this work.

In the next section we present the wall metric and the Einstein equations. We also study the conditions on the parameters which have to be satisfied so that no singularity apart from the Big Bang is present in the backward light cone of the observer. In section 6.3 we present the results for the distance-redshift relation for 'realistic' walls and for a wall universe which mimics the observed relation. In section 6.4 we conclude.

6.2 Wall Universes

In this section we study universes containing only pressure-less matter (dust) and which are symmetric under translations and rotations in a plane which we call the y-plane. They have the same number of symmetries as LTB models and can be solved analytically, see [126]. The metric is of the form

$$ds^2 = -dt^2 + a^2(t,x)dx^2 + b^2(t,x)(dy_1^2 + dy_2^2)\,. \tag{6.1}$$

Note that the only difference to the LTB geometry is that our symmetrical 2d manifolds are planes, $dy_1^2 + dy_2^2 = dr^2 + r^2 d\phi^2$ while those of LTB are spheres, $d\Omega^2 = d\theta^2 + \sin^2\theta d\phi^2$. We denote the spatial coordinates by $\mathbf{x} = (x, y_1, y_2)$ in order to reserve the letter z for the redshift. In the following a prime denotes a derivative w.r.t. x while a dot denotes derivative w.r.t. t. The Einstein equations for this geometry and for pure dust matter yield [119, 126, 93]

$$\partial_t\left(\frac{b'}{a}\right) \equiv \partial_t E = 0\,, \tag{6.2}$$

$$\dot{b}^2 - \left(\frac{b'}{a}\right)^2 = 2\frac{M(x)}{b}\,, \tag{6.3}$$

$$M' = 4\pi G\rho b^2 b' = 4\pi G\rho b^2 a E(x)\,. \tag{6.4}$$

In Eq. (6.2) we have introduced the time-independent function

$$E(x) = b'/a \tag{6.5}$$

and Eq. (6.3) defines $M(x)$ which is also time-independent. In LTB models M/G can be interpreted as mass density (Note that in the LTB case a term $b/(2G)$ has to be added to M which is a consequence of the curvature of the 2-sphere. For more details see [93].),

and $(M'/G)r^2dr$ is the mass in a shell of thickness dr. However as the mass in an infinite plane is not well defined, this interpretation is not meaningful in the planar case. In our case it is therefore not unreasonable that M may become negative even though a, b and ρ are supposed to be positive at all times.

From the matter conservation equation we also obtain $\partial_t(\rho b^2 a) = 0$, which, on the other hand, is a consequence of Eq. (6.4).

6.2.1 The solutions

Eq. (6.3) can we rewritten as

$$\dot{b}^2 = \frac{2M(x)}{b} + E(x)^2\,, \tag{6.6}$$

with parametric solutions [119, 126]

$$\begin{aligned}
\text{for } E \neq 0 \ : \qquad b &= \frac{M}{E^2}(\cosh\eta - 1) = \frac{2M}{E^2}\sinh^2(\eta/2)\,, && (6.7)\\
t &= \frac{M}{E^3}(\sinh\eta - \eta) + t_B(x), \quad \text{for } M > 0\,; && (6.8)\\
b &= -\frac{M}{E^2}(\cosh\eta + 1) = -\frac{2M}{E^2}\left(\sinh^2(\eta/2) + 1\right)\,, && (6.9)\\
t &= -\frac{M}{E^3}(\sinh\eta + \eta) + t_B(x), \quad \text{for } M < 0\,; && (6.10)\\
b &= |E|(t - t_B(x)) \quad \text{for } M = 0\,; && (6.11)
\end{aligned}$$

$$\begin{aligned}
\text{for } E = 0 \ : \qquad b &= \left(\frac{3}{2}\sqrt{2M}(t - t_B(x))\right)^{2/3}, \text{ for } M > 0\,, && (6.12)\\
b &= b_0 = \text{ const. }, \text{ for } M = 0\,. && (6.13)
\end{aligned}$$

Note that for $E = 0$ Eq. (6.6) implies that $M \geq 0$. This equation also implies

$$b \geq -\frac{2M}{E^2}$$

at all times, in all cases.

The function $t_B(x)$ is arbitrary; it is called the 'bang time'. For $M \geq 0$, at $t = t_B$, i.e $\eta = 0$, we have $b = 0$ which represents the Big Bang singularity. Positions with $M < 0$ have no Big Bang singularity but a 'bounce' at $t = t_B$. We shall simplify below to the case $t_B \equiv 0$, i.e., uniform bang time. Note that we have chosen expanding solutions. From these we can obtain the collapsing solutions simply by changing the sign of t. Since in the Einstein equations only $\dot{b}^2$ appears they are invariant under $t \to -t$.

Of course the $\{t = \text{const.}\}$ hypersurfaces are not parallel to the $\{\eta = \text{const.}\}$ hypersurfaces, but their position depends on x. For fixed position x, Eqs. (6.7,6.8) and (6.12). correspond to Friedmann solutions with curvature $K = -E^2 \leq 0$ and $M = 4\pi G\rho b^3/3$. Note that unlike in the Friedmann case, wall solutions with $M < 0$ need not be unphysical.

The parametric representation with η is chosen in order to express the solutions in terms of elementary functions, but it is of course not necessary. For example, for $M > 0$, setting

$$\tau(t, x) = -E^2\left(\frac{t}{6M}\right)^{2/3} \quad \text{and}$$

$$S(\tau) = (-3\tau)^{-1} \sinh^2\left(\frac{1}{2}\left[\sinh - \mathrm{id}\right]^{-1}\left(6\,(-\tau)^{3/2}\right)\right)$$

we obtain

$$b(t,x) = -\frac{M}{E^2} 6\tau S(\tau)\,.$$

Note that in the definition of S, $[\sinh - \mathrm{id}]^{-1}$ denotes the inverse of the function in brackets, and id is the identity function, id(x) = x. One can check that S solves the differential equation [125]

$$\frac{4}{3}\left(S + \tau S'\right)^2 + 3\tau - \frac{1}{S} = 0. \tag{6.14}$$

with initial condition $S(0) = \left(\frac{3}{4}\right)^{1/3}$. Note that this is the only regular solution, i.e solution with $S'(0) \neq \infty$. This expression will be useful in Section 6.3.3.

The function $a(x,\eta)$ can be obtained from Eq. (6.5). For example for $M > 0$ we find

$$a = E^{-1}\left(\frac{\partial b}{\partial x}\right)_t$$

$$\text{for } E \neq 0 \;:\quad a = \frac{2}{E}\left(\frac{M}{E^2}\right)' \sinh\left(\frac{\eta}{2}\right)^2 - \coth\left(\frac{\eta}{2}\right)\left[t'_B + \left(\frac{M}{E^3}\right)'(\sinh\eta - \eta)\right], \tag{6.15}$$

$$\text{for } E = 0 \;:\quad a = \frac{(t-t_B)^{2/3}}{M^{1/3}6^{1/3}}\left[M^{-1/3}\frac{M'}{E} + \frac{9(t-t_B)^{2/3}E'}{5\times 6^{1/3}}\right]. \tag{6.16}$$

(The suffix t in $\partial b/\partial x$ indicates that we have to interpret b as functions of (t,x), not (x,η), in this derivative.) Even if $E = 0$, Eq. (6.4) implies that $0 < M'/E < \infty$, so that the r.h.s. of Eq. (6.16) is well defined. Below, we shall choose the x-coordinate such that $M'/E =$constant.

Note that $M(x)$ and $E(x)$ can pass through zero so that in general different solutions from above have to be glued together at the boundary of their validity. We have checked that this gluing process can be performed in a smooth way and does not induce singularities in the scale factor b. However, for $M \to 0$ the scale factor $a \to \infty$. Nevertheless, we believe this to be a coordinate singularity, since, as we have checked, both, the Kretschmann scalar, $K \equiv R_{\alpha\beta\mu\nu}R^{\alpha\beta\mu\nu}$ and the scalar curvature remain finite for $M \to 0$. In our examples below we shall have $M > 0$ throughout and therefore we do not encounter this problem. However, when computing a from Eq. (6.5), one has to be careful to use the result (6.15) and take the limit $E \to 0$ for fixed t, hence also $\eta \to 0$. One cannot use (6.12) and (6.5), since for $E = 0$ we have $M' = 0$ so that Eq. (6.5) is identically satisfied and cannot be used to obtain $a(t,x)$.

6.2.2 Singularities

Singularities can occur when a, b or ρ become either infinite or zero. To have no singularities (apart from the Big Bang) which occurs at $t = t_B$, hence $b = 0$, in the past light cone of every possible observer we might be interested in, we must demand that all singularities lie in the future. In more precise models, when one specifies the observer location, one can relax this condition to the one that no singularity lies within the background lightcone of the specific observer.

In general, the question of singularities depends on the choice of the functions $M(x)$

and $E(x)$. From our solutions it is clear that b behaves monotonically as a function of time for fixed x. This is to be expected since no clustering goes on in the directions y_1 and y_2 described by this scale factor. Since we are interested in an expanding b, a singularity is present when the the scale factor a of the x-direction tends to zero. From Eq. (6.15) we infer that for $t_B \equiv 0$, $a = 0$ implies

$$\frac{2}{E}\frac{(M/E^2)'}{(M/E^3)'} = \frac{\cosh(\eta/2)}{\sinh^3(\eta/2)}\,(\sinh\eta - \eta) \geq 4/3\,.$$

It is easy to verify that the right hand side is an even positive function with minimum $4/3$ at $\eta = 0$. Hence there is a singularity at some finite value of η if the l.h.s. ever becomes $> 4/3$ or, equivalently, if

$$\frac{E'}{E}\frac{M/E^3}{(M/E^3)'} = \frac{\cosh(\eta/2)}{2\sinh^3(\eta/2)}\,(\sinh\eta - \eta) - 1 > -1/3$$

for some value of x.

We now consider a simple ansatz motivated by the perturbative analysis presented in Ref. [26]. We choose

$$M(x) = \frac{2}{9t_0^2}\,(1 + \epsilon h(x)) \tag{6.17}$$

and

$$4\pi G\rho b^2 a = \frac{M'}{E} = \frac{2}{3}t_0^{-2} = \text{const.} \tag{6.18}$$

so that

$$E = \epsilon\frac{h'}{3}\,. \tag{6.19}$$

In full generality $M'/E = f(x)$ could be an arbitrary positive function of x. But we can always make a coordinate transformation to $\tilde{x}(x)$ determined by

$$\frac{dx}{d\tilde{x}} = \frac{1}{6\pi G\rho b^2 a t_0^2},$$

so that with respect to the new coordinate M'/E =constant. Hence we just fix the coordinate x (up to a constant shift) by this choice. In addition, we have chosen uniform bang time, $t_B(x) \equiv 0$. This is a true restriction. With this we have reduced the three free functions of x to one, $h(x)$ which defines the density profile. Furthermore, we have introduced the parameter ϵ such that for $\epsilon = 0$ we reproduce the matter dominated Friedmann solution. We may also require $|h(x)| \leq 1$ so that ϵ indicates the amplitude of the perturbations. We do this in one of the examples below.

The above requirement for a singularity at some time $t \neq 0$ now reduces to $MM'' < M'^2/3$. (Strictly our derivation applies only for $M' \neq 0$. For $M' \propto E = 0$, one sees directly from Eq. (6.16) that $M'' \propto E' < 0$ is the necessary and sufficient condition for $a = 0$ at some time $t > t_B$.) We have found that most interesting mass profiles satisfy this condition for some values of x and therefore have singularities at some time in some places. This is not surprising but actually expected from gravitational collapse. However, when over densities become very high and we approach the collapse, pressure forces and heating become important and our simple pressure-less dust model for matter no longer holds. In order to be able to stay within the present framework, we therefore demand

that such singularities be in the future and not in the past for the density profiles under consideration.

Let us consider as a first example

$$h(x) = \cos(kx)\,.$$

Then the condition for the existence of a singularity (at $t \neq 0$) becomes

$$-\left(\epsilon\cos(kx) + \epsilon^2\cos^2(kx)\right) < (\epsilon^2/3)\sin^2(kx)\,.$$

which is always satisfied for some values of x, irrespective of k and ϵ. A similar behavior is expected whenever h is not a convex function, but a function representing several under- and over-densities cannot be convex.

However, this is not so important for our considerations. As we have said, the requirement of singularities to be absent is mainly a technical one and it is actually sufficient not to have a singularity in the past.

Using the above expression for a (for $M > 0$) and the ansatz (6.17,6.19) for M and E, we find that $a = 0$ is equivalent to

$$\frac{(1+\epsilon h)h''}{\epsilon h'^2 - 3(1+\epsilon h)h''} = -\frac{1}{3}\frac{1}{1-\frac{\epsilon h'^2}{3(1+\epsilon h)h''}} = \frac{1}{2}\frac{\cosh(\eta/2)}{\sinh^3(\eta/2)}\left(\sinh\eta - \eta\right) - 1 > -1/3\,. \quad (6.20)$$

Interestingly, in extremal positions of h, with $h' = 0$, the l.h.s. of the above expression is exactly $-1/3$. This comes from the fact that for this case $\eta = 0\ \forall\ t$ and we have to replace the condition that there is no singularity before some given time t_0 by $a(t) > 0$ for $t < t_0$ using expression (6.16) for $a(t)$. If $h''' = 0$ when $h' = 0$ (as in our example) one can show that in the positions where h has a maximum, hence $h' = 0$ and $h'' < 0$, $1 + \epsilon h > 0$, singularities occur first. Furthermore, when $1 + \epsilon h > 0$ and $h'' < 0$, the denominator of the l.h.s. of Eq. (6.20) is larger than 1 and hence the l.h.s. becomes $> -1/3$. Therefore, there exists a finite value $\eta_s(x)$ where Eq. (6.20) is satisfies and $a(x, \eta_s(x)) = 0$. If, on the contrary, $1 + \epsilon h > 0$ and $h'' > 0$ the l.h.s. of Eq. (6.20) is smaller than $-1/3$. For positions in the vicinity of an extremum this implies that if the extremum is a minimum of h, the position x does not encounter a singularity in the future while positions close to maxima do.

Let us study in more detail the request that the second singularity (not the big bang one) lies in the future, $t > t_0$. Using the expression (6.8) for t, we can rewrite the condition $a(x, \eta_s) = 0$ as

$$\frac{(1+\epsilon h)h''}{\epsilon h'^2 - 3(1+\epsilon h)h''} = \frac{9}{4}\frac{\cosh(\eta_s/2)}{\sinh^3(\eta_s/2)}\frac{t_0^2 t(x,\eta_s)\epsilon^3 h'^3}{(1+\epsilon h)} - 1\,.$$

The condition $t(x, \eta_s) > t_0$, for $h' < 0$ which we shall consider hence $\eta_s < 0$ for $t(x, \eta_s) > 0$, then becomes

$$\frac{(1+\epsilon h)}{\epsilon^3 h'^3}\left[1 + \frac{(1+\epsilon h)h''}{\epsilon h'^2 - 3(1+\epsilon h)h''}\right]\frac{4}{9t_0^3} < \frac{\cosh(\eta_s/2)}{\sinh^3(\eta_s/2)}\,.$$

This equation for $\eta_s(x)$ can only be solved numerically. However, often we realize that the l.h.s. is smallest at small $|h'|$ i.e. for small values of $|E(x)|$. Hence singularities will develop first in positions with small $|h'|$. This requires also small $|\eta_s|$ so that we may develop the

scale factor a and t in η_s. The above inequality then leads to power law relations and inserting the above expression for $E = (3/2)M' t_0^2$ yields the constraint

$$1 + \frac{(3t_0^2)^{7/3} 3^{1/3} 2^{2/3}}{80} \left(6M'' M^{1/3} - \frac{M'^2}{M^{2/3}} \right) > 0 \,,$$
$$1 - \frac{1}{20}(t_0 k)^{2/3} \left(6\epsilon \cos(kx) \left(1 + \epsilon \cos(kx)\right)^{1/3} + \frac{\epsilon^2 \left(\sin\left(kx\right)\right)^2}{\left(1 + \epsilon \cos\left(kx\right)\right)^{2/3}} \right) > 0. \quad (6.21)$$

The first inequality is general while for the second inequality we have chosen $h = \cos(kx)$. In Fig. 6.1 we plot the constraint for this case together with the condition to use the limiting solution for $E = 0$, (6.16), (which is not necessary for our analysis) in the ϵ–λ plane, where λ denotes the wavelength of the perturbation $\lambda = 2\pi/k$.

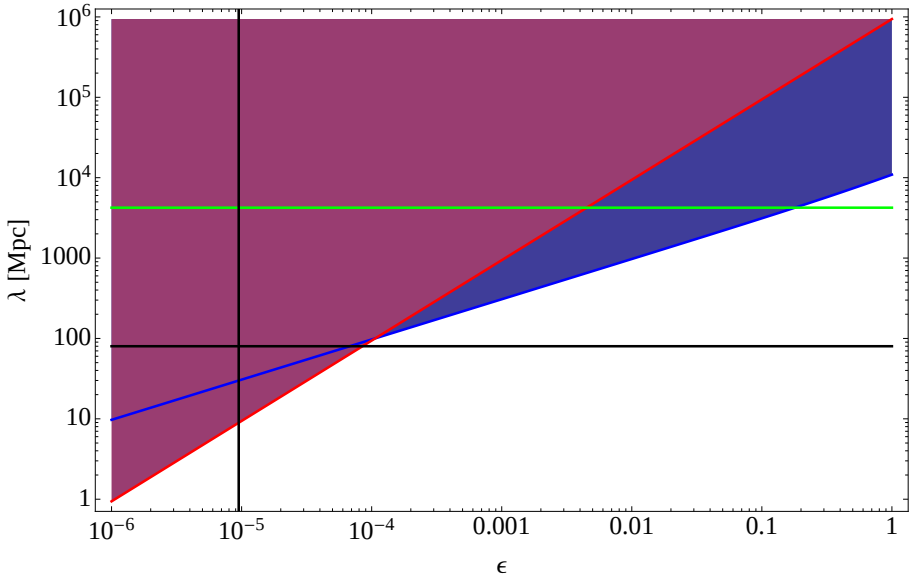

Figure 6.1: The region above the red line has singularities in the future only. While the blue line describes the condition to use the limiting solution for $E = 0$, (6.16). This can be used when $tE^3/M \ll 1$, where with "$\ll$" we mean at least two orders of magnitude smaller. The two black lines describe the physical parameters $\epsilon = 9.5 \times 10^{-6}$ and $\lambda = 80$ Mpc. The green line is the Hubble scale H_0^{-1}. With physical parameters we mean an amplitude as determined by WMAP [68] observations and a wavelength agrees with the size of the largest observed voids [45] which is about 40-90 Mpc. More precisely we find ϵ requiring that at early time there is only a single density fluctuation in each Hubble distance. This leads, at first order, to $\delta = 8\pi^2\epsilon/15$, and the matter density fluctuation at early times, $\delta \cong 5 \times 10^{-5}$ can be inferred from WMAP observations. For more details see [26].

6.3 The distance redshift relation in a wall universe

6.3.1 Generalities

6.3.1.1 Redshift

We now consider a photon emitted from a source at some position and time $(t_s, \mathbf{x}_s)$ arriving in our telescope at position and time $(t_0, \mathbf{x}_0)$. We denote the matter 4-velocity field, hence the 4-velocity of source and observer by $u(t, \mathbf{x})$ and the photon 4-velocity by n. The redshift of the source, z is then given by

$$1 + z = \frac{g(n, u)|_s}{g(n, u)|_0} \,. \tag{6.22}$$

We consider a co-moving source and observer, hence $u = \partial_t$ and normalize the affine parameter of the photon, s, such that $n^0(s_0) = 1$. The redshift then reduces to

$$1 + z = n^0|_s \tag{6.23}$$

for our geometry with $g_{00} = -1$ and $g_{0i} = 0$. From the geodesic equation for the photon we infer that its momenta in y_1- and y_2-direction are simply redshifted so that

$$J_1 \equiv b^2 n^1 = b^2 \frac{dy_1}{ds} = \text{const.} \qquad \text{and} \qquad J_2 \equiv b^2 n^2 = b^2 \frac{dy_2}{ds} = \text{const.} \tag{6.24}$$

hence

$$(n^x)^2 = \left(\frac{n^0}{a}\right)^2 - \frac{1}{a^2 b^2}\left(J_1^2 + J_1^2\right). \tag{6.25}$$

From the geodesic equation for n^0 we can now derive the evolution of the redshift:

$$\frac{dz}{ds} = -\frac{dn^0}{ds} = (1+z)^2 \frac{\dot{b}'}{b'} + \frac{J_1^2 + J_2^2}{b^2}\left(\frac{\dot{b}}{b} - \frac{\dot{b}'}{b'}\right). \tag{6.26}$$

Here we have used $a = b'/E$ to eliminate the scale factor a. Note also that the prime and the dot in the above equation denote partial derivatives while d/ds is a total derivative along the path of the photon.

6.3.1.2 Distance

The evolution of the distance to the source is given by the Sachs focussing equation [112],

$$\frac{d^2 D}{ds^2} = -\left(|\sigma|^2 + \mathcal{R}\right) D \,. \tag{6.27}$$

D is the angular diameter distance to the source, σ is the complex scalar shear of the light bundle which we define below and

$$\mathcal{R} = \frac{1}{2} R_{\mu\nu} n^\mu n^\nu = 4\pi G T_{\mu\nu} n^\mu n^\nu = 4\pi G (1+z)^2 (\rho + \bar{P}) \,. \tag{6.28}$$

Here $\bar{P} = n^i n^j P$ is the pressure in the direction of the photon. The important point is that this quantity is non-negative for any energy momentum tensor which satisfies the dominant

energy condition $\rho \geq \bar{P}$ in all directions, hence also for a cosmological constant where we have $\mathcal{R} \equiv 0$. In terms of the affine parameter of the photon, the growth of the angular diameter distance to the source is not accelerated. If the dominant energy condition is satisfied $D(s)$ is always a concave function. Furthermore, clustering which leads to the production of non-vanishing shear is only increasing the deceleration of D as function of the affine parameter s. But of course we do not measure this function but $D(z)$ which can behave very differently.

The complex shear of the light ray bundle is defined as follows [118]: We consider two spatial orthonormal vectors e_1 and e_2 which are normal to both, u and n at the observer and are parallel transported along n, such that $\nabla_n e_a = 0$ for $a = 1, 2$. The vectors e_1, e_2 are a basis of the so called 'screen'. Note that we do not require that u be parallel transported along n, hence e_1, e_2 are in general not normal to u elsewhere than at the observer, where we have given their initial conditions. The complex shear is defined by

$$\sigma = \frac{1}{2} g(\epsilon, \nabla_\epsilon n)\,, \qquad \epsilon \equiv e_1 + i e_2 \tag{6.29}$$

In order to compute the shear we must know n not only along the photon geodesic itself but we must determine its derivatives in directions normal to n. We shall directly use the transport equations [118]. For a vorticity free ray bundle (which is the case here) with expansion rate $\theta \equiv \frac{1}{2} n^\mu_{;\mu}$ these are

$$\dot{\theta} + \theta^2 + \sigma_1^2 + \sigma_2^2 = -\mathcal{R}, \tag{6.30}$$

$$\dot{\sigma}_1 + 2\theta\sigma_1 = -\mathrm{Re}\,(\mathcal{F})\,, \tag{6.31}$$

$$\dot{\sigma}_2 + 2\theta\sigma_2 = \mathrm{Im}\,(\mathcal{F})\,, \tag{6.32}$$

where $\sigma_1 = \mathrm{Re}\,(\sigma)$, $\sigma_2 = \mathrm{Im}\,(\sigma)$, and $\mathcal{F} = \frac{1}{2} R_{\alpha\mu\beta\nu} \bar{\epsilon}^\alpha \bar{\epsilon}^\beta n^\mu n^\nu$. To determine the shear σ we need to know the initial conditions for the differential equations (6.30) to (6.32). It is possible to determine the behavior of the shear and the expansion of the light near the vertex [114]. Choosing the affine parameter of the photon to vanish at the observer position, $s_0 = 0$, these are

$$\sigma(s) = -\frac{s}{3}\bar{\mathcal{F}}_0 + O\left(s^2\right), \tag{6.33}$$

$$\theta(s) = \frac{1}{s}\left(1 - \frac{1}{3}\mathcal{R}_0 s^2\right) + O\left(s^3\right). \tag{6.34}$$

$\mathcal{F}_0$ and $\mathcal{R}_0$ are the values of $\mathcal{F}$ and $\mathcal{R}$ at the observer position. The light bundle expansion θ diverges at the observer position, but we can consider an initial condition not exactly at the observer. This choice can affect the numerical precision. After determining $\mathcal{R}$, ϵ and $\mathcal{F}$ for a given geometry and photon direction, we can solve the system (6.30) to (6.32) together with the Sachs focusing equation (6.27) numerically.

6.3.2 'Realistic' walls

We want to investigate whether the system of equations derived above for $z(s)$ and $D(s)$ can lead to a distance-redshift relation close to the one observed. For wall universes we

consider,

$$\mathcal{R} = 4\pi G\rho(1+z)^2 = \frac{2(1+z)^2}{3t_0^2 b^2 a} \,. \tag{6.35}$$

For a chosen density contrast $h(x)$ we can determine $b(t,x)$ and $a(t,x)$ and solve the photon geodesic Eq. (6.26) for a given angle θ_0 of the observed photon w.r.t. the y-plane,

$$\cos\theta_0 = \frac{\sqrt{J_1^2 + J_2^2}}{b(x_0,t_0)n^0(0)} \,. \tag{6.36}$$

We again set the initial value or the affine parameter to 0, hence $x_0 = x(0)$ etc.

We have investigated two choices for $M(x)$. The first is simply $M(x) = \frac{2}{9t_0^2}\,(1+\epsilon\cos(kx))$ which we have already discussed before. The results for this case are shown in Fig. 6.2.

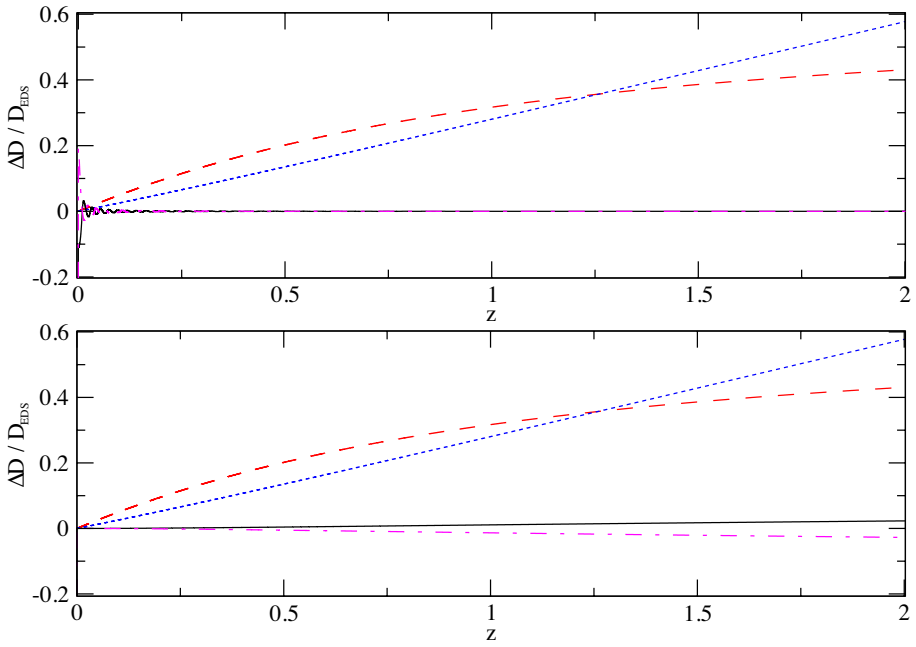

Figure 6.2: We show the relative luminosity distance redshift relation $\frac{\Delta D(z)}{D_{EdS}(z)} = \frac{D(z)-D_{EdS(z)}}{D_{EDS}(z)}$, for different models with luminosity distance $D(z)$. The blue dotted curve is for a Milne Universe, the red dashed curve is for ΛCDM universe with $\Omega_\Lambda = 0.7$ and $\Omega_M = 0.3$. The remaining two lines are our wall universe. The black solid line is in an under density while the purple dot-dashed line is in an over density. In the top panel, we consider light propagating in the x-direction only. The bottom panel is the same but for light propagating in the y-direction. The parameters for the wall model are the physical ones, $\epsilon = 9.5\times10^{-6}$ and $\lambda = 80$ Mpc.

The result is quite striking: The deviation from the Einstein-de Sitter distance-redshift relation is very small. On the level of a few percent in the most extreme case. Much smaller than the deviation for an open (Milne) Universe or even for ΛCDM. Hence voids and walls with the chosen parameters cannot simulate the observed distance redshift relation. We have also studied different values of the parameters (ϵ, k), but all cases which are such that there is no singularity before t_0 lead to small deviation from Einstein-de Sitter. Only for wavelengths of approximately Hubble scale, $k \sim H_0$, where we can choose $\epsilon \sim 10^{-3}$ do the

deviations become relatively large. But the density profile chosen here does not at all lead to a relation that resembles the observations.

As a second profile we consider thin, highly concentrated over-dense walls with an exponential profile:

$$h\left(x\right)=\frac{\lambda}{\sqrt{2\pi\sigma^{2}}}\sum_{i}\exp\left(\frac{-\left(x-x_{i}\right)^{2}}{2\sigma^{2}}\right)-1, \tag{6.37}$$

where $\lambda=x_{i+1}-x_{i}$. In the limit $\sigma\ll\lambda$ the mean of $h\left(x\right)$ vanishes and $\min_{x}h\left(x\right)=-1$. Again, we choose ϵ such that there is no singularity before t_{0}.

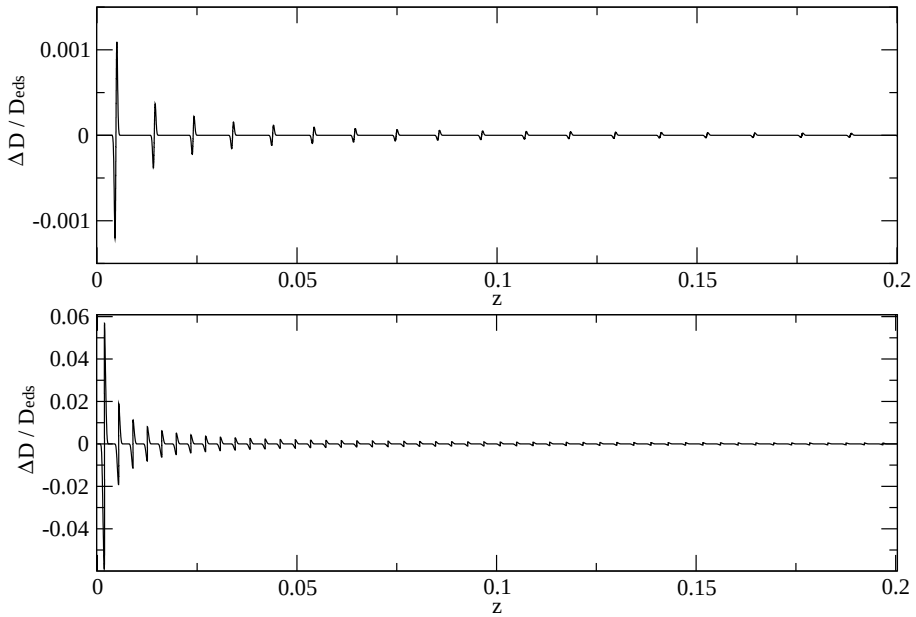

Figure 6.3: We show the relative difference between the distances in 'realistic' wall models and in EdS universe for photons propagating in x-direction. The top panel is obtained with $\epsilon=10^{-9}$, $\lambda=40$ Mpc and $\sigma=1$ Mpc, while the bottom one with $\epsilon=5\times10^{-8}$, $\lambda=15$ Mpc and $\sigma=1$ Mpc. In both cases the observer is at the center of the void. We have checked that the order of magnitude does not change for a observer in a over density. In the second case, we see that we obtain an effect of the same order of magnitude as the swiss cheese universe discussed in [84].

We have obtained the following result in these two examples (and other profiles which we do not present here explicitly): The modification of $D(z)$ never goes beyond the case of the open universe. We do not obtain acceleration by a series of dense walls. Even though we present here only two simple profiles, we think the conclusion is valid beyond these cases: if a photon passes through many *compensated* under- and over-densities in the integrated distance $D(z)$ the effect is minute as long as the time the photon spends inside a wall is much smaller than the time scale at which the gravitational potential of the wall evolves. A perturbative (first order) calculation gives a flavour of this effect. Indeed, at first order in the perturbed direction, the difference between $D(z)$ in our models and

$D_{EdS}(z)$ of a matter dominated universe can be written as

$$D_L(z_e) - D_L^{EdS} = (1+z_e)(\eta_o - \eta_e)\left(\frac{\epsilon}{3}(h(\eta_o) + h(\eta_e))\right) - (1+z_e)\int_{\eta_e}^{\eta_o} \frac{2\epsilon}{3} h(\eta)\, d\eta + (1+z_e)\int_{\eta_e}^{\eta_o} d\eta \int_{\eta_e}^{\eta} d\eta' \frac{\epsilon}{15} h''(\eta')\,\eta' - \frac{1+z_e}{\mathcal{H}_e}\int_{\eta_e}^{\eta_o} d\eta\ \frac{\epsilon}{15} h''(\eta)\,\eta \qquad (6.38)$$

where the subscripts e and o respectively mean that the conformal time is evaluated at the source (emission) or at the observer and expresses the perturbation of the energy density in under and over densities (see Appendix C for a derivation of the linearized result). From this expression, valid in the linear regime only, and for a periodic perturbation, it becomes clear that the deviation of $D_L(z)$ with respect to D_L^{EdS} depends on the amplitude ϵ of the perturbation and on the values of the conformal time at the source and at the observer. In the case of periodic perturbations, the contributions from photon path are mostly cancelled in the integral terms. Of course in the full non-linear calculation there is no simple relation between the matter over density h and the gravitational potential. In this case in principle the full non-linear Einstein equation have to be solved and Eqs. (6.26) and (6.27) govern $D_L(z)$.

Surprisingly, however, our non-linear simulations show that this result holds also to some extent in the non-linear regime. Note that, even though our value of ϵ is small, the over densities in the walls are large at late times, such that they develop singularities soon after today and we are deeply in the non-linear regime. While we do not have a proof that our conclusion holds in all cases, we have tested this also with other periodic wall profiles.

In Fig. 6.4 we show the deviations of the expansion rates with respect to the Hubble expansion in EdS universe. We note that the deviations in the unperturbed directions are small. However, in the perturbed direction these deviations can be large locally inside a wall, and they would be measurable by direct, local measurements of $H(z)$. However, they compensate when averaged over a wall thickness and do not show up in integrated quantities like $D(z)$.

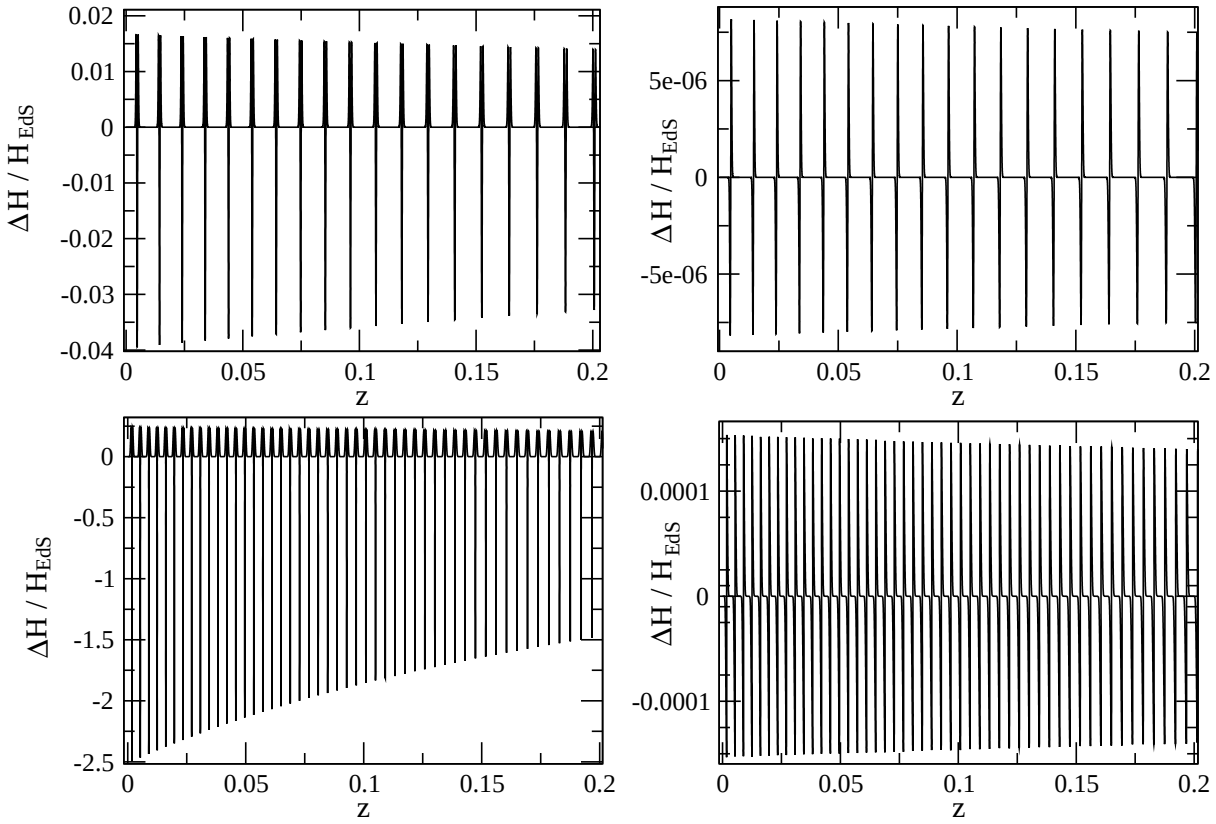

Figure 6.4: We show the relative differences between the expansion rates in the thin, highly concentrated over-dense wall model and the Hubble expansion in EdS universe. The top panels are obtained with $\epsilon = 10^{-9}$, $\lambda = 40$ Mpc and $\sigma = 1$ Mpc, while the bottom ones with $\epsilon = 5 \times 10^{-8}$, $\lambda = 15$ Mpc and $\sigma = 1$ Mpc. In both cases the observer is at the center of the void. The left panels show the expansion rates in the perturbed direction, while the right ones in the y-direction. The results for the cosine profile not shown here are similar to the two top panels.

6.3.3 Mimicking dark energy

Yoo et al. [125] have shown that in an LTB model every given distance–redshift relation can be mimicked by a suitable choice of the density profile. The same is true for a wall universe. For a given function $D(z)$ we can find a density profile which leads to exactly this distance–redshift relation for a photon coming in x-direction. First of all, for such a photon the shear vanishes for symmetry reasons and $\mathcal{R}$ is given by (6.35). To find the density profile, which is equivalent to finding $M(x)$ or $M(z) \equiv M(x(z))$ we have to solve the following coupled system of six ordinary differential equations (in principle none of the other equations couples to (6.41) since both, F_M and F_β do not depend on x explicitly),

which is very similar to the system solved in Ref. [125]:

$$\frac{dM}{ds} = F_M\left(t,z,M,\beta,\zeta\right), \tag{6.39}$$
$$\frac{d\beta}{ds} = F_\beta\left(t,z,M,\beta,\zeta\right), \tag{6.40}$$
$$\frac{dx}{ds} = \frac{F_M\left(t,z,M,\beta,\zeta\right)}{\beta} \tag{6.41}$$
$$\frac{dt}{ds} = 1+z, \tag{6.42}$$
$$\frac{dz}{ds} = \frac{\zeta}{\frac{dD}{dz}}, \tag{6.43}$$
$$\frac{d\zeta}{ds} = -4\pi\left(1+z\right)^2\rho D, \tag{6.44}$$

where we have defined

$$\zeta = \frac{dz}{ds}\frac{dD}{dz} \text{ and } \beta = \frac{\frac{dM}{ds}}{\frac{dx}{ds}} = M' = \frac{2}{3t_0^2}E\,. \tag{6.45}$$

In Appendix 6.5.1 we give the derivation of this system and the detailed expressions for F_M and F_β. There, we also explain the method used to specify the initial conditions at the observer. All the constraints are fixed by requiring the system to have no critical points. Note also that $z(s)$ need not to be monotonic. If $dz/ds = 0$ at a value of s where $\zeta = dD/ds \neq 0$, the derivative dD/dz is not well defined. This is, however, not the case of a ΛCDM Universe which we want to mimic here. We are then left with one initial condition, which we choose by requiring

$$H_0 = \left.\frac{\dot{a}}{a}\right|_{s_0} = \left.\frac{\dot{b}}{b}\right|_{s_0}, \tag{6.46}$$

i.e. the value of the Hubble rate at the observer today does not depend on direction. In Fig. 6.5 we show $M(x)$ as well as its derivative with respect to the x coordinate, $\beta\left(x\right)$, for the solution mimicking the ΛCDM expression for $D(z)$, for $\Omega_K = 0$, $\Omega_m = 0.3$ and $\Omega_{DE}(z) = 0.7$ =constant.

$$D(z) = \frac{1}{1+z}\chi_K\left(\int_0^z \frac{dz'}{H(z')}\right) \quad \text{where} \tag{6.47}$$
$$\chi_K(r) = \frac{1}{\sqrt{K}}\sin(r\sqrt{K})\,, \quad \text{and}$$
$$H(z) = H_0\Big(\Omega_m(1+z)^3 + \Omega_K(1+z)^2 + \Omega_r(1+z)^4 + \Omega_{DE}(z)\Big)^{1/2}.$$

In Fig. 6.6, we show how the luminosity distance deviates when the observer looks at photons coming in with different angles θ_0. For $\theta_0 = 90$ degrees, we have photons traveling in x-direction, in this case the luminosity distance is fitted to the one of ΛCDM by solving the system of Eqs. (6.39-6.44) with the functions $M(x)$ and $\beta(x)$ shown in Fig. 6.5. It is interesting to remark that a given angle of $\theta_0 \in [0;90]$ degrees at the observer corresponds

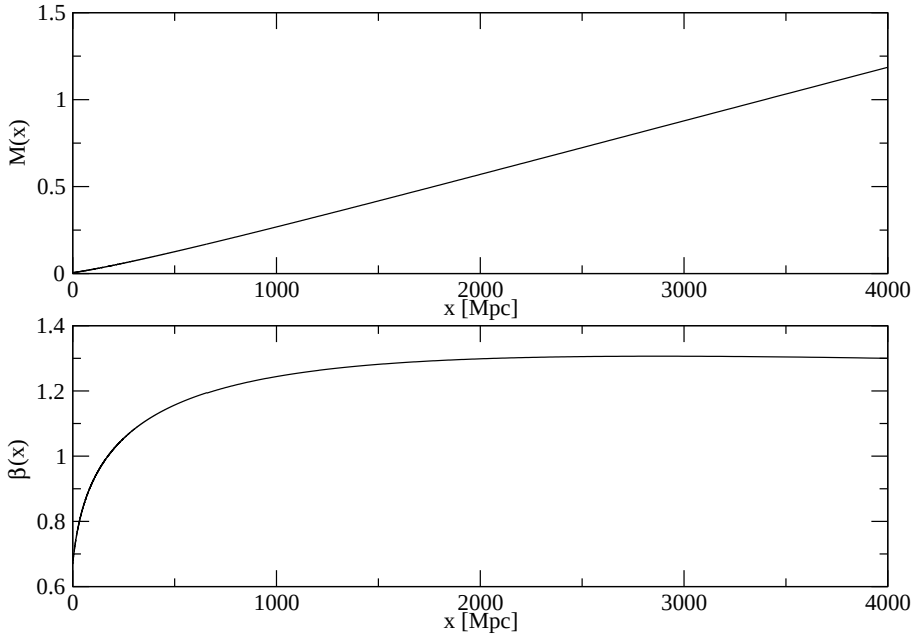

Figure 6.5: We show the function $M(x)$, top panel, and its derivative $\beta(x)$, bottom panel. In principle, there is a entire family of functions $M(x)$ parametrized by the initial value $M(0) = M_0$ that we are free to choose (appendix A). Here, we present the solutions corresponding to $H_0 = \frac{\dot{a}}{a}\big|_{s_0} = \frac{\dot{b}}{b}\Big|_{s_0}$.

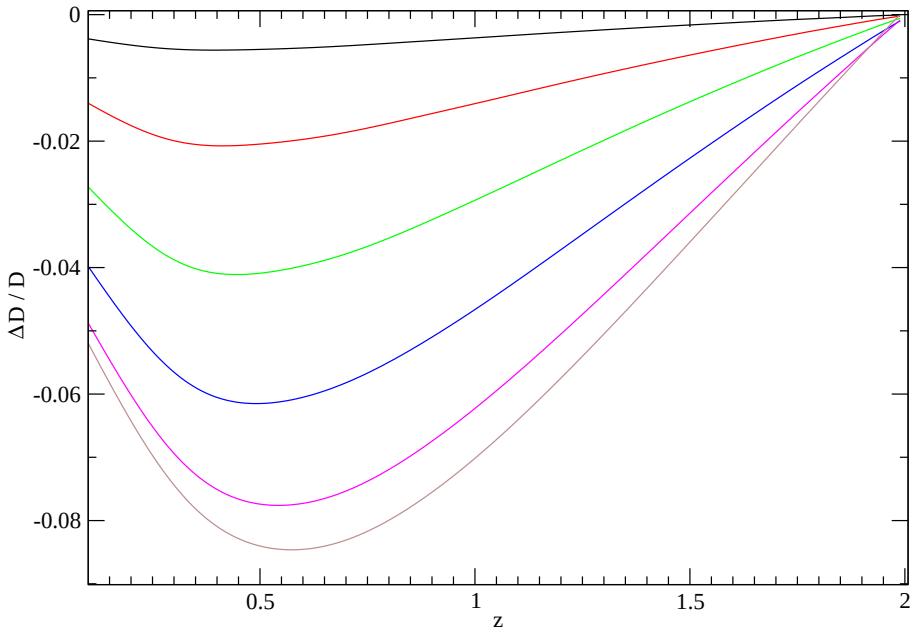

Figure 6.6: We show the relative differences between luminosity distances for photons traveling in the x-direction (perpendicular to the walls) and photons observed with an angle θ_0 (see Eq.(6.36)). From the top to the bottom, we respectively have $\theta_0 = 75,\ 60,\ 45,\ 30,\ 15,\ 5$ degrees.

to an angle at the emission $\theta_e > \theta_0$. This is a consequence of the spacetime geometry induced by the walls: due to the clustering in direction x, corresponding to $\theta = 90^o$, its expansion slows down in time.

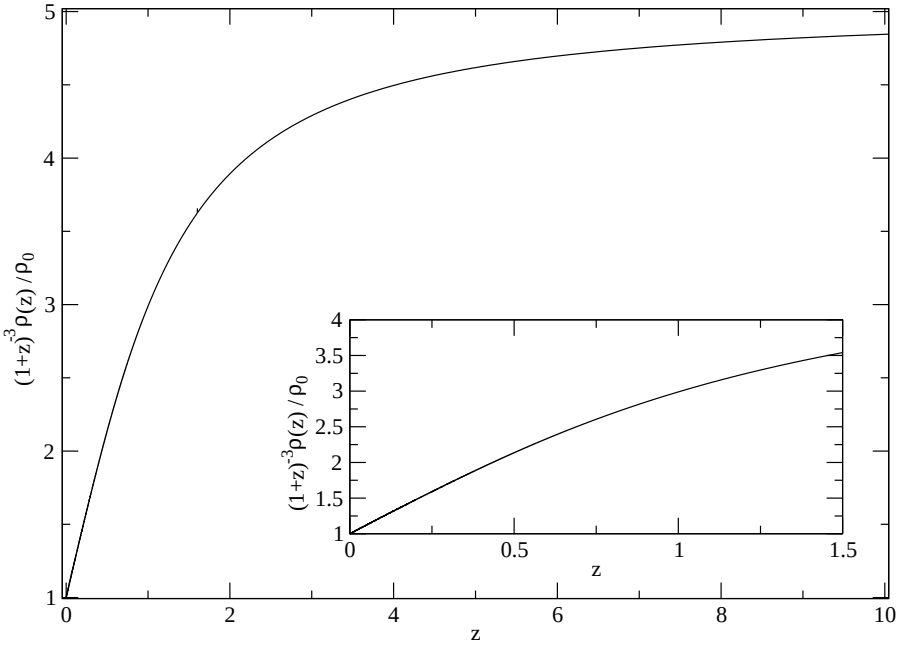

Figure 6.7: We show the ratio of our density profile to the Einstein-de Sitter one as a function of the cosmological redshift.

In Fig. 6.7, we present the density profile corrected by the isotropic expansion rate, $(1+z)^{-3}\rho(z)/\rho_0$, $\rho_0 = \rho(z=0)$, obtained for our model to mimic ΛCDM luminosity distance. Finally, in Fig. 6.8, we plot the expansion rates in the longitudinal and transverse directions, $H_a = \dot{a}/a$ and $H_b = \dot{b}/b$. It is interesting to estimate roughly the features of the under density needed to fit ΛCDM luminosity distance. For example, if one considers the highest redshift for which we have data from supernovae, at around $z \sim 1.7$. This roughly corresponds to a size $\sim H_0^{-1}$. (Of course we have another data point from the CMB. The angular size of the acoustic oscillations provides an excellent measure of the angular diameter distance to the last scattering surface, $z \simeq 1090$. But this is not very relevant in our context as the Universe is to a good approximation matter dominated from $z = 2$ to $z = 1090$.) An under density of the size of the order of the Hubble distance is necessary to mimic ΛCDM with our walls. Moreover, we can also determine the ratio of the energy density normalized at the observer to the energy density in an Einstein-de Sitter model at $z \sim 1.7$ which is about 4. At high redshift, $z \gtrsim 10$ the anisotropy is very small and the Universe is close to a Friedmann Universe with about 5 times the matter density obtained from local estimates.

6.3.4 Redshift drift

In the previous section we have fixed $M(x)$ to reproduce the distance redshift relation of ΛCDM universe. Of course, having one free function to play with, namely $M(x)$, we expect to be able to fit one function, in our case $D(z)$. If we now proceed to another, independent observable, we shall most probably not fit it. We have done this by looking at the redshift

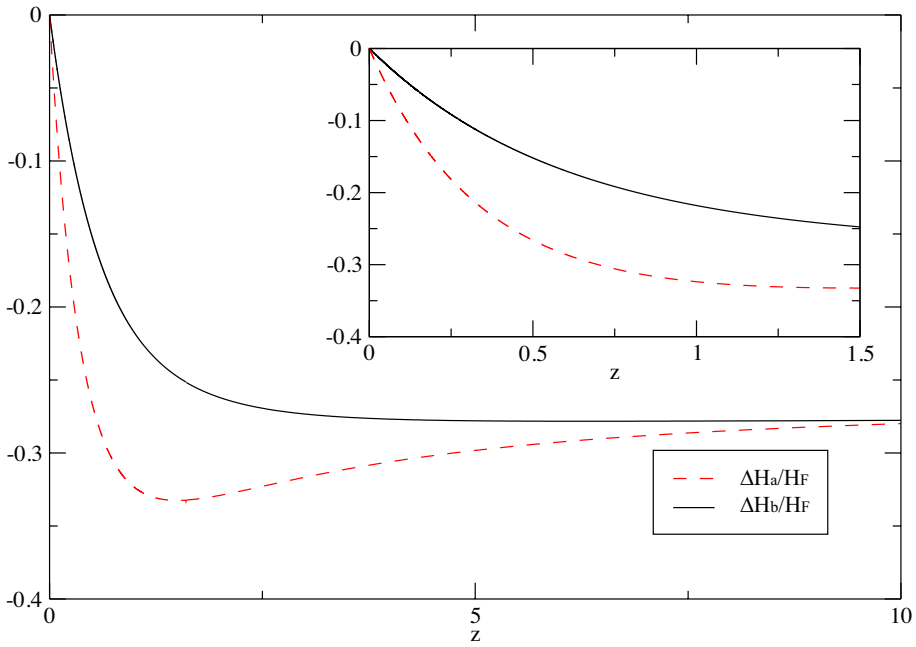

Figure 6.8: We show the relative expansion rates in the transverse and longitudinal directions as functions of the cosmological redshift. We use the following notation : $\Delta H_{a,b} = H_{a,b} - H_F$, where H_F is the expansion rate in an Einstein-de Sitter universe, and $H_{a,b}$ are the expansion rates in the longitudinal and transverse directions, normalized to the their values at the observer.

drift, defined as the rate of change of the redshift of a co-moving source per unit of observer time. In a Friedmann Universe the redshift drift is simply

$$\frac{dz}{dt_0} \equiv \lim_{\Delta t_0 \to 0} \frac{z(t_s + \Delta t_s) - z(t_s)}{\Delta t_0} = H_0(1+z) - H(z)\,, \tag{6.48}$$

where $H(z) = H(t_s)$ and H_0 denote the Hubble parameter at the source position at time t_s and at the observer at the moment t_0. We have computed the corresponding function (for light rays in x-direction) from our solution $M(x)$. The general expression for the redshift drift of a wall Universe in x–direction is (see Appendix 6.5.2),

$$\begin{aligned} \frac{dz}{dt_0} &= (1+z)\int_0^z \left(\frac{\ddot{b}'}{\dot{b}'}\right)(1+z')^{-2}\,dz' = \\ &= -(1+z)\int_0^z \left(4\pi G\rho - \frac{2M}{b^3}\right)\frac{a}{\dot{a}}\,(1+z')^{-2}\,dz'\,. \end{aligned} \tag{6.49}$$

Since we do not require $M_0 = 0$ as in LTB model, we can in principle have a positive redshift drift at low redshift; but we do not obtain this for our best fit profile $M(x)$ with $t_B(x) \equiv 0$. The result is compared with ΛCDM in Fig. 6.9.

Clearly the redshift drift for the two cosmologies are very different. We do have a second function to play with, the bang time $t_B(x)$, so that we could probably fix this observable. This has been done for LTB models in [15]. However, as it is show there, models which have both, the same redshift distance relation and the same redshift drift as ΛCDM can

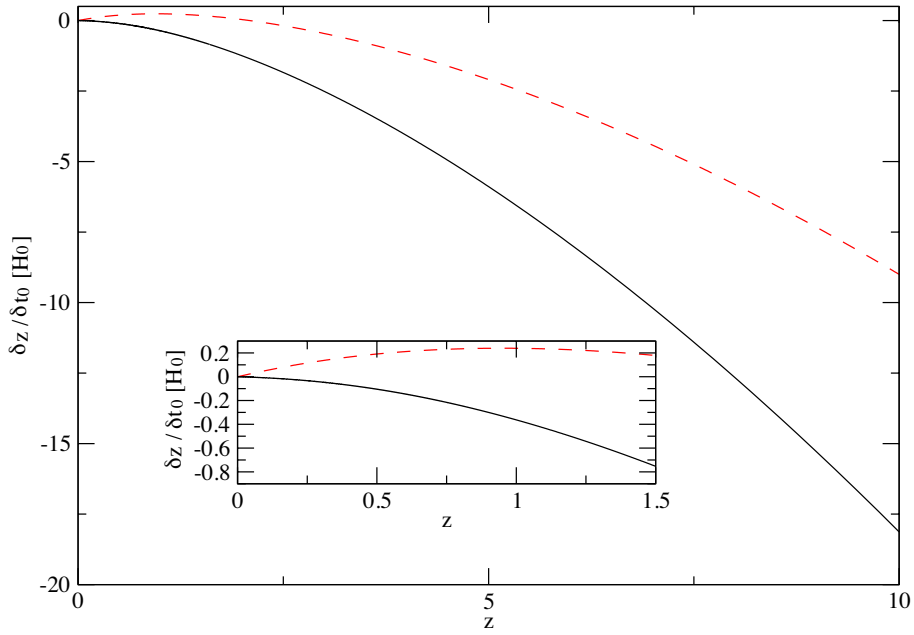

Figure 6.9: We show the redshift drift for the wall Universe (black solid line) which mimics the distance redshift relation of ΛCDM and compare it with the redshift drift of the latter (red dashed line).

be ruled out with a third observable, the kinematic Sunyaev-Zel'dovich effect which comes from the recession velocity of clusters.

6.4 Conclusions

We have studied the effect of matter perturbations on the luminosity distance in a model with planar symmetry described by the metric (6.1). Considering 'realistic' walls we find that the effect from density inhomogeneities is very small, it nearly averages out. It leads to fluctuations of the luminosity distance around the 'background' distance, but not to a significant global shift. Our results (Fig. 6.3) show that these fluctuations are due to matter inhomogeneities at the source and the observer positions, without any relevant contribution from the integrated effects of light propagation, like in the linear approach (6.38). Hence we can not mimic acceleration with many dense walls which grow by gravitational instability. Since we consider pressure-less matter only, the amplitude of density fluctuations is limited by the presence of singularities. This is a limitation of the model.

After having shown that 'realistic' wall models can not reproduce the observed distance-redshift relation, we have determined the density profile which can mimic it. We have fixed the free function of our model, $M(x)$, to mimic the luminosity (or angular) distance of the ΛCDM universe. We have shown that the observation of the redshift drift can distinguish between this model and ΛCDM. Abandoning the assumption of an uniform bang time we could arrange the second degree of freedom, $t_B(x)$, to fit the redshift drift too. We have found that the redshift drift in our model can be positive at low redshift, contrarily to the

LTB model [124].

With our solution $M(x)$ we can fit ΛCDM distance for photons coming in x-direction for positive x only. This preferred direction corresponds to the radial incoming direction for LTB model. The deviation from ΛCDM for photons coming from different angles is typically a few percent (see Fig. 6.6).

Acknowledgements

This work is supported by the Swiss National Science Foundation.

6.5 Appendices

6.5.1 Derivation of the system of differential equations and initial conditions

6.5.1.1 The system

Here we derive in more detail the system (6.39) to (6.44) and give the initial conditions used for the solution.

Since we choose the photon affine parameter such that $n^0|_0 = 1$ we have

$$1 + z(s) = n^0(s) = \frac{dt}{ds}$$

Furthermore, the null condition for a light ray in x–direction implies

$$\left(\frac{dt}{ds}\right)^2 = \left(\frac{b'}{E}\right)^2 \left(\frac{dx}{ds}\right)^2 = \left(\frac{2b'}{3t_0^2 M'}\right)^2 \left(\frac{dx}{ds}\right)^2 . \tag{6.50}$$

The geodesic equation gives

$$\frac{dz}{ds} = \frac{d^2t}{ds^2} = -\frac{\dot{a}}{a}(1+z)^2 = -\frac{\dot{b}'}{b'}(1+z)^2 . \tag{6.51}$$

Hence, when the expansion in x-direction changes into contraction, $\dot{a} = 0$, also dz/ds passes through zero. However, this does not happen in our case which mimics ΛCDM. Noting that geodesics in x-direction have no shear, the Sachs focusing equation yields

$$\frac{d^2z}{ds^2}\frac{dD}{dz} + \left(\frac{dz}{ds}\right)^2 \frac{d^2D}{dz^2} = -4\pi G\rho\,(1+z)^2\,D, \tag{6.52}$$

where we have used $\mathcal{R} = 4\pi G\,(1+z)^2\,\rho$. We can now rewrite these equations in terms of the system (6.39) to (6.44). To find the functions F_M and F_β we first derive the following

useful relations

$$\dot{\tau} = \frac{2}{3t}\tau, \tag{6.53}$$

$$\tau' = \tau\left(2\frac{\frac{d\beta}{ds}}{\frac{dM}{ds}} - \frac{2}{3}\frac{\beta}{M}\right). \tag{6.54}$$

$$b' = -\frac{8}{9t_0^4}\frac{\tau}{\beta}\left(S - 2\tau S'\right) - \frac{16}{3t_0^4}\tau^2\frac{M}{\beta^2}\frac{\frac{d\beta}{ds}}{\frac{dM}{ds}}S', \tag{6.55}$$

$$\dot{b}' = -\frac{16}{27t_0^4}\frac{\tau}{t}\frac{1}{\beta}\left(S - 3\tau S' - 2\tau^2 S''\right) - \frac{32}{9t_0^4}\frac{M}{\beta^2}\frac{\frac{d\beta}{ds}}{\frac{dM}{ds}}\frac{\tau^2}{t}\left(2S' + \tau S''\right). \tag{6.56}$$

Here S' always indicates the derivative of S with respect to its argument τ while as for all other functions of (t, x) the prime denotes the partial derivative w.r.t. x and the dot the one w.r.t. t. The null condition for the light ray can be written as

$$\frac{dM}{ds}A_1 + \frac{d\beta}{ds}B_1 = \pm 1,$$

with

$$A_1 = -\frac{16}{27t_O^6}\frac{\tau}{\beta^3\left(1+z\right)}\left(S - 2\tau S'\right), \tag{6.57}$$

$$B_1 = -\frac{32}{9t_O^6}\frac{\tau^2 M}{\beta^4\left(1+z\right)}S'. \tag{6.58}$$

The geodesic equation takes the form

$$\frac{dM}{ds}A_2 + \frac{d\beta}{ds}B_2 = 0, \tag{6.59}$$

where

$$A_2 = -\frac{\zeta}{\frac{dD}{dz}}\frac{8}{9t_0^4}\frac{\tau}{\beta}\left(S - 2\tau S'\right) - \left(1+z\right)^2\frac{16}{27t_0^4}\frac{\tau}{t}\frac{1}{\beta}\left(S - 3\tau S' - 2\tau^2 S''\right), \tag{6.60}$$

$$B_2 = -\frac{\zeta}{\frac{dD}{dz}}\frac{16}{3t_O^4}\tau^2\frac{M}{\beta^2}S' - \left(1+z\right)^2\frac{32}{9t_0^4}\frac{M}{\beta^2}\frac{\tau^2}{t}\left(2S' + \tau S''\right), \tag{6.61}$$

with $\zeta = \frac{dD}{ds} = \frac{dz}{ds}\frac{dD}{dz}$. From this we infer

$$F_M\left(t, z, M, \beta, \zeta\right) = \pm\frac{B_2}{A_1B_2 - A_2B_1}, \tag{6.62}$$

$$F_\beta\left(t, z, M, \beta, \zeta\right) = \mp\frac{A_2}{A_1B_2 - A_2B_1}. \tag{6.63}$$

Since τ is a function of M, β and t, we now have expressed everything in terms of our

variables (t, z, M, β, ζ) and the given function $D(z)$. Explicitly, F_M and F_β are given by

$$F_M = \pm\frac{3t_O^2}{4}\beta\left(\frac{6M}{t}\right)^{2/3}\frac{\frac{\zeta}{\frac{dD}{dz}}\frac{3t}{2}\frac{S'}{1+z}+(1+z)\left(2S'+\tau S''\right)}{SS'+\tau SS''-\tau S'^2}\,, \tag{6.64}$$

$$F_\beta = \pm\frac{1}{18t_O^2}\frac{1}{M}\left(\frac{6M}{t}\right)^{4/3}\frac{\frac{\zeta}{\frac{dD}{dz}}\frac{3t}{2}\frac{(S-2\tau S')}{1+z}+(1+z)\left(S-\tau S'-2\tau^2 S''\right)}{SS'+\tau SS''-\tau S'^2}\,. \tag{6.65}$$

6.5.1.2 Initial conditions

Let us now turn to the initial conditions at $s_0 = 0$. Without loss of generality we can set $x(0) = 0$. Clearly also $z(0) = 0$. From definition (6.45) we have

$$\zeta(0) = \left.\frac{dD}{ds}\right|_{s=0}. \tag{6.66}$$

Since this is an initial condition for the Sachs focusing equation, we have consistently with our affine parameter normalization [114, 91],

$$\zeta(0) = -1. \tag{6.67}$$

From (6.43) we note that our system of coupled differential equations has a critical point z_{cr} defined by

$$\left.\frac{dD}{dz}\right|_{z=z_{cr}} = 0. \tag{6.68}$$

For our ΛCDM parameters $z_{cr} \approx 1.6$. To obtain a regular solution we must therefore impose $\zeta(z_{cr}) = 0$. We remark that Eqs. (6.67) and (6.51) imply

$$\frac{\dot{a}}{a} = H_0, \tag{6.69}$$

where we have used

$$\left.\frac{dD}{dz}\right|_{z=0} = H_0^{-1}.$$

Hence the rate expansion in x-direction coincides with the measured Hubble expansion. In order to solve the system of five differential equations (Eq. (6.41) is an independent equation, since the solution $x(s)$ can also be inferred from Eq. (6.42) via the null condition), five initial conditions are needed. However, we only have two of them

$$z(0) = 0 \qquad \zeta(0) = -1. \tag{6.70}$$

We have two other constraints which we must satisfy at the critical point where (6.68) holds. Denoting the affine parameter at the critical point by s_{cr}, we have

$$z(s_{cr}) = z_{cr} \qquad \zeta(s_{cr}) = 0. \tag{6.71}$$

These lead to two other initial conditions which can be determined using the shooting method. One remaining constraint is needed and we fix it by requiring

$$\left.\frac{\dot{a}}{a}\right|_0 = \left.\frac{\dot{b}}{b}\right|_0 = H_0. \tag{6.72}$$

This last condition fixes $M(0)$ and makes sure that the Hubble rate measured today is the same in any direction. We then numerically integrate the system from the critical point to the observer by varying the three remaining conditions at the critical point until the initial conditions (6.70) and (6.72) are satisfied. This matching is obtained by using the three dimensional Newton-Raphson method. Once the desired precision has been reached, the two remaining initial conditions $\beta(0)$ and $t(0)$ can simply be read from the numerical data.

6.5.2 Derivation of the system of differential equations for the redshift drift

The redshift drift for a LTB model has been derived in [124]. This approach can also be applied to our model. The null condition for the light ray (in x-direction) and the geodesic equation lead to

$$\frac{dz}{dx} = \frac{\dot{b}'}{E}(1+z), \qquad \frac{dt}{dx} = -\frac{b'}{E}. \tag{6.73}$$

We consider two infinitesimally close geodesics at fixed comoving position x, parametrized by

$$\{z_c, t_c\} \quad \text{and} \quad \{z_c + \delta z, t_c + \delta z\}.$$

Since the geodesic $\{z_c, t_c\}$ satisfies (6.73), it follows

$$\begin{aligned} \frac{d\delta z}{dx} &= \frac{\ddot{b}'}{E}(1+z)\,\delta t + \frac{\dot{b}'}{E}\delta z, \\ \frac{d\delta t}{dx} &= -\frac{\dot{b}'}{E}\delta t. \end{aligned}$$

Then, inserting (6.73) we obtain

$$\frac{d\delta z}{dz} = \frac{\ddot{b}'}{\dot{b}'}\delta t + \frac{\delta z}{1+z}, \tag{6.74}$$

$$\frac{d\delta t}{dz} = -\frac{\delta t}{1+z}. \tag{6.75}$$

Integrating (6.75) we find

$$\delta t = \frac{\delta t_0}{1+z}.$$

This solution together with (6.74) leads to

$$\frac{d}{dz}\left(\frac{\delta z}{\delta t_0}\right) = \frac{1}{1+z}\left(\frac{\ddot{b}'}{\dot{b}'} + \frac{\delta z}{\delta t_0}\right).$$

This equation is solved by (6.49). Deriving the Einstein equation (6.3) twice (once w.r.t. x and once w.r.t. t), we obtain

$$\ddot{b}' = \frac{2Mb'}{b^3} - \frac{M'}{b^2}. \tag{6.76}$$

With (6.2) and (6.4) this results in the second line of (6.49).

6.5.3 The linearized approach

We determine the luminosity distance within linear perturbation theory for small deviations from a Friedmann–Lemaître background. Let us define

$$\begin{aligned} a(t,x) &= \bar{a}(t)\left(1+\epsilon f(t,x)\right), && (6.77)\\ b(t,x) &= \bar{a}(t)\left(1+\epsilon g(t,x)\right), && (6.78)\\ \rho(t,x) &= \bar{\rho}(t)\left(1+\epsilon\delta(t,x)\right), && (6.79) \end{aligned}$$

where the unperturbed quantities $\bar{a}(t)$, $\bar{\rho}(t)$ satisfy the Einstein equation for a flat matter dominated Friedmann universe (EdS). The perturbed quantities are determined by the Einstein equations at first order in ϵ,

$$\begin{aligned} \frac{-6t_0^{4/3}g'' + 4t^{1/3}\left(\dot{f}+2\dot{g}\right)}{3t^{4/3}} &= 8\pi G\bar{\rho}\delta, && (6.80)\\ \dot{g}' &= 0, && (6.81)\\ t^{1/3}\left(2\dot{g}+t\ddot{g}\right) &= 0, && (6.82)\\ t_0^{4/3}g'' - t^{1/3}\left(2\dot{f}+2\dot{g}+t\left(\ddot{f}+\ddot{g}\right)\right) &= 0. && (6.83) \end{aligned}$$

Neglecting the decaying mode and imposing that at the beginning the scale factors in all three directions agree, we obtain [26],

$$\begin{aligned} g &= \frac{\delta_O}{3}, && (6.84)\\ f &= \frac{3}{10}\delta_O'' t_O^{4/3} t^{2/3} + \frac{\delta_O}{3}, && (6.85) \end{aligned}$$

where $\delta_O(x) = \delta(t,x) + f(t,x) + 2g(t,x)$ is independent of time. This is a consequence of energy conservation and can also be derived by combining (6.80) to (6.83).

We are interested in finding the relation between δ_O and M, E in the perturbative regime. Following [126] we expand the solution (6.7, 6.8) around $\eta = 0$ in terms of $\frac{t_B(x)}{t} \ll 1$ and $\frac{E^3 t}{M} \ll 1$. Comparing the expanded solution with the linear one we find

$$M = \frac{2}{9t_0^2}\left(1+\epsilon\delta_O\right), \quad E = \frac{\epsilon\delta_O'}{3}. \tag{6.86}$$

With the ansatz (6.17, 6.19) we can identify $\delta_O(x)$ with $h(x)$ in the perturbative regime.

The angular distance is determined by Sachs focusing equation (6.27). We note that the shear term does not contribute to first order. Since light propagation is not affected by a conformal transformation, it is convenient to work with the conformally related geometry

$$ds^2 = -d\eta^2 + (1+2\epsilon f)\,dx^2 + (1+2\epsilon g)\left(dy_1^2 + dy_2^2\right) . \tag{6.87}$$

From this, we compute the Christoffel symbols (here we denote the derivative w.r.t. the conformal time η by a dot)

$$\Gamma^1_{10} \cong \epsilon\dot{f}, \qquad \begin{array}{c} \Gamma^0_{11} \cong \epsilon\dot{f}, \\ \Gamma^1_{11} \cong \epsilon f', \\ \Gamma^2_{20} = \Gamma^3_{30} \cong \epsilon\dot{g}, \end{array} \qquad \begin{array}{c} \Gamma^0_{22} = \Gamma^0_{33} \cong \epsilon\dot{g}, \\ \Gamma^1_{22} = \Gamma^1_{33} \cong -\epsilon g', \\ \Gamma^2_{21} = \Gamma^3_{31} \cong \epsilon g'. \end{array}$$

and the Ricci tensor

$$\begin{aligned} R_{00} &\cong -\epsilon\left(\ddot{f} + 2\ddot{g}\right), \\ R_{10} &\cong -2\epsilon\dot{g}', \\ R_{11} &\cong \epsilon\left(\ddot{f} - 2g''\right), \\ R_{22} = R_{33} &\cong \epsilon\left(\ddot{g} - g''\right). \end{aligned}$$

At 0-order we are free to parametrize the affine parameter s such that $\bar{n}^0 = 1$ and $\bar{n}^i = \delta^{i1}$ (we are interested in the distance in x-direction). With this we obtain the coefficient $\mathcal{R}$

$$\mathcal{R} = -\epsilon\left(\ddot{g} + g'' + 2\dot{g}'\right).$$

Consistently with the parametrization of the affine parameter s such that $n^0(s_0) = 1$, the initial conditions are $D(s_o) = 0$ and $D'(s_o) = -1$. After an integration by parts we find the solution to Sachs focusing equation (6.27),

$$D(s) = (s_o - s)\left(1 + \epsilon g(s_o) + \epsilon g(s)\right) + 2\int_{s_o}^{s} ds'\epsilon g\left(s'\right). \tag{6.88}$$

With the above initial conditions for the Sachs focusing equation, we consider a thin light bundle with the vertex at the observer position. Hence the solution (6.88) is the angular diameter distance, see [114]. To determine the luminosity distance we have to compute also the redshift, using the geodesic equation for n^0,

$$1 + z = \frac{g_{\mu\nu}n^\mu u^\nu|_e}{g_{\mu\nu}n^\mu u^\nu|_o} = n^0\big|_e = 1 - \int_{s_o}^{s_e} ds\ \epsilon\dot{f}, \tag{6.89}$$

where $|_e$ denotes the emission point, the source, and we denote the affine parameter at the source by s_e. With the same geodesic equation we derive the relation between the conformal time η and the affine parameter s, $n^0 = d\eta/ds$,

$$\eta_o - \eta_e = s_o - s_e + \int_{s_o}^{s_e} ds \int_{s_o}^{s} ds'\epsilon\dot{f}(s'). \tag{6.90}$$

In terms of conformal time the luminosity distance then becomes

$$D_L(\eta_e) = (\eta_o - \eta_e)\left(1 + \epsilon g_o + \epsilon g_e - 2\int_{\eta_o}^{\eta_e} d\eta\ \epsilon\dot{f}\right) + 2\int_{\eta_o}^{\eta_e} d\eta\ \epsilon g - \int_{\eta_o}^{\eta_e} d\eta \int_{\eta_o}^{\eta} d\eta' \epsilon\dot{f}. \quad (6.91)$$

All of this is valid in the conformal geometry, where the expansion of the Universe is divided out. Taking into account the expansion of the universe, changes the relation between the affine parameter and conformal time. The luminosity distance scales as [11]

$$\tilde{D}_L = \frac{\bar{a}^2(\eta_o)}{\bar{a}(\eta_e)} D_L = \frac{D_L}{\bar{a}(\eta_e)} = (1 + \bar{z}_e) D_L.$$

Since conformal time is not an observable quantity, we rewrite the distance in term of the observed redshift. We define the observed redshift as $z_e = \bar{z}_e + \delta z_e$ and we compute the correction term. The same calculation as presented in Ref. [11] leads to

$$\left(\frac{d}{dz}\tilde{D}_L\right)\delta z_e = \left((\eta_o - \eta_e) + \mathcal{H}_e^{-1}\right)\delta z_e, \quad (6.92)$$

where

$$\delta z_e = -(1 + z_e)\int_{\eta_o}^{\eta_e} d\eta\ \epsilon\dot{f}. \quad (6.93)$$

Subtracting (6.92) we obtain the distance–redshift relation

$$\begin{aligned} \tilde{D}_L(z_e) &= (1 + z_e)(\eta_o - \eta_e)\left(1 + \epsilon g_o + \epsilon g_e - \int_{\eta_o}^{\eta_e} d\eta\ \epsilon\dot{f}\right) \\ &+ (1 + z_e)\left(2\int_{\eta_o}^{\eta_e} d\eta\ \epsilon g - \int_{\eta_o}^{\eta_e} d\eta \int_{\eta_o}^{\eta} d\eta' \epsilon\dot{f}\right) + \frac{1 + z_e}{\mathcal{H}_e}\int_{\eta_o}^{\eta_e} d\eta\ \epsilon\dot{f}. \end{aligned} \quad (6.94)$$

With

$$-\int_{\eta_o}^{\eta_e} d\eta \int_{\eta_o}^{\eta} d\eta' \epsilon\dot{f} = (\eta_e - \eta_o)\int_{\eta_e}^{\eta_o} d\eta\ \epsilon\dot{f} + \int_{\eta_e}^{\eta_o} d\eta \int_{\eta_e}^{\eta} d\eta' \epsilon\dot{f},$$

we can rewrite the above expression in the form as

$$\begin{aligned} \tilde{D}_L(z_e) &= (1 + z_e)(\eta_o - \eta_e)(1 + \epsilon g_o + \epsilon g_e) \\ &+ (1 + z_e)\left(-2\int_{\eta_e}^{\eta_o} d\eta\ \epsilon g + \int_{\eta_e}^{\eta_o} d\eta \int_{\eta_e}^{\eta} d\eta' \epsilon\dot{f}\right) - \frac{1 + z_e}{\mathcal{H}_e}\int_{\eta_e}^{\eta_o} d\eta\ \epsilon\dot{f}\ . \end{aligned} \quad (6.95)$$

Using the solutions (6.84, 6.85) we express the distance in terms of $\delta_O(\eta)$. Conformal time is defined as

$$d\eta = \frac{dt}{\bar{a}(t)} \quad \Rightarrow \quad \eta(t) = 3t^{1/3}t_0^{2/3}, \quad \text{setting} \quad \eta(0) = 0.$$

This leads to

$$\begin{aligned} g\left(\eta, x\left(\eta\right)\right) &= \frac{\delta_O\left(x(\eta)\right)}{3}, \\ f\left(\eta, x\left(\eta\right)\right) &= \frac{1}{30}\delta_O''\left(x(\eta)\right)\eta^2 + \frac{\delta_O\left(x(\eta)\right)}{3}, \\ \dot{f}\left(\eta, x\left(\eta\right)\right) &= \frac{1}{15}\delta_O''\left(x(\eta)\right)\eta. \end{aligned}$$

and consequently to the following distance–redshift relation

$$\begin{aligned} D_L\left(z_e\right) &= \left(1+z_e\right)\left(\eta_O-\eta_e\right)\left(1+\frac{\epsilon}{3}\left(\delta_O\left(x(\eta_o)\right)+\delta_O\left(x(\eta_e)\right)\right)\right) - \left(1+z_e\right)\int_{\eta_e}^{\eta_o}\frac{2\epsilon}{3}\delta_O\left(x(\eta)\right)d\eta \\ &+ \left(1+z_e\right)\int_{\eta_e}^{\eta_o}d\eta\int_{\eta_e}^{\eta}d\eta'\frac{\epsilon}{15}\delta_O''\left(x(\eta')\right)\eta' - \frac{1+z_e}{\mathcal{H}_e}\int_{\eta_e}^{\eta_o}d\eta\ \frac{\epsilon}{15}\delta_O''\left(x(\eta)\right)\eta. \end{aligned} \tag{6.96}$$

Chapter 7

Conclusions

In this thesis, we focused on different aspects of non standard cosmology through four different projects. We addressed some theoretical but also some observational issues of alternative cosmological models. This is certainly of interest, since the standard model of cosmology faces many problems mainly related to the cosmological constant Λ

- the origin of this "dark" component
- the lack of understanding of the smallness of the energy density ρ_Λ associated to the cosmological constant Λ or Fine Tunning Problem
- why has the cosmological constant energy density just started to dominate the universe at the present cosmological time or the Coincidence Problem.

These problems are strong hints that the standard model of cosmology will need to be improved or even overtaken in the future, and any attempt in this direction will therefore have to integrate some aspects of non standard cosmology.

In our first project, we studied graviton production in anti-de Sitter braneworlds cosmology. In this model, the expansion of the universe is mimicked by a brane moving through a higher dimensional spacetime and the brane motion leads to particle creation via the dynamical Casimir effect. The Kaluza-Klein gravitons, which are candidates for Dark Matter, scale like $\rho_{KK} \propto a^{-6}$, and can therefore not represent Dark Matter in our setup. Furthermore, we derived a method to calculate graviton production taking into account the full generalized Neumann boundary conditions, method therefore valid for a brane moving at arbitrarily high velocities. However, for arbitrarily high velocities one has also to take into account the modification of the Friedmann equations at high energy. Implemented this effect of backreaction on the very general method developped in this project would be the next step of this study.

In our second project, we derived model-independent cosmological constraints from the CMB, i.e. we have analysed the CMB data in a way which is independent of the details of the late-time cosmology. We have presented model-independent limits on the physical densities of baryonic matter ω_b and dark matter ω_c, the spectral index n_s and the angular diameter distance to the last scattering surface $D_A(z_*)$. Every model which satisfies our limits on these cosmological parameters will automatically be in agreement with the present CMB data, except the forty lowest multipoles which have been excluded from the

analysis. A prospect for future projects would be to divide the CMB sky into patches and do a model-independent analysis for each patch. This will give the directional variation of the angular diameter distance and other cosmological parameters.

In our third project, we studied the effects on the CMB of a homogeneous magnetic field in the presence of free streaming particles. The presence of the magnetic field sources an anisotropic expansion of the universe, geometrically described by a plane-symmetric Bianchi I model. Neutrinos are particularly well suited candidates to play the role of the free streaming component. As long as the neutrinos are relativistic, their anisotropic stress cancel the magnetic field's one, and despite of the presence of the magnetic field, the expansion is isotropic. Once the temperature of the universe drops below the neutrinos mass scale, their pressures decay very fast and the effect of compensation is lost. If the neutrino masses are smaller that 0.3 eV, i.e. if they are still relativistic at photon decoupling, we found that possible signature of the anisotropic expansion due to the magnetic field on the CMB anisotropies is significantly supressed. Planck and other surveys like Euclid will most probably determine the neutrino mass scale. Once this is known, we will be able to choose between the different scenarios investigated in this project and quantify more precisely the reduction of the CMB quadrupole.

In our last project, we studied the distance-redshift relation in a universe filled with walls of pressure-less dust separated by under dense regions. We showed that for under dense regions whose diameter corresponds to observed voids, the distance remains close to what is obtained in a homogeneous and isotropic universe with pressure-less matter. We also imposed the observed distance on walls model, and found that this would require voids of size comparable to the observable universe, which are not observed. These two results disfavour our model of inhomogeneities as an alternative to dark energy: we cannot mimic acceleration with many dense walls. Our conclusions agree with previous studies where the Lemaître-Tolman-Bondi (LTB) dust universe whose distance redshift relation is equivalent to that in the standard model of cosmology is constructed. The LTB model is the spherically symmetric dust solution of Einstein's field equations. In summary, simple inhomogeneous cosmological models with plane or spherical symmetry provide strong hints that the observed accelerated expansion of the universe is a real effect sourced by some exotic and unknown component rather than a "feigned" effect of fluctuations and inhomogeneities on the average expansion rate.

The different projects achieved during this thesis point out the interest, the necessity and the opportunities of exploring cosmology beyond the standard ΛCDM model. During my thesis, I had mainly been involved on projects related to the dark energy problem, but the fundamental understanding of dark matter is also one additionnal issue of the standard model of cosmology. This fundamental understanding will certainly require to go beyond the standard model of particles, and in this domain, a lot is expected from experimental physics, above all the current experiments at the LHC. In a near future, Planck and Euclid satellites will provide more accurate cosmological data which will allow to exclude some dark energy and dark matter models, and thus, lead to a better understanding of the whole dark sector of our universe. Physics being an empirical science, it essentialy proceeds by a a combination of theoretical and observational studies, and this approach will for sure be the key of many exciting problems highlighted in this thesis.

Bibliography

[1] Amanullah R. et al., Astrophys. J. **716**, 712 (2010) [arXiv:1004.1711v1 [astro-ph.CO]];
Guy J. et al. (2010), arXiv:1010.4743v1 [astro-ph.CO];
Holsclaw T., et al., Phys. Rev. Lett. **105**, 241302 (2010) [arXiv:1011.3079v1 [astro-ph.CO]];
Suzuki N. et al. (2011), arXiv:1105.3470v1 [astro-ph.CO].

[2] Amsler C. et al. [Particle Data Group], *Review of particle physics*, *Phys. Lett.* **B667** (2008) 1

[3] Amsler C. *et al.* [Particle Data Group] Phys. Lett. **B667**, 1 (2008) and 2009 partial update for the 2010 edition.

[4] Barrow J.D., Juszkiewicz R., and Sonoda D.H., Mon. Not. R. Astron. Soc. **213**, 917 (1985);
Barrow J.D., Can. J. Phys. 164, 152 (1986);
Novikov I.D., Sov. Astron. 12, 427 (1968);
Kogut A., Hinshaw G., Barrow J.D., Jusciewicz R. and Silk J.

[5] Arkani-Hamed N., Dimopoulos S. and Dvali G., Phys. Lett. **B429**:263-272 (1998), [arXiv:hep-ph/9803315v1]

[6] Barrow J.D., Ferreira P. and Silk J., Phys. Rev. Lett. **78**, 3610 (1997) [arXiv:astro-ph/9701063]

[7] Becker R.H. et al., *Astron. J.* **22** (2001) 2850 [arXiv:astro-ph/0108097v3]
Fan X. et al.,*Ann. Rev. Astron. Astrophys.* **44** (2006) 415 [arXiv:astro-ph/0602375v2]

[8] Bennett C.L. et al., Astrophys.J.Suppl. **192**:17,2011 [arXiv:1001.4758v2 [astro-ph.CO]]

[9] Blake C. et al., Mon. Not. Roy. Ast. Soc. **418**, 1707 (2011) [arXiv:1108.2637v1 [astro-ph.CO]].

[10] Bolejko K., Célérier M-N. and Krasinski A., Class. Quantum Grav. **28**, 164002 (2011) [arXiv:1102.1449v2 [astro-ph.CO]];
Marra V. and Notari A., Class. Quantum Grav. **28**, 164004 (2011) [arXiv:1102.1015v2 [astro-ph.CO]].

[11] Bonvin C., Durrer R. and Gasparini A., Phy. Rev. **D 73**, 023523 (2006) [arXiv:astro-ph/0511183v5].

[12] Bonvin C. and Caprini C., JCAP 1005:022 (2010) [arXiv:1004.1405v2 [astro-ph.CO]].

[13] Bordag M., *Quantum Field Theory under the Influence of External Conditions* (Teuber, Stuttgart, 1996).

[14] Buchert T.,*Gen. Rel. Grav.* **40** (2008) 467 [arXiv:0707.2153v3 [gr-qc]]

[15] Bull P., Clifton T., Ferreira P. G., Phys. Rev. **D 85**, 024002 (2012) [arXiv:1108.2222v3 [astro-ph.CO]]

[16] Caldwell R.R., Doran M., Mueller C.M., Schafer G. and Wetterich C., *Astrophys. J.* **591** (2003) L75, [arXiv:astro-ph/0302505v2]
Linder E.V. and Robbers G., JCAP06(2008)004, [arXiv:0803.2877v1 [astro-ph]]

[17] Camerini R., Durrer R., Melchiorri A. and Riotto A., Phys. Rev. **D77**, 101301 (2008) [arXiv:0802.1442v1 [astro-ph]].

[18] Capozziello S. and Francaviglia M., *Gen. Rel. Grav.* **40** (2008) 357 [arXiv:0706.1146v2 [astro-ph]]

[19] Caprini C. and Durrer R., Phys. Rev. **D65**, 023517 (2001), [arXiv:astro-ph/0106244v2];
Caprini C., Durrer R. and Fenu E., JCAP **0911**, 001 (2009), [arXiv:0906.4976v1 [astro-ph.CO]].

[20] Cartier C. and Durrer R., Phys. Rev. **D71**, 064022 (2005), [arXiv:hep-th/0409287v2]

[21] Cartier C., Durrer R. and Ruser M., Phys. Rev. **D72**, 104018 (2005), [arXiv:hep-th/0510155v2]

[22] Celerier M.N., Bolejko K., Krasinski A. and Hellaby C., Astron. Astrophys. **518**:A21, 2010 [arXiv:0906.0905v5 [astro-ph.CO]]

[23] Clarkson C.,*Phys. Rev.* **D76** (2007) 104034 ,[arXiv:0708.1398v1 [gr-qc]]
Zibin J. P.,*Phys. Rev.* **D78** (2008) 043504, [arXiv:0804.1787v2 [astro-ph]]
Clarkson C., Clifton T. and February S., JCAP06(2009)025, [arXiv:0903.5040v2 [astro-ph.CO]]

[24] Clarkson C., Bassett B.A. and Lu T. H.-C., *Phys. Rev. Lett.* **101** (2008) 011301, [arXiv:0712.3457v2 [astro-ph]]
Clarkson C., Cortes M., Bassett B.A., JCAP0708(2007)011, [arXiv:astro-ph/0702670v3]
Shafieloo A. and Clarkson C., Phys.Rev. **D81**:083537,2010 [arXiv:0911.4858v2 [astro-ph.CO]]

[25] Clifton T., Ferreira P.G. and Zuntz J., JCAP07(2009)029, [arXiv:0902.1313v3 [astro-ph.CO]]

[26] Collins H.(2010), arXiv:1011.2046v1.

[27] Corasaniti P.S. and Melchiorri A., *Phys. Rev.* **D77** (2008) 103507, [arXiv:0711.4119v2 [astro-ph]]

[28] Crocce M., Dalvit D. A. R., Mazzitelli F. D., Phys. Rev. **A66**, 033811 (2002), [arXiv:quant-ph/0205104v1]

[29] Dodonov V. V., Adv. Chem. Phys. **119**, 309, (2001), [arXiv:quant-ph/0106081v1]

[30] Doran M. and Lilley M., *Mon. Not. Roy. Astron. Soc.* **330** (2002) 965, [arXiv:astro-ph/0104486v3]

[31] Doroshkevich A.G. and Khlopov M.Y., *Sov. J. Nucl. Phys.* **39** (1984) 551 (*Yad. Fiz.* **39** (1984) 869)
Turner M.S., Steigman G. and Krauss L.M., *Phys. Rev. Lett.* **52** (1984) 2090
Ferrer F., Nipoti C. and Ettori S., *Phys. Rev.* **D80** (2009) 061303 [arXiv:0905.3161 [astro-ph.CO]]

[32] Dunkley J. et al. [WMAP Collaboration], *Astrophys. J. Suppl.* **180** (2009) 306 [arXiv:0803.0586 [astro-ph]]

[33] Dunkley J. et al., Astrophys. J. **739**, 52 (2011) [arXiv:1009.0866v1 [astro-ph.CO]].

[34] Durrer R., Fund. Cosmic Phys. **15**, 209 (1994), [arXiv:astro-ph/9311041].

[35] Durrer R. , AIP Conference Proceedings 782 (2005) [arXiv:hep-th/0507006v1]

[36] Durrer R., *The Cosmic Microwave Background*, 2008 Cambridge University Press, Cambridge

[37] Durrer R. and Maartens R., *Gen. Rel. Grav.* **40** (2008) 301 [arXiv:0711.0077 [astro-ph]]

[38] Durrer R. and Ruser M. (2007), Phys. Rev. Lett. **99** , 071601 [arXiv:0704.0756v3 [hep-th]]

[39] Durrer R., Ruser M., Vonlanthen M. and Wittwer P., AIP Conference Proceedings **1122**, 39 (2009) [arXiv:astro-ph/0902.0872]

[40] Durrer R., Ruser M., Vonlanthen M. and Wittwer P., Phys. Rev. **D79**, 083529 (2009) [arXiv:astro-ph/0901.3683v3]

[41] Durrer R., Ruser M., Vonlanthen M. and Wittwer, in preparation.

[42] Durrer R., Phil. Trans. R. Soc. A **369**, 5102 (2011), doi: 10.1098/rsta.2011.0285 [arXiv:1103.5331v3 [astro-ph.CO]].

[43] Durrer R., Proceedings of the 1st Mediterranean Conference on Classical and Quantum Gravity (MCCQG). J. Phys., Conf. Ser. **222** 012021 (2010) [arXiv:1002.1389v1 [astro-ph.CO]] ;
Caprini C., Durrer R., T. Konstandin, G. Servant, Phys. Rev. **D79**, 083519 (2009) [arXiv:0901.1661v2 [astro-ph.CO]].

[44] Efstathiou G. and Bond J.R., *Mon. Not. Roy. Astron. Soc.* **304** (1999) 75 [arXiv:astro-ph/9807103]

[45] El-Ad H. and Piran T., ApJ, **491**, 421(1997) [arXiv:astro-ph/9702135v1].

[46] Elgarøy Ø. and Multamäki T., *Astron. & Astrophys.* **471** (2007) 65 [arXiv:astro-ph/0702343]

[47] Enqvist K., *Gen. Rel. Grav.* **40** (2008) 451 [arXiv:astro-ph/0709.2044]

[48] Francis C.L. and Peacock J.A., MNRAS *Mon. Not. Roy. Astron. Soc.* **406** 14 (2010) [arXiv:astro-ph/0909.2495]

[49] Fulling S.A., Davies P.C.W., Proc. Roy. Soc. Lond. A 348 (1976) 393.

[50] Galli S., Iocco F., Bertone G. and Melchiorri A., *Phys. Rev.* **D80** (2009) 023505 [arXiv:astro-ph/0905.0003]
Iocco F., Proceedings of Universe Invisible (Paris, 2009) [arXiv:arXiv:0912.1630v1 [astro-ph.CO]]

[51] Gaztañaga E., Cabré A. and Hui L., *Mon. Not. Roy. Astron. Soc.* **399** (2009) 1663 [arXiv:0807.3551 [astro-ph]]
Gaztañaga E., Miquel R. and Sánchez E., *Phys. Rev. Lett.* **103** (2009) 091302 [arXiv:0808.1921 [astro-ph]]

[52] Gondolo P. et al., JCAP07(2004)008 [arXiv:astro-ph/0406204]

[53] Gorbunov D. S., Rubakov V. A., and Sibiryakov S. M., JHEP **10**, 015 (2001) [arXiv:hep-th/0108017]

[54] Gorbunov D. S., Rubakov V. A. and Sibiryakov S. M., JHEP **10**, 015 (2001) [arXiv:hep-th/0108017].

[55] Graham P.W., Harnik R., and Rajendran S., Phys. Rev. **D82**, 063524 (2010) [arXiv:1003.0236v2 [hep-th]].

[56] Hansen F.K., Banday A.J. and Górski K.M., *Mon. Not. Roy. Astron. Soc.* **354** (2004) 641 [arXiv:astro-ph/0404206]
Huterer D.,*New Astron. Rev.* **50** (2006) 868 [arXiv:astro-ph/0608318]
Copi C.J., Huterer D., Schwarz D.J. and Starkman G.D.,*Mon. Not. Roy. Astron. Soc.* **399** (2009) 399 [arXiv:astro-ph/0808.3767]
Hoftuft J., Eriksen H.K., Banday A.J., Gorski K.M., Hansen F.K. and Lilje P.B., *Astrophys. J.* **699** (2009) 985 [arXiv:astro-ph/0903.1229]

[57] Hansen F.K., Banday A.J., Gorski K.M., Eriksen H.K. and Lilje P.B.,*Astrophys. J.* **704** (2009) 1448 [arXiv:astro-ph/0812.3795]

[58] Hinshaw G. et al.,*Astrophys. J. Suppl.* **180** (2009) 225 [arXiv:astro-ph/0803.0732]

[59] Hu W. and Sugiyama N., *Astrophys. J.* **471** (1996) 542 [arXiv:astro-ph/9510117]

[60] Hu W., Fukugita M., Zaldarriaga M. and Tegmark M., *Astrophys. J.* **549** (2001) 669 [arXiv:astro-ph/0006436]

[61] Humphreys N.P., Maartens R. and Matravers D.R., *Astrophys. J.* **477** (1997) 47 [arXiv:astro-ph/9602033]
Alnes H. and Amarzguioui M.,*Phys. Rev.* **D74** (2006) 103520 [arXiv:astro-ph/0607334]

[62] Jimenez R. and Loeb A., *Astrophys. J.* **573** (2002) 37 [arXiv:astro-ph/0106145]
Simon J., Verde L. and Jimenez R., *Phys. Rev.* **D71** (2005) 123001 [arXiv:astro-ph/0412269]

[63] Khoury J., Steinhardt P. and Turok N., Phys. Rev. Lett. **92**, 031302 (2004),[arXiv:hep-th/0307132]
Khoury J., Steinhardt P. and Turok N., Phys. Rev. Lett. **91** 161301 (2003) [arXiv:astro-ph/0302012]

[64] Kobayashi T., Kudoh H., and Tanaka T., Phys. Rev. **D68**, 044025 (2003) [arXiv:gr-qc/0305006]
Kobayashi T. and Tanaka T., Phys. Rev. **D71**, 124028 (2005) [arXiv:hep-th/0505065]
Kobayashi T. and Tanaka T., Phys. Rev. **D73**, 044005 (2006) [arXiv:hep-th/0511186]

[65] Kofman L., Pogosyan D. and Starobinsky A.A., *Sov. Astron. Lett.* **12** (1986) 175 (*Pisma Astron. Zh.* **12** (1986) 419)
Ichiki K., Oguri M. and Takahashi K., *Phys. Rev. Lett.* **93** (2004) 071302 [arXiv:astro-ph/0403164]
De Lope Amigo S., Cheung W.Y., Huang Z. and Ng S.P., JCAP06(2009)005 [arXiv:hep-th/0812.4016]

[66] Komatsu E. et al.[WMAP Collaboration],*Astrophys. J. Suppl.* **180** (2009) 330 [arXiv:astro-ph/0803.0547]

[67] Komatsu E. et al.,[arXiv:astro-ph/1001.4538]

[68] Komatsu E. et al., ApJS, **192**, 18, (2011) [arXiv:1001.4538v3 [astro-ph.CO]].

[69] Komatsu E. *et al.* [WMAP Collaboration], Astrophys. J. Supp. **192**, 18 (2011) [arXiv:0803.0547v2 [astro-ph]].

[70] Kosowsky A., Milosavlijevic M. and Jimenez R., *Phys. Rev.* **D66** (2002) 063007 [arXiv:astro-ph/0206014]

[71] Koyama K., JCAP 0409, 010 (2004) [arXiv:astro-ph/0407263]

[72] Koyama K. *Gen. Rel. Grav.* **40** (2008) 421 [arXiv:astro-ph/0706.1557]

[73] Krasinski A. and Bolejko K., Phys. Rev. **D 83**, 083503 (2011), [arXiv:1007.2083v2 [gr-qc]].

[74] Krauss L.M. and Chaboyer B., *Science* **299** (2003) 65 [arXiv:astro-ph/0111597v1]

[75] Kronberg P.P., Rept. Prog. Phys. **57**, 325 (1994)
Clarke T.E., Kronberg P.P. and Boehringer H., Astrophys. J. **547**, L111 (2001) [arXiv:astro-ph/0011281v1]

[76] Kunze K.E., Phys. Rev. **D83**, 023006 (2011) [arXiv:1007.3163v2 [astro-ph.CO]].

[77] Kurki-Suonio H., Muhonen V. and Väliviita J.,*Phys. Rev.* **D71** (2005) 063005 [arXiv:astro-ph/0412439]

[78] Larson D. *et al.* [WMAP Collaboration], Astrophys. J. Supp. **192**, 16 (2011) [arXiv:1001.4635v2 [astro-ph.CO]]

[79] Lemaître G., 1933 Ann. Soc. Sci. Bruxelles **A 53**, 51 (1933); (English translation, with historical comments: Gen. Rel. Grav. **29** 637, 1997).

[80] Lewis A. and Challinor A.,*Phys. Rept.* **429** (2006) 1 [arXiv:astro-ph/0601594v4]

[81] Lewis A., Challinor A. and Lasenby A., *Astrophys. J.* **538** (2000) 473 [arXiv:astro-ph/9911177]
Lewis A. and Bridle S., *Phys. Rev.* **D66** (2002) 103511 [arXiv:astro-ph/0205436]

[82] Linder E.V., *Gen. Rel. Grav.* **40** (2008) 339 [arXiv:astro-ph/0704.2064]

[83] Maartens R., Living Rev. Rel. **7**, 7 (2004) [arXiv:gr-qc/0312059]

[84] Marra V., Kolb E. W., Matarrese S. and Riotto A., Phys. Rev. **D 76**, 123004 (2007) [arXiv:0708.3622v3].

[85] Meures N. and Bruni M., MNRAS **419**, 1937 (2012) [arXiv:1107.4433v2] (DOI: 10.1111/j.1365-2966.2011.19850.x).

[86] Minamitsuji M., Sasaki M. and Langlois D., Phys. Rev. **D71**, 084019 (2005) [arXiv:gr-qc/0501086]

[87] Moore G.T., J. Math. Phys. **11** (1970) 2679.

[88] Mukhanov V., *Int. J. Theor. Phys.* **43** (2004) 623 [astro-ph/0303072]
Mukhanov V., *Physical Foundations of Cosmology*, 2005 Cambridge University Press, Cambridge

[89] Mukherjee P., Kunz M., Parkinson D. and Wang Y., *Planck priors for dark energy surveys*, *Phys. Rev.* **D78** (2008) 083529 [arXiv:0803.1616 [astro-ph]]

[90] Paoletti D., Finelli F. and Paci F., Mon. Not. Roy. Astron. Soc. **396**, 523 (2009) [arXiv:0811.0230v2 [astro-ph]].

[91] Perlick V., Living Reviews in Relativity, **7**, 9 (2004).

[92] Pitrou C., Class. Quant. Grav. **26**, 065006 (2009) [arXiv:0809.3036v3 [gr-qc]]

[93] Plebanski J. and Krasinski A., *An Introduction to General Relativity and Cosmology*, (Cambridge, 2006).

[94] Pontzen A., Challinor A., Mon. Not. Roy. Astron. Soc. **380**, 1387 (2007) [arXiv:0706.2075v2 [astro-ph]].

[95] de Putter R. et al, arXiv:1201.1909v1 (2012)

[96] Raftery A.E. and Lewis S.M. Bayesian Statistics 4, pp. 763-773, Cambridge University Press, Cambridge

[97] Randall L. and Sundrum R., Phys. Rev. Lett. **83**, 3370 (1999). [arXiv:hep-th/9905221]

[98] Randall L. and Sundrum R., Phys. Rev. Lett. **83**, 4690 (1999) [arXiv:hep-th/9906064]

[99] Räsänen S., JCAP11(2006)003 [arXiv:astro-ph/0607626]

[100] Räsänen S., JCAP04(2008)026 [arXiv:astro-ph/0801.2692]

[101] Räsänen S., *Phys. Rev.* **D79** (2009) 123522 [arXiv:astro-ph/0903.3013]

[102] Räsänen S., JCAP02(2009)011 [arXiv:astro-ph/0812.2872]

[103] Räsänen S., Class. Quant. Gravity **28**, 164008 (2011) [arXiv:1102.0408v2 [astro-ph.CO]].

[104] Reichardt C.L. et al.,*Astrophys. J.* **694** (2009) 1200 [arXiv:astro-ph/0801.1491v3]

[105] Riess A. et al. Astron. J. **116**, 1009 (1998) [arXiv:astro-ph/9805201v1]
S. Perlmutter et al., Astrophys. J. **517**, 565 (1999) [arXiv:astro-ph/9812133v1].

[106] Ruser M., Opt. B: Quantum Semiclass. Opt. **7**, S100 (2005) [arXiv:quant-ph/0408142]

[107] Ruser M., Phys. Rev. **A73**, 043811 (2006) [arXiv:quant-ph/0509030]

[108] Ruser M., J. Phys. **A39** (2006) 6711 [arXiv:quant-ph/0603097]

[109] Ruser M. and Durrer R., Phys. Rev. **D 76**, 104014 (2007)[arXiv:0704.0790v3 [hep-th]]

[110] Ruser M., Durrer R., Vonlanthen M. and Wittwer P., Phys.Rev.**D79**:083529,2009 [arXiv:0901.3683v3 [astro-ph.CO]]

[111] Scannapieco E. and Ferreira P.G. Phys. Rev. **D56**:7493-7497,1997 [arXiv:astro-ph/9707115v1]

[112] Schneider P., Ehlers J. and Falco E.E., *Gravitational Lenses*, (Springer Verlag, 1992).

[113] Seahra S., Phys. Rev. **D74**, 044010 (2006) [arXiv:hep-th/0602194v2]

[114] Seitz S., Schneider P. and Ehlers J., Class. Quantum Grav. **11**, 2345 (1994) [arXiv:astro-ph/9403056v1].

[115] Seljak U., *Astrophys. J.* **460** (1996) 549

[116] Shaw J. R., Lewis A., Phys. Rev. **D81**, 043517 (2010) [arXiv:0911.2714v4 [astro-ph.CO]].

[117] Spergel D N et al.[WMAP Collaboration] *Astrophys. J. Suppl.* **170** (2007) 377 [arXiv:astro-ph/0603449]

[118] Straumann N. , *General Relativity with Applications to Astrophysics*, (Springer Verlag, 2004), Appendix 7.7.3.

[119] Szekeres P., Com. Math. Phys. **41**, 55 (1975); Phys. Rev. **D12**, 2941 (1975).

[120] Tolman R.C., Proc. Nat. Acad. Sci. USA **20**, 169 (1934); (reprinted, with historical comments: Gen. Rel. Grav. **29** 931, 1997).

[121] Vale C. and White M., Astrophys. J. **592**, 699 (2003) [arXiv:astro-ph/0303555v1]
Kainulainen K. and Marra V., Phys. Rev. **D83**, 023009 (2011) [arXiv:1011.0732v2 [astro-ph.CO]].

[122] Wang Y Y. and Mukherjee P.,*Phys. Rev.* **D76** (2007) 103533 [arXiv:astro-ph/0703780]

[123] Wilson C.M., Johansson G., Pourkabirian A., Johansson J.R., Duty T., Nori F., Delsing P., arXiv:1105.4714 (2011)

[124] Yoo C.-M. , Kai T., Nakao K., Phys. Rev. **D 83**, 043527 (2011) [arXiv:1010.0091v1 [astro-ph.CO]].

[125] Yoo C.-M., Kai T., Nakao K., Prog. Theor. Phys. **120**, 937 (2008) [arXiv:0807.0932v4 [astro-ph]].

[126] Zakharov A. V. , Soviet Physics Journal **30**, 1015 (1987).

[127] Zibin J.P., Moss A. and Scott D.,*Phys. Rev. Lett.* **101** (2008) 251303 [arXiv:astro-ph/0809.3761]

[128] Zibin J.P., Moss A. and Scott D., *Phys. Rev.* **D76** (2007) 123010 [arXiv:astro-ph/0706.4482v3]

[129] Zwicky F., Helvet. Phys. Acta **6**, 110 (1933).

[130] http://www.aip.org/history/cosmology/